



**UNIVERSIDADE FEDERAL DO CEARÁ**  
**CENTRO DE CIÊNCIAS**  
**DEPARTAMENTO DE QUÍMICA ANALÍTICA E FÍSICO-QUÍMICA**  
**PROGRAMA DE PÓS-GRADUAÇÃO EM QUÍMICA**

**FRANCISCO WAGNER DE QUEIROZ ALMEIDA NETO**

**THEORETICAL, STRUCTURAL AND *IN SILICO* ANALYSIS OF  
AMINOCHALCONES DERIVATIVES WITH POTENTIAL ANTIOXIDANT AND  
ANTI-SARS-COV-2**

**FORTALEZA**

**2021**

FRANCISCO WAGNER DE QUEIROZ ALMEIDA NETO

THEORETICAL, STRUCTURAL AND *IN SILICO* ANALYSIS OF AMINOCHALCONES  
DERIVATIVES WITH POTENTIAL ANTIOXIDANT AND ANTI-SARS-COV-2

Tese apresentada ao Programa de Pós-Graduação em Química da Universidade Federal do Ceará como requisito parcial à obtenção do título de doutor em Química. Área de concentração: Físico-Química.

Orientador: Prof. Dr. Pedro de Lima Neto  
Coorientador: Prof. Dr. Emmanuel Silva Marinho

FORTALEZA

2021

Dados Internacionais de Catalogação na Publicação  
Universidade Federal do Ceará  
Biblioteca Universitária  
Gerada automaticamente pelo módulo Catalog, mediante os dados fornecidos pelo(a) autor(a)

---

- A446t Almeida Neto, Francisco Wagner de Queiroz.  
Theoretical, structural and in silico analysis of aminochalcones derivatives with potential antioxidant and anti-SARS-CoV-2 / Francisco Wagner de Queiroz Almeida Neto. – 2021.  
152 f. : il. color.
- Tese (doutorado) – Universidade Federal do Ceará, Centro de Ciências, Programa de Pós-Graduação em Química, Fortaleza, 2021.  
Orientação: Prof. Dr. Pedro de Lima Neto.  
Coorientação: Prof. Dr. Emmanuel Silva Marinho.
1. chalcone. 2. density functional theory. 3. molecular docking. 4. SPIKE. 5. ACE2. I. Título.  
CDD 540
-

FRANCISCO WAGNER DE QUEIROZ ALMEIDA NETO

THEORETICAL, STRUCTURAL AND *IN SILICO* ANALYSIS OF AMINOCHALCONES  
DERIVATIVES WITH POTENTIAL ANTIOXIDANT AND ANTI-SARS-COV-2

Tese apresentada ao Programa de Pós-Graduação em Química da Universidade Federal do Ceará, como requisito parcial à obtenção do título de doutor em Química. Área de concentração: Físico-Química.

Aprovada em: \_\_\_/\_\_\_/\_\_\_\_\_.

BANCA EXAMINADORA

---

Prof. Dr. Pedro de Lima Neto (Orientador)  
Universidade Federal do Ceará (UFC)

---

Prof. Dr. Emmanuel Silva Marinho  
Universidade Estadual do Ceará (UECE)

---

Prof. Dra. Maria da Conceição Ferreira de Oliveira  
Universidade Federal do Ceará (UFC)

---

Prof. Dr. Luiz Gonzaga de França Lopes  
Universidade Federal do Ceará (UFC)

---

Prof. Dr. Hélcio Silva dos Santos  
Universidade Vale do Acaraú (UVA)

---

Prof. Dr. Alexandre Magno Rodrigues Teixeira  
Universidade Regional do Cariri (URCA)



To God.

To my beloved mother, in loving memory.

## ACKNOWLEDGMENTS

First, I would like to thank God for the gift of my life and all the strength He has been given me in all situations.

I would like to thank my mother, Maria de Fátima Alencar Queiroz, for all the support she gave me in life. She always believed in me and always gave me the strength to pursue the career of my dreams. When I told her that, in addition to the four years of my undergraduate Chemistry course, I would still need to do a master's and a Ph.D. course if I want to be a professor and a researcher, so she didn't let me be discouraged by the long and arduous journey that awaited me. Unfortunately, she couldn't see me, in life, finish my master's degree and enter in the Ph.D. course, but all I got was for you. Your cheerful, simple, and strong way inspires me every day. I will always love you, Mom.

I would also like to thank my father, Francisco Wagner de Queiroz Almeida Júnior, my grandmother, Maria Orquídea do Nascimento Almeida, and my aunt, Ângela Maria Jucá Alencar for all kindness, love, and patience. You are everything to me. I don't know how to put into simple words all the gratitude and love I feel for you. I feel honored to be able to be a son, grandson, and nephew, respectively. Thank you for believing in me.

I would like to thank Morgana Timbó Lima, the love of my life. Your love, affection, support, comprehension, and dedication are my driving force to face any obstacle. I have a lot to thank God for, and one of those thanks is for having you in my life, for our love, our companionship, and our love story. It is a true honor to be your boyfriend, and I want to retribute giving all my love and care in all the moments of our lives.

To my inseparable and best friends: Desirée Bitencourt, Felipe Peixoto, Fernando de Brito, Mykhail Rachyd, Emanuelle Marinho, Conceição Alves, Claudio Takeuti, Lucas Lima, Leonardo Paes, Thiago Teixeira, Marcos Vinícius Aquino, Pedro Ramos, and Nicholas Oliveira. Life wouldn't have the same shiny without you. You are essential, part of my story, part of my life. I am very lucky, and I am eternally grateful to each of you.

To my "family" within the academy: my advisors Prof. Dr. Pedro de Lima Neto and Prof. Dr. Emmanuel Silva Marinho, to Prof. Dr. Márcia Machado Marinho, to Prof. Dr. Hélcio Silva dos Santos, and Prof. Dr. Alexandre Magno, you are simply amazing. It is equally difficult to put in simple words the importance of you in my life and the gratitude for all the work you have entrusted to me, for all the support, all the opportunities, and all the teaching in these years.

I would also like to thank all my family, including Katia Zoraya Saldanha, for all the support, all the support, all the strength, all the prayers, and for believing in me.

I would like to thank the Universidade Federal do Ceará (UFC), the “Programa de Pós Graduação em Química”, the “Centro Nacional de Processamento de Alto Desempenho” (CENAPAD) for the computational resources, and the “Conselho Nacional de Desenvolvimento Científico e Tecnológico” (CNPq) for the financial support, the opportunity to carry out this research, for all the knowledge and learning that I had the opportunity to acquire these four years of my Ph.D. course.

Finally, I would like to thank you who, for some reason, found my thesis. I hope that my work can help you in some way. Remember that we never reach our goals alone. I'm going to leave a very clichéd phrase: "even the darkest night will end so that a beautiful dawn can rise". Fight until the end for all your dreams, I know you can do it.

“I see now that the circumstances of one’s birth are irrelevant. It is what you do with the gift of life that determines who you are”

Mewtwo

## RESUMO

Por causa do crescente interesse na química da classe de moléculas denominadas chalconas, já que essas espécies demonstram uma ampla aplicabilidade farmacológica dependendo da natureza química dos grupos ligados aos anéis A e B, a molécula N-{4'-[(E)-3-(4-fluorofenil)-1-(fenil)-prop-2-en-1-ona]}-acetamida (PAAPF) foi recentemente sintetizada. Os cálculos químicos quânticos foram feitos para uma caracterização teórica completa (propriedades estruturais, espectroscópicas, eletrônicas e óticas não-lineares) empregando três métodos da Teoria do Funcional da Densidade (DFT) como B3LYP, mPW1PW91 e M06-2X com o conjunto de base 6-311++G(d,p). Após todas as caracterizações, a atividade antioxidante foi estudada por meio do mecanismo teórico utilizando os diferentes métodos de DFT. Em seguida, utilizando cálculos de acoplamento molecular, seis chalconas foram estudadas como potenciais antivirais para inibição de enzimas importantes do SARS-CoV-2 por causa da emergência sanitária da pandemia da COVID-19 e a busca por novos candidatos à antivirais para uma doença nova que até então não possui tratamento eficiente. Todos os três métodos DFT estudados podem descrever com grande precisão a chalcona PAAPF: os resultados da espectroscopia de infravermelho e da blindagem isotrópica de  $^1\text{H}$  e  $^{13}\text{C}$  demonstram estar em excelente concordância com os dados experimentais. Os resultados das propriedades óticas não lineares mostraram que a chalcona PAAPF pode ser usada em aparelhos óticos. Por fim, os dados experimentais da atividade antioxidante mostraram uma taxa moderada de reação com a molécula de DPPH (50,92%) e este fato foi comprovado com o mecanismo de Transferência de Átomo de Hidrogênio (HAT) sendo o mais favorável. Juntos, nossos resultados sugerem que a chalcona PAAPF, juntamente com outras cinco nomeadas N-{4'-[(E,E)-5-(fenil)-1-(fenil)-penta-2,4-dien-1-ona]}-acetamida denominada PAACN, N-{4'-[(E)-3-(fenil)-1-(fenil)-prop-2-en-1-ona]}-acetamida denominada PAAB, N-{4'-[(E)-3-(4-dimetilaminofenil)-1-(fenil)-prop-2-en-1-ona]}-acetamida denominada PAAPA, N-{4'-[(E)-3-(4-etóxfenil)-1-(fenil)-prop-2-en-1-ona]}-acetamida denominada PAAPE e N-{4'-[(E)-3-(4-metóxfenil)-1-(fenil)-prop-2-en-1-ona]}-acetamida denominada PAAPM inibem a interação do vírus com as células hospedeiras humanas através da ligação à proteína ACE2 ou SPIKE, provavelmente gerando um impedimento estérico. Além disso, as moléculas de chalconas apresentam afinidade por enzimas importantes em processos pós-traducionais, interferindo na replicação viral.

**Palavras-chave:** chalcona; teoria do funcional de densidade; acoplamento molecular; SPIKE; ACE2.

## ABSTRACT

Due to the growing interest in the chemistry of the class of molecules called chalcones, these species demonstrate broad pharmacological applicability depending on the chemical nature of the groups attached to the A and B rings, the molecule N-{4'-[(E)-3-(4-fluorophenyl)-1-(phenyl)-prop-2-en-1-one]}-acetamide (PAAPF) was recently synthesized. The quantum chemical calculations were made for the complete theoretical characterization (structural, spectroscopic, electronic, and non-linear optical properties) applying three different Density Functional Theory (DFT) methods such as B3LYP, mPW1PW91, and M06-2X with base set 6-311++G(d,p). After the characterization, the antioxidant activity was studied by the theoretical mechanisms using the different DFT methods. Then, using Molecular Docking calculations, six chalcones were studied as potential antivirals for inhibiting important enzymes of SARS-CoV-2 due to the health emergency of the COVID-19 pandemic and the search for antiviral candidates for a new disease, which until the present date, it does not have efficient treatment. All the three DFT methods used in this work can describe the PAAPF chalcone with great precision: the results of infrared spectroscopy and  $^1\text{H}$  and  $^{13}\text{C}$  isotropic shielding demonstrate to be in excellent agreement with the experimental data. The PAAPF chalcone can be used in optical devices due to its results for non-linear optical properties. Finally, the experimental data of antioxidant activity showed a moderate rate of reaction with the DPPH molecule (50.92%), and this fact was proven theoretically by the Hydrogen Atom Transfer (HAT) mechanism being the most favorable. Together, the results suggest that the PAAPF chalcone along with five others derivatives N-{4'-[(E,E)-3-(phenyl)-1-(phenyl)-prop-2-en-1-one]}-acetamide named PAACN, N-{4'-[(E)-3-(phenyl)-1-(phenyl)-prop-2,4-dien-1-one]}-acetamide named PAAB, N-{4'-[(E)-3-(4-dimethylaminophenyl)-1-(phenyl)-prop-2-en-1-one]}-acetamide named PAAPA, N-{4'-[(E)-3-(4-ethoxyphenyl)-1-(phenyl)-prop-2-en-1-one]}-acetamide named PAAPE, and N-{4'-[(E)-3-(4-methoxyphenyl)-1-(phenyl)-prop-2-en-1-one]}-acetamide named PAAPM inhibit the virus interaction with human host cells through binding to the ACE2 or SPIKE protein, probably generating a steric impediment. In addition, chalcone molecules have an affinity for important enzymes in post-translational processes, interfering with viral replication.

**Keywords:** chalcone; density functional theory; molecular docking; SPIKE; ACE2.

## LIST OF FIGURES

Figure 1	– The basic molecular structure of the chalcone molecule.....	14
Figure 2	– The general overall reaction to obtain a chalcone from the Claisen-Schmidt reaction.....	15
Figure 3	– The Claisen-Schmidt aldol condensation to obtain the chalcone molecules.....	16
Figure 4	– Chemical structures for some chalcones derivates.....	18
Figure 5	– Chalcone derivates chemical structures.....	20
Figure 6	– The chemical structure of the chalcone (E)-1-(4-aminophenyl)-3-(4-benzyloxyphenyl)-prop-2-en-1-one.....	22

## LIST OF ABBREVIATIONS

ALA	Alanine
ARG	Arginine
ASP	Aspartate
B3LYP	Becke-3-parameter-Lee-Yang-Parr exchange-correlation functional
COVID-19	Coronavirus disease 2019
DFT	Density Functional Theory
GLU	Glutamate
GLY	Glycine
OH <sup>-</sup>	Hydroxide Ion
LANL2DZ	Los Alamos National Laboratory 2-double-z
LEU	Leucine
LYS	Lysine
-OMOM	Methylmethoxy ether
Mpro	Main <i>protease</i>
PAAB	N-{4'-[( <i>E</i> )-3-(phenyl)-1-(phenyl)-prop-2,4-dien-1-one]}-acetamide
PAACN	N-{4'-[( <i>E,E</i> )-3-(phenyl)-1-(phenyl)-prop-2-en-1-one]}-acetamide
PAAPA	N-{4'-[( <i>E</i> )-3-(4-dimethylaminophenyl)-1-(phenyl)-prop-2-en-1-one]}-acetamide
PAAPE	N-{4'-[( <i>E</i> )-3-(4-ethoxyphenyl)-1-(phenyl)-prop-2-en-1-one]}-acetamide
PAAPF	N-{4'-[( <i>E</i> )-3-(4-fluorophenyl)-1-(phenyl)-prop-2-en-1-one]}-acetamide
PAAPM	N-{4'-[( <i>E</i> )-3-(4-methoxyphenyl)-1-(phenyl)-prop-2-en-1-one]}-acetamide
NMR	Nuclear Magnetic Resonance
Pd	Palladium
KOH	Potassium Hydroxide
RNA	Ribonucleic Acid
TPSSh-D3	Tao-Perdew-Staroverov-Scuseria with $\tau$ -Dependent Gradient-Corrected Correlation and using the Grimme's dispersion model
TZVP	Triple Zeta Valence Plus Polarization
UV-Vis	Ultraviolet-Visible
VAL	Valine
WHO	World Health Organization



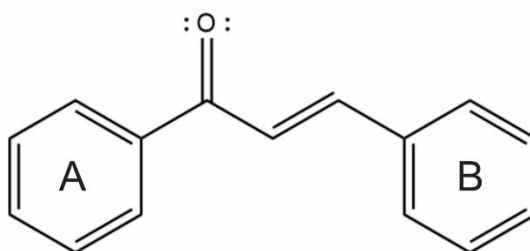
## SUMMARY

1	INTRODUCTION.....	14
2	CHARACTERIZATION OF THE STRUCTURAL, SPECTROSCOPIC, NONLINEAR OPTICAL, ELECTRONIC PROPERTIES AND ANTIOXIDANT ACTIVITY OF THE N-{4'-[( <i>E</i> )-3-(FLUOROPHENYL)-1- (PHENYL)-PROP-2-EN-1-ONE]}-ACETAMIDE.....	24
3	<i>IN SILICO</i> STUDY OF THE POTENTIAL INTERACTIONS OF 4'- ACETAMIDECHALCONES WITH PROTEIN TARGETS IN SARS-CoV-2...	102
4	CONCLUSION.....	124
	REFERENCE.....	126
	APPENDIX A – AUTHOR'S CURRICULUM DATA.....	132
	APPENDIX B – ELSEVIER'S AUTHOR RIGHTS.....	154

## 1 INTRODUCTION

The class of molecules denominated chalcone is considered open-chain molecules and derived from flavonoids and isoflavonoids, which have a natural occurrence and are important constituents of natural products such as tea, vegetables, fruits, and plants [1]. The molecular structure of chalcone consists of at least two aromatic rings linked by three highly electrophilic carbons and is called the  $\alpha,\beta$ -unsaturated system (1,3-diaryl-prop-2-en-1-one) [2,3]. The aromatic ring near to the carbonyl group is frequently called “ring A” and the other aromatic ring is “ring B”. The molecular structure of the chalcone can assume two possible geometric isomers: the *E* and the *Z* structures. Thermodynamically, in most of cases, the *E* structure is more stable. Hence, in Figure 1 is shown the basic chalcone structure using the *E* isomer [4].

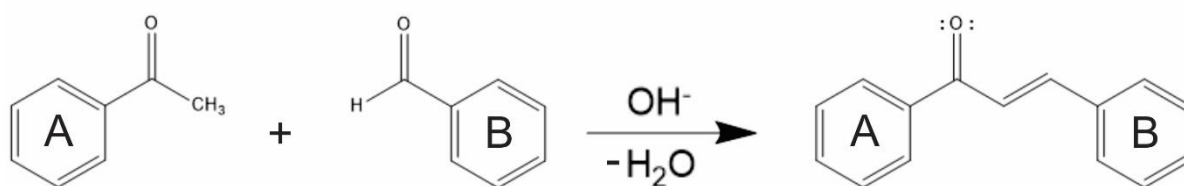
Figure 1 – The basic molecular structure of the chalcone molecule



Source: Author himself

The chalcones molecules can also be obtained through organic synthesis using several methods. In the laboratory, although there are several methods of synthesis, in this thesis, a specific method was used to synthesize these molecules, and this reaction is called Claisen-Schmidt aldol condensation [5-7]. This reaction takes place between an acetophenone molecule that has a single hydrogen and aromatic aldehydes. The general overall reaction can be seen in Figure 2. The solvent used in this reaction should be polar, and a strong base, such as potassium hydroxide (KOH), is used as a catalyst [8]. A scheme for the known mechanism is shown in Figure 3.

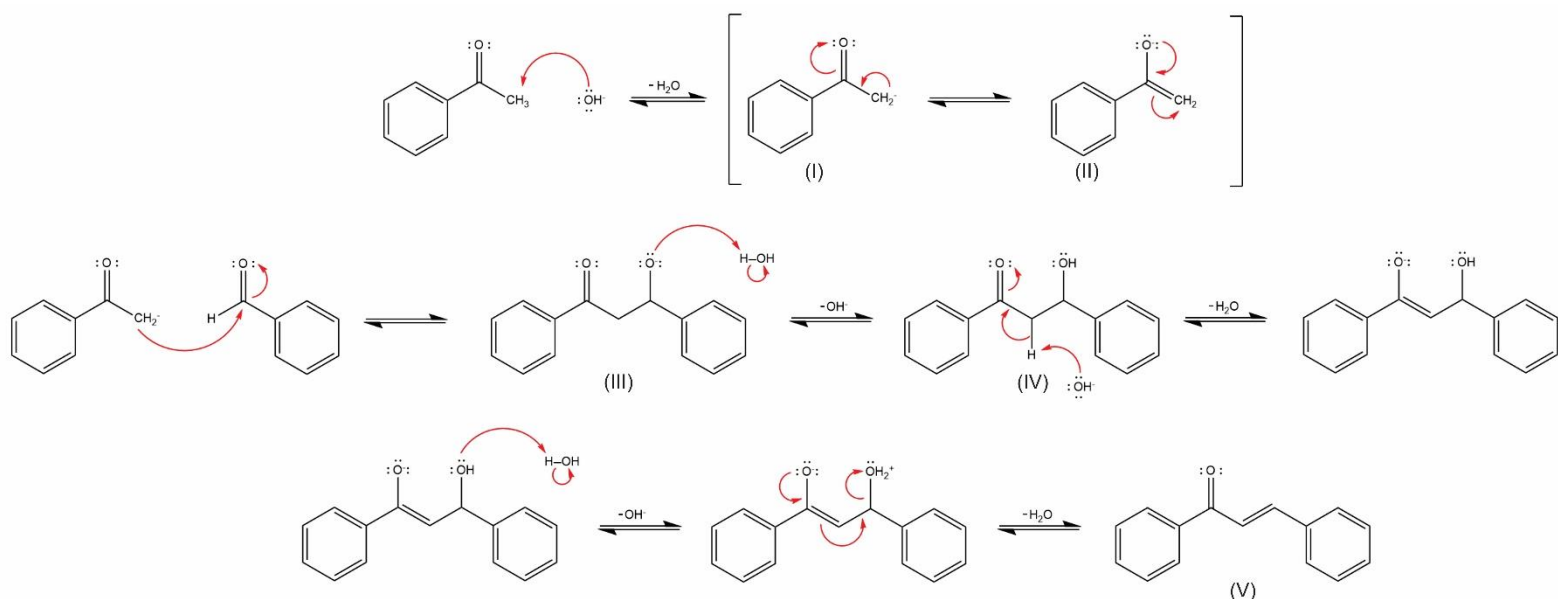
Figure 2 – The general overall reaction to obtain a chalcone from the Claisen-Schmidt reaction



Source: Author himself

Initially, due to the basic medium, there is the formation of a carbanion ion (structure I) from the acetophenone molecule by the attack of the hydroxide ion ( $\text{OH}^-$ ) and, because of the tautomeric effect, it can obtain the enolate ion (structure II). Then, it occurs the attack of the enolate ion (nucleophile) to the carbon atom of the aldehyde group (electrophile), generating an alkoxide ion (structure III). Subsequently, the alkoxide ion attacks the polar solvent molecule generating an aldol molecule (structure IV), and finally, this molecule undergoes base-catalyzed dehydration to yield the chalcone of interest (structure V). This reaction is considered one of the most used methodologies in the laboratory for the synthesis of chalcones, its duration depends on the nature of the substituent groups present in the precursor reagents, and the reaction yield can reach up to 90% [9]. It is known that the Claisen-Schmidt condensation can also be catalyzed using a strong acid, however, since the interested molecules for this thesis were synthesized using the base-catalyzed method, the text was limited to this methodology.

Figure 3 – The Claisen-Schmidt aldol condensation to obtain the chalcone molecules.



Source: Author himself

Chalcones and their derivatives are substances of great chemical-pharmacological interest and have received a great deal of attention mainly due to their relatively simple structure and the diversity of pharmacological activity they present [10-12]. The existence of conjugated double bonds between the two aromatic rings, the carbonyl group, and the olefinic bond ( $C\alpha C\beta$ ) implies the delocalization of the  $\pi$ -electronic density within the whole molecular structure. This special characteristic of chalcones makes these molecules have low reduction-oxidation potentials and exhibit a high probability of participating in reactions with electronic density transfer [13]. Furthermore, the fact that there is the possibility of anchoring different types of substituent groups in aromatic rings leads to new biological activities for each new molecule synthesized. Several recent studies in the literature show numerous pharmacological applications such as antioxidant [14,15], antiviral [16-18], anti-cancer [15,19], anti-fungal [20], antiparasitic [21], analgesic [22], anti-proliferative [23], antimicrobial [24], anticonvulsant [25], antidiabetic [26,27], anti-inflammatory [15,28], neuroprotective [15,29], and anxiolytic [2,8,30] activities. It was mentioned previously only a few examples of the most diverse application possibilities of the chalcone derivatives.

Within the huge class of chalcone molecules, it is possible to highlight the derivatives whose substitution occurred in the para position of the A ring using the amino and acetamide groups [31-36]. According to the literature, the presence of the amino group in the A ring increases the positive charge on the carbon  $C\beta$ , therefore, it increases the probability of this

chalcone derivative acting as an electrophile and attack cancer cells [37]. Dimmock *et al.* [38] and Romagnoli *et al.* [39] synthesized the base structure of the aminochalcone, and the authors measured the cytotoxicity against human cells and five cancer cell lines. The results obtained by these authors were that the aminochalcone has a satisfactory potential in the treatment of cancer, but it was found to be toxic for human cells. Since these derivatives are toxic, it was proposed in the work by Tristao *et al.* [40] that when chemically transforming the amino group into the acetamide group, there is a decrease in cytotoxicity and maintenance of the anticancer potential. Therefore, a more in-depth study of these derivatives is necessary.

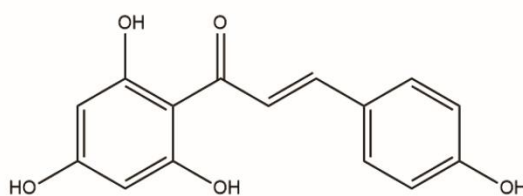
Among the mentioned applications, the possibility of using the chalcone derivatives as potential antivirals can be highlighted. The current health emergency generated by the COVID-19 pandemic caused by the new coronavirus (SARS-CoV-2) can be measured by the number of cases and deaths confirmed by the disease globally. The number of total cases in the world is higher than 241,000,000, the number of death higher than 4,900,000, and in Brazil, it has been accounting for more than 21,000,000 in the total cases and almost 600,000 deaths [41]. About a year and six months after the WHO declared that COVID-19 as a pandemic [42], until this date, there is no drug or efficient treatment against this disease. The vaccination of the population, the appropriate use of face masks, and social distancing are the only ways to slow down the spread of the virus. Hence, there is an extreme need to search for new candidates for antiviral drugs to be able to control the advance of COVID-19 [43].

It is widely known that the number of works involving computational methods is increasing in the most diverse areas. In the initial months of the pandemic, it was possible to notice an increase in the number of works that aim to study antiviral properties of different types of molecules, which can be obtained from both natural and synthetic sources, against the SARS-CoV-2. The use of computational calculations can speed up the discovery of new drugs as it is possible to predict properties with good accuracy and thus take only the promising molecules to carry out the experiments in the laboratory.

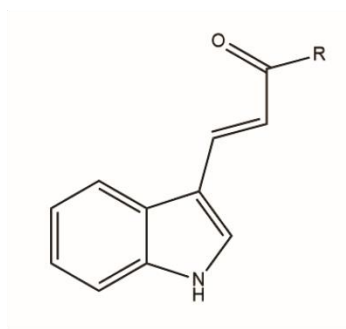
Among the computational methods most used in the literature, the Molecular Docking and the quantum calculations using the Density Functional Theory (DFT) are highlighted. With the use of those two methods, it is possible to study the chemical interactions between the interested molecules and the target proteins of the virus. Due to the great interest in the chemistry of chalcones and their known antiviral properties, this thesis aims to make a full theoretical characterization using quantum calculations (DFT method) for a chalcone derivative and subsequent application against three main target proteins of SARS-CoV-2 and the human host receptor protein to which the virus binds for entry into cells (Molecular Docking).

Vijayakumar *et al.* [44] studied *in silico* twenty-three natural flavonoids and twenty-five synthetic antituberculosis indole chalcones. The anti-SARS-CoV-2 activity was computed using the Molecular Docking. The authors chose three target proteins for the Molecular Docking calculations: the RNA-dependent RNA polymerase (rsrp), the Main protease (Mpro), and the SPIKE protein. Only a few synthetic indol chalcones (C4, C8, C12, C16, C17, C20, C22, and C23) demonstrated interaction with the RNA-dependent RNA polymerase, but it was a natural flavonoid (Cyanidin) that had the best interaction free energy; the Chalconaringenin and all the synthetic chalcones showed desirable interactions with the Mpro. The best interaction occurs with the C23 and the aminoacid residues GLU288 and ASP289; The Chalconaringenin and the indol chalcones C25 and C17 could interact with the SPIKE protein. Therefore, it can be seen that chalcones derivatives can be used as antiviral candidates according to the *in silico* studies. The chemical structures of these chalcones are shown in Figure 4.

Figure 4 – Chemical structures for some chalcones derivatives.



Chalconaringenin

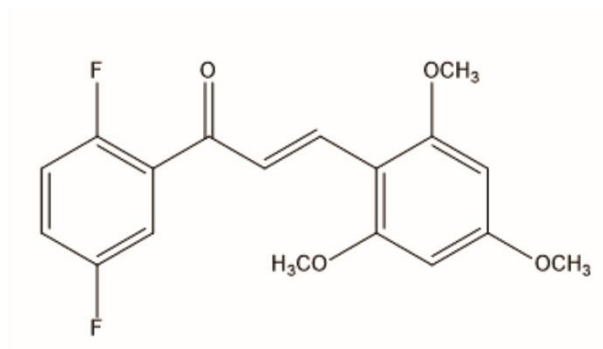


- C4. R = 4-Cl-C<sub>6</sub>H<sub>5</sub>
- C8. R = 4-OH-C<sub>6</sub>H<sub>5</sub>
- C12. R = 3,4-OCH<sub>3</sub>-C<sub>6</sub>H<sub>5</sub>
- C16. R = 4-OH-4-C<sub>6</sub>H<sub>5</sub>-piperazine
- C17. R = 1-C<sub>6</sub>H<sub>5</sub>-imidazole
- C20. R = 2-thiophenyl
- C22. R = 1,3-benzodioxole
- C23. R = 2-naphthyl
- C25. R = cyclohexyl

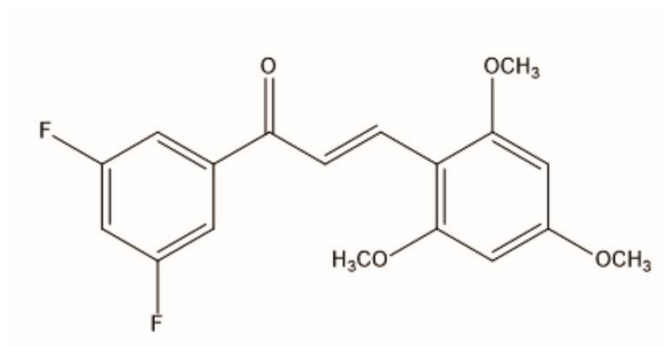
Source: Author himself

Duran *et al.* [45] studied eight new synthesized chalcones derivatives which were expected to have anti-SARS-CoV-2 activity. The authors used the Molecular Docking method with three target proteins: the RNA-dependent RNA polymerase, the Main protease (Mpro), and the SPIKE protein. The results of this works show that the chalcone derivative (E)-1-(2,5-Difluorophenyl)-3-(2,4,6-trimethoxyphenyl)prop-2-en-1-one exhibited interaction energy of -4.370 kcal/mol with the RNA-dependent RNA polymerase, interacting with the aminoacids residues SER814 (hydrogen bond) and ASP760, ASP761, and ASP618 (negatively charged interaction). The chalcone (E)-1-(2,5-Difluorophenyl)-3-(2,4,6-trimethoxyphenyl)prop-2-en-1-one demonstrated the best affinity in the molecular docking calculation with the Mpro with an interaction energy of -3.953 kcal/mol. This chalcone interacted with LYS5 by hydrogen bond, with LEU286 by hydrophobic interactions, and with ASP289 and GLU290 by negatively charged interaction. This chalcone was also the best candidate to interact with the SPIKE protein with interaction energy of -4.127 kcal/mol, and the interactions with the aminoacid residues ARG403 and GLY496 occurred by hydrogen bonds. The authors also discussed that the chalcones (E)-1-(2,5-Difluorophenyl)-3-(2,4,6-trimethoxyphenyl)prop-2-en-1-one, (E)-1-(3,5-Difluorophenyl)-3-(2,4,6-trimethoxyphenyl)prop-2-en-1-one, and (E)-1-(3,5-Bis(trifluoromethyl)phenyl)-3-(2,4,6-trimethoxyphenyl)prop-2-en-1-one showed the best antiviral activity among the eight that were tested. The authors concluded that the fluoro ligand in different positions enhanced the antiviral activity of the chalcone derivative. The molecular structure of the three chalcones derivates that exhibited best antiviral activity from the work of Duran *et al.* [45] are shown in Figure 5.

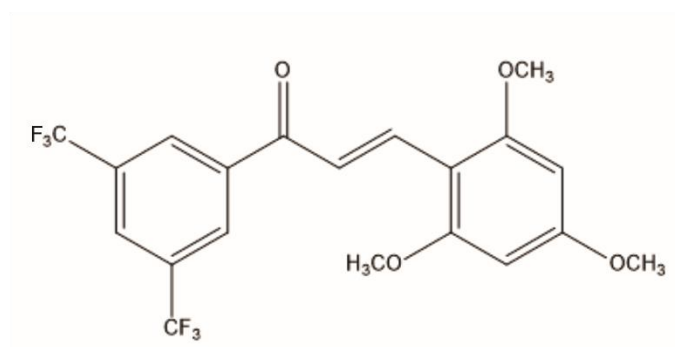
Figure 5 – Chalcone derivatives chemical structures.



(E)-1-(2,5-Difluorophenyl)-3-(2,4,6-trimethoxyphenyl)prop-2-en-1-one



(E)-1-(3,5-Difluorophenyl)-3-(2,4,6-trimethoxyphenyl)prop-2-en-1-one



(E)-1-(3,5-Bis(trifluoromethyl)phenyl)-3-(2,4,6-trimethoxyphenyl)prop-2-en-1-one

Source: Author himself

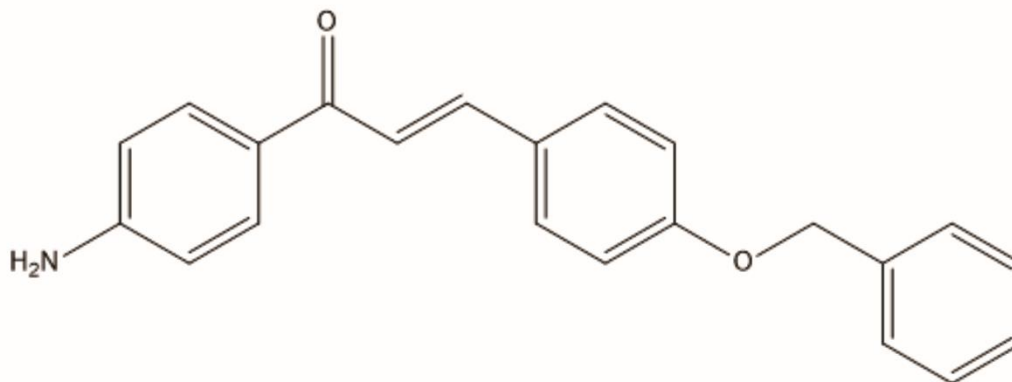
So far, it has been seen only studies that apply the Molecular Docking methodology. When the quantum calculation methodology is used, it is not possible to treat macromolecules such as the target proteins of SARS-CoV-2. However, since the molecule is a quantum entity, calculations using Density Functional Theory methodology can provide more accurate information about how interactions with target proteins occur, for example, if there is any



structural specificity of a series of candidate molecules that enhance antiviral activity. It was seen in the work by Duran *et al.* [45] that the authors proposed that the addition of fluorine groups (either the fluorine atom or the trifluoromethyl group) increase the anti-SARS-CoV-2 activity. If the authors had done quantum calculations based on the DFT, it would be possible to begin to understand the relationship between electron density withdrawn-groups and antiviral activity.

Clara *et al.* [46] used both DFT and Molecular Docking methodology to study the anti-SARS-CoV-2 properties of the chalcone derivative named (E)-1-(4-aminophenyl)-3-(4-benzyloxyphenyl)-prop-2-en-1-one (Figure 6). In this work, the chalcone derivative was geometrically optimized using the B3LYP/6-31++G(d,p) computational level in the gas phase. From the optimized structure, the full theoretical characterization was carried out: the spectroscopy analysis (vibrational,  $^1\text{H}$  and  $^{13}\text{C}$  NMR, and UV-Vis), electronic properties, thermodynamic properties, and charge analysis. Next, the Molecular Docking was done with the 6LU7 COVID-19 protein, and the interaction was compared with the FDA-approved drug against Covid-19, the ritonavir molecule. The authors showed that even the chalcone has a higher electrophilic character, the main interactions with the 6LU7 COVID-19 protein occur due to the hydrogen bonds with the aminoacids residues GLU16, ALA2, VAL3, and LEU4. The authors also found out that the chalcone can bind more effectively with the SARS-CoV-2 protein when compared to the ritonavir molecule. Therefore, it can be seen that chalcones derivatives have potential antiviral activity against the new coronavirus (SARS-CoV-2). This theoretical research is only the first step of the complete study to develop a new drug. However, it has extreme importance since it can select only the most probable candidates due to its theoretical interaction energy (Molecular Docking), and it can be proposed some relation between the molecular structure and the molecular properties to understand the chemical interactions between the chalcone and the target protein.

Figure 6 – The chemical structure of the chalcone (E)-1-(4-aminophenyl)-3-(4-benzyloxyphenyl)-prop-2-en-1-one.



(E)-1-(4-aminophenyl)-3-(4-benzyloxyphenyl)-prop-2-en-1-one

Source: Author himself

From the chalcone biological applications, it can be highlighted another important use for this class of molecules, which is the antioxidant activity. There are several recent works from the literature [47-55] concerning the antioxidant activity of chalcone derivatives. The chalcones, both natural and synthetic, have been shown excellent radical scavenging potential. The molecules 2,3,4,6-tetrahydroxy-chalcone and 2',4',3,4-tetrahydroxy-chalcone showed higher antioxidant [47] activity than the reference compounds vitamin C [56] and  $\alpha$ -tocopherol [57]. Hence, it has been seen that the presence of the hydroxyl group can increase the radical scavenging potential of a chalcone molecule [47,58].

In the work of Kostopoulou *et al.* [47], the authors synthesized fifteen derivatives from the 2'-hydroxy-chalcone, which has the hydroxyl group bonded to the ring A (phenol), to test the antioxidant activity of those chalcones. According to them, four of the fifteen molecules were synthesized for the first time. In the DPPH scavenging, the chalcones, which have the methoxy group and the alkoxymethyl protection group (-OMOM) bonded in ring B, demonstrated weak or inactive in the scavenging. However, the hydroxyl-chalcones “pure” (ring B) derivatives showed excellent results. The authors considering that the original 2'-hydroxyl group bonded in the ring A cannot react with the DPPH molecule since the existence of a strong hydrogen bond between this group and the oxygen atom from the carbonyl group. Hence, the other hydroxyl groups bonded in ring B can react with DPPH, and this enhances the

antioxidant activity. The authors also discussed that the presence of the bromine atom as a ligand can increase antioxidant activity. They showed that if they bond the bromine in position 5' (ring A), the lipid peroxidation inhibitory activity was improved about four times more when compared to the same molecule without the bromine atom. Therefore, the chalcones molecules can be excellent candidates for antioxidant molecules, which explains the reason to make more studies about this biological activity in this class of molecules, since it can be obtained several different compounds from a simple basic structure.

In the recent works of the literature, some chalcone derivatives were studied both experimental and theoretical to understand biological activities, such as antioxidant activity. In those works, the quantum chemical calculations were done using several computational levels: B3LYP/6-31+G(d,p)/LanL2DZ for Pd(II) complexes with chalcone as ligands [59]; B3LYP/6-311++G(d,p) for synthesized  $\beta$ -chalcones [60]; B3LYP using two bases set such as 6-311G(d,p) and 6-311++G(d,p) for the new chalcone derivative 1-(4-(benzylideneamino)phenyl)-3-(furan-2-yl)-prop-2-en-1-one [61]; TPSSh-D3/TZVP to obtain the optimized geometries, and the vertical and adiabatic energies of excitation for the triplet state to study the antioxidant activity against singlet oxygen [62]. Also, the quantum reactivity descriptors were computed to understand the relation between the biological activity and the chemical structure. For three of the four works, the antioxidant activity of the chalcone derivative was found to be low. However, in the work of Arif *et al.* [60], the  $\beta$ -chalcone achieve great results in the DPPH radical scavenge and Hydrogen peroxide scavenging, which show the structure-dependent of antioxidant activity. Therefore, it can be noticed that the chalcone derivatives showed low to high antioxidant activity, and it is important to understand how the structure can influence biological activity. This study can be done more easily using quantum calculations based on the Density Functional Theory method.

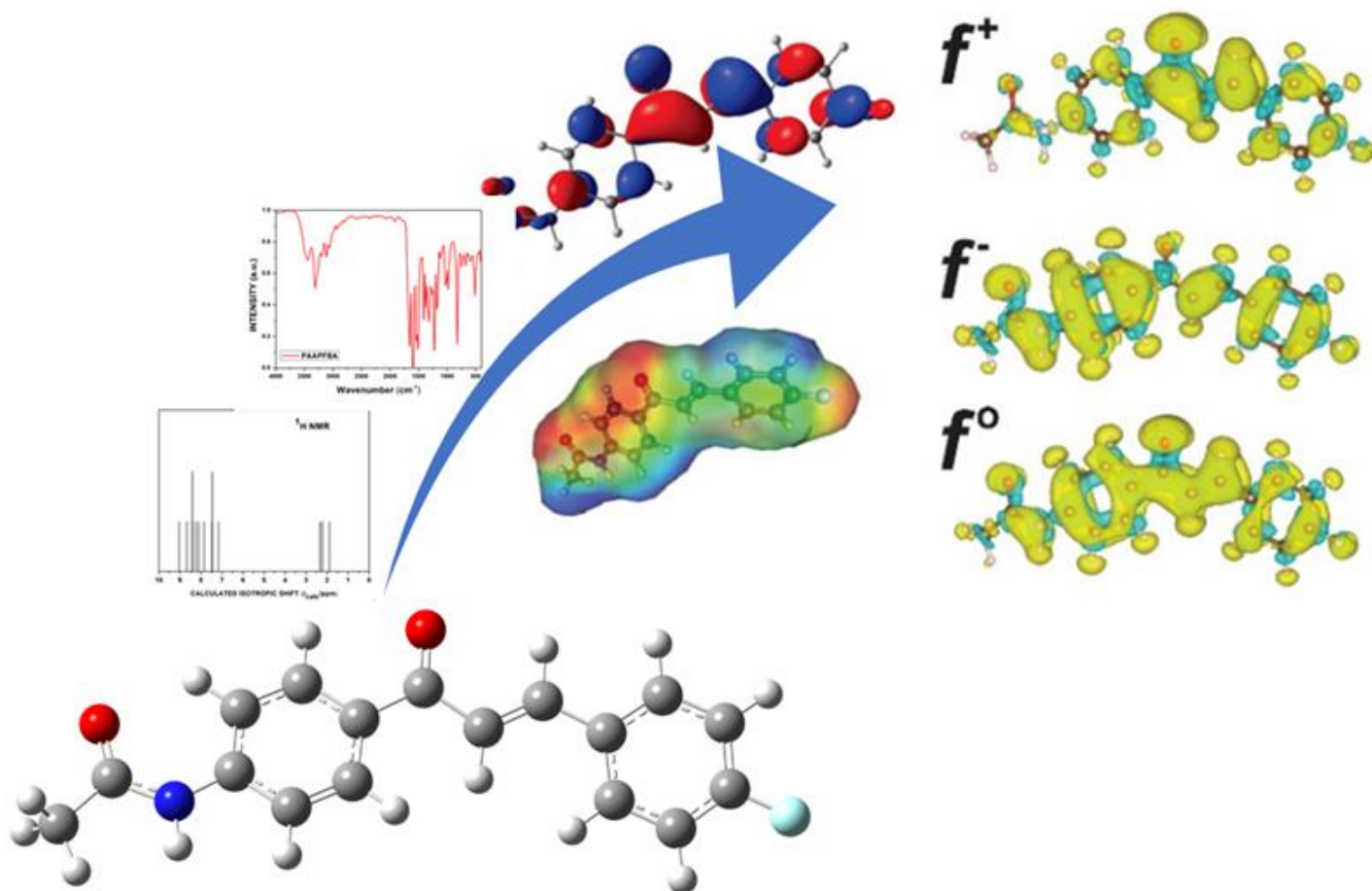
Therefore, after it has seen the importance of the chemistry of chalcones and the great relevance of at least two of its applications, as well as the growing interest in these two, this thesis aims to theoretically study a chalcone derivative making a complete characterization of its structural, electronic, spectroscopic properties and the theoretical study of two applications such as antiviral and antioxidant.

# Chapter 1

---

**Characterization of the structural, spectroscopic, nonlinear optical, electronic properties and antioxidant activity of the N-{4'-[(E)-3-(Fluorophenyl)-1-(phenyl)-prop-2-en-1-one]}-acetamide**

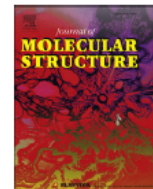
---





Contents lists available at ScienceDirect

## Journal of Molecular Structure

journal homepage: <http://www.elsevier.com/locate/molstruc>

## Characterization of the structural, spectroscopic, nonlinear optical, electronic properties and antioxidant activity of the N-{4'-[(E)-3-(Fluorophenyl)-1-(phenyl)-prop-2-en-1-one]}-acetamide

Francisco Wagner Q. Almeida-Neto <sup>a,\*</sup>, Leonardo P. da Silva <sup>a</sup>,  
 Maria Kueirislene A. Ferreira <sup>b</sup>, Francisco Rogênio S. Mendes <sup>e</sup>, Kevin K.A. de Castro <sup>d</sup>,  
 Paulo N. Bandeira <sup>c,d</sup>, Jane Eire S.A. de Menezes <sup>b</sup>, Hécio S. dos Santos <sup>d</sup>,  
 Norberto K.V. Monteiro <sup>a</sup>, Emmanuel S. Marinho <sup>e</sup>, Pedro de Lima-Neto <sup>a</sup>

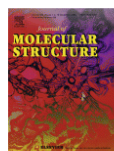
<sup>a</sup> Departamento de Química Analítica e Físico-Química, Universidade Federal do Ceará, Campus do Pici, bloco 940, 60440-900, Fortaleza, CE, Brazil

<sup>b</sup> Universidade Estadual do Ceará, Centro de Ciência e Tecnologia (CCT), Itaperi Campus, Laboratório de Química de Produtos Naturais - LQPN-S, Fortaleza, CE, Brazil

<sup>c</sup> Departamento de Química Biológica, Universidade Regional do Cariri, Crato, CE, Brazil

<sup>d</sup> Centro de Ciências Exatas e Tecnologia, Universidade Estadual do Vale do Acaraú, Sobral, CE, Brazil

<sup>e</sup> Faculdade de Filosofia Dom Aureliano Matos, Universidade Estadual do Ceará, Ceará, Brazil



Characterization of the structural, spectroscopic, nonlinear optical, electronic properties and antioxidant activity of the N-{4'-[(E)-3-(Fluorophenyl)-1-(phenyl)-prop-2-en-1-one]}-acetamide

Author: Francisco Wagner Q. Almeida-Neto, Leonardo P. da Silva, Maria Kueirislene A. Ferreira, Francisco Rogênio S. Mendes, Kevin K.A. de Castro, Paulo N. Bandeira, Jane Eire S.A. de Menezes, Hécio S. dos Santos, Norberto K.V. Monteiro, Emmanuel S. Marinho et al.

Publication: Journal of Molecular Structure

Publisher: Elsevier

Date: 15 November 2020

© 2020 Elsevier B.V. All rights reserved.

### Journal Author Rights

Please note that, as the author of this Elsevier article, you retain the right to include it in a thesis or dissertation, provided it is not published commercially. Permission is not required, but please ensure that you reference the journal as the original source. For more information on this and on your other retained rights, please visit: <https://www.elsevier.com/about/our-business/policies/copyright#Author-rights>

BACK

CLOSE WINDOW

## RESUMO

A molécula N- {4'-[(E)-3-(Fluorofenil)-1-(fenil)-prop-2-en-1-ona]} chalcona (PAAPFBA) foi recentemente sintetizada devido ao crescente interesse na química das chalconas. Os cálculos da química quântica foram realizados para fazer uma caracterização teórica completa (propriedades estruturais, espectroscópicas, ópticas não lineares e eletrônicas) empregando três métodos da Teoria do Funcional da Densidade (DFT) como B3LYP, mPW1PW91 e M06-2X com conjunto de base 6-311++G(d,p). Após todas essas caracterizações, a atividade antioxidante foi estudada utilizando a reação com o composto DPPH em solução de metanol e o mecanismo foi investigado teoricamente. Todos os três métodos de DFT usados podem descrever com grande precisão a chalcona PAAPFBA: os resultados da espectroscopia de infravermelho e da blindagem isotrópica de  $^1\text{H}$  e  $^{13}\text{C}$  demonstraram estar em excelente concordância com os dados experimentais. As propriedades ópticas não lineares (NLO) mostram que a chalcona de interesse desde trabalho pode ser usada com grande potencial em dispositivos óticos e este resultado está de acordo com a análise do Orbitais Naturais de Ligação, que mostra como a densidade eletrônica está deslocalizada por toda a molécula. Por fim, os dados experimentais da atividade antioxidante mostraram uma taxa moderada de reação com a molécula de DPPH (50,92%) e este fato está de acordo com o mecanismo teórico proposto sendo o de Transferência de Átomo de Hidrogênio como o mais favorável.

**Palavras-chave:** Energia de Dissociação de Ligação; Condensação aldólica de Claisen-Schmidt, Função de Fukui, Óptica não linear, Orbitais naturais de ligação.

### ABSTRACT

The molecule N-{4'-[(E)-3-(Fluorophenyl)-1-(phenyl)-prop-2-en-1-one]} chalcone (PAAPFBA) was recently synthesized due to the growing interest in the chemistry of the chalcone. The quantum chemical calculations were carried out to make a complete theoretical characterization (structural, spectroscopy, nonlinear optical, and electronic properties) employing three Density Functional Theory (DFT) methods like B3LYP, mPW1PW91, and M06-2X at 6-311++G(d,p) basis set. After all these characterizations, the antioxidant activity was studied using the reaction with the compound DPPH in methanol solution and the mechanism was investigated theoretically. All the three DFT methods used can describe with great accuracy the PAAPFBA chalcone: the results of infrared spectroscopy and the  $^1\text{H}$  and  $^{13}\text{C}$  isotropic shielding demonstrate to be in excellent agreement with the experimental data. The nonlinear optical (NLO) properties show that the title chalcone can be used with great potential in NLO devices and this result is in good agreement with the Natural Bond Orbital (NBO) analysis, which shows how the electronic density is delocalized within the molecule. Finally, the experimental data of the antioxidant activity showed a moderate rate of reaction with the DPPH molecule (50.92%) and this fact was proved by the theoretical mechanisms with the Hydrogen Atom Transfer (HAT) mechanism more favorable.

**Keywords:** Bond Dissociation Energy, Claisen-Schmidt aldol condensation, Fukui Function, Nonlinear Optical, Natural Bond Orbital.

## 1 INTRODUCTION

Chalcones are natural products considered as the most important subgroup of the flavonoid family. They are chemically characterized by the presence of an open chain with two phenyl rings bonded by  $\alpha,\beta$ -unsaturated carbonyl group (1,3-diphenyl-2-propen-1-ones). For the chalcones, there are two possible isomers, the E (trans) and Z (cis), being that E isomer occurs naturally and it is thermodynamically more stable [1]. The greatest interest in this class of compound lies in the fact that chalcones have many hydrogen atoms that can be replaced, thus generating the possibility of synthesis routes for several compounds with different possible applications. The chalcone can be used as anti-leishmanial, antibacterial, antimicrobial, immunosuppressive, antidepressant, anti-inflammatory, anti-obesity, hypnotic, and anti-cancer [1 – 11].

Despite these several applications, the chalcones exhibits antioxidant properties. Some examples about the great applicability of chalcone derivatives as antioxidants are given next. Arif *et al.* [12] studied the antioxidant properties of the 3-(1H-indol-3-yl)-1-p-tolylprop-2-en-1-one by DPPH radical scavenging and Hydrogen peroxide scavenging which demonstrated high antioxidant activity, Ustabas *et al.* [13] used the chalcone derivative 1-(4-(benzylideneamino)-phenyl-3-(furan-2-yl)prop-2-en-1-one as an antioxidant by the DPPH and FRAP methods which demonstrated low antioxidant activity, Uddin *et al.* [14] studied six chalcones derivatives of the 3-(4-methoxyphenyl)-prop-2-en-1-one by the total phenolic content which demonstrated good antioxidant properties, Polo *et al.* [15] studies several chalcone and bis-chalcone derivatives using sonication conditions during the synthesis and the antioxidant activity was investigated by DPPH radical scavenging and ABTS radical scavenging which demonstrated moderate antioxidant activity. Each chalcone's derivative has different values for antioxidant activity, which implies the importance of studying new derivatives in order to correlate the relationship between that antioxidant properties and the chemical structure of the chalcone's derivatives.

Given the huge and growing applicability and interest in the chemistry of chalcones, the new chalcone N-{4'-[(E)-3-(Fluorophenyl)-1-(phenyl)-prop-2-en-1-one]} acetamide (PAAPFBA) was recently experimentally synthesized by Ferreira *et al.* [16]. This derivate had the two hydrogens in the para position of the phenyl rings substituted respectively by the acetamido group in ring A and the fluorine atom in ring B. This chalcone showed an excellent result of nontoxicity and great potential for the treatment of anxiety induced by alcohol withdrawal.



Currently, it is widely known that the computational quantum chemical calculations are an important tool to study the structural, electronic, optical properties, spectroscopy characterization, and predict how the molecule behaves during a chemical reaction in different media. Hegde *et al.* [7] studied theoretically the chalcone derivative 3-(2-methoxynaphthalen-1-yl)-1-(thiophen-2-yl)-prop-2-en-1-one at DFT/B3LYP/6-311++G(d,p) to obtain the geometrical optimization, the infrared characterization, the electronic properties, and the excited states for the UV-Vis spectroscopy. Ramesh *et al.* [17] studied the 1-(3-Bromo-2-thienyl)-3-[4-(dimethylamino)-phenyl]-prop-2-en-1-one chalcone at DFT/B3LYP/6-311++G(d,p) to compute the geometrical optimization, the vibrational frequencies, the frontier molecular orbitals, the excited states (UV-Vis spectrum), the molecular electrostatic potential, and the Fukui functions. Thamarai *et al.* [18] studied the (2E)-1-(3-bromo-2-thienyl)-3-(4-chlorophenyl)-prop-2-en-1-one at B3LYP/B3PW91/M06-2 using the 6-311++G(d,p) basis set to calculate the optimize molecular structure, the vibrational frequencies, the excited states, the electronic properties, the molecular electrostatic potential, the Natural Bond Orbital (NBO) analysis, and the thermodynamics properties. Chaouiki *et al.* [19] studied several chalcones derivatives using DFT/B3LYP method at 6-311++G(d,p) basis set to determine the geometrical optimization, the frontier molecular orbitals, and the quantum molecular descriptors. Therefore, the importance of using the Density Functional Theory (DFT) method in the study of new chalcones derivatives is demonstrated with these examples of recent works.

There are also several recent theoretical researches about the fact that chalcones can also be used in optoelectronic devices and photochemical applications due to its  $\pi$ -electrons delocalization and the  $\pi$  molecular orbitals overlapping. Their optical properties can be controlled by donor or acceptor groups bonded in the two phenyl rings [7, 20, 21]. These are some examples of theoretical researches about the optical properties of the chalcones derivatives: Custodio *et al.* [22] studied the chalcone (E)-3-(2-bromophenyl)-1-[(2-phenylsulfonylamine)]-phenyl]-prop-2-en-1-one at DFT/CAM-B3LYP/6-311++G(d,p) level, Kaya *et al.* [23] studied the derivate (E)-1-(3-hydroxyphenyl)-3-(2,4,6-trimethoxyphenyl)-prop-2-en-1-one at DFT/B3LYP/6-311++G(d,p) level, Shukla *et al.* [24] studied the 1-(4-chlorophenyl)-3-(5-methylfuran-2-yl)-prop-2-en-1-one chalcone derivative at DFT/B3LYP/6-311++G(d,p) level. All authors concluded that the chalcone derivatives studied were excellent candidates for use in optical devices, which implies increasing importance in the chemistry of chalcones for optics in addition to biological applications.

In this work, the PAAPFBA chalcone was synthesized and characterized it by infrared

spectroscopy,  $^1\text{H}$  and  $^{13}\text{C}$  spectroscopy and investigated its antioxidant potential. The main objective of this work was to use quantum chemical calculations based on the Density Functional Theory (DFT) at the ground state to understand the structural, nonlinear optical, electronic properties and the antioxidant mechanism using three different DFT methods (B3LYP, mPW1PW91, and M06-2X).

## 2 Theoretical procedures

The quantum chemical calculations were done to characterize the chemical structure, electronic, reactivity, non-linear optical properties, and the antioxidant activity of the chalcone PAAPFBA and to simulate their vibrational and magnetic resonance spectra. The geometrical optimization was carried out using the Becke's three-parameter hybrid functional [25] with the Lee-Yang-Parr correlation functional [26] (B3LYP), the Perdew Wang exchange-correlation functional [27] adjusted by Adamo and Barone [28] (mPW1PW91), and the Minnesota 06 hybrid meta exchange-correlation functional [29] (M06-2X) with the Gaussian basis set 6-311++G(d,p) in Gaussian 09 program package [30] and GaussView 5.0.8 [31] to draw the input molecules. The optimization calculations were executed using the Polarizable Continuum Model [32 – 33] with the Integral Equation Formalism [34] (IEF-PCM) for the solvation method with methanol as an implicit solvent to simulate the chemical environment of the experimental application for the antioxidant activity of the PAAPFBA molecule. The thermodynamics data were obtained using the same levels of theory at temperature 298.15 K under 1 atm pressure using methanol as an implicit solvent. The vibrational frequency calculations were done using the three ground state optimized geometries to guarantee the structures were in a global minimum of energy. The calculated vibrational frequencies were multiplied by the following scaling factors: 0.967 for the B3LYP, 0.957 for the mPW1PW91, and 0.955 for the M06-2X at the 6-311++G(d,p) levels of theory. The infrared vibrational assignments were made based on the Potential Energy Distribution (PED) using the VEDA 4 [35] and, only the  $\text{PED} \geq 10\%$  were used to perform the final assignment of the molecular vibration.

The  $^1\text{H}$  and  $^{13}\text{C}$  NMR isotropic chemical shift were calculated using Gauge Independent Atomic Orbitals (GIAO) [36 – 39] proposal available in Gaussian. The correlation between the theoretical and the experimental data was made by the comparison of the theoretical shielding constant of both hydrogens ( $\sigma_{\text{H}(\text{calc})}$ ) and carbons ( $\sigma_{\text{C}(\text{calc})}$ ) atoms to the calculated shielding constant ( $\sigma_{\text{H}(\text{TMS})}$  and  $\sigma_{\text{C}(\text{TMS})}$ ) for the same elements presents in the reference compound tetramethylsilane (TMS) following the rule:  $\delta_{\text{C}} = \sigma_{\text{H}(\text{TMS})} - \sigma_{\text{H}(\text{calc})}$  and  $\delta_{\text{C}} = \sigma_{\text{C}(\text{TMS})} - \sigma_{\text{C}(\text{calc})}$ .

The Non-linear optical (NLO) calculations, such as the dipole moment ( $\mu$ ), the polarizabilities ( $\alpha$ ), and the first order hyperpolarizabilities ( $\beta$ ) at the static state were calculated at the same levels of theory. For comparison to the standard methodology available in the literature, the NLO properties were also computed at CAM-B3LYP [40], LC-BLYP [41], and  $\omega$ B97XD [42] with 6-311++G(d,p) levels of theory with methanol as an implicit solvent. These three DFT methods belong to a short (CAM-B3LYP) [43,44] and long (LC-BLYP and  $\omega$ B97XD) [44,45] range separated hybrid functional. The CAM-B3LYP shows a correct 0.65 fraction of nonlocal exchange at asymptotic distance [43,46]. The LC-BLYP and the  $\omega$ B97XD show a correct 1.00 fraction of nonlocal exchange [44,47].

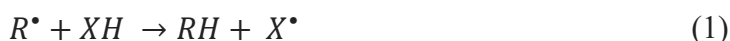
The Frontier Molecular Orbitals (FMO) energies ( $E_{HOMO}$  and  $E_{LUMO}$ ) and the global electronic properties called quantum chemical descriptors such as the energy gap ( $\Delta E_{gap}$ ), ionization potential (I), electron affinity (A), electronegativity ( $\chi$ ), global hardness ( $\eta$ ), global softness (S), electrophilicity ( $\omega$ ), and nucleophilicity ( $\epsilon$ ) using the B3LYP, mPW1PW91 and M06-2X at the 6-311++G(d,p) levels of theory.

To understand the chemical behavior of each atom, the Electronic Fukui functions were calculated from the electronic density and the Condensed Fukui functions were computed from the Hirshfeld charge population using the anionic, cationic and the radical species of the PAAPFBA molecule. Therefore, the local electronic properties such as the local hardness ( $\eta_k$ ), local softness ( $s_k$ ), philicity index ( $\omega_k$ ), dual descriptor ( $\Delta f$ ), and multiphilic index ( $\Delta\omega$ ) were estimated at the same levels of theory. The Molecular Electrostatic Potential (MEP) surface was computed using the Gabedit 2.5.0 software [48] for the PAAPFBA molecule to complement the investigation about the possibility of the electrophilic or nucleophilic reactive attack sites.

The Natural Bond Orbital (NBO) analysis was carried out by B3LYP, mPW1PW91 and M06-2X at 6-311++G(d,p) basis set to investigate the delocalization of the electron density within the title molecule using the NBO 3.1 program [49] implement in Gaussian.

To understand the antioxidant activity of the title chalcone, there are in the literature three mechanisms proposed to this analysis [50 – 54]. The Hydrogen Atom Transfer (HAT) mechanism occurs when a free radical ( $R^\bullet$ ) extract a hydrogen atom from the antioxidant molecule. The global process is shown in the equation (1). The second mechanism is called Single Electron Transfer-Proton Transfer (SET-PT) and it occurs when an electron is removed from the antioxidant and the following step is a proton transfer (equations 2a and 2b). The third mechanism is the Sequential Proton Loss Electron Transfer (SPLET) and it occurs when the proton is lost and followed by the transfer of an electron (equations 3a and 3b). All these

mechanisms can occur simultaneously, but with different rates [50 – 54].



In the HAT mechanism, the tendency of the reaction takes place can be predicted by the Bond Dissociation Energy (BDE) of the X – H chemical bond (X = C or N in this work). The lower the BDE value the higher is the reactivity of the antioxidant [50]. In the SET-PT mechanism, the reactivity is described by the Ionization Potential (IP) and the Proton Dissociation Enthalpy (PDE) from the antioxidant cation radical ( $RH^{+\bullet}$ ) species. Molecules with lower values of the IP and PDE are expected to be more reactive [50]. In the SPLET mechanism, the propensity to react is computed by the Proton Affinity (PA) of the anionic species of the antioxidant molecule ( $X^{-}$ ) and the Electron Transfer Enthalpy (ETE) which corresponds to the removal of the electron. The reactivity is measure by the lower values of the PA and ETE quantities. The mathematical expressions for those quantities are shown respectively in equations 4 – 8. The geometrical optimization of the cation radical, the radical and the anionic species were carried out using the DFT methods B3LYP/mPW1PW91/M06-2X at 6-311++G(d,p) levels of theory with methanol as implicit solvent (IEF-PCM model). All those enthalpies were calculated at 298.15 K and 1 atm of pressure. The values of the H-atom, proton and electron solvation enthalpies in methanol were taken from the work of Rimarčík *et al.* [51].

$$BDE = H(X^{\bullet}) + H(H^{\bullet}) - H(XH) \quad (4)$$

$$IP = H(X^{+\bullet}) + H(e^{-}) - H(XH) \quad (5)$$

$$PDE = H(X^{\bullet}) + H(H^{+}) - H(X^{+\bullet}) \quad (6)$$

$$PA = H(X^{-}) + H(H^{+}) - H(XH) \quad (7)$$

$$ETE = H(X^{\bullet}) + H(e^{-}) - H(X^{-}) \quad (8)$$

### 3 Experimental details

#### 3.1 Synthesis of the PAAPFBA chalcone

The title chalcone was synthesized according to the methodology proposed by Ferreira *et al.* [16]. The first step consisted in the reaction between p-Aminoacetophenone and p-Fluorobenzaldehyde by the Claisen-Schmidt aldol condensation in basic medium. The second step was the reaction with the acetic anhydride in acetic acid/sodium acetate medium at pH 4.5 under magnetic stirring at room temperature [16].

#### 3.2 Fourier transform infrared spectroscopy (FT-IR)

The sample 2 mg chalcone PAAPFBA was powdered and mixed with 200 mg of KBr, which then was pressed pellets and analysis in spectrophotometer model IRTracer-100 Shimadzu (Kyoto, Japan). The pellet was scanned, and spectra was recorded by summing 64 scans at a spectral range from 4000 to 400  $\text{cm}^{-1}$  and a resolution of 4  $\text{cm}^{-1}$  [21].

#### 3.3 DPPH Free Radical Scan

A methanol solution of DPPH was added to the methanolic solutions of the samples of chalcone (10 to 10.000  $\mu\text{g}/\text{mL}$ ). The test was performed in triplicate. After the 60-minute interval, absorbance was measured in a UV-Vis spectrophotometer at 515 nm. The antioxidant capacity was compared with a standard ascorbic acid curve and  $\text{EC}_{50}$  was determined. The control (-) was methanol and DPPH and the control (+) was done by adding standard solution (Ascorbic acid) and DPPH. In the procedure, 1 mL of the DPPH solution at a concentration of 23.7  $\mu\text{g} / \text{mL}$  was added to each concentration of the samples [55].

## 4 Results and Discussion

#### 4.1 Geometrical Optimization and Thermodynamic properties

The theoretically forecasted optimized geometries for the PAAPFBA molecule using the B3LYP/6-311++G(d,p), mPW1PW91/6-311++G(d,p) and M06-2X/6-311++G(d,p) methods are shown in Fig. 1. The optimized geometries for the three computational methods were achieved by accepting the C1 point group symmetry.

The PAAPFBA molecule exhibited seventeen C-C bonds, thirteen C-H bonds, two C-O and C-N bonds and single N-H and C-F bonds. The PAAPFBA structure can be derived from an  $\alpha, \beta$ -unsaturated carbonyl group which means a  $\pi$ -bond between the  $\alpha$  and  $\beta$  carbons

closer to a ketone group ( $R_1 - C = C - CO - R_2$ ). Therefore, when  $R_1$  is equal to the 4-fluorophenyl group and  $R_2$  is equal to the 4-acetamido-phenyl group, thus the PAAPFBA structure is formulated. The C19-C20, C20=C22, C20-H23, C22-H25 and C19=O21 bonds lengths from the  $\alpha, \beta$ -unsaturated carbonyl group are respectively 1.47960 Å, 1.34736 Å, 1.08111 Å, 1.08703 Å and 1.23322 Å (B3LYP); 1.47459 Å, 1.34377 Å, 1.08123 Å, 1.08714 Å and 1.22733 Å (mPW1PW91); 1.48436 Å, 1.33991 Å, 1.08184 Å, 1.08760 Å and 1.22110 Å (M06-2X). The three DFT methods describe the molecule in a remarkably similar way, in which the highest difference between the bond length is about 0.009772 Å between mPW1PW91 and M06-2X methods concerning the C19-C20 bond. The C20-H23 bond length predicted by the DFT methods are almost the same value 1.08111 Å (B3LYP), 1.08123 Å (mPW1PW91) and 1.08184 Å (M06-2X). Wu *et al.* [56], Cai *et al.* [57], and Prabuswamy *et al.* [58] studied, by crystallographic methods, the following chalcone derivatives: 1-Phenyl-3-(2,4,6-trimethoxyphenyl)-prop-2-en-1-one [56], (E)-1-(4-Methoxyphenyl)-3-(2,4,6-trimethoxyphenyl)-prop-2-en-1-one [57], and 1-(2-Fluorophenyl)-3-(2,4,6-trimethoxyphenyl)-prop-2-en-1-one [58], respectively, which have similar structure (the  $\alpha, \beta$ -unsaturated carbonyl group and the two phenyl rings) to the molecule investigated in this work the PAAPFBA chalcone. Hence, the values of the bonds obtained from the experimental data in the work of Wu *et al.* [56], Cai *et al.* [57], and Prabuswamy *et al.* [58] are respectively C-C (1.4611 Å, 1.4703 Å, 1.4510 Å), C=C (1.3317 Å, 1.3435 Å, 1.3450 Å), C-H (0.93 Å, 0.95 Å, 0.93 Å) and C=O (1.2244 Å, 1.2275 Å, 1.2251 Å). These experimental results are in a good agreement with the theoretical values computed from this work for the PAAPFBA chalcone.

The plane derivate by the  $\alpha, \beta$ -unsaturated carbonyl group is the C19-C20-C22-C24 angle, and then its value is 179.66871° (B3LYP), 179.58072° (mPW1PW91), and 179.26608° (M06-2X). Therefore, the molecule is not planar due to the torsion angle C4-C19-C20-C22 (176.87920° for B3LYP, 176.55675 for mPW1PW91, and 172.20156° for M06-2X) differ from the angle present in the  $\alpha, \beta$ -unsaturated carbonyl group mainly for the M06-2X method that showed the highest difference from the torsion angle (7.06452°), and it has the most deviation from the planarity. The plane distortion can also be illustrated by the angles C4-C5-C19-C20 (9.90162° for B3LYP, 10.40151° for mPW1PW91, and 18.08884° for M06-2X) and C20-C22-C24-C26 (0.03126° for B3LYP, 0.34113° for mPW1PW91, and 1.36783° for M06-2X). The M06-2X method predicted about 8.18722° more than B3LYP and 7.68733° more than mPW1PW91 method in the plane defined by the 4-acetamido-phenyl group and about 1.05523° more than B3LYP and 1.0267° more than mPW1PW91 method in-plane delimited by the 4-fluoro-phenyl group.

The two phenyl rings have the value of the C-C bonds within the expected range of 1.33 Å (double bond) to 1.54 Å (single bond) as is shown as following: C1-C2 (1.40524 Å for B3LYP, 1.40108 Å for mPW1PW91, and 1.40189 Å for M06-2X); C1-C3 (1.38707 Å for B3LYP, 1.38317 Å for mPW1PW91, and 1.38631 Å for M06-2X); C3-C4 (1.40323 Å for B3LYP, 1.39835 Å for mPW1PW91, and 1.39655 Å for M06-2X); C4-C5 (1.40482 Å for B3LYP, 1.39987 Å for mPW1PW91, and 1.39897 Å for M06-2X); C5-C6 (1.38583 Å for B3LYP, 1.38190 Å for mPW1PW91, and 1.38346 Å for M06-2X), C6-C2 (1.40437 Å for B3LYP, 1.40033 Å for mPW1PW91, and 1.40123 Å for M06-2X); C24-C26 (1.40835 Å for B3LYP, 1.40342 Å for mPW1PW91, and 1.40238 Å for M06-2X); C24-C27 (1.40649 Å for B3LYP, 1.40156 Å for mPW1PW91, and 1.40023 Å for M06-2X); C26-C28 (1.38785 Å for B3LYP, 1.38366 Å for mPW1PW91, and 1.38567 Å for M06-2X); C27-C29 (1.39135 Å for B3LYP, 1.38714 Å for mPW1PW91, and 1.38940 Å for M06-2X); C28-C30 (1.38911 Å for B3LYP, 1.38592 Å for mPW1PW91, and 1.38655 Å for M06-2X), C29-C30 (1.38477 Å for B3LYP, 1.38167 Å for mPW1PW91, and 1.38204 Å for M06-2X). These values of bonds length are in good agreement with the experimental data obtained from the work of Wu *et al.* [56], Cai *et al.* [57], and Prabuswamy *et al.* [58] with the chalcone derivatives 1-Phenyl-3-(2,4,6-trimethoxyphenyl)-prop-2-en-1-one [56], (E)-1-(4-Methoxyphenyl)-3-(2,4,6-trimethoxyphenyl)-prop-2-en-1-one [57], and 1-(2-Fluorophenyl)-3-(2,4,6-trimethoxyphenyl)-prop-2-en-1-one [58] respectively.

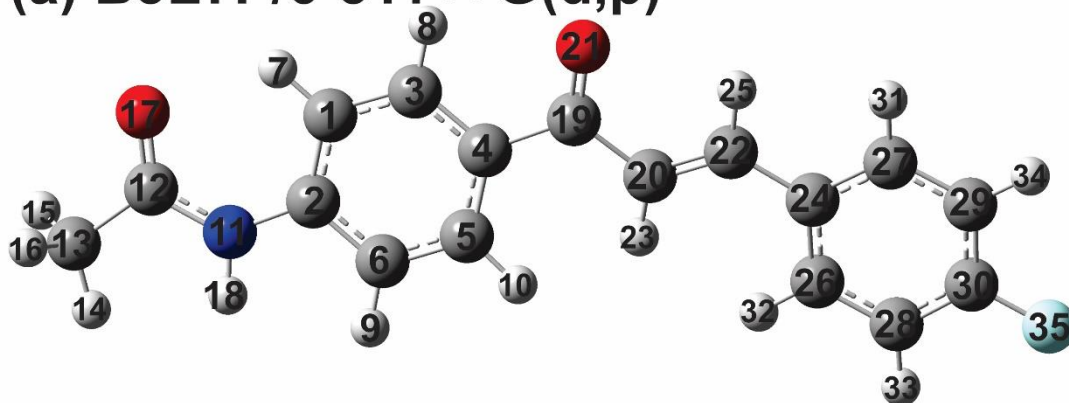
The C30-F35 bond demonstrated to have about the same value even with the change of DFT method: 1.35827 Å (B3LYP), 1.34565 Å (mPW1PW91), and 1.34612 Å (M06-2X). In the Prabuswamy *et al.* [58] work for the chalcone 1-(2-Fluorophenyl)-3-(2,4,6-trimethoxyphenyl)-prop-2-en-1-one, the experimental bond value of the C<sub>ring</sub>-F is about 1.3624 Å, which demonstrate agreement between these calculations and the experimental data. The two carbonyl groups showed the bond angle C13-C12-N11 (114.82525° for B3LYP, 114.72895° for mPW1PW91, and 114.03896° for M06-2X) and C4-C19-C20 (118.88284° for B3LYP, 118.75276° for mPW1PW91, and 118.40760° for M06-2X) expected approximated values to this functional group due to the double bond between carbons and oxygen atoms. This comparison between theoretical bond lengths and experimental data show that the used DFT methods can describe the PAAPFBA molecule satisfactorily. The results displayed in this work also show an excellent agreement in respect to the recent DFT calculations using similar structures in the works of Ramesh *et al.* [17] with the chalcone 1-(3-Bromo-2-thienyl)-3-[4-(dimethylamino)-phenyl]-prop-2-en-1-one at B3LYP/6-311++G(d,p), Thamarai *et al.* [18] with the chalcone (2E)-1-(3-bromo-2-thienyl)-3-(4-chlorophenyl)-prop-2-en-1-one at

B3LYP/B3PW91/M06-2X/6-311++G(d,p), Kaya *et al.* [23] with the chalcone (E)-1-(3-hydroxyphenyl)-3-(2,4,6-trimethoxyphenyl)-prop-2-en-1-one at DFT/B3LYP/6-311++G(d,p) and Shukla *et al.* [24] with the chalcone 1-(4-chlorophenyl)-3-(5-methylfuran-2-yl)-prop-2-en-1-one at DFT/B3LYP/6-311++G(d,p) level.

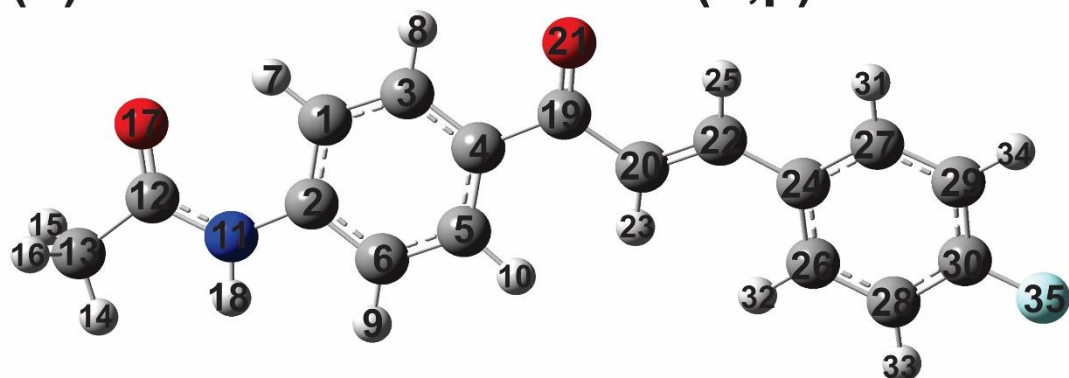
The thermodynamic data were obtained from the DFT methods (B3LYP, mPW1PW91, and M06-2X) at 6-311++G(d,p) basis set ( $T = 298.15$  K and  $P = 1$  atm). The Electronic energies ( $E_0$ ) of the most stable geometry in each method of PAAPFBA molecule are  $-961.57631892$  Hartree (B3LYP),  $-961.32942329$  Hartree (mPW1PW91), and  $-961.18171855$  Hartree (M06-2X). The zero-point vibrational energy ( $E_{ZPVE}$ ) calculated to the PAAPFBA molecule is  $169.41171$  kcal.mol<sup>-1</sup> (B3LYP),  $171.01311$  kcal.mol<sup>-1</sup> (mPW1PW91), and  $171.16780$  kcal.mol<sup>-1</sup> (M06-2X). These values for the ZPVE are similar, in which the B3LYP method describes a slightly more stable molecule. The zero-point correction, the thermal correction to the internal energy, the thermal correction to the enthalpy and the thermal correction to the Gibbs Free Energy are respectively  $0.269975$ ,  $0.288811$ ,  $0.289755$ ,  $0.219008$  Hartree/particle (B3LYP);  $0.272527$ ,  $0.291261$ ,  $0.292205$ ,  $0.221810$  Hartree/particle (mPW1PW91);  $0.272773$ ,  $0.291615$ ,  $0.292559$ ,  $0.221334$  Hartree/particle (M06-2X). Therefore, it can be possible to compute the thermodynamic properties: the Internal Energy (U), the Enthalpy (H), the Entropy and the Gibbs Free Energy (G) are respectively  $-961.287508$ ,  $-961.286564$ ,  $0.000237480068$ ,  $-961.357311$  Hartree (B3LYP);  $-961.038162$ ,  $-961.037218$ ,  $0.0002362982456$ ,  $-961.107613$  Hartree (mPW1PW91);  $-960.890103$ ,  $-960.889159$ ,  $0.0002390845295$ ,  $-960.960384$  Hartree (M06-2X). The Heat Capacity ( $C_v$ ) at constant volume was also calculated and its values are  $70.602$  cal.mol<sup>-1</sup>K<sup>-1</sup> (B3LYP),  $70.118$  cal.mol<sup>-1</sup>K<sup>-1</sup> (mPW1PW91),  $70.185$  cal.mol<sup>-1</sup>K<sup>-1</sup> (M06-2X). Finally, the rotation constants were calculated as  $1.15767$ ,  $0.08097$  and  $0.07579$  GHz (B3LYP);  $1.17178$ ,  $0.08161$  and  $0.07642$  GHz (mPW1PW91);  $1.14841$ ,  $0.08182$  and  $0.07669$  GHz (M06-2X). Therefore, the three DFT methods can be used to characterize geometrically the PAAPFBA chalcone.



(a) B3LYP/6-311++G(d,p)



(b) mPW1PW91/6-311++G(d,p)



(c) M06-2X/6-311++G(d,p)

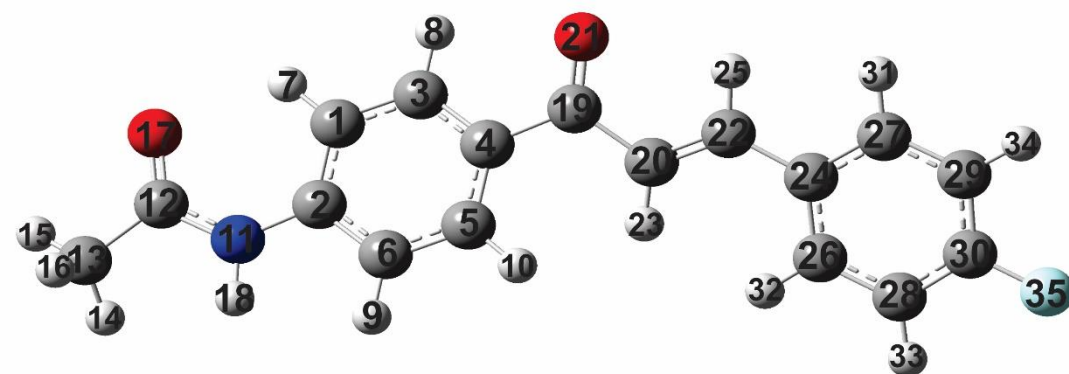


**Fig. 1** – Optimized geometries of the PAAPFBA chalcone using (a) B3LYP, (b) mPW1PW91 and (c) M06-2X at 6-311++G(d,p) levels of theory.

#### 4.2 Structural spectroscopic analysis

The theoretical FT-IR vibrational spectra were obtained from the DFT methods (B3LYP/mPW1PW91/M06-2X) at 6-311++G(d,p) computational level and they are shown in

Fig. S1 (supplementary material) together with the experimental FT-IR vibrational spectrum. The absence of negative frequencies shows that the simulated molecule is in a truly global minimum of energy for each functional. The PAAPFBA molecule is composed of 35 atoms which corresponds to a total of 99 fundamental vibrations modes ( $3N - 6$ ). The theoretical results were scaled by 0.967 (B3LYP), 0.957 (mPW1PW91), and 0.955 (M06-2X). The Potential Energy Distributions (PED) were calculated and only the results with  $\text{PED} \geq 10\%$  were computed in the vibrational assignments. To compare the theoretical data with the experimental wavenumbers, the linear fitting (Fig. 2) was made and the values of the R-squared ( $R^2$ ) are respectively 0.99791 (B3LYP), 0.99779 (mPW1PW91), and 0.99835 (M06-2X) with the linear equation respectively  $y = 1.01316x - 8.24579$  (B3LYP),  $y = 1.01385x - 6.6005$  (mPW1PW91), and  $y = 1.01408x - 10.97107$  (M06-2X). The calculated vibrational frequencies are in excellent agreement with the experimental data and all the functionals used describe accurately the PAAPFBA molecule. In Fig. S1 (supplementary material), all the Infrared intensities for both theoretical and experimental were normalized assuming the most intense peak one and the others were determined from this. The following discussion was made using only the principal vibrational modes. To see more details about all the theoretical assignments of the vibrational modes, present in the PAAPFBA molecule, they were computed in Tables S1 – S3 (supplementary material).

The strong polar bond between the nitrogen and hydrogen (N11 – H10) atoms showed a theoretical vibrational stretching at  $3609.18 \text{ cm}^{-1}$  (B3LYP),  $3651.90 \text{ cm}^{-1}$  (mPW1PW91) and  $3634.42 \text{ cm}^{-1}$  (M06-2X) against  $3437.15 \text{ cm}^{-1}$  from the experimental data with PED of 100% for each DFT method. There are differences of almost  $200 \text{ cm}^{-1}$  at the theoretical to the experimental data. Therefore, the scaling factor exhibits an important correction role: the calculated frequencies change to  $3490.08 \text{ cm}^{-1}$ ,  $3494.87 \text{ cm}^{-1}$  and  $3470.87 \text{ cm}^{-1}$  respectively with an appropriate scale factor to the DFT method. Another strong polar bond between the fluorine and carbon atoms (F35 – C30) showed IR frequencies at  $1220.91 \text{ cm}^{-1}$  (B3LYP),  $771 \text{ cm}^{-1}$  (mPW1PW91) and  $1276.98 \text{ cm}^{-1}$  (M06-2X) with PED respectively 22%, 14% and 41%.

The well-known carbonyl ( $C = O$ ) stretching were assignment at  $1711.73 \text{ cm}^{-1}$  (O17 – C12) and  $1591.41 \text{ cm}^{-1}$  (O21 – C19) for B3LYP,  $1750.20 \text{ cm}^{-1}$  (O17 – C12) and  $1723.61 \text{ cm}^{-1}$  (O21 – C19) for mPW1PW91, and  $1776.21 \text{ cm}^{-1}$  (O17 – C12) and  $1756.69 \text{ cm}^{-1}$  (O21 – C19) for M06-2X with PED respectively 73%, 41%, 76%, 44%, 78% and 60%. These results show the reason why this band is so important to characterize the carbonyl compounds since the stretching mode is responsible for most of the potential vibrational energy.

The two N11 – C12 and N11 – C2 bonds showed modes at  $966 \text{ cm}^{-1}$  (20%) and  $1276.93$

$\text{cm}^{-1}$  (25%) for B3LYP, 1259.17  $\text{cm}^{-1}$  (23%) and 1294.63  $\text{cm}^{-1}$  (26%) for mPW1PW91, 1267.66  $\text{cm}^{-1}$  (22%) and 1286.67  $\text{cm}^{-1}$  (15%) for M06-2X. The unique methyl group present in the PAAPFBA molecule showed characteristic C – H stretching at 3048.86  $\text{cm}^{-1}$  (symmetrical, 28% for C13H14, 32% for C13H15 and 40% for C13H16), 3114.54  $\text{cm}^{-1}$  (asymmetrical, 45% for C13H15 and 52% for C13H16) and 3131.75  $\text{cm}^{-1}$  (asymmetrical, 70% for C13H14 and 23% for C13H15) for the B3LYP; at 3076.12  $\text{cm}^{-1}$  (symmetrical, 29% for C13H14, 31% for C13H15 and 39% for C13H16), 3153.41  $\text{cm}^{-1}$  (asymmetrical, 42% for C13H15 and 54% for C13H16) and 3169.97  $\text{cm}^{-1}$  (asymmetrical, 27% for C13H15 and 67% for C13H14) for the mPW1PW91; at 3080.75  $\text{cm}^{-1}$  (symmetrical, 17% for C13H15, 29% for C13H14 and 54% for C13H16), 3154.69  $\text{cm}^{-1}$  (asymmetrical, 43% for C3H16 and 51% for C13H14) and 3193.18  $\text{cm}^{-1}$  (asymmetrical, 20% for C13H14 and 77% for C13H15) for the M06-2X.

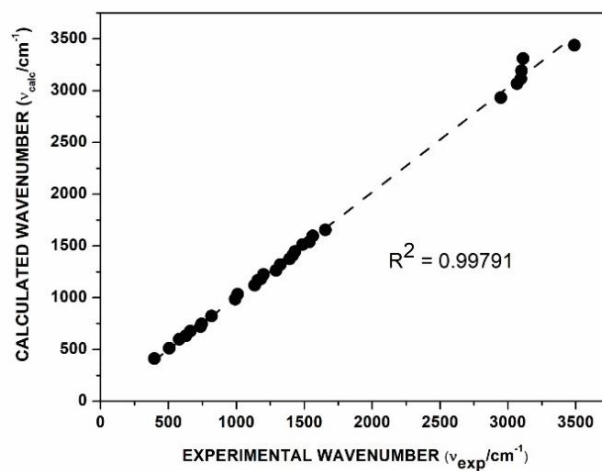
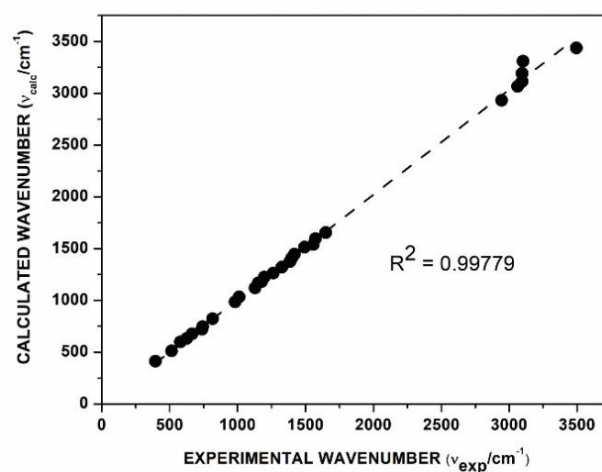
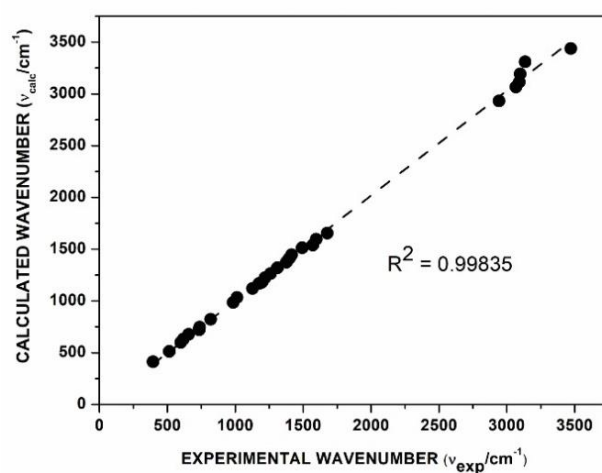
The symmetrical bending modes were assigned at 1397  $\text{cm}^{-1}$  and 1481.08  $\text{cm}^{-1}$  for B3LYP; at 1395.65  $\text{cm}^{-1}$  and 1483.25  $\text{cm}^{-1}$  for mPW1PW91; at 1401.35  $\text{cm}^{-1}$  and 1483.18  $\text{cm}^{-1}$  for M06-2X. The asymmetrical bending modes were assigned at 1052.98  $\text{cm}^{-1}$  (H15 and H16) and 1464.38  $\text{cm}^{-1}$  (H15 and H16) for B3LYP; at 1051.85  $\text{cm}^{-1}$  (H15 and H16) and 1462.59  $\text{cm}^{-1}$  (H15 and H16) for mPW1PW91; at 1464.10  $\text{cm}^{-1}$  (scissoring H14 and H16 and twisting H15 and H16) for M06-2X.

The  $\pi$ -bond from the alkene C20=C22, the C – C and the two C – H stretching were calculated respectively as 1690.20  $\text{cm}^{-1}$ , 3218.56  $\text{cm}^{-1}$  (H23), 3152.73  $\text{cm}^{-1}$  (H25) for B3LYP; as 1723.61  $\text{cm}^{-1}$ , 3241.18  $\text{cm}^{-1}$  (H23), 3177.42  $\text{cm}^{-1}$  (H25) for mPW1PW91; as 1685.99  $\text{cm}^{-1}$ , 3227.80  $\text{cm}^{-1}$  (H23), 3179.41  $\text{cm}^{-1}$  (H25) for M06-2X.

The 4-fluoro-phenyl ring shows characteristics frequencies of C – H stretching for C27 – H31 (3180.82  $\text{cm}^{-1}$ , 99%), C29 – H34 (3205.11  $\text{cm}^{-1}$ , 77%; 3205.97  $\text{cm}^{-1}$ , 15%), C28 – H33 (3189.91  $\text{cm}^{-1}$ , 21%; 3201.19  $\text{cm}^{-1}$ , 10%; 3205.11  $\text{cm}^{-1}$ , 12%; 3205.97  $\text{cm}^{-1}$ , 55%) and C26 – H32 (3190  $\text{cm}^{-1}$ , 73%; 3206  $\text{cm}^{-1}$ , 21%) for B3LYP; at C27 – H31 (3207.68  $\text{cm}^{-1}$ , 92%), C29 – H34 (3233.59  $\text{cm}^{-1}$ , 60%; 3233.97  $\text{cm}^{-1}$ , 33%), C28 – H33 (3233.59  $\text{cm}^{-1}$ , 25%; 3233.97  $\text{cm}^{-1}$ , 52%; 3216.33  $\text{cm}^{-1}$ , 18%) and C26 – H32 (3233.59  $\text{cm}^{-1}$ , 11%; 3216.33  $\text{cm}^{-1}$ , 77%) for mPW1PW91; at C27 – H31 (3211.52  $\text{cm}^{-1}$ , 93%), C29 – H34 (3237.73  $\text{cm}^{-1}$ , 91%), C28 – H33 (3218.84  $\text{cm}^{-1}$ , 11%, 3237.01  $\text{cm}^{-1}$ , 80%) and C26 – H32 (3237.01  $\text{cm}^{-1}$ , 11%; 3237.01  $\text{cm}^{-1}$ , 74%) for M06-2X.

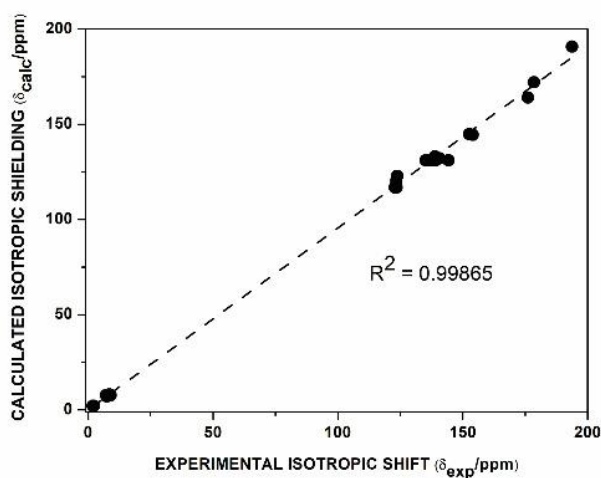
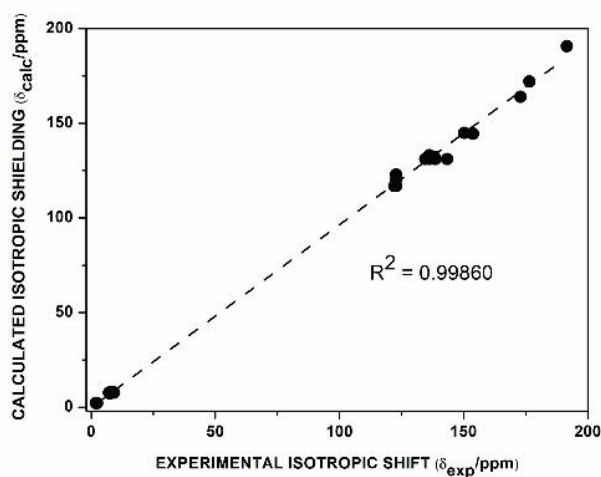
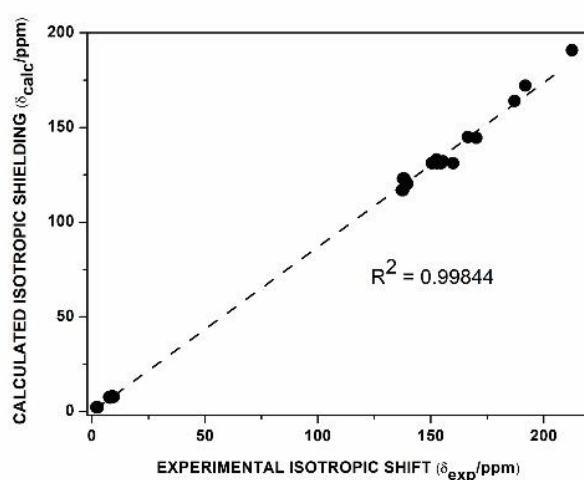
The C – C stretching were computed with higher value of PED at 1440.82  $\text{cm}^{-1}$  (C26C28, 18%), 1623.10  $\text{cm}^{-1}$  (C30C29, 13%), 834.89  $\text{cm}^{-1}$  (C28C30, 14%), 1122.21  $\text{cm}^{-1}$  (C29C27, 17%) and 1623.10  $\text{cm}^{-1}$  (C27C24, 22%) for B3LYP; at 1671.13  $\text{cm}^{-1}$  (C26C28, 15%), 1644.57  $\text{cm}^{-1}$  (C30C29, 15%), 845.65  $\text{cm}^{-1}$  (C28C30, 13%), 1455.76  $\text{cm}^{-1}$  (C29C27, 21%) and 1652.69  $\text{cm}^{-1}$

(C27C24, 21%) for mPW1PW91; at 1455.87  $\text{cm}^{-1}$  (C26C28, 19%), 1657.40  $\text{cm}^{-1}$  (C30C29, 28%), 1317.45  $\text{cm}^{-1}$  (C28C30, 19%), 1455.87  $\text{cm}^{-1}$  (C29C27, 18%) and 1317.45  $\text{cm}^{-1}$  (C27C24, 14%) for M06-2X. The C26-C24 stretching did not show the value of PED higher than 10%, thus it was not computed. Finally, for the 4-acetamido-phenyl ring show C – H stretching at 3247.14  $\text{cm}^{-1}$  (H7, 99%), 3198.20  $\text{cm}^{-1}$  (H8, 98%), 3201.19  $\text{cm}^{-1}$  (H10, 45%) and 3172.21  $\text{cm}^{-1}$  (H9, 95%) for B3LYP; at 3269.90  $\text{cm}^{-1}$  (H7, 98%), 3222.78  $\text{cm}^{-1}$  (H8, 98%), 3227.04  $\text{cm}^{-1}$  (H10, 47%) and 3200.28  $\text{cm}^{-1}$  (H9, 94%) for mPW1PW91; at 3282.60  $\text{cm}^{-1}$  (H7, 99%), 3224.10  $\text{cm}^{-1}$  (H8, 99%), 3227.80  $\text{cm}^{-1}$  (H10, 63%) and 3204.83  $\text{cm}^{-1}$  (H9, 91%) for M06-2X. The C – C ring stretching were estimated as for the C1 – C3 bond at 1431.56  $\text{cm}^{-1}$  (22%, B3LYP), 1447.44  $\text{cm}^{-1}$  (26%, mPW1PW91) and 1443.27  $\text{cm}^{-1}$  (21%, M06-2X); for the C6 – C5 bond at 1431.56  $\text{cm}^{-1}$  (19%, B3LYP), 1447.44  $\text{cm}^{-1}$  (22%, mPW1PW91) and 1443.27  $\text{cm}^{-1}$  (17%, M06-2X); for the C2 – C6 bond at 1336.63  $\text{cm}^{-1}$  (19%, B3LYP), 1294.63  $\text{cm}^{-1}$  (15%, mPW1PW91) and 1645.82  $\text{cm}^{-1}$  (24%, M06-2X); for the C4 – C3 bond at 1336.63  $\text{cm}^{-1}$  (17%, B3LYP), 1057.63  $\text{cm}^{-1}$  (17%, mPW1PW91) and 1341.36  $\text{cm}^{-1}$  (16%, M06-2X); for the C5 – C4 bond 1336.63  $\text{cm}^{-1}$  (17%, B3LYP), 1663.72  $\text{cm}^{-1}$  (12%, mPW1PW91) and 1667.56  $\text{cm}^{-1}$  (11%, M06-2X). All the DFT methods can describe the vibrational spectrum of the PAAPFBA molecule appropriately, as it was shown by the linear fitting calculation and the theoretical assignments of fundamental modes.

**(a) B3LYP/6-311++G(d,p)****(b) mPW1PW91/6-311++G(d,p)****(c) M06-2X/6-311++G(d,p)**

**Fig. 2** – The Linear correlation of the experimental wavenumbers and theoretical wavenumbers for the fundamental vibrational modes of the PAAPFBA molecule for the (a) B3LYP (b) mPW1PW91 and (c) M06-2X at 6-311++G(d,p) computational levels.

The  $^1\text{H}$  and  $^{13}\text{C}$  NMR chemical isotropic shifts analysis was carried out from the optimized molecular geometry in methanol with IEF-PCM model of the PAAPFBA using the DFT methods (B3LYP/mPW1PW91/M06-2X) at 6-311++G(d,p) level of theory with GIAO method by using the same chemical environment as the geometrical optimization. The tetramethylsilane is the reference compound and it was optimized at the same level of theory as the PAAPFBA molecule followed by the NMR calculation. The mean value of the calculated isotropic shielding constants for the hydrogen ( $\sigma_{\text{H}(TMS)}$ ) and carbon ( $\sigma_{\text{C}(TMS)}$ ) atoms were respectively:  $\sigma_{\text{H}(TMS)} = 31.9640$  ppm and  $\sigma_{\text{C}(TMS)} = 184.6196$  ppm (B3LYP);  $\sigma_{\text{H}(TMS)} = 31.8849$  ppm and  $\sigma_{\text{C}(TMS)} = 189.1702$  ppm (mPW1PW91);  $\sigma_{\text{H}(TMS)} = 32.0609$  ppm and  $\sigma_{\text{C}(TMS)} = 189.6430$  ppm (M06-2X). In Table S4 (supplementary material) is shown the values of the calculated isotropic shielding constants for the PAAPFBA molecule at DFT methods, the experimental  $^1\text{H}$  and  $^{13}\text{C}$  isotropic shifts from the Ferreira *et al.* [16] and the calculated isotropic magnetic shielding for the hydrogens ( $\delta_{\text{H}}$ ) and carbon ( $\delta_{\text{C}}$ ) atoms of PAAPFBA compound. The experimental and the theoretical  $^1\text{H}$  and  $^{13}\text{C}$  spectra are shown in Figs. S2 and S3 (supplementary material) respectively. These results show an excellent agreement with the experimental data; hence the linear fitting was made using the calculated isotropic magnetic shielding versus the experimental isotropic shifts (Fig. 3) and the values of the R-squared ( $R^2$ ) for the DFT methods are respectively 0.99865 (B3LYP), 0.99860 (mPW1PW91) and 0.99844 (M06-2X) with the linear equation respectively  $y = 0.95561x + 0.02651$  (B3LYP),  $y = 0.96623 - 0.16585$  (mPW1PW91), and  $y = 0.86899x - 0.11064$  (M06-2X). The B3LYP and the mPW1PW91 methods can describe the NMR spectra almost similarly and both are slightly better than the M06-2X method. However, all DFT methods can be used satisfactorily to describe the  $^1\text{H}$  and  $^{13}\text{C}$  NMR spectra.

**(a) B3LYP/6-311++G(d,p)****(b) mPW1PW91/6-311++G(d,p)****(c) M06-2X/6-311++G(d,p)**

**Fig. 3** – Linear correlation with the experimental  $^1\text{H}$  and  $^{13}\text{C}$  isotropic shielding and the calculated isotropic magnetic shielding by (a) B3LYP (b) mPW1PW91 and (c) M06-2X at 6-311++G(d,p) basis set.

### 4.3 Nonlinear Optics Analysis

The research for high effectiveness nonlinear optical (NLO) materials has been increasing due to its technological applicability, and the chalcone derivatives are excellent candidates due to its great optical transparency and elevated flexibility in the synthesis reactions. Therefore, the NLO calculations for the PAAPFBA molecule were carried out using the DFT methods (B3LYP/mPW1PW91/M06-2X) at 6-311++G(d,p) computational level employing the IEF-PCM model with methanol as implicit solvent. It is necessary to compare the results concerning to the reference substance with those calculated for the urea molecule, which is commonly used for this type of analysis [59 – 67]. Hence, the urea molecule was optimized, and its NLO properties were computed at the same level of theory as the PAAPFBA compound. The dipole moment ( $\mu$ ), the polarizabilities ( $\alpha$ ) and the first order hyperpolarizabilities ( $\beta$ ) at the static state ( $\omega = 0$ ) were calculated for each cartesian direction for urea and PAAPFBA molecules.

The quantities used to determine the possible usefulness of the molecular candidate are shown in the following equations (9 – 12). The hyperpolarizability is a 3D matrix with 27 elements (3 x 3 x 3), and this matrix can be reduced to only ten terms by the application of the Kleinman theorem [68, 69] in which considerer that the permutations assume the same values ( $\beta_{xyy} = \beta_{yyx} = \beta_{yyx}, \dots$ ). The value of  $\beta_0$  is often express in electrostatic units (1 a.u. =  $8.6393 \times 10^{-33}$  esu). Thus, the results of dipole moment and polarizability are shown in Table S5, and the results of the hyperpolarizability are shown in Table S6 (supplementary material).

$$\mu_{tot} = (\mu_x^2 + \mu_y^2 + \mu_z^2)^{1/2} \quad (9)$$

$$\alpha_{tot} = \frac{1}{3}(\alpha_{xx} + \alpha_{yy} + \alpha_{zz}) \quad (10)$$

$$\Delta\alpha = \frac{1}{\sqrt{2}}[(\alpha_{xx} - \alpha_{yy})^2 + (\alpha_{yy} - \alpha_{zz})^2 + (\alpha_{zz} - \alpha_{xx})^2 + 6\alpha_{xz}^2 + 6\alpha_{xy}^2 + 6\alpha_{yz}^2]^{1/2} \quad (11)$$

$$\beta_0 = [(\beta_{xxx} + \beta_{xyy} + \beta_{xzz})^2 + (\beta_{yyy} + \beta_{yzz} + \beta_{yxx})^2 + (\beta_{zzz} + \beta_{zxx} + \beta_{zyy})^2]^{1/2} \quad (12)$$

It can be observed that the PAAPFBA molecule has the  $\mu_{tot}$ ,  $\alpha_{tot}$ ,  $\Delta\alpha$ ,  $\beta_0$  respectively 1.399972, 8.27574, 20.54705 and 119.2839 (B3LYP), 1.398378, 8.291795, 20.11854 and 138.8324 (mPW1pw91), 1.375916, 7.880764, 16.77039 and 163.4927 (M06-2X) times greater than the same quantities of urea. Therefore, the chalcone PAAPFBA has a good NLO character and it may be used as a nonlinear optical material.

The NLO properties were also computed using the short (CAM-B3LYP) and long (LC-BLYP and  $\omega$ B97XD) range separated hybrid methods. The results for the calculated NLO



parameters are shown in Table S8 and S9. The total dipole moment ( $\mu_{tot}$ ), the total polarizability ( $\alpha_{tot}$ ), and the parameters  $\Delta\alpha$  and  $\beta_0$  have the values respectively 8.61189 Debye (CAM-B3LYP), 8.65791 Debye (LC-BLYP), and 8.54546 Debye ( $\omega$ B97XD); 318.5333 a.u. (CAM-B3LYP), 298.5077 a.u. (LC-BLYP), and 317.9587 a.u. ( $\omega$ B97XD); 309.5469 a.u. (CAM-B3LYP), 270.7678 a.u. (LC-BLYP), and 305.4882 a.u. ( $\omega$ B97XD);  $343.5688 \cdot 10^{-31}$  esu (CAM-B3LYP),  $268.0074 \cdot 10^{-31}$  esu (LC-BLYP), and  $329.8977 \cdot 10^{-31}$  esu ( $\omega$ B97XD). These parameters show that the PAAPFBA chalcone has a good NLO character. In Table S10 are shown the ratios for each NLO properties between the B3LYP/mPW1PW91/M06-2X methods and the short/long range separated methods (CAM-B3LYP/LC-BLYP/ $\omega$ B97XD).

For the total dipole moment, the total polarizability and for the parameter  $\Delta\alpha$ , the values between the DFT methods are in good agreement. However, for the parameter  $\beta_0$  only the M06-2X method shows a good agreement to the short/long range separated methods. Therefore, the PAAPFBA chalcone has a good NLO character as can be seen in the results from the comparison with the urea molecule and the (CAM-B3LYP/LC-BLYP/ $\omega$ B97XD) methods. All the three DFT methods (B3LYP/mPW1PW91/M06-2X) can be used to describe appropriately the total dipole moment, total polarizability, and the parameter  $\Delta\alpha$ , however only the M06-2X method described the parameter  $\beta_0$  with a good relation to the standard methods in the literature.

#### 4.4 Quantum molecular properties analysis

The Highest Occupied Molecular Orbital (HOMO) and the Lowest Occupied Molecular Orbital (LUMO) usually denominated Frontier Molecular Orbitals (FMO) play a very important role in describing the electronic properties of the organic compounds, and it was recognized firstly by Fukui [70] and explained from the DFT later [71]. The HOMO is related to the feature of nucleophilicity, and the LUMO is associated with the electrophilicity. The less negative is the value of the HOMO energy greater is the propensity of the molecule behave like a nucleophilic or donate electronic density, and the more negative is the LUMO energy greater is the tendency of the molecule to accept electronic density or behave like an electrophilic. In Fig. 4 is shown the FMOs calculated by the DFT methods (B3LYP/mPW1PW91/M06-2x) at 6-311G++(d,p) computational level rendered by the ChemCraft trial version software [72], and they are very identical with only a few differences in the mathematical signal of the wavefunction, which does not affect the probabilistic interpretation.

The HOMO is mainly spread over the  $\pi$ -bonds present in both phenyl rings, the C20=C22 bond, the dislocated electrons displayed over the amide group (O17-C12-N11) and

the fluorine (F35) atom due to its higher value of electronegativity. The LUMO is principally spread over the antibonding position of the  $\pi$ -bonds at the same set of atoms as mentioned before. Therefore, it can be concluded that the transition HOMO-LUMO occurs between the bonding molecular orbital to anti-bonding molecular orbital ( $\pi \rightarrow \pi^*$ ). The calculated HOMO energy varies according to the DFT method used: the B3LYP predicted the lowest value for the HOMO energy of -6.58330 eV and the M06-2x method predicted the highest value for the HOMO energy of -7.85 eV. The mPW1PW91 method estimated value in between of those two (-6.81297 eV), however, the value is closer to the B3LYP (-6.81297 eV) with a difference of 0.22967 eV. The method dependence was also noticed with the values of the LUMO energies: the tendency was the same as before, the B3LYP method predicted the lowest value of the LUMO energy (-2.68007 eV), the M06-2X method the highest value for the energy (-1.73556 eV), and the mPW1PW91 (-2.53367 eV) closer than B3LYP with the difference of 0.1464 eV. Despite the FMO to indicate the possible chemical behavior (nucleophilic or electrophilic), the Energy Gap ( $\Delta E_{Gap}$ ) defined by the difference between the LUMO and the HOMO energies is more used. The lowest is the value of the energy gap, the greatest is the nucleophilic/electrophilic character of the molecule. This fact is supported by an important theory: Pearson's Hard Soft Acids Bases Theory (HSAB) [73]. The calculated Energy Gap was ranked with method dependence: 6.114447 eV (M06-2x) < 4.279296 eV (mPW1PW91) < 3.903232 eV (B3LYP).

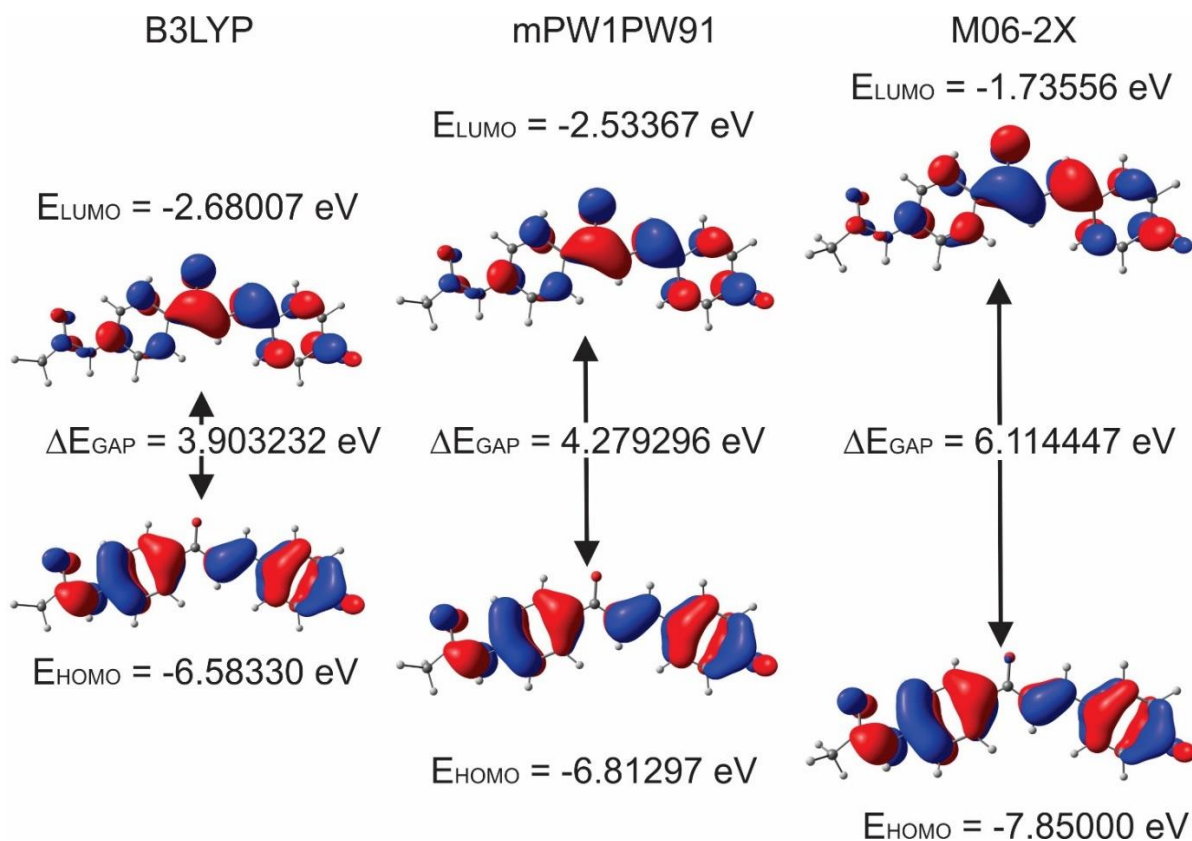


**Fig. 4** – Calculated Frontier Molecular Orbitals (FMO) for the PAAPFBA chalcone using the B3LYP/mPW1PW91/M06-2X with 6-311++G(d,p) basis set.

To study more detail the molecular electronic properties, it is used the quantum chemical descriptors, and they are computed from the values of the HOMO and LUMO (Table S11 - supplementary material).

The Ionization Potential (I) and the Electrons Affinity (A) can be determinate from the Koopmans' theorem [74] as describe below by the equations (13) and (14) respectively.

$$I = -E_{HOMO} \quad (13)$$

$$A = -E_{LUMO} \quad (14)$$

According to the results, the B3LYP method shows the lowest ionization potential ( $I = 6.583302$  eV) and the highest electron affinity ( $A = 2.68007$  eV). The M06-2x method predicts a higher ionization potential ( $I = 7.85$  eV) and lower electron affinity ( $A = 1.735556$  eV). These descriptors mean that the valence electronic density is accessible to be donated, and if the molecule receives electronic density, it will be favorable to the PAAPFBA to accommodate the extra negative charge.

The electronegativity ( $\chi$ ) can be expressed mathematically as the negative of the derivative of the energy in respect to the number of electrons at constant external potential (equation 15) [75]. The electronic chemical potential ( $\mu$ ) is the negative of the electronegativity [76]. According to the work of Iczkowski and Margrave [77], both descriptors can be expressed in function of the FMO energies (equation 16).

$$\chi = \left( \frac{\partial E}{\partial N} \right)_v = -\mu \quad (15)$$

$$\chi = -\mu = \frac{I + A}{2} = -\left( \frac{E_{HOMO} + E_{LUMO}}{2} \right) \quad (16)$$

The natural flow of the electronic density is from the regions with low electronegativity to the region with high electronegativity, thus the B3LYP method shows the lower value of electronegativity ( $\chi = 2.68007$  eV) and the highest value of chemical potential ( $\mu = -2.68007$  eV). The M06-2X method predicted the higher value of the electronegativity ( $\chi = 4.792779$  eV) and the lowest value of the electronic potential ( $\mu = -4.792779$  eV). The mPW1PW91 method predicted a value in between of the other methods:  $\chi = 4.67332$  eV and  $\mu = -4.67332$  eV.

The global hardness ( $\eta$ ) is defined as the second-order derivative of the energy in respect to the number of electrons at constant external potential [78]. This descriptor can be expressed in terms of the FMO energies as seen in equation 17 [79, 80].

$$\eta = \frac{I - A}{2} = \frac{E_{LUMO} - E_{HOMO}}{2} \quad (17)$$

According to the Maximum Hardness Principle [81], the natural arrangement of the molecule is toward the highest value of the hardness. The higher the value of the global hardness the lower is the nucleophilic/electrophilic behavior due to the larger energy gap [82]. The global hardness was computed as 1.951616 eV (B3LYP), 2.139648 eV (mPW1PW91), and 3.057223 eV (M06-2X). This order is the same as the increase of the energy gap. The global softness (S) is defined as the inverse of the global hardness (equation 17) [78]. The B3LYP method computes the highest value of the global softness ( $0.512396$  eV<sup>-1</sup>) as expected from the lowest value of

global hardness, followed by the mPW1PW91 (0.467367 eV<sup>-1</sup>) and the M06-2X (0.327094 eV<sup>-1</sup>).

The global electrophilicity index ( $\omega$ ) [83] and the global nucleophilicity index ( $\varepsilon$ ) [84] can be seen its mathematical expression in equations 18 and 19, respectively. These descriptors are related to the electrophilic and nucleophilic character of the molecule, respectively. Thus, a good nucleophile is described by lower values of the  $\omega$  and higher values of  $\varepsilon$ , and consequently, a good electrophile is described by higher values of  $\omega$  and lower values of  $\varepsilon$ . Unlike the previous results, the M06-2X method predicts the electrophilic and nucleophilic characters for the PAAPFBA molecule with the lower value of  $\omega$  (3.756797 eV) and the higher value of  $\varepsilon$  (0.266184 eV<sup>-1</sup>) against 5.496091 eV and 0.181947 eV<sup>-1</sup> from B3LYP and 5.103625 eV and 0.195939 eV<sup>-1</sup> from mPW1PW91 method.

$$\omega = \frac{\chi^2}{2\eta} \quad (18)$$

$$\varepsilon = \frac{1}{\omega} \quad (19)$$

To complete the global analysis of the quantum molecular descriptors, it may be necessary to use the electric dipole polarizability ( $\alpha_{tot}$ ) calculated at the nonlinear optical properties. The mathematical expression is the same as seen in equation 10. The hardness is a measure of chemical stability and the polarizability is a measure of chemical reactivity [85]. The Minimum Polarizability Principle [86] states that a chemical species will react until the state of minimum polarizability which means higher the value of  $\alpha_{tot}$  higher is the molecular reactivity. Thus, according to this descriptor, the predicted for the polarizability is 308.5923 a.u. (M06-2X), 330.815 a.u. (mPW1PW91), and 341.5867 a.u. (B3LYP). Therefore, the three DFT methods (B3LYP/mPW1PW91/M06-2X) can be used to describe the electronic distribution of the FMO for the PAAPFBA chalcone and all the quantum molecular descriptors can be used to describe appropriately the nucleophilic/electrophilic behavior of the title chalcone.

#### 4.6 Electronic Fukui Functions and local reactivity descriptors

It is important to understand how each atom may act to contribute to describing the entire chemical behavior of the molecular species. Along with the global quantum molecular descriptors and the local analysis, it is possible to provide a unified treatment of the selectivity and the reactivity for the compounds. The Electronic Fukui Functions can characterize the

nucleophilic, the electrophilic, and the radical regions of the molecule. The electronic Fukui function ( $f$ ) is expressed by the derivate of the electronic density ( $\rho$ ) for the number of electrons at constant external potential (equation 20). The reactivity sites can be approximated by the electronic density of the FMO as shown in equations 21 – 23.

$$f = \left( \frac{\partial \rho(r)}{\partial N} \right)_{v(r)} \quad (20)$$

$$f^+ \approx v_{LUMO} \quad (21)$$

$$f^- \approx v_{HOMO} \quad (22)$$

$$f^o \approx \frac{1}{2} (v_{LUMO} + v_{HOMO}) \quad (23)$$

The  $f^+$  is related to the molecule acting as an electrophilic (susceptible to a nucleophilic attack), the  $f^-$  is the molecule acting like a nucleophilic (susceptible to an electrophilic attack) and the  $f^o$  describe the propensity to a radical attack. They were calculated using the Multiwfn software [87] and rendered by the VESTA software [88]. The calculated isosurface of the Electronic Fukui functions for each DFT method are shown in Fig. 5. The green and the blue isosurface corresponds respectively to the positive and the negative region of the Fukui function. The  $f^+$  function appears remarkably similar in the different DFT methods. The atoms C19, O21, and C22 are more susceptible to a nucleophilic attack (the molecule acts as an electrophilic) due to the empty  $\pi^*$  antibonding, these atoms show a strong positive region for the  $f^+$ . Other atoms like C2, C3, C5, C26, C27, and C30 are also susceptible to a nucleophilic attack, but the positive regions are smaller than the C19, O21, and C22. For the  $f^-$ , the B3LYP and the mPW1PW91 predicted functions are analogous with the atoms C1, C2, C3, C4, C5, C6, N11, C12, O17, C20, C22, C24, C26, C27, C28, C29 and C30 are susceptible to an electrophilic attack (the molecule acts as a nucleophilic) due to the large positive regions of the  $f^-$  and in these atoms are mainly spread the  $\pi$  bonding molecular orbitals that can be used to donate electronic density. However, the M06-2X method only predicts that the atoms C1, C2, C3, C4, C5, C6, N11, C12, O17, and O21 are susceptible to an electrophilic attack. For the  $f^o$ , the B3LYP and mPW1PW91 functions are almost the same again. The atoms C1, C2, C3, C4, C5, C6, N11, C12, O17, C19, C20, O21, C22, C26, C27, and C30 are more susceptible to a radical attack due to the greater positive regions of the  $f^o$ . Besides, the M06-2X predicts only the atoms C1, C2, C3, C4, C5, C6, N11, C12, O17, C19 and

O21 susceptible to a radical attack.

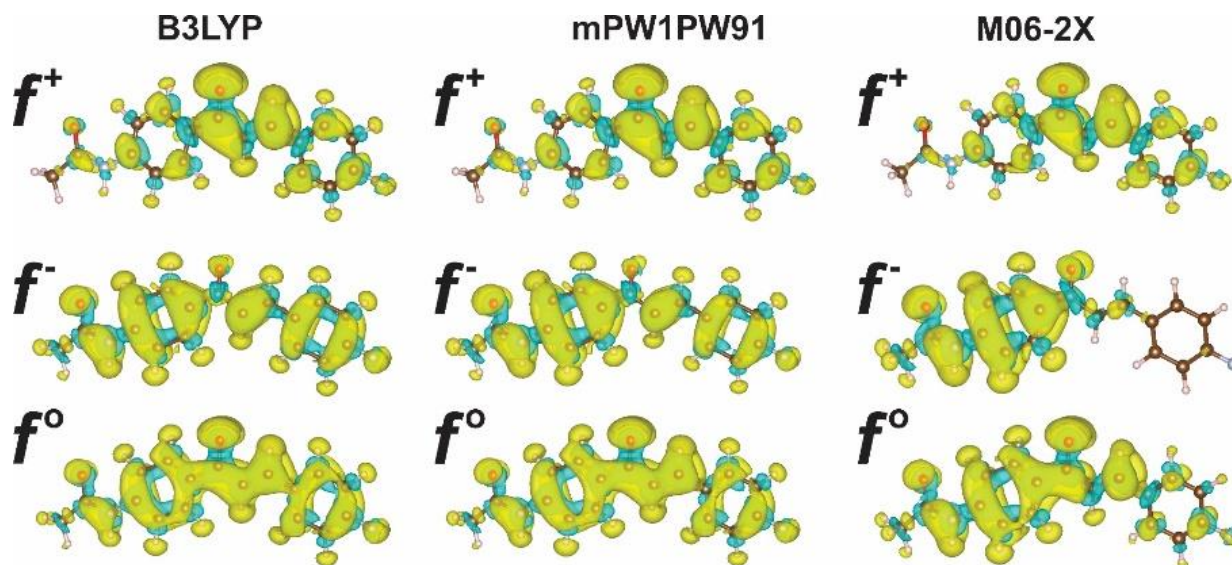


**Fig. 5** – Calculated isosurfaces for the Electronic Fukui functions using the electronic density and computed by the DFT methods (B3LYP/mPW1PW91/M06-2X) at 6-311++G(d,p) basis set.

The Fukui Functions can be approximated for each atom using an atomic population charge analysis and they are called Condensed Fukui Functions. In this work, it was used the Hirshfeld population analysis and the mathematical equations 24 - 26 are shown as follows.

$$f_k^+ = q_k(N + 1) - q_k(N) \quad (24)$$

$$f_k^- = q_k(N) - q_k(N - 1) \quad (25)$$

$$f_k^o = \frac{q_k(N + 1) - q_k(N - 1)}{2} \quad (26)$$

The  $q_k(N + 1)$ ,  $q_k(N)$  and  $q_k(N - 1)$  are respectively the atomic Hirshfeld charge on the atom  $k$  in the anionic, neutral and cationic species. According to the results, the atoms more susceptible to a nucleophilic attack are C1, C2, C4, C5, C6, N11, C12, C13, O17, C20, C24, C28, C29, C30, and F35 (B3LYP); C1, C2, C4, C5, C6, N11, C12, C13, O17, C24, C29, and F35 (mPW1PW91); C1, C2, C3, C4, C5, C6, N11, C12, C13, and O17 (M06-2X). The following atoms are more susceptible to an electrophilic attack: C3, C19, O21, C22, C26, and C27 (B3LYP); C3, C19, C20, O21, C22, C26, C27, C28, and C30 (mPW1PW91); C19, C20,

O21, C22, C24, C26, C27, C28, C29, C30, and F35 (M06-2X). For the M06-2X method, the atomic susceptibility for the electrophilic attack is the inverse when comparing to the analysis of the Electronic Fukui function. For a radical attack the most susceptible atoms are as follows: C12, C13, C24, C28, C29 and F35 (B3LYP); C12, C13, C24, C28, C29 and F35 (mPW1PW91); C12, C13, C24, C26, C27, C28, C29, C30 and F35 (M06-2X) (Table S12 - supplementary material). The Condensed Fukui functions computed from the Hirshfeld charge population are in good agreement with those Fukui functions calculated from the electronic density only for the B3LYP and mPW1PW91 methods.

Together with the global descriptors like hardness, softness and electrophilicity index, it can be generated a set of new local descriptors like local hardness ( $\eta_k$ ), local softness ( $s_k$ ) and the philicity index ( $\omega_k$ ) to understand the reactivity in each atom. The equations 27 – 29 illustrates the relations of global descriptors and the Condensed Fukui functions.

$$\eta_k^\gamma = \eta f_k^\gamma \quad (27)$$

$$s_k^\gamma = s f_k^\gamma \quad (28)$$

$$\omega_k^\gamma = \omega f_k^\gamma \quad (29)$$

Where  $\gamma = +, -$  and  $^\circ$  refer respectively to the nucleophilic, electrophilic and radical attack, the indices  $k$  refers to the atoms, and  $\eta, s, \omega$  refers to the global hardness, softness and electrophilicity index respectively. The local hardness and softness are the measure of the mainly contribution to the global hardness and softness during a chemical reaction (nucleophilic, electrophilic or radical attack). The philicity index is the measure of the propensity of an atomic site to favor a nucleophilic, electrophilic or radical site, thus the higher the value of  $\omega_k^+$ , the atomic site is most favorable to a nucleophilic attack, and the higher is the value of  $\omega_k^-$ , the atomic site is most favorable to an electrophilic attack. Consequently, the higher the value of the  $\omega_k^\circ$ , the atomic site is favorable to a radical attack. For the B3LYP method (Table S13 - supplementary material), the atoms that mainly contribute to the global hardness are C1, C4, N11, C12, C13, and O17 (nucleophilic attack); C13 and C19 (electrophilic attack); C12 (radical attack). The atoms that contribute mainly to the global softness are C1, C2, C3, C4, C5, C6, N11, C12, C13, O17, C24, C26, C27, C28, C29, and F35 (nucleophilic attack); C3, C5, C12, C13, C19, O21, C24, C26, C27, C28, C29, and F35 (electrophilic attack); C1, C3, C5, C6, N11, C12, C13, O17, C24, C26, C27, C28, C29, and F35 (radical attack). The favorable atomic sites



for the nucleophilic attack are C1, C2, C4, C5, C6, N11, C12, C13, O17, C24, C27, C28, C29, and F35; for the electrophilic attack are C3, C5, C12, C13, C19, O21, C26, C27, C28, C29, and F35; for the radical attack are C1, C3, C5, C6, N11, C12, C13, O17, C24, C26, C27, C28, C29, and F35.

For the mPW1PW91 method, the atoms that contribute mainly to the global hardness are C1, C4, C6, N11, C12, C13, O17, C24, C28, C29, and F35 (nucleophilic attack); C13, C19, C28, and C29 (electrophilic attack); C12, C28, and C29 (radical attack). The atoms that contribute mainly to the global softness are C1, C3, C4, C6, N11, C12, C13, O17, and C24 (nucleophilic attack); C13 and C19 (electrophilic attack); C12 and C13 (radical attack). The favorable nucleophilic attack (electrophilic site) is C4, N11, C12, C13, and O17. The favorable electrophilic attack (nucleophilic site) is C19, and the favorable radical attack is C13 (Table S14-supplementary material).

For the M06-2X method, the set of atoms that contribute principally to the global hardness are C4, N11, C12, C13, and O17 (nucleophilic attack); C13, C26, C27, C28, C29, C30 and F35 (electrophilic attack); C13, C28, C29, and F35. The global softness is described mainly by C1, C4, N11, C12, C13, O17 (nucleophilic attack); C13, C20, C24, C26, C27, C28, C29, C30, and F35 (electrophilic attack); C13, C28, C29, and F35 (radical attack). The suitable sites for nucleophilic attack are C4, N11, C12, C13, and O17; for the electrophilic attack are C13, C19, C24, C26, C27, C28, C29, C30, and F35; for the radical attack are C13, C24, C28, C29, and F35 (Table S15-supplementary material).

Finally, the Condensed Fukui functions can be used also to study the local reactivity and they are called the dual ( $\Delta f$ ) [89] and the multiphilic ( $\Delta\omega$ ) [90] descriptors. If both  $\Delta f$  and  $\Delta\omega$  are positive, the reactive site has an electrophilic character. If both  $\Delta f$  and  $\Delta\omega$  are negative, the site has a nucleophilic character.

$$\Delta f = f_k^+ - f_k^- \quad (30)$$

$$\Delta\omega = \omega\Delta f \quad (31)$$

The electrophilic sites of the molecule according to this analysis are C1, C2, C4, C5, C6, N11, C12, C13, O17, C20, C24, C28, C29, and F35 (B3LYP); C1, C2, C4, C5, C6, N11, C12, C13, O17, C24, and F35 (mPW1PW91); C1, C2, C3, C4, C5, C6, N11, C12, C13, and O17 (M06-2X). The nucleophilic sites are in atoms C3, C19, O21, C22, C26, and C27 (B3LYP); C3,

C19, C20, O21, C22, C26, C27, C28, and C30 (mPW1PW91); C19, C20, O21, C22, C24, C26, C27, C28, C29, C30, and F35 (M06-2X) (Table S16 - supplementary material). This result is in good agreement with the Fukui functions and the Condensed Fukui functions calculated previously.

#### 4.7 Molecular Electrostatic Potential (MEP)

The Molecular Electrostatic Potential (MEP) was calculated with the DFT methods (B3LYP/mPW1PW91/M06-2X) at 6-311++G(d,p) level of theory. This analysis has great importance concerning the nucleophilic and electrophilic reactive sites of the molecule. The MEP is colored from red to blue. The red color represents a negatively charged region and the blue color describes a positively charged region. The green color represents a neutral region, the yellow-orange color characterizes a partially negative charged region, and the light blue color is related to the partially positive charged region. The electrophilic interaction will occur with the red-colored regions due to the negative charge and the nucleophilic interaction will occur with the blue colored region due to the positive charge. As can be seen in Fig. 6 all the three MEP computes from the DFT methods are very similar: the negative regions of PAAPFBA molecule are over the oxygen atoms (O17 and O21) and the fluorine atom F35. This fact is expected due to the higher values of electronegativity of these atoms; the orange-yellow color regions appear over the  $\pi$ -bonds due to the electronic density; the green color regions describe some carbon-carbon bonds due to equal value of the electronegativity and the methyl group (C13), and the blue color regions are the hydrogen atoms and they are responsible to the nucleophilic interaction due to the high electron deficiency. The Electronic Fukui functions analysis predicts that the oxygen atoms are suitable to electrophilic attack and the hydrogen atoms have isosurface with positive values of  $f^-$ , thus this fact corroborates to these atoms are suitable to nucleophilic interaction.

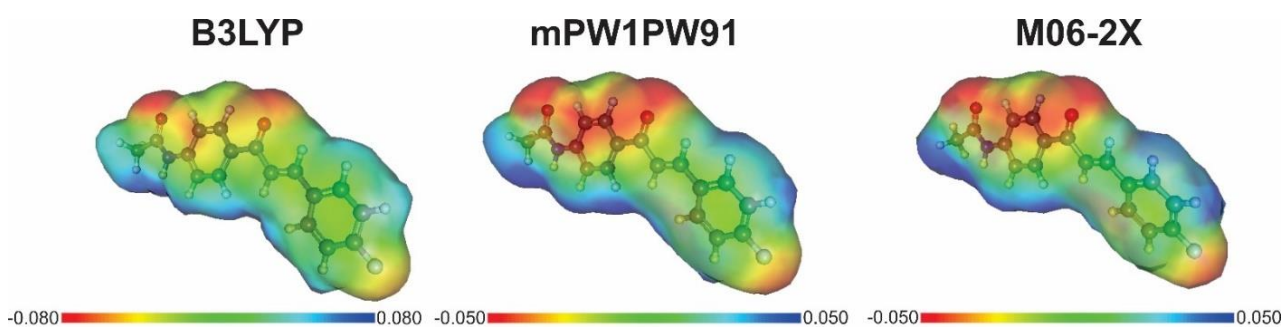


**Fig. 6** – Calculated Molecular Electrostatic Potential (MEP) for the PAAPFBA chalcone.

#### 4.8 Natural Bond Orbital (NBO) analysis

The Natural Bond Orbital (NBO) analysis is widely used to understand how the bonding and antibonding molecular orbitals can stabilize the entire chemical structure. It can be used to compute the intramolecular and intermolecular interactions and the process of conjugative interaction of bonds (delocalization of electronic density) within the molecule. To calculate the stabilization energy ( $\Delta E_{ij}$ ) from the donor-acceptor charge transfer process it is necessary to use the second-order Fock-matrix as seen in equation 32 [24,91,92].

$$\Delta E_{ij} = q_i \frac{F_{(i,j)}^2}{\varepsilon_j - \varepsilon_i} \quad (32)$$

Where the  $q_i$  is the occupancy of the donor orbital,  $\varepsilon_j$  and  $\varepsilon_i$  are the off-diagonal elements of the Fock matrix and  $F_{(i,j)}^2$  is the diagonal. The higher is the value of the stabilization energy higher is the probability of the electron delocalization process. This process can occur between the bonding molecular orbitals and lone pairs (occupied Lewis-type NBO) and antibonding molecular orbitals and Rydberg orbitals (unoccupied non-Lewis NBO). The NBO analysis was carried out using the DFT methods (B3LYP/mPW1PW91/M06-2X) at 6-311++G(d,p) levels of theory. The PAAPFBA molecule showed hyperconjugation interactions of weak, moderate and strong intensity including  $\sigma \rightarrow \sigma^*$ ,  $\pi \rightarrow \pi^*$ ,  $\pi^* \rightarrow \pi^*$ ,  $LP \rightarrow \sigma^*$  and  $LP \rightarrow \pi^*$  transitions.

For the B3LYP method, it can be seen in Table S17 (supplementary material) the results of the perturbation theory energy analysis. The higher values of the stabilization energy were due to delocalization of the  $\pi^*(C2 - C6) \rightarrow \pi^*(C1 - C3)$  and  $\pi^*(C19 - O21) \rightarrow \pi^*(C4 - C5)$  transitions with 186.44 kcal.mol<sup>-1</sup> and 196.44 kcal.mol<sup>-1</sup> respectively. This result shows how strong is the interaction between the phenyl ring present in the 4-acetamido-phenyl group and the carbonyl (C19=O21) group and the stabilization of those carbons and oxygen atoms. Also, there is moderate stabilization in this ring due to the transitions  $\pi \rightarrow \pi^*$  with values in the range of 15.38 kcal.mol<sup>-1</sup> to 24.30 kcal.mol<sup>-1</sup>. There is a weak stabilization from the  $\sigma(C4 - C19)$  to  $\sigma^*(C1 - C3)$ ,  $\sigma^*(C19 - C20)$  and  $\sigma^*(C19 - O21)$  with the value of 2.22 kcal.mol<sup>-1</sup>, 0.86 kcal.mol<sup>-1</sup> and 1.19 kcal.mol<sup>-1</sup> respectively. The moderate stabilization due to the  $\pi \rightarrow \pi^*$  transition is also present in the phenyl ring of the 4-fluorine-phenyl group with values in the range of 17.33 kcal.mol<sup>-1</sup> to 21.34 kcal.mol<sup>-1</sup>. The  $\sigma(C30 - F35) \rightarrow \sigma^*(C28 - H33)$  transition is responsible for a weak stabilization of 1.58 kcal.mol<sup>-1</sup>. The bond  $\sigma(N11 - H18)$  can donate

weakly electronic density to the  $\sigma^*(\text{C1} - \text{C2})$  and  $\sigma^*(\text{C12} - \text{O17})$  with the energy of 4.16 kcal.mol<sup>-1</sup> and 4.59 kcal.mol<sup>-1</sup> respectively. The lone pair (LP) of the nitrogen atom (N11) is responsible to stabilize the carbonyl (C12=O17) group about 59.71 kcal.mol<sup>-1</sup>. The lone pairs of the two oxygen atoms can stabilize antibonding molecular orbital as follows: LP(O17)  $\rightarrow$   $\sigma^*(\text{N11} - \text{C12})$  with 24.48 kcal.mol<sup>-1</sup>, LP(O17)  $\rightarrow$   $\sigma^*(\text{C12} - \text{C13})$  with 17.49 kcal.mol<sup>-1</sup>, LP(O21)  $\rightarrow$   $\sigma^*(\text{C4} - \text{C19})$  with 18.09 kcal.mol<sup>-1</sup>, and LP(O21)  $\rightarrow$   $\sigma^*(\text{C19} - \text{C20})$  with 18.19 kcal.mol<sup>-1</sup>. The  $\pi$ -bond between C20 and C22 can transfer charge moderately to the  $\pi^*(\text{C19} - \text{O21})$  and  $\pi^*(\text{C24} - \text{C27})$  with 21.72 kcal.mol<sup>-1</sup> and 11.55 kcal.mol<sup>-1</sup> respectively. The  $\pi^*(\text{C20} - \text{C22})$  bond is stabilized by the donation of the  $\pi^*(\text{C19} - \text{O21})$  and  $\pi^*(\text{C24} - \text{C27})$  with the energy of 52.58 kcal.mol<sup>-1</sup> and 88.45 kcal.mol<sup>-1</sup> respectively. The electronic density of the  $\sigma$ -bonds of C20 - H23 and C22 - H25 have weakly spread over  $\sigma^*$  molecular orbitals. Finally, the methyl group is responsible for a weak stabilization due to the hyperconjugation  $\sigma \rightarrow \sigma^*$  which the higher value for the energy is only 5.07 kcal.mol<sup>-1</sup> for the transition  $\sigma(\text{C13} - \text{H16}) \rightarrow \sigma^*(\text{C12} - \text{O17})$  (Table S17 - supplementary material).

For the mPW1PW91 method, the higher value of the stabilization energy is 193.42 kcal.mol<sup>-1</sup> for the transition  $\pi^*(\text{C2} - \text{C6}) \rightarrow \pi^*(\text{C1} - \text{C3})$ . This value differs from the B3LYP method of about 3.02 kcal.mol<sup>-1</sup>. Nevertheless, this result shows how strong is the delocalization of the electronic density in the phenyl ring. According to Table S18 (supplementary material), the values of the stabilization energy for the  $\pi \rightarrow \pi^*$  transitions are in the range 16.43 kcal.mol<sup>-1</sup> for  $\pi(\text{C2} - \text{C6}) \rightarrow \pi^*(\text{C1} - \text{C3})$  to 26.43 kcal.mol<sup>-1</sup> for  $\pi(\text{C2} - \text{C6}) \rightarrow \pi^*(\text{C4} - \text{C5})$ . The weak stabilization energies due to the  $\sigma(\text{C4} - \text{C19})$  are 2.29 kcal.mol<sup>-1</sup> ( $\sigma^* \text{C1} - \text{C3}$ ), 2.30 kcal.mol<sup>-1</sup> ( $\sigma^* \text{C3} - \text{C4}$ ) and 2.45 kcal.mol<sup>-1</sup> ( $\sigma^* \text{C4} - \text{C5}$ ). The phenyl ring of the 4-fluorine-phenyl group shows a moderate stabilization from 18.42 kcal.mol<sup>-1</sup> ( $\pi \text{C29} - \text{C30} \rightarrow \pi^* \text{C26} - \text{C28}$ ) to 23.42 kcal.mol<sup>-1</sup> ( $\pi \text{C29} - \text{C30} \rightarrow \pi^* \text{C24} - \text{C27}$ ). The  $\sigma$ -bond between the carbon C30 and fluorine F35 shows a value of 1.66 kcal.mol<sup>-1</sup> to donate electronic density to the  $\sigma^*(\text{C28} - \text{H33})$ . The  $\sigma(\text{N11} - \text{H18})$  bond donate its electronic density to  $\sigma^*(\text{C1} - \text{C2})$  and  $\sigma^*(\text{C12} - \text{O17})$  with the energy of 4.30 kcal.mol<sup>-1</sup> and 4.72 kcal.mol<sup>-1</sup> respectively. The lone pairs from the nitrogen and oxygen atoms participate to the following charge transfer process: LP(N11)  $\rightarrow$   $\pi^*(\text{C12} - \text{O17})$ , LP(O17)  $\rightarrow$   $\sigma^*(\text{N11} - \text{C12})$ , LP(O17)  $\rightarrow$   $\sigma^*(\text{C12} - \text{C13})$ , LP(O21)  $\rightarrow$   $\sigma^*(\text{C4} - \text{C19})$ , and LP(O21)  $\rightarrow$   $\sigma^*(\text{C19} - \text{C20})$  which the energy values are respectively 62.85 kcal.mol<sup>-1</sup>, 25.67 kcal.mol<sup>-1</sup>, 18.43 kcal.mol<sup>-1</sup>, 19.08 kcal.mol<sup>-1</sup> and 19.25 kcal.mol<sup>-1</sup>. The  $\pi(\text{C20} - \text{C22})$  can interact with the  $\pi^*(\text{C19} - \text{O21})$  and  $\pi^*(\text{C24} - \text{C27})$  with stabilization energy of 22.87 kcal.mol<sup>-1</sup> and 11.91 kcal.mol<sup>-1</sup>, thus the electronic

density of the  $\pi$ -bond can spread over the resonance effect that reduces the total energy of the molecule. The  $\sigma$ -bonds C20 – H23 and C22 – H25 can slightly stabilize respectively the  $\sigma^*(\text{C22} - \text{H25})$  and  $\sigma^*(\text{C20} - \text{H23})$  with the energy of 4.47 kcal.mol<sup>-1</sup> and 5.73 kcal.mol<sup>-1</sup>. Also, those bonds can interact with the  $\sigma^*(\text{C20} - \text{C22})$  with the energy of 1.73 kcal.mol<sup>-1</sup> and 1.36 kcal.mol<sup>-1</sup>. The methyl group is responsible for a weak donation of charge to the carbonyl (C12=O17) group with the transitions  $\sigma(\text{C13} - \text{H14}) \rightarrow \sigma^*(\text{C12} - \text{O17})$  with 4.41 kcal.mol<sup>-1</sup> and  $\sigma(\text{C13} - \text{H16}) \rightarrow \pi^*(\text{C12} - \text{O17})$  with 5.63 kcal.mol<sup>-1</sup>.

For the M06-2X method (Table S19), the higher value of the stabilization energy is for the transition of the lone pair of the nitrogen atom (N11) to the  $\pi^*(\text{C12} - \text{O17})$  with the energy of 72.62 kcal.mol<sup>-1</sup>. This result shows a great difference from the other methods. The delocalization of the  $\pi$  electrons occurs due to the  $\pi \rightarrow \pi^*$  as follow: C1 – C2  $\rightarrow$  C3 – C4 (35.76 kcal.mol<sup>-1</sup>); C1 – C2  $\rightarrow$  C5 – C6 (23.11 kcal.mol<sup>-1</sup>); C3 – C4  $\rightarrow$  C1 – C2 (25.01 kcal.mol<sup>-1</sup>); C3 – C4  $\rightarrow$  C5 – C6 (31.44 kcal.mol<sup>-1</sup>); C3 – C4  $\rightarrow$  C19 – O21 (21.79 kcal.mol<sup>-1</sup>); C5 – C6  $\rightarrow$  C1 – C2 (30.08 kcal.mol<sup>-1</sup>); C5 – C6  $\rightarrow$  C3 – C4 (23.11 kcal.mol<sup>-1</sup>). There is a weak donation of electronic density through the 4-acetamido-phenyl ring from the  $\sigma(\text{C4} - \text{C19})$  to the  $\sigma^*(\text{C1} - \text{C3})$ ,  $\sigma^*(\text{C3} - \text{C4})$  and  $\sigma^*(\text{C4} - \text{C5})$  with stabilization energy of 2.43 kcal.mol<sup>-1</sup>, 2.53 kcal.mol<sup>-1</sup> and 2.58 kcal.mol<sup>-1</sup> respectively. The 4-fluorine-phenyl ring shows a delocalization of the  $\pi$  electronic density over the  $\pi^*$  molecular orbitals of the carbon atoms of the ring and the C20=C22: C24 – C27  $\rightarrow$  C20 – C22 (19.37 kcal.mol<sup>-1</sup>); C24 – C27  $\rightarrow$  C26 – C28 (29.02 kcal.mol<sup>-1</sup>); C26 – C28  $\rightarrow$  C24 – C27 (24.52 kcal.mol<sup>-1</sup>); C29 – C30  $\rightarrow$  C24 – C27 (31.26 kcal.mol<sup>-1</sup>); C29 – C30  $\rightarrow$  C26 – C28 (24.32 kcal.mol<sup>-1</sup>). The lone pair of the nitrogen atom is responsible for the highest stabilization energy however, this non-bonding pair can also interact with the  $\pi^*(\text{C1} - \text{C2})$  with the energy of 44.16 kcal.mol<sup>-1</sup>. The lone pairs of the oxygen atom O17 donate negative charge to the  $\sigma^*(\text{N11} - \text{C12})$  (29.71 kcal.mol<sup>-1</sup>) and  $\sigma^*(\text{C12} - \text{C13})$  (20.82 kcal.mol<sup>-1</sup>). The lone pair of the O21 interact with the  $\sigma^*(\text{C4} - \text{C19})$  (21.67 kcal.mol<sup>-1</sup>) and  $\sigma^*(\text{C19} - \text{C20})$  (22.19 kcal.mol<sup>-1</sup>). The  $\pi(\text{C20} - \text{C22})$  can stabilize the  $\pi^*(\text{C19} - \text{O21})$  (24.28 kcal.mol<sup>-1</sup>) and  $\pi^*(\text{C24} - \text{C27})$  (12.19 kcal.mol<sup>-1</sup>). The  $\sigma$ -bonds between the C20 – H23 and C22 – H25 can spread the electronic density through hyperconjugation respectively with the  $\sigma^*(\text{C20} - \text{C22})$  (2.14 kcal.mol<sup>-1</sup>);  $\sigma^*(\text{C22} - \text{H25})$  (4.95 kcal.mol<sup>-1</sup>) and  $\sigma^*(\text{C20} - \text{H23})$  (6.27 kcal.mol<sup>-1</sup>);  $\sigma^*(\text{C24} - \text{C26})$  (5.09 kcal.mol<sup>-1</sup>). The methyl group can donate electrons as the following transition:  $\sigma(\text{C13} - \text{H14}) \rightarrow \sigma^*(\text{C12} - \text{O17})$  (3.99 kcal.mol<sup>-1</sup>);  $\sigma(\text{C13} - \text{H15}) \rightarrow \sigma^*(\text{N11} - \text{C12})$  (4.42 kcal.mol<sup>-1</sup>);  $\sigma(\text{C13} - \text{H16}) \rightarrow \sigma^*(\text{C12} - \text{O17})$  (7.59 kcal.mol<sup>-1</sup>) (Table S19 -supplementary material). Despite the M06-2X did not predict any charge transfer process with

a large value of  $\Delta E_{ij}$ , all the energies computed for this method are higher than for the others.

All the results exhibit that the PAAPFBA molecule has delocalized electronic density which agrees with the NLO properties, the FMO spread over the entire molecule, and the difference of each atom behavior obtained in the Fukui functions analysis.

#### 4.9 Antioxidant activity

The experimental data from the DPPH free radical scan reveal that the PAAPFBA chalcone exhibit a moderate antioxidant activity of 50.92% when compared to the (+) control of ascorbic acid. According to the results of the Fukui functions and the Condensed Fukui functions show that there are several atoms are susceptible to a radical attack. Based on these results and in the NBO analysis, to understand how the PAAPFBA molecule can behave as an antioxidant compound the atoms N11, C13, C20, and C22 were chosen to compute the parameters (equations 4 – 8) for each antioxidant mechanisms. The antioxidant mechanisms were calculated using the DFT methods (B3LYP/mPW1PW91/M06-2X) at 6-311++G(d,p) levels of theory. Each enthalpy value was computed at  $T = 298.15$  K and 1 atm of pressure. The results of the BDE, IP, PDE, PA and ETE parameters for the bonds N11 – H18, C13 – H, C20 – H23 and C22 – H 25 are shown in Table 1.

For the HAT mechanism, the lower value of the BDE ( $96.98 \text{ kcal mol}^{-1}$  for the B3LYP,  $96.79 \text{ kcal mol}^{-1}$  for the mPW1PW91, and  $96.63 \text{ kcal mol}^{-1}$  for the M06-2X) is for the radical attack on the carbon atom (C13) of the methyl group. These results agree with the Condensed Fukui functions, which predicts that the C13 is the most atom susceptible to a radical attack due to the highest value of the  $f^0$  for the three DFT methods. Also, it can be seen from the NBO analysis, the stabilization due to the  $\sigma$ -bonds from the methyl is very low when it is comparing to the delocalization of the other bonds, thus the methyl can be the best target for a radical to react. The carbon C20 shows the highest value of the BDE ( $105.97 \text{ kcal mol}^{-1}$  for the B3LYP,  $105.82 \text{ kcal mol}^{-1}$  for the mPW1PW91, and  $105.53 \text{ kcal mol}^{-1}$  for the M06-2X) due to the lack of the electronic delocalization process, the molecular geometry change when the bond C20 – H23 break, thus this radical is the less stable. The nitrogen N11 (BDE =  $96.98 \text{ kcal mol}^{-1}$  for the B3LYP,  $98.77 \text{ kcal mol}^{-1}$  for the mPW1PW91, and  $99.99 \text{ kcal mol}^{-1}$  for the M06-2X) may present stabilization of the radical structure by the resonance effect, but it has BDE values higher than the BDE values for the methyl group because more atoms with high electronegativity (oxygen and nitrogen) will have electron deficiency. The carbon C22 (BDE =  $104.36 \text{ kcal mol}^{-1}$  for the B3LYP,  $104.36 \text{ kcal mol}^{-1}$  for the mPW1PW91, and  $105.13 \text{ kcal mol}^{-1}$  for the M06-2X), although it can also stabilize the radical structure through the resonance

effect, this relocation would occur with the phenyl ring of the 4-fluorophenyl group, in this case, this ring has an electronic deficiency because it has a ligand with high electronegativity, the which hinders the resonant effect and the radical is not as stable, thus showing high BDE values.

For the SET-PT mechanism, the first step is equal for the four bonds in each DFT method (IP = 125.589 kcal.mol<sup>-1</sup> for the B3LYP, 126.958 kcal.mol<sup>-1</sup> for the mPW1PW91, and 131.699 kcal.mol<sup>-1</sup> for the M06-2X) because it is the loss of the electron by the molecule. The second step is the loss of the proton  $H^+$  for each bond: The methyl group shows the lower value of the PDE in each method (16.064 kcal.mol<sup>-1</sup> for the B3LYP, 14.499 kcal.mol<sup>-1</sup> for the mPW1PW91, and 9.605 kcal.mol<sup>-1</sup> for the M06-2X) which agree with the HAT mechanism, but the PDE for the nitrogen N11 is very similar to the methyl (16.583 kcal.mol<sup>-1</sup> for the B3LYP, 16.483 kcal.mol<sup>-1</sup> for the mPW1PW91, and 12.962 kcal.mol<sup>-1</sup> for the M06-2X) since they have a similar effect of electronic delocalization when the radical is formed. Also, the bond N11 – H18 is shorter than the C13 – H bond, thus more energy is needed to break the N – H bond which explains the slightly higher value of the PDE for the nitrogen. The carbons C20 and C22 show the PDE value of 25.050 kcal.mol<sup>-1</sup> and 23.440 kcal.mol<sup>-1</sup> for the B3LYP; 23.537 kcal.mol<sup>-1</sup> and 22.075 kcal.mol<sup>-1</sup> for the mPW1PW91; and 18.498 kcal.mol<sup>-1</sup> and 18.103 kcal.mol<sup>-1</sup> for the M06-2X respectively. These values reflect in the formation of the radical: for the C20 it is not possible the stabilization due to the resonance effect, thus the radical for the C20 is less stable and it shows the highest total energy (IP + PDE) for the SET-PT mechanism (150.639 kcal.mol<sup>-1</sup> for the B3LYP, 150.495 kcal.mol<sup>-1</sup> for the mPW1PW91, and 150.197 kcal.mol<sup>-1</sup> for the M06-2X) differing from the methyl of 8.986 kcal.mol<sup>-1</sup>, for the nitrogen of 8.467 kcal.mol<sup>-1</sup> and the C22 atom of 1.610 kcal.mol<sup>-1</sup> (B3LYP); for the methyl 9.038 kcal.mol<sup>-1</sup>, for the nitrogen of 7.054 kcal.mol<sup>-1</sup> and the C22 atom of 1.462 kcal.mol<sup>-1</sup> (mPW1PW91); for the methyl 8.893 kcal.mol<sup>-1</sup>, for the nitrogen of 5.536 kcal.mol<sup>-1</sup> and the C22 atom of 0.395 kcal.mol<sup>-1</sup> (M06-2X).

For the SPLET mechanism, the nitrogen N11 exhibited the lower value of the PA (50.500 kcal.mol<sup>-1</sup> for the B3LYP, 51.935 kcal.mol<sup>-1</sup> for the mPW1PW91, and 49.074 kcal.mol<sup>-1</sup> for the M06-2X). For the four atoms chosen, the nitrogen can accommodate better the negative charge in the formation of the anion in the first step of this mechanism. When the carbanion is formed in the methyl group (PA = 66.148 kcal.mol<sup>-1</sup> for the B3LYP, 67.629 kcal.mol<sup>-1</sup> for the mPW1PW91, and 64.975 kcal.mol<sup>-1</sup> for the M06-2X), this negative charge can be delocalized over the carbonyl group (C12=O17) with part of the extra charge spread over the oxygen atom. The carbon C20 (PA = 73.200 kcal.mol<sup>-1</sup> for the B3LYP, 74.212 kcal.mol<sup>-1</sup> for the mPW1PW91, and 70.301 kcal.mol<sup>-1</sup> for the M06-2X) shows the PA value lower than the carbon C22 (PA = 88.426 kcal.mol<sup>-1</sup> for the B3LYP, 89.463 kcal.mol<sup>-1</sup> for the mPW1PW91, and 84.546 kcal.mol<sup>-1</sup>

<sup>1</sup> for the M06-2X) since in C20 the delocalization occurs with the carbonyl group (C19=O21) which spread the negative charge over the oxygen atom, but the C22 can spread the charge over carbons atoms present in the 4-fluorine-phenyl ring. However, the loss of the electron in the second step is more difficult to the nitrogen atom due to the higher stability of the anion structure which corresponds to the higher value of ETE (91.672 kcal.mol<sup>-1</sup> for the B3LYP, 91.507 kcal.mol<sup>-1</sup> for the mPW1PW91, and 95.586 kcal.mol<sup>-1</sup> for the M06-2X). The carbon C22 shows the lower value of ETE (60.603 kcal.mol<sup>-1</sup> for the B3LYP, 59.571 kcal.mol<sup>-1</sup> for the mPW1PW91, and 65.255 kcal.mol<sup>-1</sup> for the M06-2X) due to the stabilization of the radical when compared with the anion. The carbon atoms C13 and C20 exhibited similar ETE values of 75.504 kcal.mol<sup>-1</sup> and 77.439 kcal.mol<sup>-1</sup> for the B3LYP, 73.828 kcal.mol<sup>-1</sup> and 76.283 kcal.mol<sup>-1</sup> for the mPW1PW91, and 76.328 kcal.mol<sup>-1</sup> and 79.896 kcal.mol<sup>-1</sup> for the M06-2X respectively. The total energy change (PA + ETE) of the mechanism increases in the order C13 < N11 < C22 < C20. This tendency is the same for all the three mechanisms and agreed with the previous results of the Fukui functions and NBO.

The theoretical antioxidant activity analysis shows that the methyl group is the most susceptible to the radical attack due to the lower values of the enthalpies for each mechanism. The values of the global parameters (BDE; IP + PDE; PA + ETE) used in this discussion are higher than 80 kcal.mol<sup>-1</sup>, thus it is expected that the PAAPFBA molecule exhibits a moderate antioxidant activity. The most probable mechanism to explain the behavior of the title chalcone is the Hydrogen Atom Transfer (HAT) due to the lower values of the enthalpies. All three DFT methods used in this calculation present similar values of the thermodynamics parameters, therefore the antioxidant activity can be evaluated independently of the method chosen.

Table 1 – Calculated enthalpy parameters: the Bond Dissociation Energy (BDE), the Ionization Potential (IP) and the Proton Dissociation Enthalpy (PDE), the Proton Affinity (PA), and the Electron Transfer Enthalpy (ETE) for the PAAPFBA chalcone using the B3LYP/mPW1PW91/M06-2X at 6-311++G(d,p) levels of theory.

<b>Bond</b>	<b>BDE (kcal.mol<sup>-1</sup>)</b>	<b>IP (kcal.mol<sup>-1</sup>)</b>	<b>PDE (kcal.mol<sup>-1</sup>)</b>	<b>PA (kcal.mol<sup>-1</sup>)</b>	<b>ETE (kcal.mol<sup>-1</sup>)</b>	<b>DFT Method</b>
N11 – H18	97.50	125.589	16.583	50.500	91.672	B3LYP
C20 – H23	105.97	125.589	25.050	73.200	77.439	
C22 – H25	104.36	125.589	23.440	88.426	60.603	
C13 – H	96.98	125.589	16.064	66.148	75.504	



N11 – H18	98.77	126.958	16.483	51.935	91.507	mPW1PW91
C20 – H23	105.82	126.958	23.537	74.212	76.283	
C22 – H25	104.36	126.958	22.075	89.463	59.571	
C13 – H	96.79	126.958	14.499	67.629	73.828	
N11 – H18	99.99	131.699	12.962	49.074	95.586	M06-2X
C20 – H23	105.53	131.699	18.498	70.301	79.896	
C22 – H25	105.13	131.699	18.103	84.546	65.255	
C13 – H	96.63	131.699	9.605	64.975	76.328	

## 5 Conclusion

The DFT methods were capable to achieve the global minimum of the energy for the PAAPFBA molecule. Also, they predicted that the molecule is not planar, in which the M06-2X method showed the higher value of the distortion angle. According to the experimental results and the comparison with the results of other calculations, the PAAPFBA molecule was well-described by all DFT methods.

The thermodynamics properties predicted were similar independent of the method used. Also, the infrared fundamental vibrational modes were in excellent agreement with the experimental data regardless of the method. This fact was observed by the R-squared ( $R^2$ ) which are respectively 0.99791 (B3LYP), 0.99779 (mPW1PW91), and 0.99835 (M06-2X). The  $^1\text{H}$  and  $^{13}\text{C}$  NMR also exhibited an excellent agreement with the experimental data with R-squared ( $R^2$ ) of 0.99865 (B3LYP), 0.99860 (mPW1PW91) and 0.99844 (M06-2X). The nonlinear optical properties predicted by the DFT methods show that the PAAPFBA molecule can be used as NLO material because of the higher values of the dipole moment, polarizability, and static first hyperpolarizability. Although the Frontier Molecular Orbital (FMO) analysis predicted a similar electronic density distribution of the HOMO and the LUMO among the methods, the quantum molecular descriptors show very different values when the method is shifted due to the change of the mathematical approximation within to the method itself.

To understand how each atom behavior during a chemical reaction, the Electronic Fukui functions, the Condensed Fukui functions, the local descriptors, and the Natural Bond Orbitals (NBO) were calculated. The B3LYP and mPW1PW91 methods could describe the molecule very similarly, however, the M06-2X illustrates differences in the reactive sites (radical attack) and the electronic density was predicted to be more delocalized (higher value of the stabilization energy). According to those results, the antioxidant activity was carried out with the DFT methods to investigate the three mechanisms: HAT, SET-PT, and SLET. All the global

thermodynamic parameters computed (BDE, IP + PDE, PA + ETE) were higher than 80 kcal.mol<sup>-1</sup> for every method used, which explains the moderate experimental value of 50.92%. The mechanism thermodynamically favorable is the Hydrogen Atom Transfer (HAT) using each method. Therefore, all the DFT methods (B3LYP, mPW1PW91, and M06-2X) used in this work are in excellent agreement to a structural, electronic, nonlinear optical, and antioxidant activity characterization.

## Acknowledgment

This study was financed by two Brazilian agencies: Coordenação de Aperfeiçoamento de Pessoal de Nível Superior (CAPES) and Conselho Nacional de Desenvolvimento Científico e Tecnológico (CNPq). Leonardo P. da Silva thanks CAPES for his scholarship. Francisco Wagner Q. Almeida-Neto thanks CNPq for his grant. Pedro de Lima-Neto thanks the financial support received from CNPq project: 304152/2018-8. The authors also thanks Centro Nacional de Processamento de Alto Desempenho (CENAPAD) of the Federal University of Ceará (UFC) for providing computational resources.

## Reference

- [1] M.N. Gomes, E.N. Muratov, M. Pereira, J.C. Peixoto, L.P. Rosseto, P.V.L. Cravo, C.H. Andrade, B.J. Neves, Chalcone Derivatives: Promising Starting Points for Drug Design, (n.d.). doi:10.3390/molecules22081210.
- [2] S.F. Nielsen, S.B. Christensen, G. Cruciani, A. Kharazmi, T. Liljefors, Antileishmanial Chalcones : Statistical Design , Synthesis , and Three-Dimensional Quantitative Structure - Activity Relationship Analysis, (1998) 4819–4832.
- [3] R. Selvam, The effect of anthracene-based chalcone derivatives in the resazurin dye reduction assay mechanisms for the investigation of Gram-positive and Gram-negative bacterial and fungal infection †, *New J. Chem.* (2017). doi:10.1039/C7NJ04125J.
- [4] Y.R. Prasad, P.R. Kumar, C.H.A. Deepti, Synthesis and Antimicrobial Activity of Some Novel Chalcones of 2-Hydroxy -1-Acetonaphthone and 3-Acetyl Coumarin, 3 (2006) 236–241.
- [5] B.P. Bandgar, S.A. Patil, B.L. Korbadi, S.H. Nile, C.N. Khobragade, Synthesis and biological evaluation of b -chloro vinyl chalcones as inhibitors of TNF- a and IL-6 with antimicrobial activity, *Eur. J. Med. Chem.* 45 (2010) 2629–2633. doi:10.1016/j.ejmech.2010.01.050.

- [6] M. Liu, P. Wilairat, S.L. Croft, A.L. Tan, M. Go, Structure – Activity Relationships of Antileishmanial and Antimalarial Chalcones, 11 (2003) 2729–2738. doi:10.1016/S0968-0896(03)00233-5.
- [7] H. Hegde, R.K. Sinha, S.D. Kulkarni, N.S. Shetty, Journal of Photochemistry & Photobiology A : Chemistry Synthesis , photophysical and DFT studies of naphthyl chalcone and nicotinonitrile derivatives, J. Photochem. Photobiol. A Chem. 389 (2020) 112222. doi:10.1016/j.jphotochem.2019.112222.
- [8] C. Thirumurugan, P. Vadivel, A. Lalitha, S. Lakshmanan, Synthesis , characterization of novel quinoline-2- carboxamide based chalcone derivatives and their molecular docking , photochemical studies, Synth. Commun. 0 (2020) 1–9. doi:10.1080/00397911.2020.1720737.
- [9] S. Khanapure, M. Jagadale, P. Bansode, P. Choudhari, Anticancer activity of ruthenoceny chalcones and their molecular docking studies, J. Mol. Struct. 1173 (2018) 142–147. doi:10.1016/j.molstruc.2018.06.091.
- [10] D. Kar, S. Kumar, V. Asati, S. Kumar, European Journal of Medicinal Chemistry Perspectives of medicinally privileged chalcone based metal coordination compounds for biomedical applications, Eur. J. Med. Chem. 174 (2019) 142–158. doi:10.1016/j.ejmech.2019.04.032.
- [11] P. Singh, A. Anand, V. Kumar, European Journal of Medicinal Chemistry Recent developments in biological activities of chalcones : A mini review, Eur. J. Med. Chem. 85 (2014) 758–777. doi:10.1016/j.ejmech.2014.08.033.
- [12] R. Arif, M. Rana, S. Yasmeen, S. Khan, M. Abid, M.S. Khan, Facile synthesis of chalcone derivatives as antibacterial agents : Synthesis , DNA binding , molecular docking , DFT and antioxidant studies, J. Mol. Struct. 1208 (2020) 127905. doi:10.1016/j.molstruc.2020.127905.
- [13] R. Ustabaş, N. Süleymanoğlu, N. Özdemir, N. Kahriman, E. Bektaş, Y. Ünver, New Chalcone Derivative: Synthesis, Characterization, Computational Studies and Antioxidant Activity, (2020) 46–53. doi:10.2174/1570178616666181130163115.
- [14] M.N. Uddin, M.N.H. Knock, M. Uzzaman, M.M.H. Bhuiyan, A.F.M. Sanaullah, W. Shumi, H.M. Sadrul, Amin, Microwave assisted synthesis , characterization , molecular docking and pharmacological activities of some new 2-O-hydroxychalcone derivatives, J. Mol. Struct. 1206 (2020) 127678. doi:10.1016/j.molstruc.2020.127678.
- [15] E. Polo, N. Ibarra-arellano, L. Prent-peñaloza, A. Morales-bayuelo, J. Henao, A. Galdámez, M. Gutiérrez, Bioorganic Chemistry Ultrasound-assisted synthesis of novel

- chalcone , heterochalcone and bis- chalcone derivatives and the evaluation of their antioxidant properties and as acetylcholinesterase inhibitors, *Bioorg. Chem.* 90 (2019) 103034. doi:10.1016/j.bioorg.2019.103034.
- [16] M.K.A. Ferreira, A.W. da Silva, F.C.O. Silva, C.L.A. Holanda, S.M. Barroso, J. dos R. Lima, A.E. Vieira Neto, A.R. Campos, P.N. Bandeira, H.S. dos Santos, T.L.G. de Lemos, S.M.C. Siqueira, F.E.A. Magalhães, J.E.S.A. de Menezes, Anxiolytic-like effect of chalcone N- $\{(4'-(E)-3-(4\text{-fluorophenyl})-1\text{-phenyl})\text{prop-2-en-1-one}\}$  acetamide on adult zebrafish (*Danio rerio*): Involvement of the GABAergic system, *Behav. Brain Res.* 374 (2019) 3–8. doi:10.1016/j.bbr.2019.03.040.
- [17] P. Ramesh, M. Lydia Caroline, S. Muthu, B. Narayana, M. Raja, S. Aayisha, Spectroscopic and DFT studies, structural determination, chemical properties and molecular docking of 1-(3-bromo-2-thienyl)-3-[4-(dimethylamino)-phenyl]prop-2-en-1-one, *J. Mol. Struct.* 1200 (2020) 127123. doi:10.1016/j.molstruc.2019.127123.
- [18] A. Thamarai, R. Vadamar, M. Raja, S. Muthu, B. Narayana, P. Ramesh, S. Sevvanthi, S. Aayisha, Molecular structure conformational analyses, solvent-electronic studies through theoretical studies and biological profiling of (2E)-1-(3-bromo-2-thienyl)-3-(4-chlorophenyl)-prop-2-en-1-one, *J. Mol. Struct.* 1202 (2020) 127349. doi:10.1016/j.molstruc.2019.127349.
- [19] A. Chaouiki, H. Lgaz, R. Salghi, M. Cha, H. Oudda, K.S. Bhat, Assessing the impact of electron-donating-substituted chalcones on inhibition of mild steel corrosion in HCl solution : Experimental results and molecular-level insights, 588 (2020). doi:10.1016/j.colsurfa.2019.124366.
- [20] D. Coskun, B. Gunduz, M. Fatih, Synthesis , characterization and significant optoelectronic parameters of 1- ( 7-methoxy-1-benzofuran-2-yl ) substituted chalcone derivatives, *J. Mol. Struct.* 1178 (2019) 261–267. doi:10.1016/j.molstruc.2018.10.043.
- [21] A. Praveen, A. Jayarama, H.J. Ravindra, *Materials Today : Proceedings Investigation of physical , spectral and thermal properties of a dimethoxy substituted chalcone for optoelectronic device applications*, *Mater. Today Proc.* (2020). doi:10.1016/j.matpr.2020.02.543.
- [22] J.M.F. Custodio, C. Noda, C. Valverde, F.A.P. Osório, H.B. Napolitano, Enhanced nonlinear optics properties of a bromine chalcone from a novel polymorph, *Chem. Phys. Lett.* 738 (2020) 136852. doi:10.1016/j.cplett.2019.136852.
- [23] S. Kaya, H. Gökce, T. Arslan, G. Alpaslan, Synthesis, spectroscopic characterization, DFT computations, nonlinear optical profile and molecular docking study of a novel chalcone derivative, *J. Mol. Struct.* 1202 (2020) 1–11.

doi:10.1016/j.molstruc.2019.127270.

- [24] S. Shukla, A. Srivastava, K. Srivastava, P. Tandon, J. Jamalis, R.B. Singh, Non-covalent interactions and spectroscopic study of chalcone derivative 1-(4-chlorophenyl)-3-(5-methylfuran-2-yl) prop-2-en-1-one, *J. Mol. Struct.* 1201 (2020) 127145. doi:10.1016/j.molstruc.2019.127145.
- [25] A.D. Becke, Density functional thermochemistry. I. The effect of the exchange only gradient correction, *J. Chem. Phys.* 96 (1992) 2155–2160. doi:10.1063/1.462066.
- [26] C. Lee, W. Yang, R.G. Parr, Development of the Colle-Salvetti correlation-energy formula into a functional of the electron density, *Phys. Rev. B.* 37 (1988) 785–789. doi:10.1103/PhysRevB.37.785.
- [27] K. Burke, J.P. Perdew, Y. Wang, Derivation of a Generalized Gradient Approximation: The PW91 Density Functional, *Electron. Density Funct. Theory.* (1998) 81–111. doi:10.1007/978-1-4899-0316-7\_7.
- [28] C. Adamo, V. Barone, Exchange functionals with improved long-range behavior and adiabatic connection methods without adjustable parameters: The mPW and mPW1PW models, *J. Chem. Phys.* 108 (1998) 664–675. doi:10.1063/1.475428.
- [29] Y. Zhao, D.G. Truhlar, The M06 suite of density functionals for main group thermochemistry, thermochemical kinetics, noncovalent interactions, excited states, and transition elements: Two new functionals and systematic testing of four M06-class functionals and 12 other function, *Theor. Chem. Acc.* 120 (2008) 215–241. doi:10.1007/s00214-007-0310-x.
- [30] M.J. Frisch, G.W. Trucks, H.B. Schlegel, G.E. Scuseria, M.A. Robb, J.R. Cheeseman, G. Scalmani, V. Barone, G.A. Petersson, H. Nakatsuji, X. Li, M. Caricato, A. Marenich, J. Bloino, B.G. Janesko, R. Gomperts, B. Mennucci, H.P. Hratchian, J. V. Ortiz, A.F. Izmaylov, J.L. Sonnenberg, D. Williams-Young, F. Ding, F. Lipparini, F. Egidi, J. Goings, B. Peng, A. Petrone, T. Henderson, D. Ranasinghe, V.G. Zakrzewski, J. Gao, N. Rega, G. Zheng, W. Liang, M. Hada, M. Ehara, K. Toyota, R. Fukuda, J. Hasegawa, M. Ishida, T. Nakajima, Y. Honda, O. Kitao, H. Nakai, T. Vreven, K. Throssell, J.A. Montgomery, J.E. Peralta, F. Ogliaro, M. Bearpark, J.J. Heyd, E. Brothers, K.N. Kudin, V.N. Staroverov, T. Keith, R. Kobayashi, J. Normand, K. Raghavachari, A. Rendell, J.C. Burant, S.S. Iyengar, J. Tomasi, M. Cossi, J.M. Millam, M. Klene, C. Adamo, R. Cammi, J.W. Ochterski, R.L. Martin, K. Morokuma, O. Farkas, J.B. Foresman, D.J. Fox, *Gaussian 09, Revision A.02*, (2009).
- [31] R. Dennington, T. Keith, J. Millam, *GaussView, Version 5*, (2009).

- [32] J. Tomasi, R. Cammi, Remarks on the Use of the Apparent Surface Charges (ASC) Methods in Solvation Problems: Iterative versus Matrix-Inversion Procedures and Renormalization of the Apparent Charges, *J. Comput. Chem.* 16 (1995) 1449–1458.
- [33] B. Mennucci, E. Cancès, J. Tomasi, Evaluation of solvent effects in isotropic and anisotropic dielectrics and in ionic solutions with a unified integral equation method: Theoretical bases, computational implementation, and numerical applications, *J. Phys. Chem. B.* 101 (1997) 10506–10517. doi:10.1021/jp971959k.
- [34] E. Cancès, B. Mennucci, J. Tomasi, A new integral equation formalism for the polarizable continuum model: Theoretical background and applications to Isotropic and anisotropic dielectrics, *J. Chem. Phys.* 107 (1997) 3032–3041. doi:10.1063/1.474659.
- [35] Michal, H. Jamroz, *Vibrational Energy Distribution Analysis VEDA 4*, (2010).
- [36] R. McWeeny, Perturbation Theory for the Fock-Dirac Density Matrix, *Phys. Rev.* 126 (1962) 1028–1034. doi:10.1103/PhysRev.126.1028.
- [37] R. Ditchfield, Self-consistent perturbation theory of diamagnetism I. A gauge-invariant LCAO method for N.M.R. Chemical shifts, *Mol. Phys.* 27 (1974) 789–807. doi:10.1080/00268977400100711.
- [38] K. Wolinski, J.F. Hinton, P. Pulay, Efficient Implementation of the Gauge-Independent Atomic Orbital Method for NMR Chemical Shift Calculations, *J. Am. Chem. Soc.* 112 (1990) 8251–8260. doi:10.1021/ja00179a005.
- [39] J.R. Cheeseman, A comparison of models for calculating nuclear magnetic resonance shielding tensors, *J. Chem. Phys.* 104 (1996) 5497–5509. doi:10.1063/1.471789.
- [40] T. Yanai, D.P. Tew, N.C. Handy, A new hybrid exchange-correlation functional using the Coulomb-attenuating method (CAM-B3LYP), *Chem. Phys. Lett.* 393 (2004) 51–57. doi:10.1016/j.cplett.2004.06.011.
- [41] H. Iikura, T. Tsuneda, T. Yanai, K. Hirao, A long-range correction scheme for generalized-gradient-approximation exchange functionals, *J. Chem. Phys.* 115 (2001) 3540–3544. doi:10.1063/1.1383587.
- [42] J. Da Chai, M. Head-Gordon, Long-range corrected hybrid density functionals with damped atom-atom dispersion corrections, *Phys. Chem. Chem. Phys.* 10 (2008) 6615–6620. doi:10.1039/b810189b.
- [43] N. Kosar, K. Shehzadi, K. Ayub, T. Mahmood, Theoretical study on novel superalkali doped graphdiyne complexes: Unique approach for the enhancement of electronic and

- nonlinear optical response, *J. Mol. Graph. Model.* 97 (2020) 107573. doi:10.1016/j.jmglm.2020.107573.
- [44] H. Sajid, K. Ayub, T. Mahmood, Exceptionally high NLO response and deep ultraviolet transparency of superalkali doped macrocyclic oligofuran rings, *New J. Chem.* 44 (2020) 2609–2618. doi:10.1039/c9nj05065e.
- [45] H. Tahir, N. Kosar, K. Ayub, T. Mahmood, Outstanding NLO response of thermodynamically stable single and multiple alkaline earth metals doped C<sub>20</sub> fullerene, *J. Mol. Liq.* 305 (2020) 112875. doi:10.1016/j.molliq.2020.112875.
- [46] A. Boruah, M.P. Borpuzari, R. Kar, Performance of Range Separated Density Functional in Solvent Continuum: Tuning Long-range Hartree–Fock Exchange for Improved Orbital Energies, *J. Comput. Chem.* 41 (2020) 295–304. doi:10.1002/jcc.26101.
- [47] S. Munsif, Maria, S. Khan, A. Ali, M.A. Gilani, J. Iqbal, R. Ludwig, K. Ayub, Remarkable nonlinear optical response of alkali metal doped aluminum phosphide and boron phosphide nanoclusters, *Elsevier B.V.*, 2018. doi:10.1016/j.molliq.2018.08.121.
- [48] A.R. Allouche, Gabedita - A graphical user interface for computational chemistry softwares, *J. Comput. Chem.* 32 (2010) 174–182. doi:10.1002/jcc.21600.
- [49] E.D. Gledening, A.E. Reed, J.E. Carpenter, F. Weinhold, NBO Version 3.1, (n.d.).
- [50] Y. Xue, Y. Zheng, L. An, Y. Dou, Y. Liu, Density functional theory study of the structure – antioxidant activity of polyphenolic deoxybenzoins, *FOOD Chem.* 151 (2014) 198–206. doi:10.1016/j.foodchem.2013.11.064.
- [51] J. Rimarcík, V. Lukeš, E. Klein, M. Ilcin, *Journal of Molecular Structure* : THEOCHEM Study of the solvent effect on the enthalpies of homolytic and heterolytic N – H bond cleavage in p -phenylenediamine and tetracyano- p -phenylenediamine, 952 (2010) 25–30. doi:10.1016/j.theochem.2010.04.002.
- [52] Y. Zheng, G. Deng, Q. Liang, D. Chen, R. Guo, R. Lai, Antioxidant Activity of Quercetin and Its Glucosides from Propolis: A Theoretical Study, *Sci. Rep.* (2017) 1–11. doi:10.1038/s41598-017-08024-8.
- [53] J. Chen, J. Yang, L. Ma, J. Li, N. Shahzad, C.K. Kim, Structure-antioxidant activity relationship of methoxy, phenolic hydroxyl, and carboxylic acid groups of phenolic acids, (2020) 1–9.
- [54] D.Q. Huong, T. Duong, P.C. Nam, An experimental and computational study of

- antioxidant activity of N-phenylthiourea and N-phenylselenourea analogues, 57 (2019) 469–479. doi:10.1002/vjch.201900091.
- [55] S.M. Morais, K.S.B. Lima, S.M.C. Siqueira, E.S.B. Cavalcanti, M.S.T. Souza, J.E.S.A. Menezes, M.T.S. Trevisan, Correlação entre as atividades antiradical , antiacetilcolinesterase e teor de fenóis totais de extratos de plantas medicinais de farmácias vivas, (2013) 575–582.
- [56] J. Wu, L. Zhang, J. Wang, S. Yang, X. Li, 1-Phenyl-3-(2,4,6-trimethoxy-phen-yl)prop-2-en-1-one, Acta Crystallogr. Sect. E Struct. Reports Online. 65 (2009). doi:10.1107/S1600536809041877.
- [57] Y. Cai, Z. Wang, Z. Li, M. Zhang, J. Wu, (E)-1-(4-Meth-oxyphenyl)-3-(2,4,6-trimeth-oxyphenyl)prop-2-en-1-one, Acta Crystallogr. Sect. E Struct. Reports Online. 67 (2011). doi:10.1107/S1600536811017788.
- [58] M. Prabuswamy, S. Madan Kumar, D. Bhuvaneshwar, C.S.S.S. Murthy, N.K. Lokanath, 1-(2-Fluorophenyl)-3-(2,4,6-trimethoxyphenyl)prop-2-en-1-one, Acta Crystallogr. Sect. E Struct. Reports Online. 68 (2012). doi:10.1107/S1600536812043139.
- [59] I.N. Ribeiro, R.L.G. de Paula, P.R.S. Wenceslau, F.S. Fernandes, V.S. Duarte, W.F. Vaz, G.R. Oliveira, C. Valverde, H.B. Napolitano, B. Baseia, Growth and characterization of a new chlorine substituted chalcone: A third order nonlinear optical material, J. Mol. Struct. 1201 (2020) 127137. doi:10.1016/j.molstruc.2019.127137.
- [60] D.A. Zainuri, M. Abdullah, S. Arshad, M.S.A. Aziz, G. Krishnan, H. Bakhtiar, I.A. Razak, Crystal structure, spectroscopic and third-order nonlinear optical susceptibility of linear fused ring dichloro-substituent chalcone isomers, Opt. Mater. (Amst). 86 (2018) 32–45. doi:10.1016/j.optmat.2018.09.032.
- [61] D. Haleshappa, A. Jayarama, R. Bairy, S. Acharya, P.S. Patil, Second and third order nonlinear optical studies of a novel thiophene substituted chalcone derivative, Phys. B Condens. Matter. 555 (2019) 125–132. doi:10.1016/j.physb.2018.11.046.
- [62] J.M.F. Custodio, J.J.A. Guimarães-Neto, R. Awad, J.E. Queiroz, G.M.V. Verde, M. Mottin, B.J. Neves, C.H. Andrade, G.L.B. Aquino, C. Valverde, F.A.P. Osório, B. Baseia, H.B. Napolitano, Molecular modelling and optical properties of a novel fluorinated chalcone, Arab. J. Chem. 13 (2020) 3362–3371. doi:10.1016/j.arabjc.2018.11.010.
- [63] P.P. Vinaya, A.N. Prabhu, K. Subrahmanya Bhat, V. Upadhyaya, Synthesis, growth and characterization of a long-chain  $\pi$ -conjugation based methoxy chalcone derivative single crystal; a third order nonlinear optical material for optical limiting applications,



- Opt. Mater. (Amst). 89 (2019) 419–429. doi:10.1016/j.optmat.2019.01.061.
- [64] C. Valverde, F.A.P. Osório, T.L. Fonseca, B. Baseia, DFT study of third-order nonlinear susceptibility of a chalcone crystal, Chem. Phys. Lett. 706 (2018) 170–174. doi:10.1016/j.cplett.2018.06.001.
- [65] E. Mathew, V. V. Salián, I. Hubert Joe, B. Narayana, Third-order nonlinear optical studies of two novel chalcone derivatives using Z-scan technique and DFT method, Opt. Laser Technol. 120 (2019) 105697. doi:10.1016/j.optlastec.2019.105697.
- [66] S.R. Maidur, J.R. Jahagirdar, P.S. Patil, T.S. Chia, C.K. Quah, Structural characterizations, Hirshfeld surface analyses, and third-order nonlinear optical properties of two novel chalcone derivatives, Opt. Mater. (Amst). 75 (2018) 580–594. doi:10.1016/j.optmat.2017.11.008.
- [67] S. Veeramanikandan, H.B. Sherine, A. Dhandapani, S. Subashchandrabose, Synthesis, solid state structure, Hirshfeld surface, nonlinear optics and DFT studies on novel bischalcone derivative, J. Mol. Struct. 1180 (2019) 798–811. doi:10.1016/j.molstruc.2018.12.045.
- [68] K.S. Thanthiriwatte, K.M. Nalin de Silva, Non-linear optical properties of novel fluorenyl derivatives - Ab initio quantum chemical calculations, J. Mol. Struct. THEOCHEM. 617 (2002) 169–175. doi:10.1016/S0166-1280(02)00419-0.
- [69] D.A. Kleinman, Nonlinear dielectric polarization in optical media, Phys. Rev. 126 (1962) 1977–1979. doi:10.1103/PhysRev.126.1977.
- [70] K. Fukui, Role of frontier orbitals in chemical reactions, Science (80-. ). 218 (1982) 747–754. doi:10.1126/science.218.4574.747.
- [71] R.G. Parr, W. Yang, Density Functional Theory of Atoms and Molecules, Oxford University Press, Oxford, 1989.
- [72] Chemcraft - graphical software for visualization of quantum chemistry computations., (2004).
- [73] R.G. Pearson, Hard and Soft Acids and Bases, J. Am. Chem. Soc. 85 (1963) 3533–3539. doi:10.1021/ja00905a001.
- [74] T. Koopmans, Über die Zuordnung von Wellenfunktionen und Eigenwerten zu den Einzelnen Elektronen Eines Atoms, Physica. 1 (1934) 104–113. doi:10.1016/S0031-8914(34)90011-2.
- [75] H. Chermette, Chemical reactivity indexes in density functional theory, J. Comput.

- Chem. 20 (1999) 129–154. doi:10.1002/(SICI)1096-987X(19990115)20:1<129::AID-JCC13>3.0.CO;2-A.
- [76] L.H. Mendoza-Huizar, C.H. Rios-Reyes, Chemical reactivity of Atrazine employing the Fukui function, *J. Mex. Chem. Soc.* 55 (2011) 142–147.
- [77] R.P. Iczkowski, J.L. Margrave, Electronegativity, *J. Am. Chem. Soc.* 83 (1961) 3547–3551. doi:10.1021/ja01478a001.
- [78] W. Yang, R.G. Parr, Hardness, softness, and the fukui function in the electronic theory of metals and catalysis., *Proc. Natl. Acad. Sci. U. S. A.* 82 (1985) 6723–6726. doi:10.1073/pnas.82.20.6723.
- [79] J.F. Janak, Proof that  $\partial E/\partial n_i = \epsilon_i$  in density-functional theory, *Phys. Rev. B.* 18 (1978) 7165–7168. doi:10.1103/PhysRevB.18.7165.
- [80] L. Von Szentpály, Studies on electronegativity equalization. Part 1. Consistent diatomic partial charges, *J. Mol. Struct. THEOCHEM.* 233 (1991) 71–81. doi:10.1016/0166-1280(91)85055-C.
- [81] R.G. Parr, P.K. Chattaraj, Principle of Maximum Hardness, *J. Am. Chem. Soc.* 113 (1991) 1854–1855. doi:10.1021/ja00005a072.
- [82] R.G. Pearson, Recent advances in the concept of hard and soft acids and bases, *J. Chem. Educ.* 64 (1987) 561–567. doi:10.1021/ed064p561.
- [83] R.G. Parr, L. V. Szentpály, S. Liu, Electrophilicity index, *J. Am. Chem. Soc.* 121 (1999) 1922–1924. doi:10.1021/ja983494x.
- [84] P.K. Chattaraj, S. Giri, S. Duley, Update 2 of: Electrophilicity index, *Chem. Rev.* 111 (2011). doi:10.1021/cr100149p.
- [85] I.B. Obot, D.D. Macdonald, Z.M. Gasem, Density functional theory (DFT) as a powerful tool for designing new organic corrosion inhibitors: Part 1: An overview, *Corros. Sci.* 99 (2015) 1–30. doi:10.1016/j.corsci.2015.01.037.
- [86] P.K. Chattaraj, S. Sengupta, Popular electronic structure principles in a dynamical context, *J. Phys. Chem.* 100 (1996) 16126–16130. doi:10.1021/jp961096f.
- [87] T. Lu, F. Chen, Multiwfn : A Multifunctional Wavefunction Analyzer, (2011). doi:10.1002/jcc.22885.
- [88] K. Momma, F. Izumi, VESTA 3 for three-dimensional visualization of crystal , volumetric and morphology data, (2011) 1272–1276.

- doi:10.1107/S0021889811038970.
- [89] C. Morell, A. Toro-labbe, New Dual Descriptor for Chemical Reactivity, (2005) 205–212.
- [90] J. Padmanabhan, R. Parthasarathi, M. Elango, V. Subramanian, B.S. Krishnamoorthy, D.R. Roy, P.K. Chattaraj, Multiphilic descriptor for chemical reactivity and selectivity, (2007) 9130–9138.
- [91] S. Shahab, M. Sheikhi, L. Filippovich, M. Atroshko, M. Drachilovskaya, Quantum-chemical modeling, spectroscopic (FT-IR, excited states, UVVis, polarization, and Dichroism) studies of two new benzo[d]oxazole derivatives, J. Mol. Struct. 1202 (2020) 127352. doi:10.1016/j.molstruc.2019.127352.
- [92] A. Viji, V. Balachandran, S. Babiyana, B. Narayana, V. V Saliyan, Molecular docking and quantum chemical calculations of 4-methoxy-{2-[3-(4-chlorophenyl)-5-(4-(propane-2-yl) PHENYL)-4, 5-dihydro-1H-pyrazol-1-yl]- 1, 3-thiazol-4-yl}phenol, J. Mol. Struct. 1203 (2020) 127452. doi:10.1016/j.molstruc.2019.127452.

## Supplementary Material

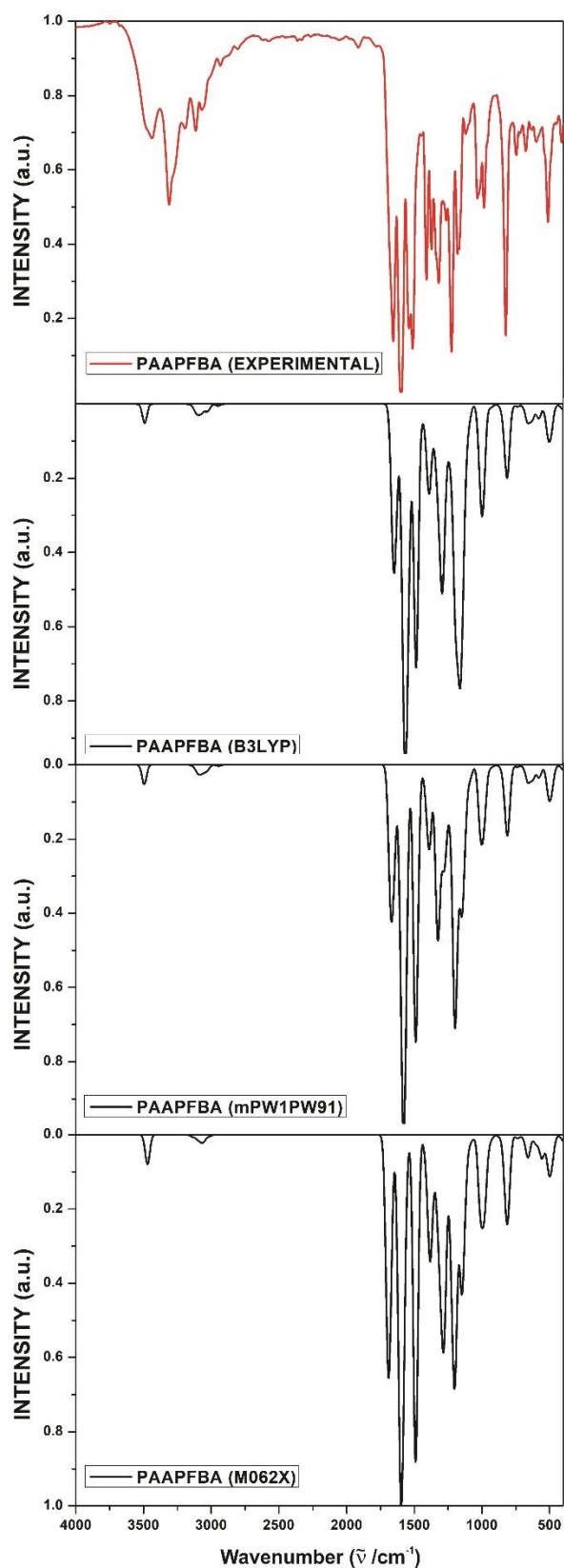
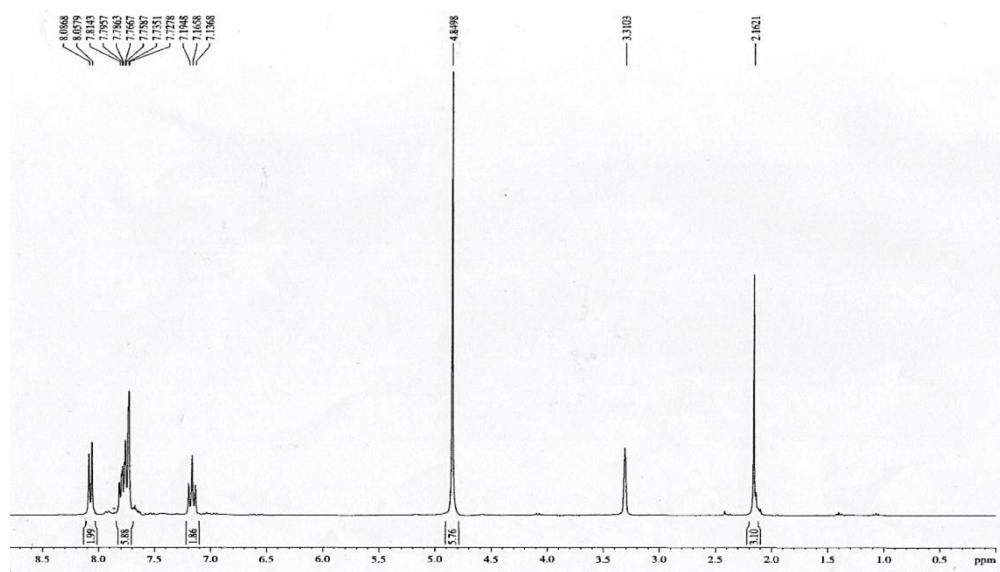


**Fig. S1** – Experimental and calculated Infrared Spectra of the PAAPFBA chalcone using the DFT methods: (a) B3LYP, (b) mPW1PW91 and (c) M06-2X at 6-311++G(d,p) basis set.

## (a) $^1\text{H}$ NMR Experimental



## (b) $^{13}\text{C}$ NMR Experimental

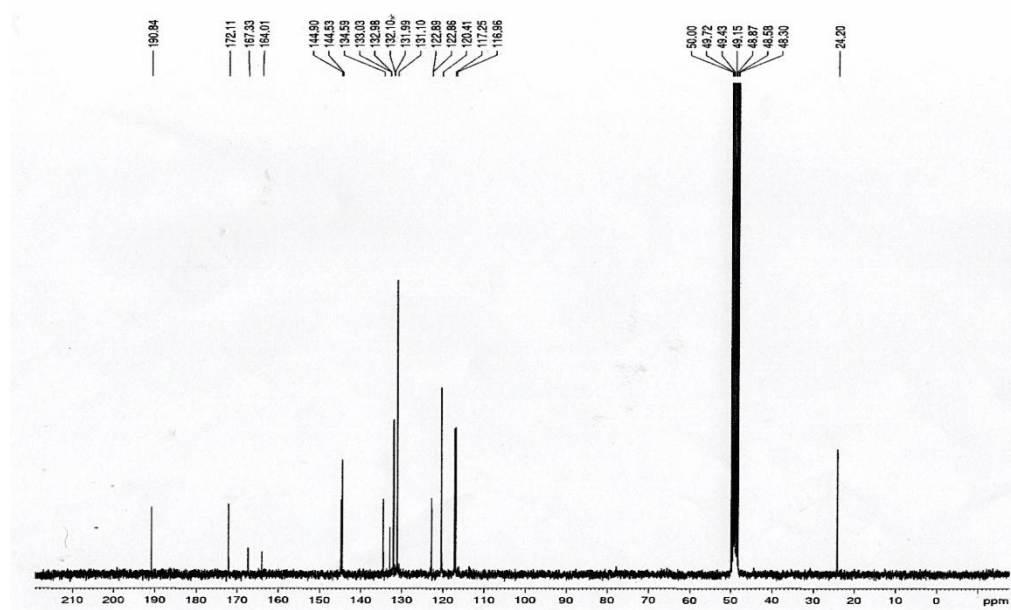
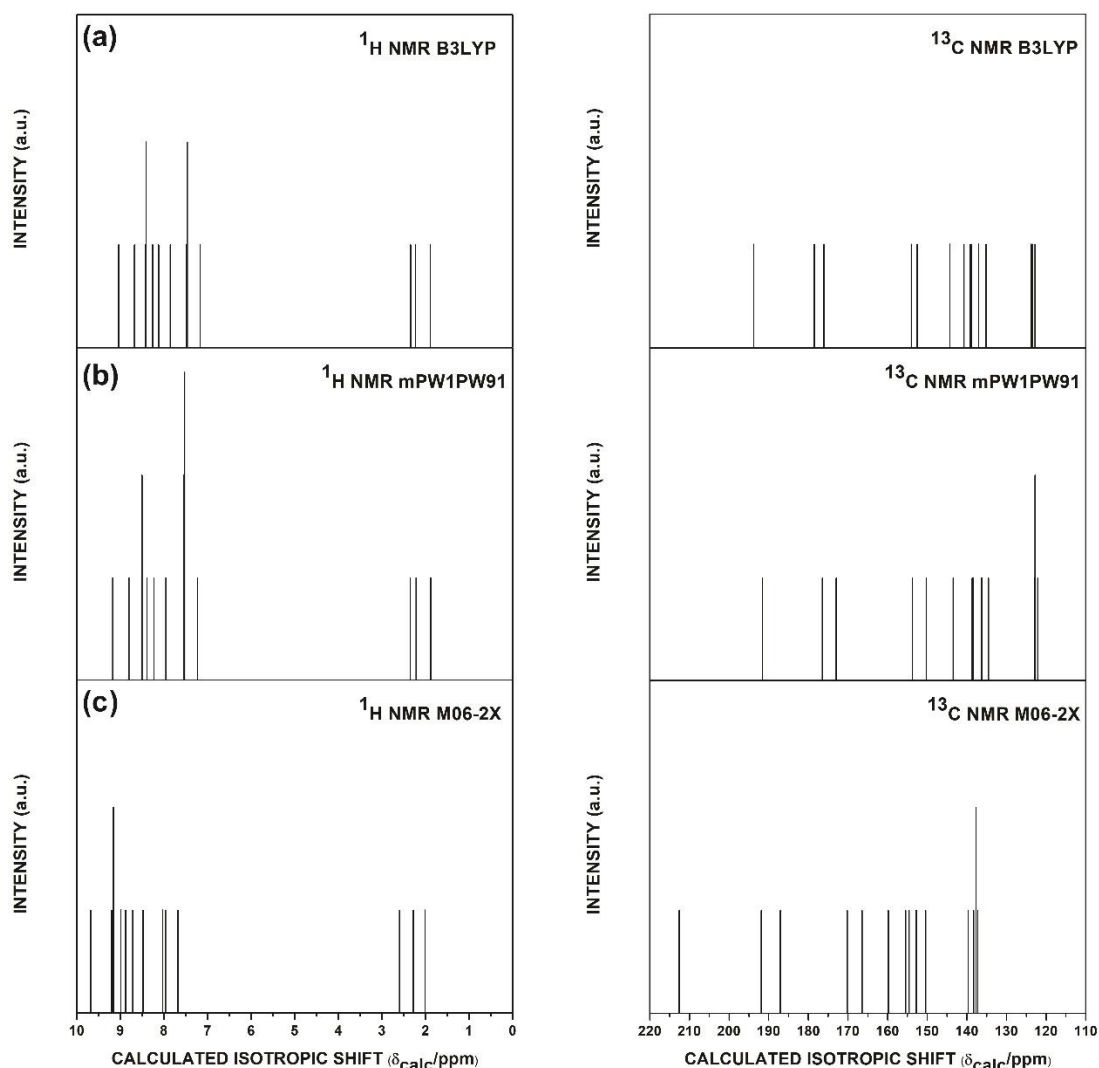


Fig. S2 – Experimental  $^1\text{H}$  and  $^{13}\text{C}$  spectra of the PAAPFBA chalcone.



**Fig. S3** – Theoretical  $^1\text{H}$  and  $^{13}\text{C}$  NMR spectra of the PAAPFBA chalcone using the DFT methods: (a) B3LYP, (b) mPW1PW91 and (c) M06-2X at 6-311++G(d,p) basis set.

Table S1 – Calculated, scaled and experimental wavenumbers for the Infrared spectra using the B3LYP/mPW1PW91/M06-2X at 6-311++G(d,p) basis set.

B3LYP		mPW1PW91		M06-2X		Experimental
Calculated	Scaled	Calculated	Scaled	Calculated	Scaled	
410.18	396.6441	413.41	395.6334	414.71	396.0481	412.76662
523.71	506.4276	537.56	514.4449	538.27	514.0479	513.06506
600.17	580.3644	605.87	579.8176	626.56	598.3648	597.93296
649.77	628.3276	654.38	626.2417	647.7	618.5535	630.72283
684.38	661.7955	695.27	665.3734	688.91	657.9091	677.01442
761.21	736.0901	771.38	738.2107	769.88	735.2354	721.37718
769.63	744.2322	775.86	742.498	773.41	738.6066	746.45179

846.13	818.2077	853.49	816.7899	857.57	818.9794	823.60443
1024.8	990.9816	1025.5	981.4035	1031.86	985.4263	985.62498
1044.1	1009.645	1057.63	1012.152	1060.55	1012.825	1033.84538
1174.43	1135.674	1180.59	1129.825	1180.39	1127.272	1120.6421
1198.23	1158.688	1204.1	1152.324	1230.85	1175.462	1168.8625
1220.91	1180.62	1230.62	1177.703	1253.61	1197.198	1180.43539
1242.27	1201.275	1250.31	1196.547	1276.98	1219.516	1224.79816
1336.63	1292.521	1320.15	1263.384	1320.19	1260.781	1263.37448
1369.68	1324.481	1385.47	1325.895	1373.76	1311.941	1319.31014
1440.82	1393.273	1447.44	1385.2	1443.27	1378.323	1373.31699
1464.38	1416.055	1462.59	1399.699	1464.1	1398.216	1409.9645
1481.08	1432.204	1483.25	1419.47	1483.18	1416.437	1446.612
1539.5	1488.697	1560.59	1493.485	1563.61	1493.248	1512.68112
1591.41	1538.893	1628.25	1558.235	1645.82	1571.758	1539.19517
1616.01	1562.682	1644.57	1573.853	1671.4	1596.187	1595.13083
1711.73	1655.243	1750.2	1674.941	1776.21	1696.281	1654.92413
3048.86	2948.248	3076.12	2943.847	3080.75	2942.116	2931.80032
3172.21	3067.527	3200.28	3062.668	3211.52	3067.002	3066.81744
3201.19	3095.551	3233.59	3094.546	3237.73	3092.032	3113.10902
3205.97	3100.173	3233.97	3094.909	3244.58	3098.574	3192.19048
3218.56	3112.348	3241.18	3101.809	3282.6	3134.883	3309.84826
3609.18	3490.077	3651.9	3494.868	3634.42	3470.871	3437.15011

Table S2 – Theoretical assignments for the fundamental vibrational modes of the PAAPFBA chalcone using B3LYP/6-311++G(d,p) level of theory.

<b>B3LYP</b>		
Wavenumber (cm <sup>-1</sup> )	IR intensity (a.u.)	Vibrational Mode Assignment
17.45	0.0406	$\varphi$ C22C20C19C4 (41) + $\varphi$ C27C24C22C20 (30)
21.89	5.7283	$\varphi$ C20C19C4C3 (63)
39.06	1.0267	$\delta$ C22C20C19 (24) + $\delta$ C24C22C20 (24) + $\delta$ C20C19C4 (15)
44.88	3.3198	$\varphi$ C12N11C2C6 (57) + $\varphi$ C27C24C22C20 (10)
52.44	7.4709	$\varphi$ C13C12N11C2 (32) + $\varphi$ H16C13C12N11 (13) + $\varphi$ H15C13C12N11 (12) + $\varphi$ C12N11C2C6 (10)

67.01	2.2451	$\varphi C29C27C24C22$ (17) + $\varphi C22C20C19C4$ (11)
74.39	3.1048	$\varphi C29C27C24C22$ (23) + $\varphi C24C22C20C19$ (18)
102.46	1.2831	$\varphi C27C24C22C20$ (19) + $\varphi C22C20C19C4$ (14)
119.69	1.0245	$\delta N11C2C1$ (22) + $\delta C12N11C2$ (20) + $\delta C19C4C5$ (11)
157.10	3.1688	$\varphi C13C12N11C2$ (21) + $\phi C19C3C5C4$ (16)
176.72	4.4692	$\delta C20C19C4$ (11) + $\delta C27C24C22$ (10)
201.05	0.1823	$\varphi C24C22C20C19$ (27) + $\varphi C28C30C29C27$ (24) + $\phi F35C28C29C30$ (14)
208.74	6.7583	$\delta C22C20C19$ (15) + $\delta C12N11C2$ (14)
281.46	13.8688	$\delta O21C19C20$ (16) + $\delta C19C4C5$ (16) + $\delta C13C12N11$ (16) + $\delta C22C20C19$ (12)
311.05	2.4092	$\phi C19C3C5C4$ (17) + $\varphi C2C6C5C4$ (16)
324.55	7.8480	$\phi C19C3C5C4$ (11) + $\varphi C2C6C5C4$ (10)
374.57	7.7686	$\delta N11C2C1$ (30) + $\delta C13C12N11$ (23)
375.51	1.3332	$\phi F35C28C29C30$ (25) + $\varphi C29C27C24C22$ (23) + $\varphi C26C28C30C29$ (15) + $\varphi C24C22C20C19$ (14)
410.18	19.9843	$\delta F35C30C29$ (50)
418.73	0.1533	$\varphi C1C3C4C5$ (32) + $\varphi C6C5C4C3$ (28) + $\varphi H10C5C6C2$ (16) + $\varphi H8C3C1C2$ (11)
423.15	0.2900	$\varphi C26C28C30C29$ (24) + $\varphi C28C30C29C27$ (21) + $\varphi C29C27C24C22$ (13) + $\varphi H32C26C28C30$ (11) + $\varphi H31C27C29C30$ (11)
451.43	2.7693	$\delta O17C12C13$ (21) + $vC19C4$ (15) + $\delta C27C24C22$ (10)
502.05	61.7623	$\delta C20C19C4$ (19)
512.48	11.8655	$\phi F35C28C29C30$ (15) + $\phi N11C6C1C2$ (14)
523.71	70.6939	$\phi F35C28C29C30$ (17) + $\phi N11C6C1C2$ (16)
537.74	32.5287	$\delta C24C20C22$ (22) + $\delta C20C19C4$ (13) + $\delta C29C27C24$ (12) + $\delta C27C24C22$ (10)
581.76	8.1310	$\delta O17C12C13$ (29) + $vC3C12$ (13)
600.17	46.5726	$\varphi H18N11C2C6$ (35) + $\phi O17C13N11C12$ (35)
646.69	6.8324	$\delta C6C5C4$ (25) + $\delta C1C3C4$ (14)
648.21	0.3446	$\delta C30C29C27$ (26) + $\delta C29C27C24$ (17) + $\delta C26C28C30$ (14)
649.77	45.6116	$\varphi H18N11C2C6$ (56) + $\phi O17C13N11C12$ (31)
684.38	48.9127	$vC13C12$ (14) + $\delta O21C19C20$ (14)
689.21	12.0318	$\phi O21C4C20C19$ (27) + $\varphi C30C29C27C24$ (10)
726.46	3.2605	$\varphi C30C29C27C24$ (35) + $\varphi C26C28C30C29$ (14) + $\varphi C28C30C29C27$ (13)
761.21	5.9635	$vF35C30$ (15) + $\delta C29C27C24$ (14) + $vC24C22$ (12)
769.63	3.4377	$\phi N11C6C1C2$ (23) + $\phi C19C3C5C4$ (10)
822.04	0.4647	$\varphi H33C28C30C29$ (31) + $\varphi H34C29C30C28$ (29) + $\varphi H32C26C28C30$ (21) + $\varphi H31C27C29C30$ (18)
834.30	74.6343	$\varphi H9C6C2N11$ (47) + $\varphi H10C5C6C2$ (34)
834.89	66.7129	$vC28C30$ (14) + $vF35C30$ (13) + $vC29C30$ (12)
846.13	127.2174	$\varphi H31C27C29C30$ (12) + $\phi F35C28C29C30$ (11) + $\varphi H32C26C28C30$ (11)



857.75	9.2057	$\delta C3C4C5$ (23)
871.25	21.8480	$\varphi H7C1C2N11$ (35) + $\varphi H8C3C1C2$ (21) + $\varphi H23C20C22C24$ (10)
898.43	1.8102	$\varphi H23C20C22C24$ (53) + $\phi O21C4C20C19$ (12)
904.72	1.6187	$\delta C22C20C19$ (15) + $\delta C28C30C29$ (12) + $\delta O21C19C20$ (10)
958.05	2.8431	$\varphi H31C27C29C30$ (24) + $\varphi H32C26C28C30$ (21) + $\varphi H34C29C30C28$ (17) + $\varphi H33C29C30C28$ (16)
965.69	9.0205	$vC13C12$ (28) + $vN11C12$ (20)
973.68	1.6863	$\varphi H10C5C6C2$ (28) + $\varphi H9C6C2N11$ (27) + $\varphi C2C6C5C4$ (26)
976.43	0.0275	$\varphi H32C26C28C30$ (24) + $\varphi H31C27C29C30$ (23) + $\varphi H33C28C30C29$ (23) + $\varphi H34C29C30C28$ (20)
1006.72	0.7803	$\varphi H8C3C1C2$ (39) + $\varphi H7C1C2N11$ (35) + $\varphi C1C3C4C5$ (13)
1018.59	47.9133	$\varphi H25C22C24C26$ (63) + $\varphi C30C29C27C24$ (10)
1022.21	3.8340	$\delta C1C3C4$ (28) + $\delta C6C5C4$ (15) + $\delta C3C4C5$ (11)
1024.80	206.8406	$\varphi H16C13C13N11$ (18) + $\varphi H15C13C12N11$ (16)
1026.30	29.0454	$\delta C26C28C30$ (36) + $\delta C27C29C30$ (21) + $\delta C28C29C30$ (14) + $\delta H33C28C30$ (11) + $\delta H34C29C30$ (11)
1044.10	176.0769	$vC19C20$ (34) + $vC3C4$ (17)
1052.98	12.9373	$\varphi H14C13C12N11$ (51) + $\phi O17C13N11C12$ (19) + $\delta H15C13H14$ (14) + $\delta H14C13H16$ (12)
1122.82	14.1112	$\delta H34C29C30$ (21) + $vC29C27$ (17) + $\delta H33C28C30$ (16) + $\delta H32C26C28$ (12) + $\delta H31C27C29$ (11) + $vC2628$ (10)
1141.56	69.0745	$\delta H8C1C3$ (32) + $\delta H7C3C1$ (25)
1174.43	332.6504	$\delta H33C28C30$ (18) + $\delta H34C29C30$ (16) + $vC30F35$ (11)
1198.23	732.4341	$\delta H10C5C6$ (25) + $\delta H9C6C2$ (21)
1220.91	192.3285	$vC30F35$ (22) + $\delta H31C27C29$ (15) + $\delta H25C22C24$ (11)
1231.03	280.2440	$vC22C24$ (17) + $vC4C19$ (13)
1327.82	52.0783	$vC30F35$ (11)
1242.27	289.1947	$vN11C12$ (16)
1276.93	157.8015	$vN11C2$ (25) + $vC2C6$ (15) + $\delta H18N11C2$ (12)
1314.10	156.3930	$vC22C24$ (14) + $vC27C29$ (10) + $vC27C24$ (10)
1321.07	9.4844	$\delta H23C20C22$ (11) + $\delta H9C6C2$ (11) + $\delta H10C5C6$ (11) + $\delta H8C3C1$ (10)
1329.49	20.9898	$\delta H32C26C28$ (17) + $\delta H31C27C29$ (15)
1336.63	495.4703	$vC2C6$ (19) + $vC3C4$ (17)
1351.49	73.8365	$vC24C27$ (11) + $\delta H25C22C24$ (11) + $vC20C22$ (10)
1369.68	213.6758	$\delta H23C20C22$ (39)
1397.41	72.3858	$\delta H16C13H15$ (60) + $\delta H14C13H16$ (47) + $\delta H15C13H14$ (33)
1431.51	137.1281	$vC1C3$ (22) + $vC6C5$ (19) + $\delta H10C5C6$ (10)
1440.82	184.3337	$vC26C28$ (18) + $vC27C29$ (18) + $\delta H34C29C30$ (10)
1464.38	14.0702	$\delta H14C13H16$ (47) + $\delta H15C13H14$ (33) + $\varphi H14C13C12N11$ (11)

1481.08	40.0927	$\delta\text{H15C13H14}$ (33) + $\delta\text{H16C13H15}$ (22) + $\delta\text{H14C13H16}$ (16) + $\phi\text{H15C13C12N11}$ (14) + $\phi\text{H16C13C12N11}$ (10)
1532.26	428.9511	$\delta\text{H31C27C29}$ (16) + $\delta\text{H33C28C30}$ (15) + $\delta\text{H32C26C28}$ (14) + $\delta\text{H34C29C30}$ (12)
1536.84	261.9342	$\delta\text{H7C1C3}$ (17) + $\delta\text{H18N11C2}$ (10) + $\nu\text{C3C4}$ (10)
1539.50	267.8041	$\delta\text{H18N11C2}$ (29) + $\delta\text{H9C6C2}$ (18) + $\delta\text{H10C5C6}$ (14) + $\nu\text{C4C5}$ (13)
1591.41	366.4863	$\nu\text{O21C19}$ (41) + $\nu\text{C20C22}$ (12)
1616.01	804.5153	$\nu\text{C2C6}$ (13) + $\nu\text{C30C29}$ (12)
1623.10	246.4152	$\nu\text{C27C24}$ (22) + $\nu\text{C30C29}$ (13) + $\nu\text{C28C30}$ (11)
1634.15	138.0322	$\nu\text{C26C28}$ (16)
1641.15	206.9205	$\nu\text{C1C3}$ (14)
1690.20	298.6628	$\nu\text{C19O21}$ (34) + $\nu\text{C20C22}$ (32)
1711.73	426.0448	$\nu\text{C12O17}$ (73)
3048.86	6.5719	$\nu\text{C13H16}$ (40) + $\nu\text{C13H15}$ (32) + $\nu\text{C13H14}$ (28)
3114.54	6.2898	$\nu\text{C13H16}$ (52) + $\nu\text{C13H15}$ (45)
3131.75	21.0337	$\nu\text{C13H14}$ (70) + $\nu\text{C13H15}$ (23)
3152.73	3.4070	$\nu\text{C22H25}$ (99)
3172.21	17.8251	$\nu\text{C6H9}$ (95)
3180.82	7.3486	$\nu\text{C27H31}$ (92)
3189.91	5.8248	$\nu\text{C26H32}$ (73) + $\nu\text{C28H33}$ (21)
3198.20	4.0832	$\nu\text{C3H8}$ (98)
3201.19	1.3071	$\nu\text{C5H10}$ (45) + $\nu\text{C20H23}$ (41) + $\nu\text{C28H33}$ (10)
3201.15	4.5052	$\nu\text{C29H34}$ (77) + $\nu\text{C28H33}$ (12)
3205.97	5.0553	$\nu\text{C28H33}$ (55) + $\nu\text{C26H32}$ (21) + $\nu\text{C29H34}$ (15)
3218.56	18.7668	$\nu\text{C20H23}$ (53) + $\nu\text{C5H10}$ (43)
3247.14	2.8826	$\nu\text{C1H7}$ (98)
3609.18	68.7200	$\nu\text{N11H18}$ (100)

Table S3 – Theoretical assignments for the fundamental vibrational modes of the PAAPFBA chalcone using mPW1PW91/6-311++G(d,p) level of theory.

<b>mPW1PW91</b>		
Wavenumber (cm <sup>-1</sup> )	IR intensity (a.u.)	Vibrational Mode Assignment
19.64	0.357	$\phi\text{C22C20C19C4}$ (34) + $\phi\text{C27C24C22C20}$ (23) + $\phi\text{C20C19C4C3}$ (17) + $\phi\text{C12N11C2C6}$ (10)
23.62	5.8794	$\phi\text{C20C19C4C3}$ (46) + $\phi\text{C27C24C22C20}$ (19) + $\phi\text{C22C20C19C4}$ (11)
39.25	1.279	$\delta\text{C22C20C19}$ (24) + $\delta\text{C24C22C20}$ (23) + $\delta\text{C20C19C4}$ (15)
45.88	1.2095	$\phi\text{C12N11C2C6}$ (46)
51.89	8.2907	$\phi\text{C13C12N11C2}$ (29) + $\phi\text{C12N11C2C6}$ (19) + $\phi\text{H16C13C12N11}$ (13) + $\phi\text{H15C13C12N11}$ (13)

65.52	1.9323	$\varphi C14C13C12N11$ (11) + $\varphi C29C27C24C22$ (10)
74.55	3.4877	$\varphi C29C27C24C22$ (28) + $\varphi C24C22C20C19$ (17) + $\varphi C20C19C4C3$ (10)
103.23	1.4588	$\varphi C27C24C22C20$ (15) + $\varphi C22C20C19C4$ (14)
120.82	0.964	$\delta N11C2C1$ (22) + $\delta C12N11C2$ (19) + $\delta C19C4C5$ (10)
157.31	3.1372	$\varphi C13C12N11C2$ (21) + $\phi C19C3C5C4$ (15)
178.38	4.2315	$\delta C20C19C4$ (11)
203.82	0.1677	$\varphi C24C22C20C19$ (26) + $\varphi C28C30C29C27$ (24) + $\phi F35C28C29C30$ (13)
209.23	6.38	$\delta C22C20C19$ (16) + $\delta C12N11C2$ (14)
281.24	15.1113	$\delta O21C19C20$ (16) + $\delta C19C4C5$ (16) + $\delta C13C12N11$ (16) + $\delta C22C20C19$ (12)
312.79	1.8206	$\phi C19C3C5C4$ (18) + $\varphi C2C6C5C4$ (16)
327.55	7.7818	$\phi C19C3C5C4$ (10)
374.84	7.7623	$\delta N11C2C1$ (31) + $\delta C13C12N11$ (25)
380.62	1.3024	$\phi F35C28C29C30$ (24) + $\varphi C29C27C24C22$ (24) + $\varphi C26C28C30C29$ (17) + $\varphi C24C22C20C19$ (16)
413.41	19.2293	$\delta F35C30C29$ (51)
419.53	0.0904	$\varphi C1C3C4C5$ (31) + $\varphi C6C5C4C3$ (27) + $\varphi H10C5C6C2$ (15) + $\varphi H8C3C1C2$ (10)
424.26	0.3376	$\varphi C28C30C29C27$ (21) + $\varphi C26C28C30C29$ (17) + $\varphi C29C27C24C22$ (15) + $\varphi H31C27C29C30$ (11) + $\varphi H32C26C28C30$ (10)
453.41	1.9719	$\delta O17C12C13$ (22) + $\nu C19C4$ (14) + $\delta C27C24C22$ (10)
504.55	59.7191	$\delta C20C19C4$ (20)
516.09	11.3754	$\phi N11C6C1C2$ (18) + $\phi F35C28C29C30$ (12)
527.51	73.1005	$\phi F35C28C29C30$ (19) + $\phi N11C6C1C2$ (13)
537.56	32.6061	$\delta C24C20C22$ (22) + $\delta C20C19C4$ (12) + $\delta C29C27C24$ (13) + $\delta C27C24C22$ (10)
586.83	5.5681	$\delta O17C12C13$ (27) + $\nu C3C12$ (12)
605.38	45.1366	$\varphi H18N11C2C6$ (36) + $\phi O17C13N11C12$ (33)
645.87	6.8085	$\delta C6C5C4$ (28) + $\delta C1C3C4$ (16) + $\delta C2C6C5$ (11) + $\nu C4C5$ (10)
648.43	0.0937	$\delta C30C29C27$ (29) + $\delta C29C27C24$ (18) + $\delta F35C30C29$ (10)
654.38	46.0957	$\varphi H18N11C2C6$ (36) + $\phi O17C13N11C12$ (32)
690.23	51.0633	$\delta O21C19C20$ (14) + $\nu C13C12$ (13)
695.27	12.7835	$\phi O21C4C20C19$ (25) + $\varphi C30C29C27C24$ (10)
731.1	3.6955	$\varphi C30C29C27C24$ (35) + $\varphi C26C28C30C29$ (14) + $\varphi C28C30C29C27$ (13)
771.38	4.5388	$\delta C29C27C24$ (15) + $\nu F35C30$ (14) + $\nu C24C22$ (12)
775.86	3.824	$\phi C21C4C20C19$ (24) + $\phi N11C6C1C2$ (10)
830.46	0.7233	$\varphi H33C28C30C29$ (30) + $\varphi H34C29C30C28$ (29) + $\varphi H32C26C28C30$ (21) + $\varphi H31C27C29C30$ (17)
840.78	8032364	$\varphi H9C6C2N11$ (47) + $\varphi H10C5C6C2$ (34)
845.65	58.4184	$\nu C29C30$ (13) + $\nu C28C30$ (13) + $\nu F35C30$ (12)
853.49	134.017	$\varphi H31C27C29C30$ (12) + $\phi F35C28C29C30$ (11) + $\varphi H32C26C28C30$ (11) + $\varphi H8C3C1C2$ (10)

		+ φH7C1C2N11 (10)
869.28	13.1275	δC3C4C5 (22)
877.47	19.0684	φH7C1C2N11 (34) + φH8C3C1C2 (21) + φH23C20C22C24 (10)
905.26	1.981	φH23C20C22C24 (52) + φH7C1C2N11 (10)
912.77	1.6239	δC22C20C19 (13) + δC28C30C29 (13)
962.28	2.4958	φH31C27C29C30 (24) + φH32C26C28C30 (22) + φH33C29C30C28 (18) + φH34C29C30C28 (16)
978.23	2.0963	φH10C5C6C2 (27) + φH9C6C2N11 (25) + φC2C6C5C4 (24)
982.35	8.0275	vC13C12 (24) + vN11C12 (19)
988.17	0.0203	φH31C27C29C30 (24) + φH32C26C28C30 (23) + φH33C28C30C29 (22) + φH34C29C30C28 (20)
1012.15	0.8573	φH8C3C1C2 (38) + φH7C1C2N11 (35) + φC1C3C4C5 (12)
1025.5	51.1463	φH25C22C24C26 (64)
1026.42	4.017	δC1C3C4 (15) + φH15C13C12N11 (15) + φH16C13C12N11 (17)
1030.63	75.4853	δC1C3C4 (14) + δC6C5C4 (10) + φH16C13C12N11 (10)
1031.61	59.3394	δC26C28C30 (27) + δC30C29C27 (16) + δC28C29C30 (10)
1051.85	15.5571	φH14C13C12N11 (51) + φO17C13N11C12 (19) + δH15C13H14 (15) + δH14C13H16 (12)
1057.63	210.0214	vC19C20 (37) + vC2C6 (17)
1126.21	13.9725	δH33C28C30 (17) + vC29C27 (15) + δH31C27C29 (12) + δH32C26C28 (12) + vC2628 (10)
1143.17	41.9534	δH8C1C3 (34) + δH7C3C1 (27)
1180.59	202.5512	δH33C28C30 (20) + δH34C29C30 (17) + δH31C27C29 (12) + δH32C26C28 (12)
1204.1	453.5349	δH10C5C6 (27) + δH9C6C2 (26)
1230.62	62.2979	δH25C22C24 (25) + δH31C27C29 (15) + δH23C20C22 (12) + vC27C24 (10)
1250.31	667.022	vC4C19 (25) + vC22C24 (11) + δH7C1C3 (11)
1259.17	213.3767	vN11C12 (23) + vC13C12 (13)
1260.99	112.8575	vF35C30 (35) + vC26C24 (11) + δH32C26C28 (10)
1294.63	138.7782	vN11C12 (26) + vC2C6 (15) + δH18N11C2 (15)
1320.15	8.4467	vC22C24 (14) + vC27C29 (10) + vC27C24 (10)
1328.74	119.9946	δH32C26C28 (11) + δH8C3C1 (10)
1337.03	217.8104	δH25C22C24 (16) + δH31C27C29 (14) + vC28C30 (10)
1355.85	85.9839	δH23C20C22 (16)
1372.32	64.3798	vC3C4 (15) + vC27C24 (12) + vC2C6 (10) + δH25C22C24 (10)
1385.47	476.7799	δH23C20C22 (24)
1395.65	143.2562	δH16C13H15 (59) + δH14C13H16 (15) + δH15C13H14 (10)
1447.44	152.4646	vC1C3 (26) + vC6C5 (22)
1455.76	155.84	vC26C28 (22) + vC29C27 (21) + δH34C29C30 (10)
1462.59	15.991	δH14C13H16 (48) + δH15C13H14 (32) + φH14C13C12N11 (12)
1483.25	52.2478	δH15C13H14 (35) + δH16C13H15 (21) + δH14C13H16 (16) + φH15C13C12N11 (13)

1549.06	335.9576	$\delta$ H31C27C29 (16) + $\delta$ H33C28C30 (14) + $\delta$ H32C26C28 (13) + $\delta$ H34C29C30 (11)
1552.79	128.1346	$\delta$ H9C6C2 (20) + $\delta$ H10C5C6 (16) + $\delta$ H18N11C2 (15)
1560.59	648.056	$\delta$ H18N11C2 (27) + $\delta$ H7C1C3 (11) + $\nu$ N11C12 (10)
1628.25	255.2234	$\nu$ O21C19 (30) + $\nu$ C2C6 (13) + $\nu$ C20C22 (10)
1644.57	712.7984	$\nu$ C30C29 (15) + $\nu$ C22C20 (10)
1652.69	284.179	$\nu$ C27C24 (21) + $\nu$ C30C29 (12) + $\nu$ C28C30 (10)
1663.72	349.7252	$\nu$ C1C3 (15) + $\nu$ C5C4 (12) + $\nu$ C26C28 (10)
1671.13	170.1567	$\nu$ C26C28 (15) + $\nu$ C30C29 (12) + $\nu$ C20C22 (10)
1723.61	302.5793	$\nu$ C19O21 (44) + $\nu$ C20C22 (27)
1750.2	472.8702	$\nu$ C12O17 (76)
3076.12	4.6056	$\nu$ C13H16 (39) + $\nu$ C13H15 (31) + $\nu$ C13H14 (29)
3153.12	4.4776	$\nu$ C13H16 (54) + $\nu$ C13H15 (42)
3169.97	16.8996	$\nu$ C13H14 (67) + $\nu$ C13H15 (27)
3177.42	3.0005	$\nu$ C22H25 (99)
3200.28	15.7295	$\nu$ C6H9 (94)
3207.68	6.1675	$\nu$ C27H31 (92)
3216.33	5.3671	$\nu$ C26H32 (77) + $\nu$ C28H33 (18)
3222.78	3.8936	$\nu$ C3H8 (98)
3227.04	0.7493	$\nu$ C5H10 (47) + $\nu$ C20H23 (43)
3233.59	0.9627	$\nu$ C28H33 (52) + $\nu$ C29H34 (33) + $\nu$ C26H32 (11)
3233.97	6.956	$\nu$ C29H34 (60) + $\nu$ C28H33 (25) + $\nu$ C26H32 (11)
3241.18	17.2718	$\nu$ C20H23 (52) + $\nu$ C5H10 (43)
3241.18	3.9369	$\nu$ C1H7 (98)
3651.9	74.8179	$\nu$ N11H18 (100)

Table S4 – Theoretical assignments for the fundamental vibrational modes of the PAAPFBA chalcone using M06-2X/6-311++G(d,p) level of theory.

### M06-2X

Wavenumber	IR intensity	Vibrational Mode Assignment
16.66	0.1018	$\varphi$ C27C24C22C20 (46) + $\varphi$ C22C20C19C4 (38)
22.77	5.7404	$\varphi$ C20C19C4C3 (49) + $\varphi$ C27C24C22C20 (12) + $\varphi$ C12C11C2C6 (12)
36.41	2.4991	$\delta$ C22C20C19 (19) + $\delta$ C24C22C20 (17) + $\delta$ C20C19C4 (15)
39.24	6.6737	$\varphi$ C20C19C4C3 (49) + $\varphi$ C12N11C2C6 (12)
49.01	1.5714	$\varphi$ H16C13C13N11 (35) + $\varphi$ H14C13C12N11 (26) + $\varphi$ H15C13C12N11 (11)
53.67	3.1674	$\varphi$ C13C12N11C2 (16) + $\varphi$ C6C5C4C3 (13) + $\varphi$ C27C24C22C20 (11) + $\varphi$ C19C3C5C4 (10)
69.02	1.0944	$\varphi$ C29C27C24C22 (28) + $\varphi$ C22C20C19C4 (18) + $\varphi$ C13C12N11C2 (13) + $\varphi$ C24C22C20C19 (11)

96.28	4.2346	$\varphi C20C19C4C3 (10) + \varphi C24C22C20C19 (10) + \varphi C22C20C19C4 (10)$
126.16	0.7788	$\delta N11C2C1 (19) + \delta C12N11C2 (14) + \delta C19C4C5 (10) + \varphi C13C12N11C2 (10)$
144.91	3.0503	$\varphi C13C12N11C2 (20) + \varphi C19C3C5C4 (15) + \delta C12N11C2 (13)$
144.91	2.9313	$\delta C20C19C4 (11)$
201.19	0.3588	$\varphi C24C22C20C19 (29) + \varphi C28C30C29C27 (25) + \varphi F35C28C29C30 (13)$
215.84	8.2082	$\delta C12N11C2 (16) + \delta C22C20C19 (13) + \delta C13C12N11 (10)$
282.58	12.4542	$\delta C19C4C5 (15) + \delta C13C12N11 (16) + \delta O21C19C20 (13) + \delta C22C20C19 (11)$
300.97	0.384	$\varphi C19C3C5C4 (21) + \varphi C2C6C5C4 (14)$
331.11	6.8743	$\varphi C19C3C5C4 (11)$
373.81	5.9592	$\delta N11C2C1 (32) + \delta C13C12N11 (24)$
380.41	1.9725	$\varphi C29C27C24C22 (26) + \varphi F35C28C29C30 (24) + \varphi C26C28C30C29 (17) + \varphi C24C22C20C19 (15)$
414.71	18.8068	$\delta F35C30C29 (37)$
418.84	1.1789	$\varphi C1C3C4C5 (22) + \varphi C6C5C4C3 (21) + \delta F35C30C29 (18) + \varphi H10C5C6C2 (10)$
422.46	0.4102	$\varphi C28C30C29C27 (23) + \varphi C26C28C30C29 (23) + \varphi C29C27C24C22 (15) + \varphi H31C27C29C30 (11) + \varphi H32C26C28C30 (11)$
454.21	1.5128	$vC19C4 (25) + \delta O17C12C13 (19) + \delta C27C24C22 (11)$
501.21	44.5784	$\varphi N11C6C1C2 (16) + \delta C20C19C4 (15)$
516.41	12.7879	$\varphi F35C28C29C30 (19)$
526.16	79.43	$\varphi N11C6C1C2 (15) + \varphi F35C28C29C30 (11)$
538.27	24.9425	$\delta C24C20C22 (19) + \delta C20C19C4 (15) + \delta C29C27C24 (10)$
580.94	59.7852	$\varphi H18N11C2C6 (50) + \varphi O17C13N11C12 (16) + \varphi H15C13C12N11 (11)$
594.62	14.5426	$\varphi H18N11C2C6 (36) + \varphi O17C13N11C12 (33)$
626.56	23.0304	$\delta C17C12C13 (19) + vC13C12 (10) + \varphi H18N11C2C6 (10)$
644.88	5.8009	$\delta C6C5C4 (28) + \delta C1C3C4 (16) + \delta C2C6C5 (10) + vC5C4 (10)$
647.7	0.0903	$\varphi H18N11C2C6 (36) + \varphi O17C13N11C12 (32)$
688.91	40.9909	$\delta C30C29C27 (30) + \delta C29C27C24 (18) + \delta C26C28C30 (16)$
695.73	30.3251	$vC13C12 (13) + \delta O21C19C20 (10)$
728.19	4.0628	$\varphi C30C29C27C24 (35) + \varphi C26C28C30C29 (14) + \varphi C28C30C29C27 (12)$
769.88	6.7462	$\delta C29C27C24 (15) + vF35C30 (14) + vC24C22 (12)$
773.41	4.0624	$\varphi C21C4C20C19 (11)$
839.52	1.2492	$\varphi H33C28C30C29 (30) + \varphi H34C29C30C28 (27) + \varphi H32C26C28C30 (20) + \varphi H31C27C29C30 (16)$
844.01	89.8635	$\varphi H9C6C2N11 (44) + \varphi H10C5C6C2 (34)$
846.47	51.668	$vC28C30 (10) + vF35C30 (10)$
857.57	132.2999	$\varphi H7C1C2N11 (13) + \varphi H8C3C1C2 (12) + \varphi H31C27C29C30 (12) + \varphi F35C28C29C30 (11)$
867.67	17.4108	$\delta C3C4C5 (19)$
876.64	17.685	$\varphi H7C1C2N11 (35) + \varphi H8C3C1C2 (21)$

909.91	1.6226	$\varphi H23C20C22C24$ (48) + $\phi O21C4C20C19$ (11)
914.66	3.0362	$\delta C22C20C19$ (12) + $\delta C28C30C29$ (12) $\varphi H32C26C28C30$ (23) + $\varphi H31C27C29C30$ (22) + $\varphi H33C29C30C28$ (20) + $\varphi H34C29C30C28$ (14)
971.01	2.8316	(14)
984.62	9.723	$\nu C13C12$ (18) + $\varphi H10C5C6C2$ (12) + $\varphi H9C6C2N11$ (11) + $\varphi C2C6C5C4$ (11) + $\nu C11C12$ (10)
986.91	5.9355	$\varphi H10C5C6C2$ (22) + $\varphi C2C6C5C4$ (18) + $\varphi H9C6C2N11$ (15) $\varphi H31C27C29C30$ (27) + $\varphi H32C26C28C30$ (21) + $\varphi H33C28C30C29$ (21) + $\varphi H34C29C30C28$ (21)
997.91	0.0209	$\varphi H8C3C1C2$ (37) + $\varphi H7C1C2N11$ (33) + $\varphi C1C3C4C5$ (11)
1014.09	0.8854	$\varphi H16C13C12N11$ (20) + $\varphi H14C13C12N11$ (13)
1020.73	24.3477	$\varphi C25C22C24C26$ (60)
1026.64	54.5151	$\delta C6C5C4$ (28) + $\delta C1C3C4$ (16)
1029.57	85.1374	$\delta C26C28C30$ (25) + $\delta C30C29C27$ (14)
1031.86	55.9812	$\varphi H14C13C12N11$ (25) + $\phi O17C13N11C12$ (25) + $\varphi H15C13C12N11$ (19)
1057.81	16.4466	$\nu C19C20$ (35) + $\nu C4C3$ (16)
1060.55	194.0859	$\delta H33C28C30$ (18) + $\nu C29C27$ (17) + $\delta H32C26C28$ (11) + $\delta H31C27C29$ (11) + $\nu C2628$ (11)
1123.85	12.7495	$\delta H8C1C3$ (31) + $\delta H7C3C1$ (24) + $\nu C1C3$ (10)
1151.62	18.4365	$\delta H33C28C30$ (20) + $\delta H34C29C30$ (18) + $\delta H31C27C29$ (13) + $\delta H32C26C28$ (13)
1180.39	118.9829	$\delta H10C5C6$ (25) + $\delta H9C6C2$ (23)
1204.02	422.2817	$\delta H25C22C24$ (22) + $\nu C27C24$ (14) + $\nu C22C24$ (13) + $\delta H31C27C29$ (12) + $\delta H23C20C22$ (11)
1230.85	24.8096	(11)
1253.61	552.5258	$\nu C4C19$ (25) + $\delta H23C20C22$ (11)
1267.66	140.1719	$\nu N11C12$ (22) + $\nu C13C12$ (13) + $\nu N11C12$ (12)
1276.98	137.5165	$\nu F35C30$ (41) + $\nu C26C28$ (12)
1286.67	120.6389	$\nu C2C6$ (19) + $\nu N11C2$ (15) + $\delta H18N11C2$ (11)
1317.45	51.1358	$\nu C28C30$ (19) + $\nu C27C29$ (15) + $\nu C27C24$ (14) + $\nu C22C24$ (11)
1320.19	6.4841	$\delta H32C26C28$ (18) + $\delta H31C27C29$ (15) + $\delta H33C28C30$ (10)
1330.4	27.2177	$\delta H9C6C2$ (15) + $\delta H10C5C6$ (14) + $\delta H8C3C1$ (14) + $\delta H7C1C3$ (12)
1341.36	479.764	$\nu C4C3$ (16) + $\nu C2C6$ (14) + $\nu N11C2$ (14) + $\nu C6C5$ (11)
1354.01	96.24	$\delta H25C22C24$ (42)
1373.76	281.0456	$\delta H23C20C22$ (40)
1401.35	103.1562	$\delta H16C13H15$ (39) + $\delta H14C13H16$ (33)
1443.27	266.2137	$\nu C1C3$ (21) + $\nu C6C5$ (17) + $\delta H10C5C6$ (10)
1455.87	118.1555	$\nu C26C28$ (19) + $\nu C29C27$ (18) + $\delta H34C29C30$ (10)
1464.1	25.8261	$\delta H14C13H16$ (44) + $\delta H16C13H15$ (24) + $\varphi H16C13C12N11$ (12)
1483.18	35.5159	$\delta H15C13H14$ (62) + $\delta H16C13H15$ (15) + $\varphi H15C13C12N11$ (15)
1554.7	131.8311	$\delta H9C6C2$ (11)
1556.21	249.85	$\delta H9C6C2$ (10)

1563.61	648.5509	$\delta$ H18N11C2 (35)
1645.82	177.5135	vC2C6 (24) + vC5C4 (11) + $\delta$ H18N11C2 (11)
1657.4	184.6935	vC30C29 (28) + vC27C24 (13)
1667.56	210.9449	vC1C3 (11) + vC5C4 (10)
1671.4	447.4624	vC26C28 (16) + vC1C3 (12)
1685.99	404.7131	vC22C20 (29) + vO21C19 (14) + vC29C30 (10)
1756.69	330.9729	vC19O21 (60) + vC20C22 (19)
1776.21	529.2085	vO17C12 (78)
3080.75	0.571	vC13H16 (54) + vC13H14 (29) + vC13H15 (17)
3154.69	4.5557	vC13H14 (51) + vC13H16 (43)
3179.41	1.2164	vC22H25 (99)
3193.18	6.3067	vC13H15 (70) + vC13H14 (20)
3204.83	10.0958	vC6H9 (91)
3211.52	3.4218	vC27H31 (93)
3218.84	3.942	vC26H32 (74) + vC28H33 (11) + vC20H23 (10)
3224.1	1.7992	vC3H8 (99)
3227.8	0.8915	vC5H10 (63) + vC20H23 (19)
3237.01	0.4018	vC28H33 (80) + vC26H32 (11)
3237.73	2.5757	vC29H34 (91)
3244.58	9.4052	vC20H23 (68) + vC5H10 (22)
3282.6	6.597	vC1H7 (99)
3634.42	90.7483	vN11H18 (100)

Table S5 – Experimental isotropic shifts ( $\delta_{exp}$ ), calculated isotropic shielding ( $\sigma_{calc}$ ), and calculated isotropic magnetic shielding ( $\delta_{calc}$ ) for the PAAPFBA chalcone using the B3LYP/mPW1PW91/M06-2x at 6-311++G(d,p) basis set.

Atom	$\delta_{exp}$	B3LYP/6-311++G(d,p)		mPW1PW91/6-311++G(d,p)		M06-2X/6-311++G(d,p)	
		$\sigma_{calc}$	$\delta_{calc}$	$\sigma_{calc}$	$\delta_{calc}$	$\sigma_{calc}$	$\delta_{calc}$
H7	7.73	22.9245	9.039492	22.709	9.175942	22.3799	9.681025
H8	8.07	23.2891	8.674892	23.0822	8.802742	22.9013	9.159625
H9	7.73	24.7941	7.169892	24.6525	7.232442	24.3834	7.677525
H10	8.07	23.5558	8.408192	23.3751	8.509842	23.0701	8.990825
H14	2.16	30.074	1.889992	30.0075	1.877442	29.7816	2.279325
H15	2.16	29.7364	2.227592	29.6696	2.215342	30.0501	2.010825
H16	2.16	29.6222	2.341792	29.5367	2.348242	29.4645	2.596425
H23	7.72	23.842	8.121992	23.6543	8.230642	23.3454	8.715525



H25	7.81	23.7028	8.261192	23.4983	8.386642	23.1819	8.879025
H31	7.76	24.1087	7.855292	23.9288	7.956142	23.5802	8.480725
H32	7.76	23.5393	8.424692	23.3835	8.501442	22.8584	9.202525
H33	7.16	24.4801	7.483892	24.34	7.544942	24.0319	8.029025
H34	7.16	24.5014	7.462592	24.3593	7.525642	24.0974	7.963525
C1	122.9	60.7972	123.8224	66.3324	122.8378	51.3253	138.3178
C2	144.9	32.0822	152.5374	38.8985	150.2717	23.1826	166.4605
C3	131.1	45.4927	139.1269	50.5401	138.6301	35.0692	154.5739
C4	132.1	43.8748	140.7448	50.8205	138.3497	34.1681	155.475
C5	131.1	47.588	137.0316	52.8628	136.3074	36.8379	152.8052
C6	122.9	60.8753	123.7443	66.3921	122.7781	51.9725	137.6706
C12	172.1	6.1025	178.5171	12.6887	176.4815	-2.2202	191.8633
C19	190.8	-9.1641	193.7837	-2.4186	191.5888	-22.9224	212.5655
C20	120.4	61.1729	123.4467	66.2502	122.92	49.9848	139.6583
C22	144.5	30.6146	154.005	35.4162	153.754	19.4458	170.1973
C24	133.1	45.7068	138.9128	52.9449	136.2253	37.0038	152.6393
C26	131.1	49.4334	135.1862	54.5879	134.5823	39.2171	150.426
C27	131.1	40.3391	144.2805	45.7316	143.4386	29.8093	159.8338
C28	116.9	61.1196	123.5	66.3878	122.7824	51.9394	137.7037
C29	116.9	61.8149	122.8047	67.0439	122.1263	52.3784	137.2647
C30	164.0	8.5405	176.0791	16.2018	172.9684	2.5654	187.0777

Table S6 – Calculated the dipole moment in each cartesian direction ( $\mu_x$ ,  $\mu_y$  and  $\mu_z$ ), the total dipole moment ( $\mu_{tot}$ ), the polarizabilities ( $\alpha$ ), the total polarizability and the parameter  $\Delta\alpha$  for the urea and the PAAPFBA molecules using the DFT methods at 6-311++G(d,p) levels of theory.

	B3LYP (Urea)	mPW1PW91 (Urea)	M06-2X (Urea)	B3LYP (PAAPFBA)	mPW1PW91 (PAAPFBA)	M06-2X (PAAPFBA)
$\mu_x$ (Debye)	-0.7045	-0.6834	-0.7554	-0.6323	-0.6556	-1.0366
$\mu_y$ (Debye)	-2.2931	-2.2943	-2.2731	-7.8316	-7.8099	-7.5466
$\mu_z$ (Debye)	-5.0778	-5.0730	-5.0282	0.2815	0.3268	0.8367
$\mu_{tot}$ (Debye)	5.6159	5.6095	5.5696	7.8621	7.8442	7.6633
$\alpha_{xx}$ (a.u.)	30.276	29.211	28.627	544.710	523.220	461.326

$\alpha_{yy}$ (a.u.)	45.968	44.386	43.450	303.915	296.662	288.710
$\alpha_{zz}$ (a.u.)	47.583	46.093	45.396	176.135	172.563	175.741
$\alpha_{xz}$ (a.u.)	-3.257	-3.137	-3.149	93.649	89.815	80.301
$\alpha_{xy}$ (a.u.)	-0.548	-0.514	-0.540	-6.981	-6.298	-3.519
$\alpha_{yz}$ (a.u.)	1.278	1.323	1.497	5.971	5.861	3.492
$\alpha_{tot}$ (a.u.)	41.276	39.897	39.158	341.587	330.815	308.592
$\Delta\alpha$ (a.u.)	17.65827	17.16578	17.02058	362.8255	345.3505	285.4418

Table S7 – Calculated hyperpolarizabilities and the parameter  $\beta_0$  for the urea and the PAAPFBA molecules using the DFT methods at 6-311++G(d,p) levels of theory.

	B3LYP (Urea)	mPW1PW91 (Urea)	M06-2X (Urea)	B3LYP (PAAPFBA)	mPW1PW91 (PAAPFBA)	M06-2X (PAAPFBA)
$\beta_{xxx}$ (a.u.)	25.3491	22.9450	24.7271	188.783	-37.9062	-408.116
$\beta_{xyy}$ (a.u.)	2.88211	0.438257	-1.5407	-290.073	-251.678	-152.11
$\beta_{xzz}$ (a.u.)	-0.231099	-1.10871	-2.18118	176.651	146.499	63.277
$\beta_{yyy}$ (a.u.)	120.884	116.906	128.746	-37.373	-51.0298	-16.4008
$\beta_{yzz}$ (a.u.)	-114.26	-108.795	-108.38	251.888	228.164	164.065
$\beta_{yxx}$ (a.u.)	-22.6641	-20.3658	-19.2649	5046.49	4583.74	3327.27
$\beta_{zzz}$ (a.u.)	-19.6227	-16.8157	0.747332	48.9393	42.0916	39.0853
$\beta_{zxx}$ (a.u.)	-41.9774	-36.7625	-33.351	469.301	372.16	122.925
$\beta_{zyy}$ (a.u.)	31.2634	30.3821	37.0017	-41.6402	-37.2174	-16.9461
$\beta_{xyz}$ (a.u.)	14.0277	14.2156	15.4876	1134.16	1036.04	783.983
$\beta_0$ ( $\times 10^{-31}$ esu)	3.82635	2.97322	1.85649	456.422	412.779	303.523

Table S8 – Calculated the dipole moment in each cartesian direction ( $\mu_x$ ,  $\mu_y$  and  $\mu_z$ ), the total dipole moment ( $\mu_{tot}$ ), the polarizabilities ( $\alpha$ ), the total polarizability ( $\alpha_{tot}$ ) and the parameter  $\Delta\alpha$  for the PAAPFBA molecules using the DFT methods (CAM-B3LYP/LC-BLYP/ $\omega$ B97XD) at 6-311++G(d,p) levels of theory.

	CAM-B3LYP (PAAPFBA)	LC-BLYP (PAAPFBA)	$\omega$ B97XD (PAAPFBA)
$\mu_x$ (Debye)	-0.98830	-1.18890	-0.94200
$\mu_y$ (Debye)	-8.55280	-8.57300	-8.49140
$\mu_z$ (Debye)	-0.19380	-0.22270	-0.18360

$\mu_{tot}$ (Debye)	8.61189	8.65791	8.54546
$\alpha_{xx}$ (a.u.)	487.5960	442.6690	484.5330
$\alpha_{yy}$ (a.u.)	296.1750	286.8250	296.5080
$\alpha_{zz}$ (a.u.)	171.8290	166.0290	172.8350
$\alpha_{xz}$ (a.u.)	81.0930	71.8110	80.0830
$\alpha_{xy}$ (a.u.)	-5.1540	-3.4460	-5.0620
$\alpha_{yz}$ (a.u.)	5.9170	5.9100	5.8950
$\alpha_{tot}$ (a.u.)	318.5333	298.5077	317.9587
$\Delta\alpha$ (a.u.)	309.5469	270.7678	305.4882

Table S9 – Calculated hyperpolarizabilities and the parameter  $\beta_0$  for the PAAPFBA molecules using the DFT methods (CAM-B3LYP/LC-BLYP/  $\omega$ B97XD) at 6-311++G(d,p) levels of theory.

	CAM-B3LYP (PAAPFBA)	LC-BLYP (PAAPFBA)	$\omega$ B97XD (PAAPFBA)
$\beta_{xxx}$ (a.u.)	-587.7070	-624.7830	-642.3580
$\beta_{xyy}$ (a.u.)	-191.7550	-123.7450	-177.4900
$\beta_{xzz}$ (a.u.)	81.1264	45.4119	71.4209
$\beta_{yyy}$ (a.u.)	-48.6281	-71.1506	-52.4783
$\beta_{yzz}$ (a.u.)	189.7430	151.0590	183.0880
$\beta_{yxx}$ (a.u.)	3770.3700	2940.4500	3611.3600
$\beta_{zzz}$ (a.u.)	20.9908	6.5433	16.4644
$\beta_{zxx}$ (a.u.)	171.5280	88.5672	144.4450
$\beta_{zyy}$ (a.u.)	-26.2299	-13.6268	-23.0985
$\beta_{xyz}$ (a.u.)	854.0880	674.8040	818.0620
$\beta_0$ (x $10^{-31}$ esu)	343.5688	268.0074	329.8977

Table S10 – Computed ratio between the B3LYP/mPW1PW91/M06-2X methods and the range separated methods (CAM-B3LYP/LC-BLYP/  $\omega$ B97XD) at 6-311++G(d,p) levels of theory for the PAAPFBA molecule.

	$\mu_{tot}$ (Debye)	$\alpha_{tot}$ (a.u.)	$\Delta\alpha$ (a.u.)	$\beta_0$ (x $10^{-31}$ esu)
	CAM-B3LYP			
B3LYP	1.0954	0.9325	0.8532	0.7527
mPW1PW91	1.0979	0.9629	0.8963	0.8323

M06-2X	1.1238	1.0322	1.0844	1.1319
LC-BLYP				
B3LYP	1.1012	0.8739	0.7463	0.5872
mPW1PW91	1.1037	0.9023	0.7840	0.6493
M06-2X	1.1298	0.9673	0.9486	0.8830
$\omega$ B97XD				
B3LYP	1.0869	0.9308	0.8420	0.7228
mPW1PW91	1.0894	0.9611	0.8846	0.7992
M06-2X	1.1151	1.0304	1.0702	1.0869

Table S11 – Calculated quantum reactivity descriptors for the PAAPFBA chalcone using the DFT methods (B3LYP/mPW1PW91/M06-2X) at 6-311++G(d,p) levels of theory.

Quantum reactivity descriptor	B3LYP	mPW1PW91	M06-2X
HOMO ( $E_{HOMO}/eV$ )	-6.5833	-6.81297	-7.85000
LUMO ( $E_{LUMO}/eV$ )	-2.68007	-2.53367	-1.73556
Energy Gap ( $\Delta E_{gap}/eV$ )	3.903232	4.279296	6.114447
Ionization Potential (I/eV)	6.583302	6.812968	7.850002
Electron Affinity (A/eV)	2.68007	2.533672	1.735556
Electronegativity ( $\chi/eV$ )	4.631686	4.67332	4.792779
Electronic Chemical Potential ( $\mu/eV$ )	-4.63169	-4.67332	-4.79278
Global Hardness ( $\eta/eV$ )	1.951616	2.139648	3.057223
Global Softness (S/eV <sup>-1</sup> )	0.512396	0.467367	0.327094
Electrophilicity index ( $\omega/eV$ )	5.496091	5.103625	3.756797
Nucleophilicity index ( $\varepsilon/eV^{-1}$ )	0.181947	0.195939	0.266184
Electric Dipole Polarizability (a.u.)	341.5867	330.815	308.5923

Table S12 – Condensed Fukui functions calculated by the Hirshfeld charge population for the PAAPFBA molecule.

Atom	B3LYP			mPW1PW91			M06-2X		
	$f_k^+$	$f_k^-$	$f_k^o$	$f_k^+$	$f_k^-$	$f_k^o$	$f_k^+$	$f_k^-$	$f_k^o$
C1	-0.02015	-0.04606	-0.03311	-0.01961	-0.05155	-0.03558	-0.01779	-0.07173	-0.04476
C2	-0.03638	-0.05047	-0.04343	-0.03612	-0.05725	-0.04668	-0.03327	-0.08173	-0.0575
C3	-0.03875	-0.03317	-0.03596	-0.03851	-0.03638	-0.03745	-0.0361	-0.04704	-0.04157
C4	-0.01727	-0.06216	-0.03971	-0.01634	-0.0715	-0.04392	-0.01382	-0.10939	-0.0616

C5	-0.02948	-0.03058	-0.03003	-0.02944	-0.03362	-0.03153	-0.02783	-0.0425	-0.03517
C6	-0.02137	-0.04323	-0.0323	-0.02065	-0.04995	-0.0353	-0.01799	-0.08289	-0.05044
H7	-0.01163	-0.02042	-0.01602	-0.01129	-0.02245	-0.01687	-0.01039	-0.03119	-0.02079
H8	-0.02248	-0.01884	-0.02066	-0.02192	-0.02034	-0.02113	-0.02041	-0.02727	-0.02384
H9	-0.01309	-0.0206	-0.01685	-0.0127	-0.02303	-0.01787	-0.01141	-0.03467	-0.02304
H10	-0.01462	-0.0165	-0.01556	-0.01449	-0.0181	-0.0163	-0.01484	-0.02497	-0.01991
N11	-0.00948	-0.05274	-0.03111	-0.00934	-0.06095	-0.03514	-0.00818	-0.09792	-0.05305
C12	-0.01506	-0.0247	-0.01988	-0.01412	-0.02725	-0.02069	-0.01062	-0.03633	-0.02348
C13	-0.00495	-0.00908	-0.00702	-0.00466	-0.01002	-0.00734	-0.00365	-0.01417	-0.00891
H14	-0.00324	-0.00652	-0.00488	-0.00305	-0.00723	-0.00514	-0.00271	-0.01124	-0.00698
H15	-0.00496	-0.0092	-0.00708	-0.00467	-0.01022	-0.00744	-0.00334	-0.01406	-0.0087
H16	-0.00503	-0.00923	-0.00713	-0.00475	-0.01026	-0.0075	-0.00349	-0.01367	-0.00858
O17	-0.01888	-0.04946	-0.03417	-0.01793	-0.05574	-0.03683	-0.01465	-0.08037	-0.04751
H18	-0.00731	-0.02138	-0.01435	-0.00709	-0.02406	-0.01557	-0.00637	-0.03721	-0.02179
C19	-0.10152	-0.01601	-0.05876	-0.10448	-0.0148	-0.05964	-0.11205	-0.01796	-0.065
C20	-0.06057	-0.06226	-0.06142	-0.06235	-0.05238	-0.05737	-0.06522	-0.00324	-0.03423
O21	-0.11403	-0.02828	-0.07116	-0.11703	-0.02706	-0.07204	-0.1252	-0.04711	-0.08615
C22	-0.0987	-0.0427	-0.0707	-0.1011	-0.03938	-0.07024	-0.1111	-0.01876	-0.06493
H23	-0.02636	-0.0178	-0.02208	-0.02692	-0.01533	-0.02112	-0.02922	-0.005	-0.01711
C24	-0.02142	-0.03801	-0.02972	-0.02087	-0.03144	-0.02616	-0.01991	-0.00237	-0.01114
H25	-0.03941	-0.01848	-0.02895	-0.03954	-0.01667	-0.02811	-0.04288	-0.00819	-0.02554
C26	-0.03767	-0.03135	-0.03451	-0.03749	-0.02672	-0.0321	-0.03781	-0.00505	-0.02143
C27	-0.03484	-0.03298	-0.03391	-0.03498	-0.02839	-0.03168	-0.03505	-0.00611	-0.02058
C28	-0.02237	-0.02569	-0.02403	-0.02185	-0.02151	-0.02168	-0.02099	-0.00361	-0.0123
C29	-0.02333	-0.02765	-0.02549	-0.02269	-0.0231	-0.02289	-0.02153	-0.00377	-0.01265
C30	-0.04021	-0.04444	-0.04233	-0.04008	-0.03789	-0.03899	-0.04008	-0.00659	-0.02333
H31	-0.01699	-0.01578	-0.01638	-0.0168	-0.01338	-0.01509	-0.01692	-0.00289	-0.00991
H32	-0.01775	-0.01414	-0.01595	-0.01746	-0.01189	-0.01467	-0.01768	-0.00224	-0.00996
H33	-0.01348	-0.01444	-0.01396	-0.01316	-0.01209	-0.01263	-0.01275	-0.00227	-0.00751
H34	-0.01384	-0.01496	-0.0144	-0.01347	-0.01253	-0.013	-0.01296	-0.00242	-0.00769
F35	-0.02291	-0.03048	-0.0267	-0.02266	-0.02544	-0.02405	-0.02142	-0.00396	-0.01269

Table S13 – Calculated local reactivity descriptors for the title chalcone using the B3LYP/6-311++G(d,p) basis set.

Atom	B3LYP								
	$\eta_k^+$	$\eta_k^-$	$\eta_k^o$	$s_k^+$	$s_k^-$	$s_k^o$	$\omega_k^+$	$\omega_k^-$	$\omega_k^o$
C1	-0.03933	-0.0899	-0.06461	-0.01033	-0.0236	-0.01696	-0.11076	-0.25317	-0.18196
C2	-0.071	-0.0985	-0.08475	-0.01864	-0.02586	-0.02225	-0.19995	-0.27739	-0.23867
C3	-0.07563	-0.06473	-0.07018	-0.01986	-0.01699	-0.01843	-0.21299	-0.18229	-0.19764
C4	-0.0337	-0.12131	-0.07751	-0.00885	-0.03185	-0.02035	-0.0949	-0.34164	-0.21827
C5	-0.05754	-0.05968	-0.05861	-0.01511	-0.01567	-0.01539	-0.16204	-0.16808	-0.16506
C6	-0.04171	-0.08437	-0.06304	-0.01095	-0.02215	-0.01655	-0.11745	-0.2376	-0.17752
H7	-0.02269	-0.03985	-0.03127	-0.00596	-0.01046	-0.00821	-0.0639	-0.11224	-0.08807
H8	-0.04386	-0.03677	-0.04032	-0.01152	-0.00965	-0.01059	-0.12352	-0.10356	-0.11354
H9	-0.02555	-0.04021	-0.03288	-0.00671	-0.01056	-0.00863	-0.07197	-0.11323	-0.0926
H10	-0.02853	-0.03221	-0.03037	-0.00749	-0.00846	-0.00797	-0.08034	-0.09071	-0.08552
N11	-0.01849	-0.10293	-0.06071	-0.00486	-0.02703	-0.01594	-0.05208	-0.28988	-0.17098
C12	-0.02938	-0.04821	-0.0388	-0.00771	-0.01266	-0.01019	-0.08275	-0.13576	-0.10925
C13	-0.00967	-0.01772	-0.01369	-0.00254	-0.00465	-0.00359	-0.02722	-0.0499	-0.03856
H14	-0.00632	-0.01272	-0.00952	-0.00166	-0.00334	-0.0025	-0.01779	-0.03583	-0.02681
H15	-0.00968	-0.01796	-0.01382	-0.00254	-0.00471	-0.00363	-0.02727	-0.05057	-0.03892
H16	-0.00981	-0.01802	-0.01392	-0.00258	-0.00473	-0.00365	-0.02764	-0.05074	-0.03919
O17	-0.03685	-0.09653	-0.06669	-0.00967	-0.02534	-0.01751	-0.10377	-0.27185	-0.18781
H18	-0.01427	-0.04173	-0.028	-0.00375	-0.01096	-0.00735	-0.04019	-0.11752	-0.07886
C19	-0.19812	-0.03124	-0.11468	-0.05202	-0.0082	-0.03011	-0.55795	-0.08797	-0.32296
C20	-0.11822	-0.12151	-0.11986	-0.03104	-0.0319	-0.03147	-0.33292	-0.34219	-0.33756
O21	-0.22254	-0.0552	-0.13887	-0.05843	-0.01449	-0.03646	-0.62672	-0.15544	-0.39108
C22	-0.19263	-0.08332	-0.13798	-0.05057	-0.02188	-0.03623	-0.54248	-0.23466	-0.38857
H23	-0.05145	-0.03474	-0.0431	-0.01351	-0.00912	-0.01132	-0.14489	-0.09785	-0.12137
C24	-0.04181	-0.07419	-0.058	-0.01098	-0.01948	-0.01523	-0.11774	-0.20893	-0.16334
H25	-0.07691	-0.03607	-0.05649	-0.02019	-0.00947	-0.01483	-0.21658	-0.10159	-0.15909
C26	-0.07351	-0.06119	-0.06735	-0.0193	-0.01606	-0.01768	-0.20702	-0.17231	-0.18966
C27	-0.06799	-0.06436	-0.06618	-0.01785	-0.0169	-0.01737	-0.19148	-0.18125	-0.18637

C28	-0.04366	-0.05013	-0.04689	-0.01146	-0.01316	-0.01231	-0.12296	-0.14117	-0.13206
C29	-0.04552	-0.05397	-0.04975	-0.01195	-0.01417	-0.01306	-0.1282	-0.15199	-0.14009
C30	-0.07848	-0.08674	-0.08261	-0.0206	-0.02277	-0.02169	-0.22101	-0.24426	-0.23264
H31	-0.03315	-0.03079	-0.03197	-0.0087	-0.00808	-0.00839	-0.09336	-0.08671	-0.09003
H32	-0.03465	-0.0276	-0.03112	-0.0091	-0.00725	-0.00817	-0.09758	-0.07772	-0.08765
H33	-0.02631	-0.02818	-0.02724	-0.00691	-0.0074	-0.00715	-0.0741	-0.07935	-0.07672
H34	-0.02701	-0.02919	-0.0281	-0.00709	-0.00766	-0.00738	-0.07607	-0.0822	-0.07914
F35	-0.04471	-0.05949	-0.0521	-0.01174	-0.01562	-0.01368	-0.12591	-0.16754	-0.14672

Table S14 – Calculated local reactivity descriptors for the title chalcone using the mPW1PW91/6-311++G(d,p) basis set.

Atom	mPW1PW91								
	$\eta_k^+$	$\eta_k^-$	$\eta_k^o$	$s_k^+$	$s_k^-$	$s_k^o$	$\omega_k^+$	$\omega_k^-$	$\omega_k^o$
C1	-0.04195	-0.11029	-0.07612	-0.00916	-0.02409	-0.01663	-0.10007	-0.26307	-0.18157
C2	-0.07728	-0.12249	-0.09989	-0.01688	-0.02676	-0.02182	-0.18434	-0.29217	-0.23826
C3	-0.0824	-0.07784	-0.08012	-0.018	-0.017	-0.0175	-0.19655	-0.18567	-0.19111
C4	-0.03496	-0.15298	-0.09397	-0.00764	-0.03342	-0.02053	-0.0834	-0.3649	-0.22415
C5	-0.063	-0.07193	-0.06747	-0.01376	-0.01571	-0.01474	-0.15027	-0.17158	-0.16092
C6	-0.04418	-0.10688	-0.07553	-0.00965	-0.02335	-0.0165	-0.10537	-0.25495	-0.18016
H7	-0.02416	-0.04803	-0.03609	-0.00528	-0.01049	-0.00788	-0.05763	-0.11457	-0.0861
H8	-0.04689	-0.04352	-0.0452	-0.01024	-0.00951	-0.00987	-0.11185	-0.1038	-0.10782
H9	-0.02718	-0.04928	-0.03823	-0.00594	-0.01077	-0.00835	-0.06483	-0.11756	-0.09119
H10	-0.03101	-0.03872	-0.03487	-0.00677	-0.00846	-0.00762	-0.07397	-0.09236	-0.08317
N11	-0.01999	-0.1304	-0.0752	-0.00437	-0.02848	-0.01643	-0.04769	-0.31104	-0.17936
C12	-0.03021	-0.05831	-0.04426	-0.0066	-0.01274	-0.00967	-0.07206	-0.13908	-0.10557
C13	-0.00997	-0.02143	-0.0157	-0.00218	-0.00468	-0.00343	-0.02378	-0.05111	-0.03745
H14	-0.00653	-0.01547	-0.011	-0.00143	-0.00338	-0.0024	-0.01559	-0.03689	-0.02624
H15	-0.00999	-0.02187	-0.01593	-0.00218	-0.00478	-0.00348	-0.02382	-0.05216	-0.03799
H16	-0.01015	-0.02195	-0.01605	-0.00222	-0.0048	-0.00351	-0.02422	-0.05236	-0.03829
O17	-0.03837	-0.11925	-0.07881	-0.00838	-0.02605	-0.01721	-0.09151	-0.28445	-0.18798
H18	-0.01516	-0.05147	-0.03332	-0.00331	-0.01124	-0.00728	-0.03616	-0.12277	-0.07947
C19	-0.22355	-0.03167	-0.12761	-0.04883	-0.00692	-0.02787	-0.53322	-0.07554	-0.30438

C20	-0.13342	-0.11207	-0.12274	-0.02914	-0.02448	-0.02681	-0.31823	-0.26731	-0.29277
O21	-0.2504	-0.0579	-0.15415	-0.05469	-0.01265	-0.03367	-0.59726	-0.1381	-0.36768
C22	-0.21632	-0.08426	-0.15029	-0.04725	-0.0184	-0.03283	-0.51598	-0.20098	-0.35848
H23	-0.05759	-0.0328	-0.04519	-0.01258	-0.00716	-0.00987	-0.13737	-0.07823	-0.1078
C24	-0.04466	-0.06727	-0.05596	-0.00975	-0.01469	-0.01222	-0.10652	-0.16046	-0.13349
H25	-0.0846	-0.03567	-0.06013	-0.01848	-0.00779	-0.01314	-0.2018	-0.08507	-0.14344
C26	-0.08021	-0.05716	-0.06869	-0.01752	-0.01249	-0.015	-0.19132	-0.13635	-0.16383
C27	-0.07484	-0.06074	-0.06779	-0.01635	-0.01327	-0.01481	-0.17852	-0.14487	-0.1617
C28	-0.04676	-0.04602	-0.04639	-0.01021	-0.01005	-0.01013	-0.11153	-0.10977	-0.11065
C29	-0.04854	-0.04942	-0.04898	-0.0106	-0.0108	-0.0107	-0.11578	-0.11789	-0.11683
C30	-0.08576	-0.08107	-0.08342	-0.01873	-0.01771	-0.01822	-0.20456	-0.19338	-0.19897
H31	-0.03595	-0.02862	-0.03229	-0.00785	-0.00625	-0.00705	-0.08575	-0.06828	-0.07701
H32	-0.03735	-0.02544	-0.0314	-0.00816	-0.00556	-0.00686	-0.08909	-0.06069	-0.07489
H33	-0.02816	-0.02587	-0.02702	-0.00615	-0.00565	-0.0059	-0.06718	-0.0617	-0.06444
H34	-0.02883	-0.02681	-0.02782	-0.0063	-0.00586	-0.00608	-0.06876	-0.06395	-0.06635
F35	-0.04849	-0.05443	-0.05146	-0.01059	-0.01189	-0.01124	-0.11566	-0.12984	-0.12275

Table S15 – Calculated local reactivity descriptors for the title chalcone using the M06-2X/6-311++G(d,p) basis set.

Atom	M06-2X								
	$\eta_k^+$	$\eta_k^-$	$\eta_k^o$	$s_k^+$	$s_k^-$	$s_k^o$	$\omega_k^+$	$\omega_k^-$	$\omega_k^o$
C1	-0.05438	-0.21931	-0.13684	-0.00582	-0.02346	-0.01464	-0.06682	-0.26949	-0.16816
C2	-0.10172	-0.24986	-0.17579	-0.01088	-0.02673	-0.01881	-0.125	-0.30704	-0.21602
C3	-0.11035	-0.14381	-0.12708	-0.01181	-0.01539	-0.0136	-0.1356	-0.17671	-0.15616
C4	-0.04224	-0.33442	-0.18833	-0.00452	-0.03578	-0.02015	-0.05191	-0.41094	-0.23143
C5	-0.08509	-0.12994	-0.10751	-0.0091	-0.0139	-0.0115	-0.10456	-0.15968	-0.13212
C6	-0.05499	-0.2534	-0.1542	-0.00588	-0.02711	-0.0165	-0.06757	-0.31139	-0.18948
H7	-0.03175	-0.09537	-0.06356	-0.0034	-0.0102	-0.0068	-0.03902	-0.11719	-0.0781
H8	-0.0624	-0.08338	-0.07289	-0.00668	-0.00892	-0.0078	-0.07668	-0.10246	-0.08957
H9	-0.03489	-0.10601	-0.07045	-0.00373	-0.01134	-0.00754	-0.04288	-0.13026	-0.08657
H10	-0.04537	-0.07634	-0.06086	-0.00485	-0.00817	-0.00651	-0.05575	-0.09381	-0.07478
N11	-0.02502	-0.29935	-0.16218	-0.00268	-0.03203	-0.01735	-0.03075	-0.36785	-0.1993



C12	-0.03247	-0.11108	-0.07178	-0.00347	-0.01188	-0.00768	-0.0399	-0.1365	-0.0882
C13	-0.01114	-0.04331	-0.02723	-0.00119	-0.00463	-0.00291	-0.01369	-0.05322	-0.03346
H14	-0.0083	-0.03437	-0.02133	-0.00089	-0.00368	-0.00228	-0.0102	-0.04224	-0.02622
H15	-0.0102	-0.043	-0.0266	-0.00109	-0.0046	-0.00285	-0.01254	-0.05284	-0.03269
H16	-0.01067	-0.04179	-0.02623	-0.00114	-0.00447	-0.00281	-0.01311	-0.05135	-0.03223
O17	-0.04479	-0.24572	-0.14525	-0.00479	-0.02629	-0.01554	-0.05504	-0.30194	-0.17849
H18	-0.01948	-0.11375	-0.06662	-0.00208	-0.01217	-0.00713	-0.02394	-0.13978	-0.08186
C19	-0.34255	-0.05492	-0.19873	-0.03665	-0.00588	-0.02126	-0.42093	-0.06749	-0.24421
C20	-0.1994	-0.00991	-0.10465	-0.02133	-0.00106	-0.0112	-0.24503	-0.01218	-0.1286
O21	-0.38275	-0.14403	-0.26339	-0.04095	-0.01541	-0.02818	-0.47033	-0.17698	-0.32366
C22	-0.33965	-0.05735	-0.1985	-0.03634	-0.00614	-0.02124	-0.41738	-0.07047	-0.24393
H23	-0.08934	-0.01528	-0.05231	-0.00956	-0.00163	-0.0056	-0.10978	-0.01877	-0.06428
C24	-0.06086	-0.00724	-0.03405	-0.00651	-0.00077	-0.00364	-0.07478	-0.0089	-0.04184
H25	-0.13111	-0.02503	-0.07807	-0.01403	-0.00268	-0.00835	-0.16111	-0.03076	-0.09593
C26	-0.11559	-0.01542	-0.06551	-0.01237	-0.00165	-0.00701	-0.14204	-0.01895	-0.0805
C27	-0.10715	-0.01868	-0.06291	-0.01146	-0.002	-0.00673	-0.13166	-0.02295	-0.07731
C28	-0.06416	-0.01104	-0.0376	-0.00686	-0.00118	-0.00402	-0.07884	-0.01357	-0.0462
C29	-0.06582	-0.01151	-0.03867	-0.00704	-0.00123	-0.00414	-0.08088	-0.01414	-0.04751
C30	-0.12254	-0.02013	-0.07133	-0.01311	-0.00215	-0.00763	-0.15058	-0.02474	-0.08766
H31	-0.05174	-0.00882	-0.03028	-0.00554	-0.00094	-0.00324	-0.06358	-0.01084	-0.03721
H32	-0.05405	-0.00683	-0.03044	-0.00578	-0.00073	-0.00326	-0.06642	-0.0084	-0.03741
H33	-0.03899	-0.00695	-0.02297	-0.00417	-0.00074	-0.00246	-0.04791	-0.00854	-0.02822
H34	-0.03961	-0.0074	-0.02351	-0.00424	-0.00079	-0.00251	-0.04868	-0.00909	-0.02888
F35	-0.06549	-0.01211	-0.0388	-0.00701	-0.0013	-0.00415	-0.08048	-0.01488	-0.04768

Table S16 – Calculated the Dual ( $\Delta f$ ) and the multiphlic descriptors ( $\Delta\omega$ ) for the PAAPFBA chalcone.

Atom	B3LYP		mPW1PW91		M06-2X	
	$\Delta f$	$\Delta\omega$	$\Delta f$	$\Delta\omega$	$\Delta f$	$\Delta\omega$
C1	0.025911	0.142409	0.031938	0.16300	0.053947	0.202668
C2	0.01409	0.07744	0.021128	0.10783	0.048456	0.182039
C3	-0.00559	-0.0307	-0.00213	-0.01088	0.010943	0.041111

C4	0.044895	0.246747	0.055157	0.28150	0.095568	0.35903
C5	0.001099	0.00604	0.004177	0.02132	0.014671	0.055116
C6	0.02186	0.120145	0.029307	0.14957	0.064901	0.24382
H7	0.008795	0.048338	0.011157	0.05694	0.020808	0.078171
H8	-0.00363	-0.01997	-0.00158	-0.00805	0.006864	0.025787
H9	0.007508	0.041265	0.010331	0.05273	0.023261	0.087387
H10	0.001886	0.010366	0.003603	0.01839	0.010131	0.03806
N11	0.043267	0.237799	0.051601	0.26335	0.089731	0.337101
C12	0.009645	0.05301	0.013132	0.06702	0.025711	0.096591
C13	0.004126	0.022677	0.005356	0.02734	0.010521	0.039525
H14	0.003284	0.018049	0.004174	0.02130	0.008529	0.032042
H15	0.00424	0.023303	0.005553	0.02834	0.010727	0.040299
H16	0.004203	0.0231	0.005515	0.02815	0.010179	0.03824
O17	0.030582	0.168081	0.037804	0.19294	0.065721	0.2469
H18	0.01407	0.07733	0.01697	0.08661	0.030836	0.115845
C19	-0.08551	-0.46998	-0.08968	-0.45768	-0.09408	-0.35344
C20	0.001687	0.009272	-0.00998	-0.05092	-0.06198	-0.23285
O21	-0.08575	-0.47128	-0.08997	-0.45916	-0.07809	-0.29335
C22	-0.05601	-0.30782	-0.06172	-0.31500	-0.09234	-0.3469
H23	-0.00856	-0.04705	-0.01159	-0.05915	-0.02423	-0.09101
C24	0.016591	0.091186	0.010569	0.05394	-0.01754	-0.06589
H25	-0.02092	-0.11499	-0.02287	-0.11673	-0.0347	-0.13035
C26	-0.00632	-0.03471	-0.01077	-0.05497	-0.03276	-0.12309
C27	-0.00186	-0.01023	-0.00659	-0.03365	-0.02894	-0.10871
C28	0.003313	0.018209	-0.00035	-0.00176	-0.01737	-0.06527
C29	0.004329	0.023793	0.000414	0.00211	-0.01777	-0.06674
C30	0.004231	0.023254	-0.00219	-0.01118	-0.0335	-0.12584
H31	-0.00121	-0.00665	-0.00342	-0.01747	-0.01404	-0.05274
H32	-0.00361	-0.01986	-0.00556	-0.02840	-0.01545	-0.05802
H33	0.000955	0.005249	-0.00107	-0.00548	-0.01048	-0.03938
H34	0.001115	0.006128	-0.00094	-0.00481	-0.01054	-0.03959

F35	0.007574	0.041627	0.002778	0.01418	-0.01746	-0.0656
-----	----------	----------	----------	---------	----------	---------

Table S17 – Natural Bond Orbital (NBO) results of the significant donor-acceptor transitions and the second-order perturbation theory analysis of the Fock matrix for the PAAPFBA chalcone using the B3LYP/6-311++G(d,p) basis set.

Type	Donor	Type	Acceptor	$\Delta E_{ij}$ (kcal.mol <sup>-1</sup> )	$E_{(j)} - E_{(i)}$ (a.u.)	$F_{(i,j)}$ (a.u.)
$\sigma$	C1 - C2	$\sigma^*$	C1 - C3	2.6	1.28	0.052
$\pi$	C1 - C3	$\pi^*$	C2 - C6	23.2	0.27	0.072
$\pi$	C1 - C3	$\pi^*$	C4 - C5	17.03	0.28	0.063
$\pi$	C2 - C6	$\pi^*$	C1 - C3	15.38	0.29	0.062
$\pi$	C2 - C6	$\pi^*$	C4 - C5	24.3	0.29	0.075
$\pi$	C4 - C5	$\pi^*$	C1 - C3	20.99	0.29	0.071
$\pi$	C4 - C5	$\pi^*$	C2 - C6	18.65	0.27	0.064
$\pi$	C4 - C5	$\pi^*$	C19 - O21	20.97	0.27	0.069
$\sigma$	C4 - C19	$\text{RY}^*$	C20	1.32	1.65	0.042
$\sigma$	C4 - C19	$\text{RY}^*$	O21	0.8	1.46	0.031
$\sigma$	C4 - C19	$\sigma^*$	C1 - C3	2.22	1.23	0.047
$\sigma$	C4 - C19	$\sigma^*$	C19 - C20	0.86	1.09	0.028
$\sigma$	C4 - C19	$\sigma^*$	C19 - O21	1.19	1.21	0.034
$\sigma$	C4 - C19	$\sigma^*$	C20 - C22	1.61	1.28	0.041
$\sigma$	C5 - C6	$\sigma^*$	C2 - C6	3.07	1.26	0.056
$\sigma$	C5 - C6	$\sigma^*$	C2 - N11	3.6	1.13	0.057
$\sigma$	C5 - C6	$\sigma^*$	C4 - C5	3.25	1.28	0.057
$\sigma$	C5 - C6	$\sigma^*$	C4 - C19	3.24	1.14	0.055
$\sigma$	C5 - C6	$\sigma^*$	C5 - H10	1.02	1.16	0.031
$\sigma$	C5 - C6	$\sigma^*$	C6 - H9	1.21	1.15	0.033
$\sigma$	N11 - H18	$\sigma^*$	C1 - C2	4.16	1.21	0.064
$\sigma$	N11 - H18	$\sigma^*$	C12 - O17	4.59	1.25	0.068
$\sigma$	C12 - O17	$\sigma^*$	N11 - H18	1.13	1.46	0.036
$\sigma$	C12 - O17	$\sigma^*$	C12 - C13	1.2	1.44	0.038
$\pi$	C12 - O17	$\pi^*$	C12 - O17	0.86	0.38	0.017
$\sigma$	C13 - H14	$\sigma^*$	N11 - C12	0.58	0.96	0.021

$\sigma$	C13 - H14	$\sigma^*$	C12 - O17	4.78	1.1	0.065
$\sigma$	C13 - H15	$\sigma^*$	N11 - C12	2.06	0.95	0.04
$\sigma$	C13 - H15	$\pi^*$	C12 - O17	4.18	0.51	0.044
$\sigma$	C13 - H16	$\sigma^*$	N11 - C12	1.56	0.95	0.035
$\sigma$	C13 - H16	$\pi^*$	C12 - O17	5.07	0.51	0.049
$\sigma$	C19 - C20	$\sigma^*$	C22 - C24	3.93	1.14	0.06
$\sigma$	C19 - O21	$\sigma^*$	C4 - C5	1.33	1.61	0.042
$\pi$	C19 - O21	$\pi^*$	C4 - C5	4.35	0.4	0.041
$\pi$	C19 - O21	$\pi^*$	C20 - C22	3.55	0.41	0.035
$\pi$	C20 - C22	$\pi^*$	C19 - O21	21.72	0.29	0.072
$\pi$	C20 - C22	$\pi^*$	C24 - C27	11.55	0.3	0.055
$\sigma$	C20 - H23	$\sigma^*$	C19 - O21	3.88	1.09	0.058
$\sigma$	C20 - H23	$\sigma^*$	C20 - C22	1.59	1.15	0.038
$\sigma$	C20 - H23	$\sigma^*$	C22 - H25	4.35	1	0.059
$\sigma$	C22 - H25	$\sigma^*$	C19 - C20	0.6	0.95	0.021
$\sigma$	C22 - H25	$\sigma^*$	C20 - C22	1.27	1.14	0.034
$\sigma$	C22 - H25	$\sigma^*$	C20 - H23	5.49	0.95	0.065
$\sigma$	C22 - H25	$\sigma^*$	C24 - C26	4.88	1.07	0.065
$\pi$	C24 - C27	$\pi^*$	C20 - C22	17.65	0.29	0.069
$\pi$	C24 - C27	$\pi^*$	C26 - C28	20.65	0.28	0.069
$\pi$	C26 - C28	$\pi^*$	C24 - C27	17.33	0.29	0.064
$\pi$	C29 - C30	$\pi^*$	C24 - C27	21.34	0.3	0.072
$\pi$	C29 - C30	$\pi^*$	C26 - C28	17.32	0.3	0.065
$\sigma$	C30 - F35	$\sigma^*$	C28 - H33	1.58	5.56	0.084
LP (1)	N11	$\pi^*$	C2 - C6	35.2	0.29	0.091
LP (1)	N11	$\pi^*$	C12 - O17	59.71	0.28	0.117
LP (1)	O17	RY*	C12	16.55	1.72	0.151
LP (2)	O17	$\sigma^*$	N11 - C12	24.48	0.71	0.119
LP (2)	O17	$\sigma^*$	C12 - C13	17.49	0.64	0.097
LP (1)	O21	RY*	C19	13.3	1.6	0.13
LP (2)	O21	$\sigma^*$	C4 - C19	18.09	0.69	0.101

LP (2)	O21	$\sigma^*$	C19 - C20	18.19	0.7	0.102
$\pi^*$	C2 - C6	$\pi^*$	C1 - C3	186.48	0.01	0.081
$\pi^*$	C19 - O21	$\pi^*$	C4 - C5	196.44	0.01	0.072
$\pi^*$	C19 - O21	$\pi^*$	C20 - C22	52.58	0.02	0.073

Table S18 – Natural Bond Orbital (NBO) results of the significant donor-acceptor transitions and the second-order perturbation theory analysis of the Fock matrix for the PAAPFBA chalcone using the mPW1PW91/6-311++G(d,p) basis set.

Type	Donor	Type	Acceptor	$\Delta E_{ij}$ (kcal.mol <sup>-1</sup> )	$E_{(j)} - E_{(i)}$ (a.u.)	$F_{(i,j)}$ (a.u.)
$\sigma$	C1 - C2	$\sigma^*$	C1 - C3	2.79	1.32	0.054
$\pi$	C1 - C2	$\sigma^*$	C1 - H7	1.18	1.21	0.034
$\sigma$	C1 - C2	$\sigma^*$	C2 - C6	4.2	1.29	0.066
$\pi$	C1 - C3	$\pi^*$	C2 - C6	25.01	0.29	0.077
$\pi$	C1 - C3	$\pi^*$	C4 - C5	18.28	0.3	0.067
$\pi$	C2 - C6	$\pi^*$	C1 - C3	16.43	0.31	0.065
$\pi$	C2 - C6	$\pi^*$	C4 - C5	26.43	0.3	0.08
$\pi$	C4 - C5	$\pi^*$	C1 - C3	22.63	0.3	0.076
$\pi$	C4 - C5	$\pi^*$	C2 - C6	19.75	0.29	0.068
$\pi$	C4 - C5	$\pi^*$	C19 - O21	21.75	0.29	0.073
$\sigma$	C4 - C19	$\sigma^*$	C1 - C3	2.29	1.27	0.048
$\sigma$	C4 - C19	$\sigma^*$	C3 - C4	2.3	1.24	0.048
$\sigma$	C4 - C19	$\sigma^*$	C4 - C5	2.45	1.26	0.05
$\sigma$	C5 - C6	$\sigma^*$	C2 - C6	3.27	1.3	0.058
$\sigma$	C5 - C6	$\sigma^*$	C2 - N11	3.65	1.17	0.059
$\sigma$	N11 - H18	RY*	C2	1.83	2.13	0.056
$\sigma$	N11 - H18	RY*	C12	1.49	2.57	0.055
$\sigma$	N11 - H18	$\sigma^*$	C1 - C2	4.3	1.25	0.066
$\sigma$	N11 - H18	$\sigma^*$	C12 - O17	4.72	1.3	0.07
$\sigma$	C13 - H14	RY*	C12	0.72	2.42	0.037
$\sigma$	C13 - H14	$\sigma^*$	N11 - C12	0.65	1	0.023
$\sigma$	C13 - H14	$\sigma^*$	C12 - O17	4.97	1.14	0.067

$\sigma$	C13 - H15	$\sigma^*$	N11 - C12	2.19	0.99	0.042
$\sigma$	C13 - H15	$\pi^*$	C12 - O17	4.41	0.54	0.046
$\sigma$	C13 - H16	RY*	C12	0.54	1.81	0.028
$\sigma$	C13 - H16	$\sigma^*$	N11 - C12	1.54	0.99	0.035
$\sigma$	C13 - H16	$\pi^*$	C12 - O17	5.63	0.54	0.052
$\sigma$	C20 - C22	$\sigma^*$	C4 - C19	2.01	1.21	0.044
$\sigma$	C20 - C22	$\sigma^*$	C19 - C20	2.49	1.22	0.05
$\sigma$	C20 - C22	$\sigma^*$	C20 - H23	1.75	1.22	0.041
$\sigma$	C20 - C22	$\sigma^*$	C22 - C24	3.23	1.26	0.057
$\sigma$	C20 - C22	$\sigma^*$	C22 - H25	1.27	1.26	0.036
$\sigma$	C20 - C22	$\sigma^*$	C24 - C27	2.04	1.34	0.047
$\pi$	C20 - C22	$\pi^*$	C19 - O21	22.87	0.31	0.077
$\pi$	C20 - C22	$\pi^*$	C24 - C27	11.91	0.31	0.058
$\sigma$	C20 - H23	$\sigma^*$	C19 - O21	3.97	1.13	0.06
$\sigma$	C20 - H23	$\sigma^*$	C20 - C22	1.73	1.19	0.041
$\sigma$	C20 - H23	$\sigma^*$	C22 - H25	4.47	1.03	0.061
$\sigma$	C22 - H25	$\sigma^*$	C19 - C20	0.67	0.98	0.023
$\sigma$	C22 - H25	$\sigma^*$	C20 - C22	1.36	1.17	0.036
$\sigma$	C22 - H25	$\sigma^*$	C20 - H23	5.73	0.98	0.067
$\sigma$	C22 - H25	$\sigma^*$	C24 - C26	4.99	1.11	0.066
$\pi$	C24 - C27	$\pi^*$	C20 - C22	18.48	0.31	0.073
$\pi$	C24 - C27	$\pi^*$	C26 - C28	22.29	0.3	0.074
$\pi$	C26 - C28	$\pi^*$	C24 - C27	18.52	0.3	0.068
$\pi$	C29 - C30	$\pi^*$	C24 - C27	23.42	0.31	0.077
$\pi$	C29 - C30	$\pi^*$	C26 - C28	18.42	0.32	0.069
$\sigma$	C30 - F35	$\sigma^*$	C28 - H33	1.66	5.65	0.087
LP (1)	N11	$\pi^*$	C2 - C6	37.54	0.3	0.096
LP (1)	N11	$\pi^*$	C12 - O17	62.85	0.3	0.124
LP (1)	O17	RY*	C12	16.67	1.79	0.154
LP (2)	O17	$\sigma^*$	N11 - C12	25.67	0.74	0.125
LP (2)	O17	$\sigma^*$	C12 - C13	18.43	0.68	0.102

LP (1)	O21	RY*	C19	13.44	1.65	0.133
LP (2)	O21	$\sigma^*$	C4 - C19	19.08	0.73	0.106
LP (2)	O21	$\sigma^*$	C19 - C20	19.25	0.74	0.108
LP (1)	F35	RY*	C30	8.1	2.26	0.121
$\pi^*$	C2 - C6	$\pi^*$	C1 - C3	193.42	0.02	0.084
$\pi^*$	C19 - O21	$\pi^*$	C20 - C22	59.03	0.02	0.075
$\pi^*$	C24 - C27	$\pi^*$	C20 - C22	84.83	0.02	0.069

Table S19 – Natural Bond Orbital (NBO) results of the significant donor-acceptor transitions and the second-order perturbation theory analysis of the Fock matrix for the PAAPFBA chalcone using the M06-2X/6-311++G(d,p) basis set.

Type	Donor	Type	Acceptor	$\Delta E_{ij}(\text{kcal.mol}^{-1})$	$E_{(j)} - E_{(i)}$ (a.u.)	$F_{(i,j)}$ (a.u.)
$\sigma$	C1 - C3	$\sigma^*$	C1 - C2	3.45	1.4	0.062
$\sigma$	C1 - C3	$\sigma^*$	C1 - H7	1.55	1.32	0.041
$\sigma$	C1 - C3	$\sigma^*$	C2 - N11	4.99	1.27	0.071
$\sigma$	C1 - C3	$\sigma^*$	C3 - C4	4.11	1.39	0.068
$\pi$	C1 - C2	$\pi^*$	C3 - C4	35.76	0.36	0.101
$\pi$	C1 - C2	$\pi^*$	C5 - C6	23.11	0.36	0.083
$\sigma$	C2 - C6	$\sigma^*$	C1 - C2	4.45	1.4	0.071
$\sigma$	C2 - C6	$\sigma^*$	C1 - H7	2.37	1.33	0.05
$\sigma$	C2 - C6	$\sigma^*$	C2 - N11	1.23	1.27	0.035
$\sigma$	C2 - C6	$\sigma^*$	C5 - C6	3.36	1.43	0.062
$\sigma$	C2 - C6	$\sigma^*$	C5 - H10	2.33	1.31	0.049
$\sigma$	C2 - C6	$\sigma^*$	C6 - H9	1.1	1.29	0.034
$\sigma$	C2 - C6	$\sigma^*$	N11 - C12	3.36	1.29	0.06
$\pi$	C3 - C4	$\pi^*$	C1 - C2	25.01	0.34	0.083
$\pi$	C3 - C4	$\pi^*$	C5 - C6	31.44	0.35	0.095
$\pi$	C3 - C4	$\pi^*$	C19 - O21	21.79	0.36	0.083
$\sigma$	C4 - C5	$\sigma^*$	C3 - C4	4.63	1.39	0.072
$\sigma$	C4 - C5	$\sigma^*$	C3 - H8	2.56	1.31	0.052
$\sigma$	C4 - C5	$\sigma^*$	C4 - C19	1.95	1.27	0.045

$\sigma$	C4 - C19	$\sigma^*$	C1 - C3	2.43	1.37	0.052
$\sigma$	C4 - C19	$\sigma^*$	C3 - C4	2.53	1.34	0.052
$\sigma$	C4 - C19	$\sigma^*$	C4 - C5	2.58	1.36	0.053
$\sigma$	C4 - C5	$\sigma^*$	C5 - C6	3.41	1.43	0.062
$\pi$	C5 - C6	$\pi^*$	C1 - C2	30.08	0.36	0.094
$\pi$	C5 - C6	$\pi^*$	C3 - C4	23.11	0.36	0.083
$\sigma$	C13 - H14	$\text{RY}^*$	C12	0.53	2.52	0.033
$\sigma$	C13 - H14	$\sigma^*$	C12 - O17	3.99	1.26	0.063
$\sigma$	C13 - H14	$\pi^*$	C12 - O17	2.76	0.64	0.04
$\sigma$	C13 - H15	$\sigma^*$	N11 - C12	4.42	1.08	0.063
$\sigma$	C13 - H15	$\sigma^*$	C12 - O17	0.63	1.26	0.025
$\sigma$	C13 - H15	$\pi^*$	C12 - O17	0.78	0.63	0.021
$\sigma$	C13 - H16	$\sigma^*$	C12 - O17	1.05	1.26	0.033
$\sigma$	C13 - H16	$\pi^*$	C12 - O17	7.59	0.63	0.066
$\pi$	C20 - C22	$\pi^*$	C19 - O21	24.28	0.4	0.089
$\pi$	C20 - C22	$\pi^*$	C24 - C27	12.19	0.38	0.065
$\sigma$	C20 - H23	$\sigma^*$	C19 - O21	4.01	1.25	0.063
$\sigma$	C20 - H23	$\sigma^*$	C20 - C22	2.14	1.29	0.047
$\sigma$	C20 - H23	$\sigma^*$	C22 - H25	4.95	1.15	0.067
$\sigma$	C22 - H25	$\sigma^*$	C19 - C20	0.79	1.07	0.026
$\sigma$	C22 - H25	$\sigma^*$	C20 - C22	1.63	1.27	0.041
$\sigma$	C22 - H25	$\sigma^*$	C20 - H23	6.27	1.09	0.074
$\sigma$	C22 - H25	$\sigma^*$	C24 - C26	5.09	1.21	0.07
$\sigma$	C24 - C26	$\sigma^*$	C22 - C24	3.13	1.31	0.057
$\sigma$	C24 - C26	$\sigma^*$	C24 - C27	4.15	1.4	0.068
$\sigma$	C24 - C26	$\sigma^*$	C26 - C28	3.21	1.43	0.061
$\pi$	C24 - C27	$\pi^*$	C20 - C22	19.37	0.38	0.083
$\pi$	C24 - C27	$\pi^*$	C26 - C28	29.02	0.35	0.092
$\pi$	C26 - C28	$\pi^*$	C24 - C27	24.52	0.36	0.085
$\pi$	C29 - C30	$\pi^*$	C24 - C27	31.26	0.37	0.097
$\pi$	C29 - C30	$\pi^*$	C26 - C28	24.32	0.37	0.086



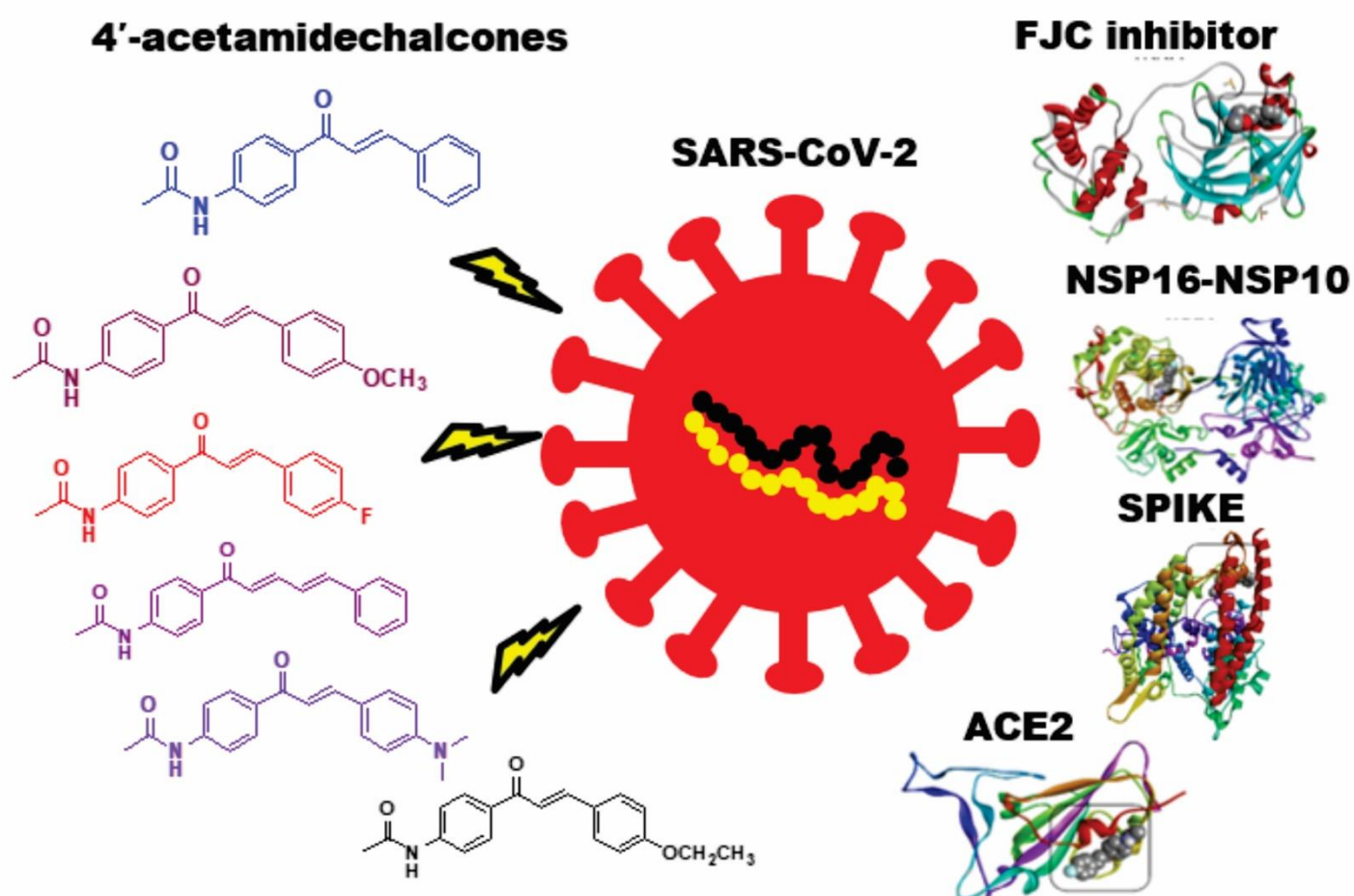
LP (1)	N11	$\pi^*$	C1 - C2	44.16	0.37	0.115
LP (1)	N11	$\pi^*$	C12 - O17	72.62	0.37	0.15
LP (1)	O17	RY*	C12	18.27	1.84	0.164
LP (2)	O17	$\sigma^*$	N11 - C12	29.71	0.85	0.143
LP (2)	O17	$\sigma^*$	C12 - C13	20.82	0.79	0.116
LP (1)	O21	RY*	C19	14.76	1.74	0.143
LP (2)	O21	$\sigma^*$	C4 - C19	21.67	0.83	0.121
LP (2)	O21	$\sigma^*$	C19 - C20	22.19	0.84	0.123
$\pi^*$	C19 - O21	$\pi^*$	C20 - C22	62.86	0.02	0.078
$\pi^*$	C24 - C27	$\pi^*$	C20 - C22	52.62	0.03	0.073

# Chapter 2

---

*In silico* study of the potential interactions of 4'-acetamidochalcones with protein targets in SARS-CoV-2

---





Contents lists available at ScienceDirect

## Biochemical and Biophysical Research Communications

journal homepage: [www.elsevier.com/locate/ybbrc](http://www.elsevier.com/locate/ybbrc)

## *In silico* study of the potential interactions of 4'-acetamidechalcones with protein targets in SARS-CoV-2



Francisco Wagner Q. Almeida-Neto<sup>a</sup>, Maria Geysillene Castro Matos<sup>b</sup>,  
 Emanuelle Machado Marinho<sup>a</sup>, Márcia Machado Marinho<sup>c</sup>,  
 Ramon Róseo Paula Pessoa Bezerra de Menezes<sup>d</sup>, Tiago Lima Sampaio<sup>d</sup>,  
 Paulo Nogueira Bandeira<sup>e</sup>, Carla Freire Celedonio Fernandes<sup>f</sup>,  
 Alexandre Magno Rodrigues Teixeira<sup>b</sup>, Emmanuel Silva Marinho<sup>h</sup>, Pedro de Lima-Neto<sup>a</sup>,  
 Hélcio Silva dos Santos<sup>b, e, i, \*</sup>

<sup>a</sup> Universidade Federal do Ceará, Departamento de Química Analítica e Físico-Química, Campus do Pici, Fortaleza, CE, Brazil

<sup>b</sup> Universidade Regional do Cariri, Departamento de Química Biológica, Crato, CE, Brazil

<sup>c</sup> Faculdade de Educação, Ciência e Letras de Iguatu, Universidade Estadual do Ceará, Iguatu, CE, Brazil

<sup>d</sup> Departamento de Análises Clínicas e Toxicológicas, Universidade Federal do Ceará, Fortaleza, CE, Brazil

<sup>e</sup> Universidade Estadual do Vale do Acaraú, Centro de Ciências Exatas e Tecnologia, Sobral, CE, Brazil

<sup>f</sup> Fundação Oswaldo Cruz, Laboratório Multiusuário de Pesquisa e Desenvolvimento - Plataforma de Anticorpos e Nanocorpos, Eusébio, CE, Brazil

<sup>h</sup> Universidade Estadual do Ceará, Faculdade de Filosofia Dom Aureliano Matos, Limoeiro do Norte, CE, Brazil

<sup>i</sup> Universidade Estadual do Ceará, Centro de Ciências e Tecnologia, Programa de Pós-Graduação Ciências Naturais, Fortaleza, CE, Brazil

CCC | RightsLink<sup>®</sup>

Home ? Live Chat Sign in Create Account



### In silico study of the potential interactions of 4'-acetamidechalcones with protein targets in SARS-CoV-2

Author: Francisco Wagner Q. Almeida-Neto, Maria Geysillene Castro Matos, Emanuelle Machado Marinho, Márcia Machado Marinho, Ramon Róseo Paula Pessoa Bezerra de Menezes, Tiago Lima Sampaio, Paulo Nogueira Bandeira, Carla Freire Celedonio Fernandes et al.

Publication: Biochemical and Biophysical Research Communications

Publisher: Elsevier

Date: 22 January 2021

© 2020 Elsevier Inc. All rights reserved.

#### Journal Author Rights

Please note that, as the author of this Elsevier article, you retain the right to include it in a thesis or dissertation, provided it is not published commercially. Permission is not required, but please ensure that you reference the journal as the original source. For more information on this and on your other retained rights, please visit: <https://www.elsevier.com/about/our-business/policies/copyright#Author-rights>

BACK

CLOSE WINDOW

## RESUMO

A emergência sanitária gerada pela pandemia da COVID-19 instiga a busca de estratégias científicas para mitigar os danos causados pela doença a diferentes setores da sociedade. A doença causada pelo coronavírus, SARS-CoV-2, já atingiu 216 países/territórios, onde cerca de 20 milhões de pessoas foram notificadas com a infecção. Destes, mais de 740.000 morreram. Diante da situação, as estratégias envolvendo o desenvolvimento de novas moléculas antivirais são extremamente importantes. O presente trabalho avaliou, por meio de ensaios de docking molecular, as interações dos derivados da 4'-acetamida-chalcona com alvos enzimáticos e estruturais do SARS-CoV-2 e com a ACE2 do hospedeiro, que é reconhecida pelo vírus, facilitando assim sua entrada nas células. Portanto, observou-se que, em relação às interações das chalconas com a protease principal (Mpro), a chalcona N-(4'-[(2E)-3-(4-fluorofenil)-1-(fenil) prop-2-en-1-ona]) acetamida (PAAPF) tem potencial para se acoplar na mesma região que o inibidor natural FJC por meio de fortes ligações de hidrogênio. A formação de duas fortes ligações de hidrogênio entre N-(4'-[(2E)-3-(fenil)-1-(fenil)-prop-2-en-1-ona]) acetamida (PAAB) e o heterodímero NSP16-NSP10 metiltransferase também foi observada. As chalconas N-(4'-[(2E)-3-(4-metoxifenil)-1-(fenil)-prop-2-en-1-ona]) acetamida (PAAPM) e N-(4'-[(2E)-3-(4-etoxifenil)-1-(fenil) prop-2-en-1-ona]) acetamida (PAAPE) mostraram pelo menos uma forte interação com a proteína SPIKE. A chalcona N-(4'-[(2E)-3-(4-dimetilaminofenil)-1-(fenil)-prop-2-en-1-ona]) acetamida (PAAPA) teve melhor afinidade com ACE2 do hospedeiro humano, mostrando fortes interações via ligação de hidrogênio. Nossos resultados sugerem que as 4'-acetamida-chalconas inibem a interação do vírus com as células hospedeiras através da ligação à proteína ACE2 ou SPIKE, provavelmente gerando um impedimento estérico. Além disso, as chalconas apresentam afinidade por enzimas importantes em processos pós-traducionais, interferindo na replicação viral.

**Palavras-chave:** Chalconas, *Docking* molecular, SPIKE, ACE2.

### ABSTRACT

The sanitary emergency generated by the pandemic COVID-19, instigates the search for scientific strategies to mitigate the damage caused by the disease to different sectors of society. The disease caused by the coronavirus, SARS-CoV-2, reached 216 countries / territories, where about 20 million people were reported with the infection. Of these, more than 740,000 died. In view of the situation, strategies involving the development of new antiviral molecules are extremely important. The present work evaluated, through molecular docking assays, the interactions of 4' -acetamidechalcones with enzymatic and structural targets of SARS-CoV-2 and with the host's ACE2, which is recognized by the virus, facilitating its entry into cells. Therefore, it was observed that, regarding the interactions of chalcones with Main protease (Mpro), the chalcone N-(4' [(2E)-3-(4-fluorophenyl)-1-(phenyl)prop-2-en-1-one]) acetamide (PAAPF) has the potential for coupling in the same region as the natural inhibitor FJC through strong hydrogen bonding. The formation of two strong hydrogen bonds between N-(4[(2E)-3-(phenyl)-1-(phenyl)-prop-2-en-1-one]) acetamide (PAAB) and the NSP16-NSP10 heterodimer methyltransferase was also noted. N-(4[(2E)-3-(4-methoxyphenyl)-1-(phenyl)prop-2-en-1-one]) acetamide (PAAPM) and N-(4-[(2E)-3-(4-ethoxyphenyl)-1-(phenyl)prop-2-en-1-one]) acetamide (PAAPE) chalcones showed at least one strong intensity interaction of the SPIKE protein. N-(4[(2E)-3-(4-dimethylaminophenyl)-1-(phenyl)-prop-2-en-1-one]) acetamide (PAAPA) chalcone had a better affinity with ACE2, with strong hydrogen interactions. Together, our results suggest that 4' -acetamidechalcones inhibit the interaction of the virus with host cells through binding to ACE2 or SPIKE protein, probably generating a steric impediment. In addition, chalcones have an affinity for important enzymes in post-translational processes, interfering with viral replication.

**Keywords:** Chalcone, Molecular Docking, SPIKE, ACE2.

## 1 Introduction

The health problem caused by the COVID-19 pandemic can be measured by the numbers of cases and deaths confirmed by the disease globally. In Brazil, community transmission is observed, with the collapse of the Health System in some regions. As it is an infection triggered by a new coronavirus (SARS-CoV-2), the pathophysiology of COVID-19 is little known and there is no specific treatment for the disease [1,2].

The search for new candidates for antiviral drugs has made great progress in recent years with the discovery of molecular targets, the development of organic synthesis and the discovery of new bioactives substances. A big number of techniques have been used in the search for new antiviral drugs. Despite the great progress, the arsenal of antiviral drugs is still small [1]. In this sense, strategies involving the development and validation of new antiviral molecules have been considered.

Chalcones, known as  $\alpha$ ,  $\beta$ -unsaturated ketones (1,3-diaryl-2-propene-1-one) are a class of naturally occurring compounds belonging to the flavonoid family. They can be obtained from natural sources or by synthesis, and are widely distributed in fruits, vegetables, and tea [3]. The double connection together with carbonyl group are possibly responsible for diverse biological activities such as antibacterial, antioxidant, anti-inflammatory and antiparasitic [4].

Antiviral properties of chalcones have been recorded in studies with plant viruses and human rhinoviruses [5]. Antiviral studies [6] with chalcones containing hydroxy and methoxy groups, confirm that the activity is dependent on the nature of the group and its positions in the aromatic rings. Santos [7] reports in a recent study the evaluation of the antiviral activity of hydroxychalcones and synthetic curcuminoids against infection caused by HPV *in vitro*.

Therefore, in this work, for the first time acetamide chalcones will be study theoretically by the Molecular Docking to characterize the inhibition power of the chalcones with the enzyme Mpro, methyltransferase, the SPIKE, and ACE2 proteins by the interaction energy and the distance of the compounds and the target protein's amino acids.

## 2 Material and methods

### 2.1 Chalcones

Using the methodological principle of synthesis the Claisen-Schmith reaction (in basic medium) [8], chalcones were synthesized from benzaldehydes and 4-aminoacetophenone, both at a concentration of 2mmol. The reagents were added in a volumetric flask (25 mL), to which 5 mL of ethanolic NaOH solution (50%) were added. After

adding the ethanol solution, the mixtures were kept under stirring for 48 hours (at room temperature). TLC (n-hexane: ethyl acetate, 2: 1) was used to monitor the progress of the reaction. After 48 h, the reaction mixture was neutralized with diluted HCl (10%) and ice water added. The products were obtained using the filtration technique under reduced pressure, washing with cold water and recrystallization in ethanol. To obtain the 4'-acetamidocalcones (1-6) (Figure 1), the acetylation reaction of the 4'-aminocalcones (2 mmol) with acetic anhydride (2 mmol) in buffered medium (5 mL) at pH = 5.0 with AcOH / AcONa was used [9].

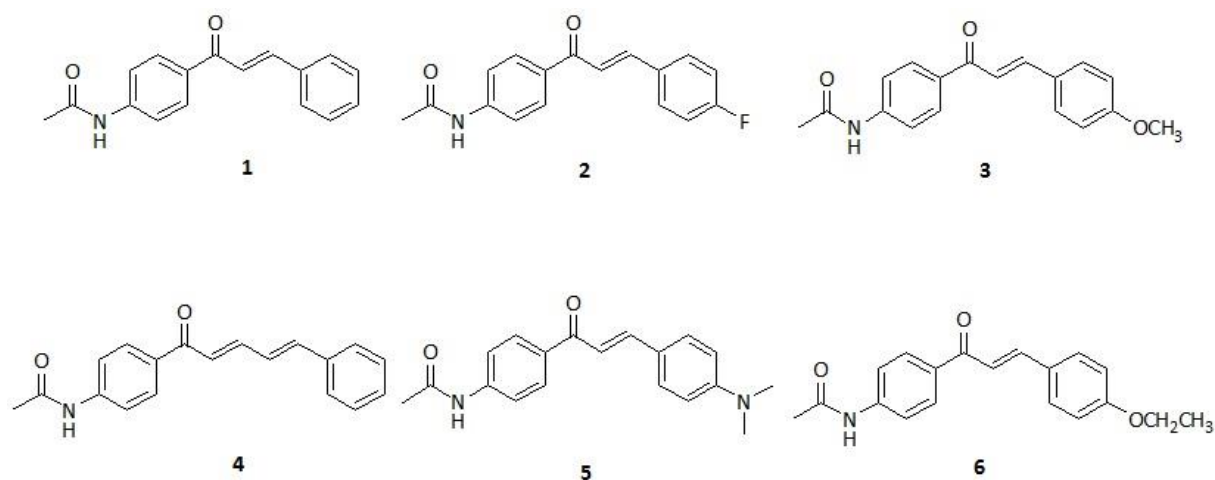


**Fig. 1.** Structural representation of the chalcones (1) PAAB (2) PAAPF (3) PAAPM (4) PAACN (5) PAAPA (6) PAAPE.

From the data available in the database, Protein Data Bank (<https://www.rcsb.org/>), the structures of the following target proteins were obtained: Main protease COVID-19 (Mpro), NSP16-NSP10 SARS-CoV-2, SPIKE, and ACE2. Then, the proteins were prepared for analysis by removing all residues and adding polar hydrogens, producing favorable protonation states for molecular docking. The Main protease COVID-19 (Mpro) was identified in the repository as “The crystal structure of COVID-19 main protease in complex with an inhibitor N3” (PDB ID: 6LU7). The structure of this enzyme is deposited in the Protein Data Bank with a resolution of 2.16 Å, determined from X-ray diffraction R-Value Free: 0.235, R-Value Work: 0.202, R-Value Observed: 0.204), classified as viral protein, Bat SARS-like coronavirus organism and *Escherichia coli* BL21 (DE3) expression system [10].

The enzyme structure of the methyltransferase complex, the NSP16-NSP10 SARS-CoV-2 heterodimer, was identified in the repository as “1.98 Angstrom Resolution Crystal Structure of NSP16-NSP10 Heterodimer from SARS-CoV-2 in Complex with Sinefungin”

(PDB ID: 6WKQ). The structure was deposited in the Protein Data Bank with a resolution of 1.98 Å, determined from X-ray diffraction (R-Value Free: 0.180, R-Value Work: 0.162), classified as viral protein, severe acute respiratory syndrome coronavirus 2, and expression system *Escherichia coli* BL21 (DE3), *Escherichia coli* BL21 [11].

The structures of the SPIKE protein and the ACE2 enzyme were identified in the repository as “Crystal structure of SARS-CoV-2 spike receptor-binding domain bound with ACE2” (PDB ID: 6MOJ). The structures were deposited in the Protein Data Bank with a resolution of 2.45 Å, determined from X-ray diffraction (R-Value Free: 0.227, R-Value Work: 0.192, R-Value Observed: 0.194), classified as viral protein/hydrolase, Homo sapiens organism, severe acute respiratory syndrome coronavirus 2, and Trichoplusia ni expression system [12].

## 2.2 Molecular docking

The interaction simulations between the selected inhibitors and proteins were performed using AutoDock Vina code (version 1.1.2), using 3-way multithreading, Lamarckian Genetic Algorithm [13]. The docking parameters: grid box sizes, centers, spacing and exhaustiveness to the proteins are given in Table S1 (Supplementary material). All grid boxes were configured to fit all the protein in the simulation for seeking the greater amplitude in the selection of molecular positions. As a standard procedure, one hundred (100) independent simulations were performed for all the target proteins, and it was obtained ten (10) positions each. As selection criteria, the simulations that showed positions with free binding energy ( $\Delta G$ ) below  $-6.0 \text{ kcal.mol}^{-1}$  [14] and RMSD (Root Mean Square Deviation) values less than two thousand (2,000) [15] were analyzed.

For results analysis, image plotting, and generation of bi and tri-country maps, the Discovery Studio Visualizer [16] and UCSF Chimera [17] codes were used. For statistical analysis, the Morpheus® online server (<https://software.broadinstitute.org/morpheus/>) was used, in which heat maps were generated to identify the ligand-residue interaction and similarity profiles by the Pearson statistical test [18].

Based on observations of the interactions of the molecules with the enzyme, the hydrogen bonds were plotted and classified according to previous studies that group interactions with distances between 2.5 and 3.1 Å as strong, from 3.1 to 3.55 Å as average and  $> 3.55 \text{ Å}$  as weak [19].



### 3 Results

#### 3.1 Interaction between the 4'-acetamidechalcones molecules and the Main protease (Mpro)

The positions shown in Figure 2A were obtained from the simulations of interactions of 4'-acetamidechalcones with Mpro by molecular docking. After comparative analyzes, it was noted that the PAAPF interacted with the enzyme at a site like that of the FJC inhibitor. Likewise, PAAB interacted at the same site as the antibiotic Azithromycin. Also, the reference drugs Anakinra and Remdesivir interacted in common sites, the same as for PAAPA. Additionally, PAAPM, PAACN, and PAAPE interacted with distinct sites from each other and different from any other reference inhibitor.

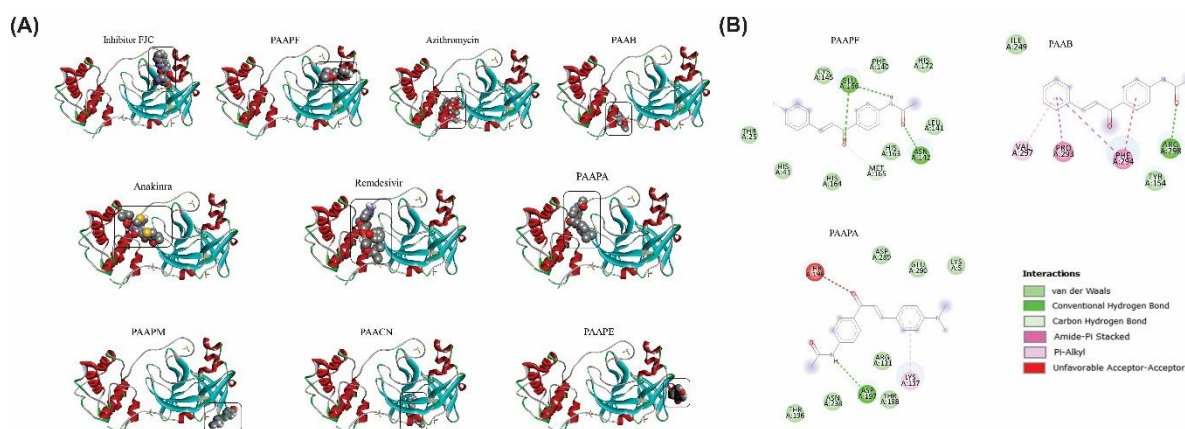


**Fig. 2.** Theoretical calculations of the interaction between the FJC inhibitor, the reference drugs, and the chalcone derivatives with the enzyme Mpro (A). The bi-dimensional map of the hydrogen bonds and the hydrophobic interaction of the chalcone derivatives with the enzyme Mpro (B).

To analyze the intensity and affinity of the interactions obtained in the molecular docking simulations, the values of the interaction energy and RMSD were collected, plotted, and compared (Table S2, Supplementary material). Interactions with energy  $< -6.0$  kcal.mol<sup>-1</sup> and RMSD  $< 2.0$  were considered satisfactory. Therefore, based on these criteria, only the chalcone PAACN showed an affinity of  $-6.1$  kcal.mol<sup>-1</sup> with the enzyme Mpro, although this molecule does not have a binding site in common with the inhibitors, especially the natural inhibitor FJC. Concerning the reference inhibitor, azithromycin did not show good affinity when presenting energy of  $-5.8$  kcal.mol<sup>-1</sup>.

To examine and describe the intrinsic characteristics of the interactions of 4'-acetamidechalcones molecules with the enzyme, the hydrogen bonds, and hydrophobic interactions were highlighted and compared with the reference ligands (Figure 2B). Since PAAPM, PAACN, and PAAPE did not show similarities with the reference ligands, those molecules were not considered for analysis. Table S3 (Supplementary material) shows the interaction distances between chalcones and the amino acid residues of the enzyme Mpro. Thus, detailed information about the interactions of the molecules with the enzyme was obtained. Initially, for the PAAPF chalcone, which has the potential for coupling in the same region as the FJC inhibitor, it has two significant interactions with the GLU166 residue, one of which is a strong hydrogen bond. The PAAB chalcone presented only interaction of hydrogen with the residue ARG298, which the Azithromycin did not interact; moreover, the Azithromycin presents most hydrophobic interactions, all with a distance higher than 3.5 Å. The PAAPA chalcone interacted with the enzyme through two hydrogen bonds, highlighting the ASP197 residue in common with Anakinra and Remdesivir; it is important to notice that, among the reference drugs, Remdesivir interacted with the enzyme through five hydrogen bonds, mostly of moderate to strong intensity.

### 3.2 Interaction with the methyltransferase heterodimer NSP16-NSP10 SARS-CoV-2

The interactions of chalcones with the NSP16-NSP10 are illustrated in Figure 3A. Among the studied structures, PAACN and PAAPE did not show significant interaction with the enzyme. Besides, the other chalcones interacted in similar places. Table S4 (Supplementary material) lists the energies of the interactions and the respective RMSD; thus, it was possible to observe affinity values  $< -6.0 \text{ kcal.mol}^{-1}$  for the four chalcones, obtaining values of up to  $-8.2 \text{ kcal.mol}^{-1}$  for PAAPF. All RMSD values were less than 2.0 Å, suggesting a satisfactory interaction between the molecules and the enzyme.

The specification of the interactions of chalcones with the enzyme is illustrated in the bi-dimensional maps contained in Figure 3B. The distances of the interactions are specified in Table S4 (Supplementary material). Therefore, it is possible to understand the formation of two strong hydrogen bonds between PAAB and the methyltransferase. The other chalcones also had two hydrogen bonds each, however, with an intermediate to weak intensity.

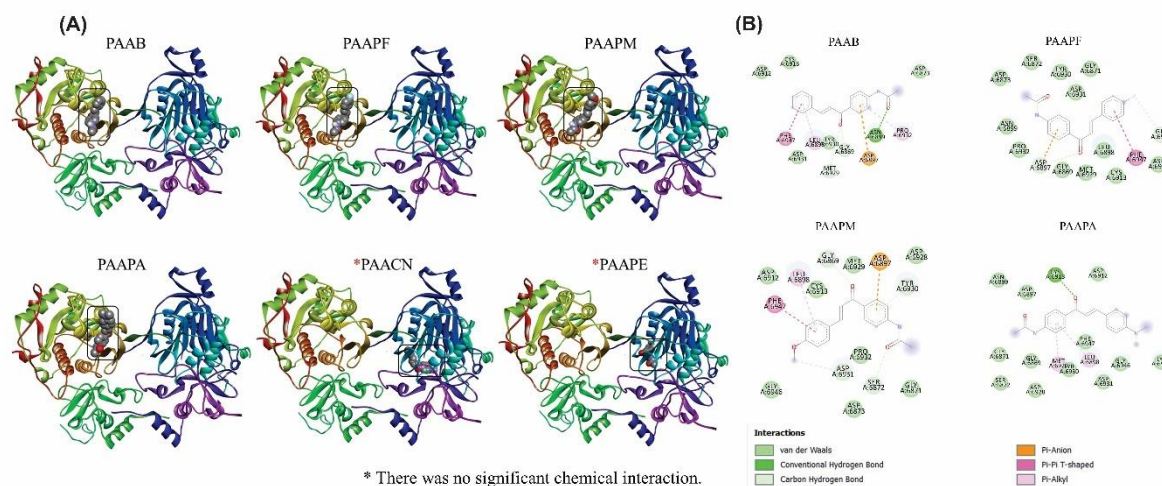


**Fig. 3.** Simulated interaction between the chalcones derivatives and the enzyme NSP16-NSP10 SARS-CoV-2 heterodimer methyltransferase (A). The bi-dimensional map of the hydrogen bonds and the hydrophobic interaction between the chalcones derivatives and the enzyme NSP16-NSP10 SARS-CoV-2 heterodimer methyltransferase (B).

### 3.3 Interactions with the SPIKE protein of the SARS-CoV-2 and with the ACE2

To study the potential of the chalcone acetamide derivatives to inhibit the interaction of the virus that causes COVID-19 with the target cells, a simulation of the interaction of the chalcones with the heterodimeric proteins of the virus, the Spike proteins, was carried out. The illustrations of the coupling simulations are contained in Figure 4A. It was possible to observe that all chalcones had connections with similar regions of the protein. According to data of interaction energy and RMSD contained in Table S2 (Supplementary material), it is observed that all chalcones had satisfactory affinity  $< -6.0$  Kcal/mol. In particular, the PAAPA and PAACN derivatives showed the best affinity values ( $-7.0$  and  $-6.9$ , respectively), demonstrating the link of greater stability between chalcones.

The interactions with the amino acid residues of Spike protein heterodimer and the chalcones molecules were represented in bi-dimensional maps, corroborating with the information collected in the molecular docking simulations (Figure 4C). Besides, the specific interactions of the chalcones derivatives with the Spike protein are shown in Table S5 (Supplementary material). It is possible to observe that the chalcone derivatives showed a pattern of interaction with the protein, as with the SER371 residue, which the derivatives interacted through the hydrogen of moderate intensity. Furthermore, the PAAPM and PAAPE chalcones showed, at least, one interaction of strong intensity, and the chalcone PAAPA did not

show hydrogen bonds with the Spike protein.

Additionally, it is known that the interaction of the SPIKE protein with ACE2 is necessary for the virus to enter the host cells, hence the simulations of the interactions of the chalcone derivatives with this enzyme were performed, as shown in Figure 4B. It is possible to observe that the chalcones interacted in similar sites, except for PAACN, which may have interacted at a non-specific site. Those data are reinforced by the affinity energy of the connections and RMSD, which the PAACN presented higher values, indicating an interaction of lower stability. PAAB and PAAPA had lower affinity values, with PAAPA having the best-suggested interaction, with an affinity of -8.0 Kcal/mol associated with a low RMSD value (1,355 Å).

Those results are reinforced when characterizing the interactions of the chalcones derivatives with the ACE2 protein, as illustrated in the bi-dimensional maps (Figure 4D) and the interaction distances are shown in Table S5 (Supplementary material). The chalcones PAAPA and PAAPF stood out for presenting two interactions of strong hydrogen bonds. Also, the chalcones derivatives had common binding sites, such as the ILE291 residue, in which the PAAPA even had a hydrogen bond.

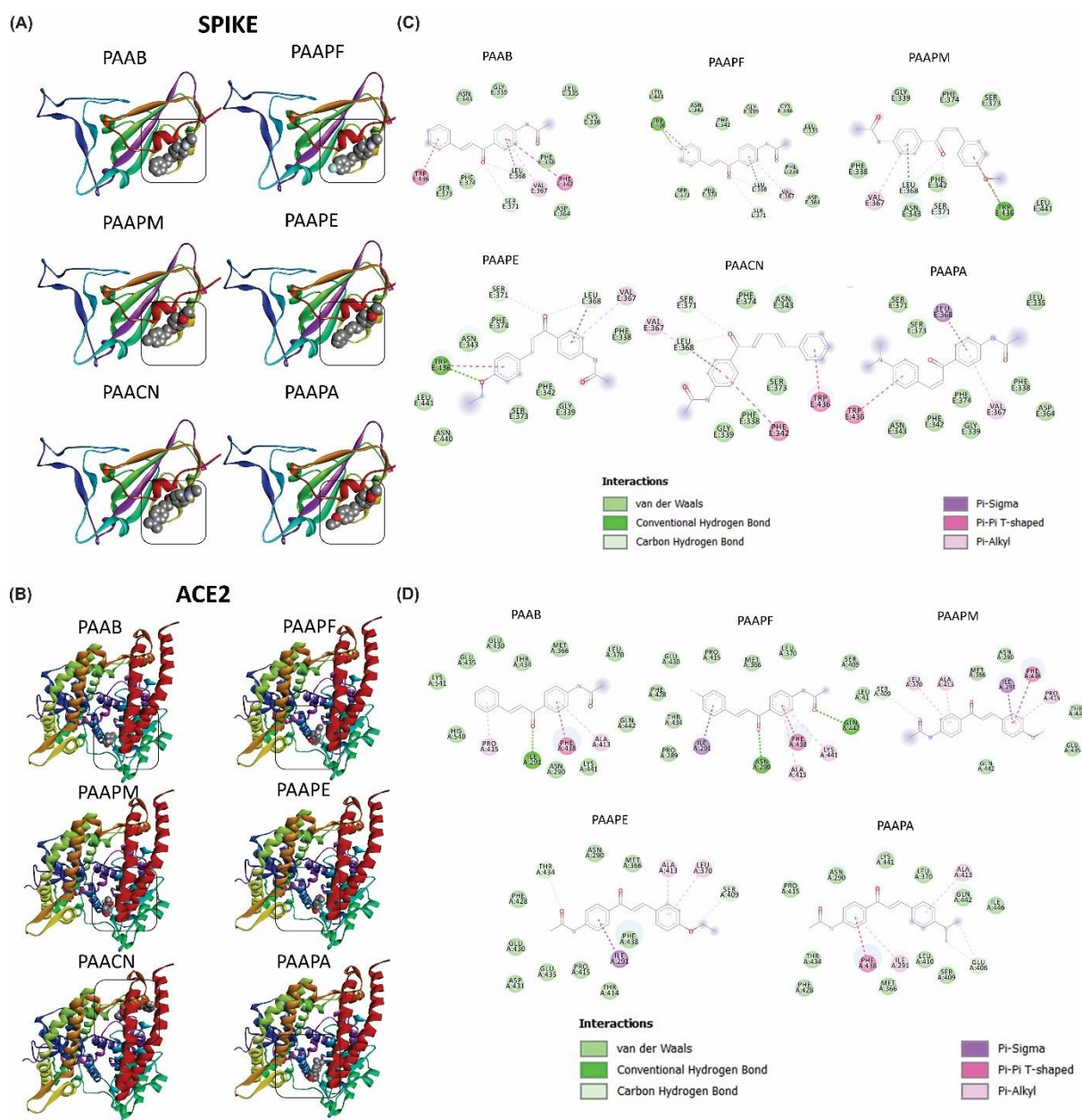


**Fig. 4.** Calculated interaction positions of the studied chalcones with the SPIKE (A) protein and the ACE2 protein of the human host (B). The bi-dimensional map of the hydrogen bonds and hydrophobic interactions between the chalcones and the SPIKE protein of the SARS-CoV-2 (C) and between the ACE2 protein of the human host (D).

#### 4 Discussion

Overall, the present work evaluated, through molecular docking assays, the interactions of chalcone acetamide derivatives with enzymatic and structural targets of SARS-CoV-2 and with the host's ACE2, which is recognized by the virus, facilitating its entry into cells. Therefore, it was observed that, regarding the interactions of chalcones with Main protease (Mpro), the PAAPF derivative has the potential for coupling in the same region as the natural inhibitor FJC

through strong hydrogen bonding. The formation of two strong hydrogen bonds between PAAB and the NSP16-NSP10 heterodimer methyltransferase was also noted. PAAPM and PAAPE showed at least one strong intensity interaction of the SPIKE protein. PAAPA had a better affinity with ACE2, with strong hydrogen interactions.

These results are relevant, as several chalcones have been described as having antiviral activity. A work performed by Park et al [20] showed that chalcones isolated from *Angelica Keiskei* inhibit the chymotrypsin protease (3CL (pro)) and a papain protease (PL (pro)) in SARS-CoV. Proteases are important for post-translational modifications of structural proteins in the viral particle. Therefore, the inhibition of proteases interferes with the viral replication process [20]. Literature data suggest the inhibition of viral proteases by flavonoids and related compounds. For example, flavonoids such herbacetin, isobavachalcone, quercetin 3- $\beta$ -d-glucoside and helicrysetin have been described as potent inhibitors of the Middle Eastern respiratory syndrome-coronavirus protease (MERS-CoV 3CLpro), indicating that flavonol and chalcones are favorite structures for binding to the catalytic site, suggesting that modifications in the more hydrophobic molecules or with carbohydrates attached to their main structures have a good inhibitory effect [21].

In fact, synthetic flavonoids and chalcones are described for potential antiviral properties. In a previous study, substituted chalcones, showed inhibition of viral translation in cells infected with hepatitis C virus (HCV) by the ablation of ribosomal protein phosphorylation 6 (rps6) [22]. Additionally, several reports in the literature demonstrate that derivatives of chalcones present antiviral activity better than the reference drugs in experimental models, including synergistic effects with these. For example, a previous study showed that thienyl-chalcone derivatives showed moderate to excellent antiviral activity, with higher *in vitro* potency against human cytomegalovirus compared to the standard drug Ganciclovir [23]. These data corroborate the findings of the present study, in which the chalcone derivatives interacted with the virus protease at sites and with similar affinities to the clinically used drugs and the theoretical inhibitor FJC.

Binding and inhibiting the enzymatic activity of proteases and methyltransferases can lead to a disruption in the viral capsid construction process, interrupting the flow of transmission. In this sense, the importance of *in silico* screening of phytochemical compounds is ratified, allowing a preliminary and rational analysis of a high number of molecules. For example, an investigation of phytochemicals as antiviral agents against dengue has shown that secondary phenolic plant metabolites such as alkaloids, terpenoids, chalcones, flavonoids, coumarins, and quinones have the potential to bind to targets such as protease (NS2B-NS3pro),

helicase (NS3 helicase), methyltransferase (MTase) and dengue virus envelope protein [24].

Therefore, it is evident that it is feasible to study the interaction of drugs and antiviral molecules with structural proteins of these viruses, in addition to enzyme targets. Flavone derivatives, such as luteolin and semisynthetic derivatives of gallic acid have been described as potential binders to the SARS-CoV surface SPIKE protein and, therefore, may interfere with the entry of the virus into its host cells. This connection has been shown to happen with great avidity, with surface proteins linked to natural compounds being detected by frontal affinity chromatography coupled with mass spectrometry [25].

The inhibition of the interaction of virus structural proteins with receptors in host cells is a line of research that has been highlighted. It is described that when binding the SPIKE protein to the angiotensin-converting enzyme 2 (ACE2) in the lung and intestinal cells, the virus enters the cells, releasing proteins such as the high-mobility group box 1 protein (HMGB1), allowing the occurrence of sepsis. Phenolic compounds have been described as steric inhibitors of the interaction of the viral structure with ACE2 and / or the release of HMGB1, reducing infectivity [26].

Together, these results suggest that chalcone derivatives inhibit the interaction of the virus with host cells through binding to ACE2 or SPIKE protein, probably generating a steric impediment. In addition, chalcones have an affinity for important enzymes in post-translational processes, interfering with viral replication.

## 5 Conclusion

The 4'-acetamidechalcones presented inhibitory potential over the SARS-CoV-2 proteins, detaching the PAAPF that has the potential to couple to Mpro (same region as the natural inhibitor FJC through strong hydrogen bonds), PAAB that can bind to NSP16- NSP10 methyltransferase, PAAPM and PAAPE that can interact with the protein Spike and PAAPA that demonstrated a strong affinity with ACE2, these results being a strong indication of the pharmacological potential of 4'-acetamidechalcones on important enzymes in post-translational processes, interfering in the viral replication of SARS-CoV-2, being an indication for the feasibility of *in vitro* tests. Emphasizing that the present work represents a fundamental step in the process of developing a pharmacological tool for COVID-19 based on chalcones.



### Interest conflicts

The authors declare no conflicts of interest.

### Acknowledgment

The authors thank PROGRAMA INOVA FIOCRUZ - CE/FUNCAP, CAPES and CNPq for financial support and scholarship. Hécio S. dos Santos also acknowledges financial support from the FUNCAP-BPI (BP4-0172-00075.01.00/20).

### Reference

- [1] A.E. Gorbalenya, S.C. Baker, R.S. Baric, R.J. de Groot, C. Drosten, A.A. Gulyaeva, B.L. Haagmans, C. Lauber, A.M. Leontovich, B.W. Neuman, D. Penzar, S. Perlman, L.L.M. Poon, D.V. Samborskiy, I.A. Sidorov, I. Sola, J. Ziebuhr, V. Coronaviridae Study Group of the International Committee on Taxonomy of, The species Severe acute respiratory syndrome-related coronavirus: classifying 2019-nCoV and naming it SARS-CoV-2, *Nat Microbiol* 5 (2020) 536-544. <https://doi.org/10.1038/s41564-020-0695-z>.
- [2] Y. Chen, Q. Liu, D. Guo, Emerging coronaviruses: Genome structure, replication, and pathogenesis, *J Med Virol* 92 (2020) 418-423. <https://doi.org/10.1002/jmv.25681>.
- [3] A.A. Siddiqui, A. Rahman, Shaharyar, R. Mishra, Synthesis and anticonvulsant activity of some substituted 3,5-diphenyl-2-pyrazoline-1-carboxamide derivatives, *Chem Sci J* 1 (2010). <https://doi.org/10.4172/2150-3494.1000006>.
- [4] P.T.da Silva, J.daCunhaXavier, T.S.Freitas,M.M.Oliveira, H.D.M.Coutinho, A.L.A.B.Leal, H.M.Barreto, P.N.Bandeira, C.E.S.Nogueira, D.M.SenaJr., F.W.Q.Almeida-Neto, E.S.Marinho, H.S.Santos, A.M.R.Teixeira, Synthesis, spectroscopic characterization and antibacterial evaluation by chalcones derived of acetophenone isolated from *Croton anisodontus* Müll.Arg., *J Mol Struct* 1226 (2021). <https://doi.org/10.1016/j.molstruc.2020.129403>.
- [5] Z. Nowakowska, A review of anti-infective and anti-inflammatory chalcones, *Eur J Med Chem* 42 (2007) 125-137. <https://doi.org/10.1016/j.ejmech.2006.09.019>.
- [6] J.C. Onyilagha, B. Malhotra, M. Elder, C.J. French, G.H.N. Towers, Comparative



- studies of inhibitory activities of chalcones on tomato ringspot virus (ToRSV), *Can J Plant Pathol* 19 (1997) 133-137. <https://doi.org/10.1080/07060669709500541>.
- [7] I.A. Santos, Atividade antiviral de compostos naturais brasileiros e hidroxichalconas e curcuminoides sintéticos. , Universidade Federal de Uberlândia-Instituto de Ciências Biomédicas, 2018.
- [8] B.A. Bhat, K.L. Dhar, S.C. Puri, A.K. Saxena, M. Shanmugavel, G.N. Qazi, Synthesis and biological evaluation of chalcones and their derived pyrazoles as potential cytotoxic agents, *Bioorg Med Chem Lett* 15 (2005) 3177-3180. <https://doi.org/10.1016/j.bmcl.2005.03.121>.
- [9] P.N. Bandeira, T.L.G. Lemos, H.S. Santos, M.C.S. de Carvalho, D.P. Pinheiro, M.O. de Moraes, C. Pessoa, F.W.A. Barros-Nepomuceno, T.H.S. Rodrigues, P.R.V. Ribeiro, H.S. Magalhaes, A.M.R. Teixeira, Synthesis, structural characterization, and cytotoxic evaluation of chalcone derivatives, *Med Chem Res* 28 (2019) 2037–2049. <https://doi.org/10.1007/s00044-019-02434-1>.
- [10] Z. Jin, X. Du, Y. Xu, Y. Deng, M. Liu, Y. Zhao, B. Zhang, X. Li, L. Zhang, C. Peng, Y. Duan, J. Yu, L. Wang, K. Yang, F. Liu, R. Jiang, X. Yang, T. You, X. Liu, X. Yang, F. Bai, H. Liu, X. Liu, L.W. Guddat, W. Xu, G. Xiao, C. Qin, Z. Shi, H. Jiang, Z. Rao, H. Yang, Structure of Mpro from SARS-CoV-2 and discovery of its inhibitors, *Nature* 582 (2020) 289-293. <https://doi.org/10.1038/s41586-020-2223-y>.
- [11] M. Rosas-Lemus, G. Minasov, L. Shuvalova, N.L. Inniss, O. Kiryukhina, G. Wiersum, Y. Kim, R. Jedrzejczak, N.I. Maltseva, M. Endres, L. Jaroszewski, A. Godzik, A. Joachimiak, K.J.F. Satchell, The crystal structure of nsp10-nsp16 heterodimer from SARS-CoV-2 in complex with S-adenosylmethionine, *bioRxiv* (2020) 2020.2004.2017.047498. <https://doi.org/10.1101/2020.04.17.047498>.
- [12] J. Lan, J. Ge, J. Yu, S. Shan, H. Zhou, S. Fan, Q. Zhang, X. Shi, Q. Wang, L. Zhang, X. Wang, Structure of the SARS-CoV-2 spike receptor-binding domain bound to the ACE2 receptor, *Nature* 581 (2020) 215-220. <https://doi.org/10.1038/s41586-020-2180-5>.
- [13] O. Trott, A.J. Olson, AutoDock Vina: Improving the speed and accuracy of docking with a new scoring function, efficient optimization, and multithreading, *Journal of Computational Chemistry* 31 (2010) 455-461. <https://doi.org/10.1002/jcc.21334>.

- [14] S. Shityakov, C. Förster, In silico predictive model to determine vector-mediated transport properties for the blood-brain barrier choline transporter, *Adv Appl Bioinform Chem* 7 (2014) 23-36. <https://doi.org/10.2147/aabc.s63749>.
- [15] D. Yusuf, A.M. Davis, G.J. Kleywegt, S. Schmitt, An Alternative Method for the Evaluation of Docking Performance: RSR vs RMSD, *J Chem Inf Model* 48 (2008) 1411-1422. <https://doi.org/10.1021/ci800084x>.
- [16] D.S. Biovia, H.M. Berman, J. Westbrook, Z. Feng, G. Gilliland, T.N. Bhat, H. Weissig, I.N. Shindyalov, P.E. Bourne, T. Darden, D. York, L.G. Pedersen, G. Bussi, D. Donadio, M. Parrinello, U. Essmann, L. Perera, M.L. Berkowitz, T. Darden, H. Lee, L.G. Pedersen, M. Parrinello, A. Rahman, V. Hornak, R. Abel, A. Okur, B. Strockbine, A. Roitberg, C. Simmerling, M.J. Abraham, T. Murtola, R. Schulz, S. Páll, J.C. Smith, B. Hess, E. Lindahl, H.J.C. Berendsen, J.P.M. Postma, W.F. Van Gunsteren, A. Dinola, J.R. Haak, R.W. Hockney, S.P. Goel, J.W. Eastwood, C.A. Davey, D.F. Sargent, K. Luger, A.W. Maeder, T.J. Richmond, Dassault Systèmes BIOVIA, Discovery Studio Visualizer, v.17.2, San Diego: Dassault Systèmes, *J Chem Phys* 10 (2000). [https://doi.org/10.1016/0021-9991\(74\)90010-2](https://doi.org/10.1016/0021-9991(74)90010-2).
- [17] E.F. Pettersen, T.D. Goddard, C.C. Huang, G.S. Couch, D.M. Greenblatt, E.C. Meng, T.E. Ferrin, UCSF Chimera—A visualization system for exploratory research and analysis, *Journal of Computational Chemistry* 25 (2004) 1605-1612. <https://doi.org/10.1002/jcc.20084>.
- [18] F.A. Ruffinatti, T. Genova, F. Mussano, L. Munaron, MORPHEUS: An automated tool for unbiased and reproducible cell morphometry, *J Cell Physiol* 235 (2020) 10110-10115. <https://doi.org/10.1002/jcp.29768>.
- [19] A. Imberty, K.D. Hardman, J.P. Carver, S. Perez, Molecular modelling of protein-carbohydrate interactions. Docking of monosaccharides in the binding site of concanavalin A, *Glycobiology* 1 (1991) 631-642. <https://doi.org/10.1093/glycob/1.6.631>.
- [20] J.-Y. Park, J.-A. Ko, D.W. Kim, Y.M. Kim, H.-J. Kwon, H.J. Jeong, C.Y. Kim, K.H. Park, W.S. Lee, Y.B. Ryu, Chalcones isolated from *Angelica keiskei* inhibit cysteine proteases of SARS-CoV, *J Enzyme Inhib Med Chem* 31 (2016) 23-30. <https://doi.org/10.3109/14756366.2014.1003215>.

- [21] S. Jo, H. Kim, S. Kim, D.H. Shin, M.-S. Kim, Characteristics of flavonoids as potent MERS-CoV 3C-like protease inhibitors, *Chem Biol Drug Des* 94 (2019) 2023-2030. <https://doi.org/10.1111/cbdd.13604>.
- [22] N. Mateeva, S.V.K. Eyunni, K.K. Redda, U. Ononuju, T.D. Hansberry, C. Aikens, A. Nag, Functional evaluation of synthetic flavonoids and chalcones for potential antiviral and anticancer properties, *Bioorg Med Chem Lett* 27 (2017) 2350-2356. <https://doi.org/10.1016/j.bmcl.2017.04.034>.
- [23] V. Patil, S.A. Patil, R. Patil, A. Bugarin, K. Beaman, S.A. Patil, Exploration of (hetero)aryl Derived Thienylchalcones for Antiviral and Anticancer Activities, *Med Chem* 15 (2019) 150-161. <https://doi.org/10.2174/1573406414666180524074648>.
- [24] C.N. Powers, W.N. Setzer, An In-Silico Investigation of Phytochemicals as Antiviral Agents Against Dengue Fever, *Comb Chem High Throughput Screen* 19 (2016) 516-536. <https://doi.org/10.2174/1386207319666160506123715>.
- [25] L. Yi, Z. Li, K. Yuan, X. Qu, J. Chen, G. Wang, H. Zhang, H. Luo, L. Zhu, P. Jiang, L. Chen, Y. Shen, M. Luo, G. Zuo, J. Hu, D. Duan, Y. Nie, X. Shi, W. Wang, Y. Han, T. Li, Y. Liu, M. Ding, H. Deng, X. Xu, Small Molecules Blocking the Entry of Severe Acute Respiratory Syndrome Coronavirus into Host Cells, *J Virol* 78 (2004) 11334. <https://doi.org/10.1128/JVI.78.20.11334-11339.2004>.
- [26] M. Wyganowska-Swiatkowska, M. Nohawica, K. Grocholewicz, G. Nowak, Influence of Herbal Medicines on HMGB1 Release, SARS-CoV-2 Viral Attachment, Acute Respiratory Failure, and Sepsis. A Literature Review, *Int J Mol Sci* 21 (2020). <https://doi.org/10.3390/ijms21134639>.

## Supplementary Material

**Table S1.** Protein, grid box centres, sizes, spacing and exhaustiveness used for molecular docking simulations.

Protein	Center			Size			Spacing	Exhaustiveness
	x	y	z	x	y	z		
Mpro	-	13.009	56.185	94	112	108	0.642	8
	26.734							
NSP16-NSP10	78.486	-1.045	-9.341	102	126	108	0.764	8
SPIKE	-	29.339	21.745	92	104	126	0.453	8
	31.044							
ACE2	-	19.272		126	126	126	0.564	8
	20.871		27.086					

Legend: Methyltransferase (NSP16-NSP10).

**Table S2.** Interaction energy and RMSD in molecular docking assay with Main protease, Methyltransferase, SPIKE and ACE2.

Ligands	Mpro		Methyltransferase		SPIKE		ACE2	
	Energy	RMSD	Energy	RMSD	Energy	RMSD	Energy	RMSD
Chalcones								
PAAB	-5.2	1.689	-7.4	1.743	-6.8	1.763	-8.2	1.847
PAACN	-6.1	1.853			-6.9	1.590	-7.4	1.866
PAAPA	-5.5	1.822	-8.0	1.930	-6.6	1.168	-8.0	1.355
PAAPE	-5.5	1.635			-6.6	1.456	-7.7	1.644
PAAPF	-5.6	1.721	-8.2	1.947	-7.0	1.759	-7.7	1.658
PAAPM	-5.3	1.505	-7.1	1.260	-6.8	1.229	-7.6	1.481
Inhibitors								
FJC	-6.7	1.580						
Anakinra	-6.5	1.998						
Azithromycin	-5.8	1.244						
Remdesivir	-6.8	1.643						

Legend: Energy (Kcal/mol); RMSD (Å).

**Table S3.** Interaction distances (Å) between the compounds and the amino acid residues of

the enzyme Mpro.

Chalcon/Residue	PAAB	PAAPA	PAAPF	FJC	Anakinra	Azithromycin	Remdesivir
LYS5					2.69		3.23*
THR25			2.95*				
GLN10						2.40*	
LYS137		3.69			3.14*		3.54
LEU141			3.29				
ANS142			2.31*				
GLY143				2.56*			
SER144				3.45*			
CYS145				1.93*			
TYR154				-		3.93	
HIS164				2.36*			
MET165				3.88			
GLU166			3.92	1.83*			
GLU166			2.64*				
GLN189				3.03			
ASP197		3.03*			2.31*		3.22*
ANS238		3.43*					
ILE249						3.67	
GLU288							2.49*
ASP289					3.41*		1.88*
GLU290		3.76			2.33		3.61*
PRO293	3.62					3.65	
PHE294	3.66					3.59	
PHE294	3.85					3.58	
VAL297	3.80						
ARG298	2.60*						

Legend: \*Hydrogen bounds.

**Table S4.** Interaction distances (Å) between the compounds and the amino acid residues of the enzyme NSP16-NSP10 SARS-CoV-2 heterodimer methyltransferase.

Chalcon/Residue	PAAB	PAAPA	PAAPF	PAAPM
GLY6869			3.30*	

ASP6873	3.70				
LEU6898	3.52	3.43	3.23	3.22	
LEU6898		3.46	2.57*	2.98*	
LEU6898			3.00*	3.49*	
ASN6899	2.29*				
TYR6930	2.87*				
MET6929		3.76		3.81	
CYS6913		2.11*			
ASP6931	3.75		3.80	3.88	
PRO6932	3.90				
PHE6947	3.53		3.60	3.70	

Legend: \*Hydrogen bounds.

**Table S5.** Interaction distances (Å) between the compounds and the amino acid residues of the SPIKE protein and ACE2.

Chalcon/Residue	PAAB	PAACN	PAAPA	PAAPE	PAAPF	PAAPM
<b>SPIKE</b>						
PHE338	3.57	3.48	3.70	3.45	3.58	3.46
GLY339	3.51*	3.26*		3.35*		3.31*
PHE342		3.72	3.48			
VAL367	3.71	3.78	3.69	3.73	3.67	3.72
LEU368	3.65	3.73	3.60	3.64	3.66	3.67
SER371	3.45*	3.37*	-	3.38*	3.52*	3.33*
PHE374	3.46	3.90	3.40	3.42	3.50	3.58
TRP436	3.57		4.95	3.45	3.55	2.58*
TRP436			3.75	2.62*	4.72	3.58
LEU441				3.93		
<b>ACE2</b>						
ANS290					2.61*	
ILE291	2.11*		3.06*	3.83	3.64	3.67
ILE291	3.56		3.43	3.94	3.42	3.89
ILE291			3.82	3.75		3.64
LEU370				3.93	3.93	

LEU370				3.82	3.93	
SER409				3.60*	-	
ALA413				3.63	4.00	
PRO415	3.38	-	-	-	-	3.86
GLU430	3.66	-	-	3.77	-	-
THR434	-	-	-	-	3.71	-
GLU435	3.32	-	-	3.58	-	-
PHE438	3.38	-	3.81	3.55	3.22	3.69
PHE438	3.66	-	3.47	-	3.54	4.40
LYS441	-	-	3.01*	-	3.83	-
GLN442	-	-	-	-	2.93*	-

---

Legend: \*Hydrogen bounds.

## CONCLUSION

All the structural, electronic, spectroscopy, non-linear optical properties, and antioxidant activity characterizations were possible since all the three quantum methods used were able to achieve an optimized geometry with no imaginary frequencies. Furthermore, the quantum methods predicted that the PAAPFBA molecule has not the two aromatic rings in the same plane delimited by the  $\alpha,\beta$ -unsaturated system. The M06-2X method had the highest distortion angle value with a difference of  $7.06452^\circ$  in comparison with the other methods. The structural parameters were compared with experimental results from literature and with the results of other calculations. The results were that the PAAPFBA molecule was well described by all the DFT methods that were used due to excellent correlation.

The thermodynamic properties were similar, and the fundamental infrared vibrational modes were in excellent agreement with the experimental data, regardless of the method again. The values computed for  $R^2$  showed the excellent agreement between experimental and theoretical results., which were respectively 0.99791 for the B3LYP, 0.99779 for the mPW1PW91), and 0.99835 for the M06-2X method. The  $^1\text{H}$  and  $^{13}\text{C}$  theoretical chemical shifts also exhibited excellent agreement with the experimental data with the  $R^2$  of 0.99865 fo the B3LYP, 0.99860 for the mPW1PW91, and 0.99844 for the M06-2X method. All three methods showed that the chalcone PAAPFBA can be used to make non-linear optical devices since this molecule has higher values for the total dipole moment, polarizability, and first hyperpolarizability. The Frontier Molecular Orbital analysis predicted a similar HOMO and LUMO distribution between the methods. However, the quantum molecular descriptors showed different values when the method is shifted. This happens due to the change in the mathematical approximation within the method itself.

The Fukui Electronics and Condensed functions, the local descriptors, and the analysis of the Natural Bond Orbitals were carried out to characterize locally the electronic properties of the PAAPFBA chalcone. The B3LYP and mPW1PW91 methods can describe the molecule very similarly. However, the M06-2X illustrates differences in reactive sites (radical attack), and the electron density was predicted to be more delocalized (higher stabilization energy value).

Next, the antioxidant activity was determined using all the three DFT methods to investigate the possible three mechanisms: HAT, SET-PT, and SLET. All global thermodynamic parameters calculated were found to be above  $80 \text{ kcal.mol}^{-1}$  regardless of the method, which



explains the moderate experimental value of 50.92% in the DPPH scavenging. Therefore, the most thermodynamically favorable mechanism is the HAT for all methods.

Finally, once the quantum calculation methodology was determined to optimize the chalcone derivatives, six chalcone derivatives denominated PAAPFBA, PAAB, PAAPM, PAAPE, PAAPA, and PAACN were used to study the antiviral activity of chalcones. The results showed an inhibitory potential on SARS-CoV-2 target proteins, highlighting the coupling to Main protease (Mpro) in the same region as the natural inhibitor FJC by strong hydrogen bonds for the PAAPFBA molecule. The chalcone PAAB interacted with the NSP16-NSP10 methyltransferase, while the PAAPM and PAAPE interacted with the SPIKE protein. Hence, these chalcones can interfere in the replication of the virus and blocking it from the bond with the human host cells. In addition, the chalcone PAAPA was found to have a strong interaction with the ACE2 of the human host. Hence this molecule can also block the bond of the SPIKE protein of SARS-CoV-2 with the human cells.

These results are a strong indication of the pharmacological potential of chalcone derivatives containing the 4-acetamido group on important enzymes in post-translational processes, interfering with the viral replication of SARS-CoV-2, being an indication for the viability of in vitro tests.

## REFERENCES

- [1] XAVIER, J. DA C. et al. Spectroscopic analysis by NMR, FT-Raman, ATR-FTIR, and UV-vis, evaluation of antimicrobial activity, and in silico studies of chalcones derived from 2-hydroxyacetophenone. **Journal of Molecular Structure**, [s.l.], v. 1241, p. 130647, 2021.
- [2] XAVIER, J. DA C. et al. Structural characterization, electronic properties, and anxiolytic-like effect in adult zebrafish (*Danio rerio*) of cinnamaldehyde chalcone. **Journal of Molecular Structure**, [s.l.], v. 1222, 2020.
- [3] DA CUNHA XAVIER, J. et al. Structural characterization, DFT calculations, ADMET studies, antibiotic potentiating activity, evaluation of efflux pump inhibition and molecular docking of chalcone (E)-1-(2-hydroxy-3,4,6-trimethoxyphenyl)-3-(4-methoxyphenyl)prop-2-en-1-one. **Journal of Molecular Structure**, [s.l.], v. 1227, p. 129692, 2021.
- [4] GOMES, M. N. et al. Chalcone derivatives: Promising starting points for drug design. **Molecules**, [s.l.], v. 22, n. 8, 2017.
- [5] SCHMIDT, J. G. Ueber die Einwirkung von Aceton auf Furfurol und auf Bittermandelöl in Gegenwart von Alkalilauge. **Ber. Dtsch. Chem. Ges**, [s.l.], v. 14, p. 1459–1461, 1881.
- [6] CLAISEN, L.; CLAPARÈDE, A. Condensationen von Ketonen mit Aldehyden. **Ber. Dtsch. Chem. Ges.**, [s.l.], v. 14, p. 2460–2468, 1881.
- [7] ELAMATHI, P.; CHANDRASEKAR, G.; BALAMURALI, M. M. Nanoporous AlSBA-15 catalysed Claisen–Schmidt condensation for the synthesis of novel and biologically active chalcones. **Journal of Porous Materials**, [s.l.], v. 27, n. 3, p. 817–829, 2020.
- [8] FERREIRA, M. K. A. et al. Anxiolytic-like effect of chalcone N-{(4-[(E)-3-(4-fluorophenyl)-1-(phenyl) prop-2-en-1-one]} acetamide on adult zebrafish (*Danio rerio*): Involvement of the GABAergic system. **Behavioural Brain Research**, [s.l.], v. 374, n. December 2018, p. 3–8, 2019.
- [9] LI, J. T.; et al. Improved synthesis of chalcones under Ultrasonal irradiation. **Ultrasonics Sonochemistry**, [s.l.], v.9, p. 237-239, 2002.
- [10] DIMMOCK, J.R.; ELIAS, D.W.; BENAZELY, M.A.; KANDEPU, N.M. Bioactivities of chalconas. **Curr Med Chem**, [s.l.], v. 6, n. 12, p. 1125–11249, 1999.
- [11] NI, L.; MENG, C.Q.; SIKOKSKI, J.A. Recent advances in therapeutic chalcones. **Expert Opinion on Therapeutic Patents**, [s.l.], v. 14, n. 12, p. 1669 - 1691, 2004.
- [12] NOWAKOWSKA, Z.A. A review of anti-inflammatory chalcones. **European Journal of Chemistry**, [s.l.], v. 42, p. 125–137, 2007.

- [13] DA SILVA, P. T. et al. Synthesis, spectroscopic characterization and antibacterial evaluation by chalcones derived of acetophenone isolated from *Croton anisodontus* Müll.Arg. **Journal of Molecular Structure**, [s.l.], v. 1226, 2021.
- [14] VANANGAMUDI, G.; SUBRAMANIAN, M.; THIRUNARAYANAN, G. Synthesis, spectral linearity, antimicrobial, antioxidant, and insect antifeedant activities of some 2,5-dimethyl-3-thienyl chalcones. **Arabian Journal of Chemistry**, [s.l.], v. 10, S1254–S1266, 2017.
- [15] WANG, M. et al. Pharmacological review of isobavachalcone, a naturally occurring chalcone. **Pharmacological Research**, [s.l.], v. 165, n. December 2020, p. 105483, 2021.
- [16] FU, Y. et al. New chalcone derivatives: Synthesis, antiviral activity, and mechanism of action. **RSC Advances**, [s.l.], v. 10, n. 41, p. 24483–24490, 2020.
- [17] ALAAELDIN, R. et al. In vitro inhibition and molecular docking of a new ciprofloxacin-chalcone against SARS-CoV-2 main protease. **Fundamental and Clinical Pharmacology**, [s.l.], n. 6, p. 1–11, 2021.
- [18] ZHOU, X. et al. Design, synthesis and anti-TMV activity of novel  $\alpha$ -aminophosphonate derivatives containing a chalcone moiety that induce resistance against plant disease and target the TMV coat protein. **Pesticide Biochemistry and Physiology**, [s.l.], v. 172, n. October 2020, p. 104749, 2021.
- [19] LEAL, A. L. A. B. et al. Structural and spectroscopic analysis and evaluation of cytotoxic activity of 2-hydroxychalcones against human cancer cell lines. **Journal of Molecular Structure**, [s.l.], v. 1245, p. 131135, 2021.
- [20] MELLADO, M. et al. Design, synthesis, antifungal activity, and structure–activity relationship studies of chalcones and hybrid dihydrochromane–chalcones. **Molecular Diversity**, [s.l.], v. 24, n. 3, p. 603–615, 2020.
- [21] DÍAZ-CARRILLO, J. T. et al. Synthesis of leading chalcones with high antiparasitic, against *hymenolepis nana*, and antioxidant activities. **Brazilian Journal of Pharmaceutical Sciences**, [s.l.], v. 54, n. 3, p. 1–13, 2018.
- [22] HUANG, Z. H. et al. Screening of chalcone analogs with anti-depressant, anti-inflammatory, analgesic, and COX-2-inhibiting effects. **Bioorganic and Medicinal Chemistry Letters**, [s.l.], v. 30, n. 11, p. 127173, 2020.
- [23] DOS SANTOS, M. B. et al. Antiproliferative activity and p53 upregulation effects of chalcones on human breast cancer cells. **Journal of Enzyme Inhibition and Medicinal Chemistry**, [s.l.], v. 34, n. 1, p. 1093–1099, 2019.
- [24] VÁSQUEZ-MARTÍNEZ, Y. A. et al. Antimicrobial, anti-inflammatory and antioxidant activities of polyoxygenated chalcones. **Journal of the Brazilian Chemical Society**, [s.l.], v. 30, n. 2, p. 286–304, 2019.
- [25] BEYHAN, N. et al. Synthesis and anticonvulsant activity of some 2-pyrazolines derived from chalcones. **Arabian Journal of Chemistry**, [s.l.], v. 10, p. S2073–S2081, 2017.

- [26] ROCHA, S. et al. A Systematic Review on Anti-diabetic Properties of Chalcones. **Current Medicinal Chemistry**, [s.l.], v. 27, n. 14, p. 2257–2321, 2018.
- [27] WELDAY KAHSSAY, S.; HAILU, G. S.; DESTA, K. T. Design, synthesis, characterization, and in vivo antidiabetic activity evaluation of some chalcone derivatives. **Drug Design, Development and Therapy**, [s.l.], v. 15, p. 3119–3129, 2021.
- [28] TANG, Y. L. et al. Synthesis and anti-inflammatory evaluation of new chalcone derivatives bearing bispiperazine linker as IL-1- $\beta$ -inhibitors. **Bioorganic Chemistry**, [s.l.], v. 98, n. 3, p. 103748, 2020.
- [29] SOOKNUAL, P. et al. Synthesis and neuroprotective effects of novel chalcone-triazole hybrids. **Bioorganic Chemistry**, [s.l.], v. 105, p. 104384, 2020.
- [30] FERREIRA, M. K. A. et al. Anxiolytic-like effect of chalcone N-{4'-[(2E)-3-(3-nitrophenyl)-1-(phenyl)prop-2-en-1-one]} acetamide on adult zebrafish (*Danio rerio*): Involvement of the 5-HT system. **Biochemical and Biophysical Research Communications**, [s.l.], v. 526, n. 2, p. 505–511, 2020.
- [31] LIMA, I. K. C. et al. Structural and spectroscopic investigation of the chalcones (E)-1-(4-aminophenyl)-3-(4'-ethoxyphenyl)-prop-2-en-1-one and (E)-1-(aminophenyl)-3-(4'-methoxyphenyl)-prop-2-en-1-one. **Vibrational Spectroscopy**, [s.l.], v. 110, n. July, p. 103118, 2020.
- [32] N. BANDEIRA, P. et al. Synthesis, structural characterization, and cytotoxic evaluation of chalcone derivatives. **Medicinal Chemistry Research**, [s.l.], v. 28, n. 11, p. 2037–2049, 2019.
- [33] ATLA, S. R.; SISTLA, R.; YEJELLA, R. P. STUDY OF THE ANTI-TUMOR ACTIVITY OF SYNTHETIC PYRIDO [2,3-d]PYRIMIDINES, PYRIMIDINES AND CORRESPONDING CHALCONE DERIVATIVES. **International Journal of Pharmaceutical Sciences and Research**, [s.l.], v. 9, n. 9, p. 3804–3814, 2018.
- [34] SEBA, V. et al. Chalcone derivatives 4'-amino-1-naphthyl-chalcone (D14) and 4'-amino-4-methyl-1-naphthyl-chalcone (D15) suppress migration and invasion of osteosarcoma cells mediated by p53 regulating emt-related genes. **International Journal of Molecular Sciences**, [s.l.], v. 19, n. 9, p. 1–13, 2018.
- [35] SANTOS, M. B. et al. Antiproliferative and pro-apoptotic activities of 2'- and 4'-aminochalcones against tumor canine cells. **European Journal of Medicinal Chemistry**, [s.l.], v. 138, p. 884–889, 2017.
- [36] ZERAIK, M. L. et al. 4'-Aminochalcones as Novel Inhibitors of the Chlorinating Activity of Myeloperoxidase. **Current Medicinal Chemistry**, [s.l.], v. 19, n. 31, p. 5405–5413, 2012.
- [37] IRFAN, R. et al. A comprehensive review of aminochalcones. **Molecules**, [s.l.], v. 25, n. 22, 2020.

- [38] DIMMOCK, J. R. et al. Cytotoxic 4'-Aminochalcones and Related Compounds. **Pharmazie**, [s.l.], v. 58, p. 227–232, 2003.
- [39] ROMAGNOLI, R. et al. Hybrid  $\alpha$ -bromoacryloylamido chalcones. Design, synthesis, and biological evaluation. **Bioorganic and Medicinal Chemistry Letters**, [s.l.], v. 19, n. 7, p. 2022–2028, 2009.
- [40] TRISTÃO, T. C. et al. Antimicrobial and cytotoxicity potential of acetamido, amino and nitrochalcones. **Arzneimittel-Forschung/Drug Research**, [s.l.], v. 62, n. 12, p. 590–594, 2012.
- [41] COVID-19 CORONAVIRUS PANDEMIC. **Worldometer COVID-19**, [s.l.]. Disponível em: <https://www.worldometers.info/coronavirus/>. Acessado em 16 out. 2021.
- [42] COVID-19 OUTBREAK A PANDEMIC. **World Health Organization**, [s.l.]. Disponível em: <https://www.euro.who.int/en/health-topics/health-emergencies/coronavirus-covid-19/news/news/2020/3/who-announces-covid-19-outbreak-a-pandemic>. Acessado em: 16 out. 2021.
- [43] HOW TO PROTECT YOURSELF & OTHERS. **Centers for Disease Control and Prevention**, [s.l.]. Disponível em: <https://www.cdc.gov/coronavirus/2019-ncov/prevent-getting-sick/prevention.html>. Acessado em: 16 out. 2021.
- [44] VIJAYAKUMAR, B. G. et al. In silico pharmacokinetic and molecular docking studies of natural flavonoids and synthetic indole chalcones against essential proteins of SARS-CoV-2. **European Journal of Pharmacology**, [s.l.], v. 886, p. 173448, 2020.
- [45] DURAN, N. et al. New Chalcone Derivatives as Effective Anti-SARS-CoV-2 Agents. **The International Journal of Clinical Practice**, [s.l.], 2021.
- [46] HANNAH CLARA, T.; MUTHU, S.; CHRISTIAN PRASANA, J. Quantum mechanical, spectroscopic and docking studies of (2E)-1-(4-aminophenyl)-3-(4-benzyloxyphenyl)-prop-2-en-1-one Chalcone derivative by density functional theory - A prospective respiratory drug. **Materials Today: Proceedings**, [s.l.], 2020.
- [47] KOSTOPOULOU, I. et al. Exploring the 2'-hydroxy-chalcone framework for the development of dual antioxidant and soybean lipoxygenase inhibitory agents. **Molecules**, [s.l.], v. 26, n. 9, 2021.
- [48] USTABAŞ, R. et al. New Chalcone Derivative: Synthesis, Characterization, Computational Studies and Antioxidant Activity. **Letters in Organic Chemistry**, [s.l.], v. 17, p. 46–53, 2020.
- [49] SALEHI, B. et al. Pharmacological Properties of Chalcones: A Review of Preclinical Including Molecular Mechanisms and Clinical Evidence. **Frontiers in Pharmacology**, [s.l.], v. 11, 2021.

- [50] JASIM, H. A. et al. Chalcones: Synthetic chemistry follows where nature leads. **Biomolecules**, [s.l.], v. 11, n. 8, 2021.
- [51] RAWAT, P. et al. Study of antimicrobial and antioxidant activities of pyrrole-chalcones. **Journal of Molecular Structure**, [s.l.], v. 1228, p. 129483, 2021.
- [52] GUAZELLI, C. F. S. et al. Antioxidant and anti-inflammatory effects of hesperidin methyl chalcone in experimental ulcerative colitis. **Chemico-Biological Interactions**, [s.l.], v. 333, n. 6 2020, p. 109315, 2021.
- [53] EDEN, W. T. et al. Synthesis of Chalcone Derivative from Clove Leaf Waste as a Natural Antioxidant. **Pharmaceutical Chemistry Journal**, [s.l.], v. 55, n. 3, p. 269–274, 2021.
- [54] ALISI, I. O.; UZAIRU, A.; IDRIS, S. O. Ligand-based design of chalcone analogues and thermodynamic analysis of their mechanism of free radical scavenge. **Journal of Molecular Modeling**, [s.l.], v. 27, n. 3, 2021.
- [55] CHE, Y.-F. et al. The Antioxidant, Anti-Inflammatory, and Neuroprotective Properties of the Synthetic Chalcone Derivative AN07. **Molecules**, [s.l.], v. 25, n. 12, p. 1–20, 2020.
- [56] XUE, Y. et al. Antioxidant and spectral properties of chalcones and analogous aurones: Theoretical insights. **International Journal of Quantum Chemistry**, [s.l.], v. 119, n. 3, p. 21–25, 2019.
- [57] CHEN, W. J. et al. Butein, a more effective antioxidant than  $\alpha$ -tocopherol. **Journal of Molecular Structure: THEOCHEM**, [s.l.], v. 763, n. 1–3, p. 161–164, 2006.
- [58] MATHEW, B. et al. Anti-oxidant behavior of functionalized chalcone-a combined quantum chemical and crystallographic structural investigation. **Journal of Molecular Structure**, [s.l.], v. 1146, p. 301–308, 2017.
- [59] GABER, M.; AWAD, M. K.; ATLAM, F. M. Pd (II) complexes of bidentate chalcone ligands: Synthesis, spectral, thermal, antitumor, antioxidant, antimicrobial, DFT and SAR studies. **Journal of Molecular Structure**, [s.l.], v. 1160, p. 348–359, 2018.
- [60] ARIF, R. et al. Facile synthesis of chalcone derivatives as antibacterial agents : Synthesis , DNA binding , molecular docking , DFT and antioxidant studies. **Journal of Molecular Structure**, [s.l.], v. 1208, p. 127905, 2020.
- [61] USTABAŞ, R. et al. New Chalcone Derivative: Synthesis, Characterization, Computational Studies and Antioxidant Activity, **Letters in Organic Chemistry**, [s.l.], v. 17, n. 1, p. 46-53, 2020.
- [62] DIAZ-URIBE, C. et al. Furanyl chalcone derivatives as efficient singlet oxygen quenchers. An experimental and DFT/MRCI study. **Tetrahedron**, [s.l.], v. 76, n. 24, 2020.

## APPENDIX A – AUTHOR'S CURRICULUM DATA



### Francisco Wagner de Queiroz Almeida Neto

Bolsista de Doutorado do CNPq

Endereço para acessar este CV: <http://lattes.cnpq.br/6426529527198879>

ID Lattes: **6426529527198879**

Última atualização do currículo em 26/08/2021

Graduado em Química Bacharelado pela Universidade Federal do Ceará (2015). Mestre em Química pela Universidade Federal do Ceará (2017). Doutorado em Química pela Universidade Federal do Ceará, atuando na área de Físico-Química no Grupo de Química Teórica (GQT) trabalhando em parceria com o Grupo de Química Teórica e Eletroquímica (GQTE) da Universidade Estadual do Ceará. Trabalhou em parceria com LabInício do Departamento de Física da Universidade Federal do Ceará (2016 - 2018). Foi monitor da disciplina de Química Geral (2013) e bolsista de Iniciação Científica no Laboratório de Materiais Funcionais Avançados (LaMFA) do Departamento de Física da Universidade Federal do Ceará (2014 - 2015). **(Texto informado pelo autor)**

### Identificação

<b>Nome</b>	Francisco Wagner de Queiroz Almeida Neto
<b>Nome em citações bibliográficas</b>	ALMEIDA-NETO, FRANCISCO W.Q.;ALMEIDA-NETO, F. W. Q.;ALMEIDA NETO, FRANCISCO WAGNER DE QUEIROZ;ALMEIDA-NETO, FRANCISCO WAGNER Q.;ALMEIDA NETO, FRANCISCO WAGNER Q.;ALMEIDA-NETO, FRANCISCO WAGNER QUEIROZ;ALMEIDA-NETO, F.W.Q.;ALMEIDA-NETO, FRANCISCO WAGNER DE QUEIROZ;Q. ALMEIDA-NETO, FRANCISCO WAGNER;QUEIROZ ALMEIDA NETO, FRANCISCO WAGNER;DE ALMEIDA-NETO, FRANCISCO W.Q.;Francisco Wagner de Queiroz Almeida-Neto;Francisco Wagner Queiroz Almeida-Neto;ALMEIDA-NETO, FRANCISCO W. Q.
<b>Lattes iD</b>	<a href="http://lattes.cnpq.br/6426529527198879">http://lattes.cnpq.br/6426529527198879</a>
<b>Orcid iD</b>	<a href="https://orcid.org/0000-0003-3317-5029">https://orcid.org/0000-0003-3317-5029</a>

### Endereço

### Formação acadêmica/titulação

<b>2018</b>	Doutorado em andamento em Química (Conceito CAPES 6). Universidade Federal do Ceará, UFC, Brasil. Orientador: Pedro de Lima Neto. Coorientador: Emmanuel Silva Marinho. Bolsista do(a): Conselho Nacional de Desenvolvimento Científico e Tecnológico, CNPq, Brasil.
<b>2016 - 2017</b>	Mestrado em Química (Conceito CAPES 6). Universidade Federal do Ceará, UFC, Brasil. Título: Propriedades Estruturais, Eletrônicas, Óticas e Vibracionais das ligas Ca1-xMgxO e Ba1-ySryO via DFT, Ano de Obtenção: 2018. Orientador:  Pedro de Lima Neto. Bolsista do(a): Coordenação de Aperfeiçoamento de Pessoal de Nível Superior, CAPES, Brasil. Palavras-chave: Ligas Ternárias; Compostos Iônicos; Óxidos alcalinos terrosos. Grande área: Ciências Exatas e da Terra
<b>2012 - 2016</b>	Graduação em Química. Universidade Federal do Ceará, UFC, Brasil. Título: FUNCIONALIZAÇÃO DE SUPERFÍCIE DE VIDRO COM ORGANOSILANO. Orientador: Amauri Jardim de Paula.
<b>2007 - 2009</b>	Ensino Médio (2º grau). Organização Educacional Farias Brito, OEFB, Brasil.

### Formação Complementar

<b>2016 - 2016</b>	Cromatografia Gasosa - Fundamentos e Perspectiva Prática. (Carga horária: 8h). Universidade Federal do Ceará, UFC, Brasil.
<b>2014 - 2014</b>	Princípios Básicos de Corrosão. (Carga horária: 8h). Universidade Federal do Ceará, UFC, Brasil.
<b>2012 - 2012</b>	Fundamentos de Absorção Atômica. (Carga horária: 8h). Universidade Federal do Ceará, UFC, Brasil.

## Atuação Profissional

Universidade Federal do Ceará, UFC, Brasil.

### Vínculo institucional

**2014 - 2015** Vínculo: Bolsista, Enquadramento Funcional: Bolsista de Iniciação Científica, Carga horária: 16

### Outras informações

Foi Bolsista de Iniciação Científica no Laboratório de Materiais Funcionais Avançados (LaMFA) - Departamento de Física UFC, atuando no projeto PRODUÇÃO DE SISTEMAS HÍBRIDOS A BASE DE GRAFENO E HIDROGÊIS DE PLURONIC F-127 PARA APLICAÇÕES MÉDICAS"

### Vínculo institucional

**2013 - 2013**

### Outras informações

Vínculo: Bolsista, Enquadramento Funcional: Monitor de Química Geral, Carga horária: 12  
Monitor de Química Geral para os cursos de Química Bacharelado, Química Licenciatura, Engenharias e outros.

## Áreas de atuação

1. Grande área: Ciências Exatas e da Terra / Área: Química.
2. Grande área: Ciências Exatas e da Terra / Área: Química / Subárea: Físico-Química.

## Idiomas

**Inglês** Compreende Bem, Fala Razoavelmente, Lê Bem, Escreve Bem.

## Prêmios e títulos

**2016** Distinção Acadêmica Magna Cum Laude, Universidade Federal do Ceará.

## Produções

### Produção bibliográfica

### Artigos completos publicados em periódicos

Ordenar por

Ordem Cronológica

1. DA CUNHA XAVIER, JAYZE ; **ALMEIDA-NETO, FRANCISCO WAGNER DE QUEIROZ** ; DA SILVA, PRISCILA TEIXEIRA ; DE SOUSA, AMANDA PEREIRA ; MARINHO, EMMANUEL SILVA ; MARINHO, MÁRCIA MACHADO ; ROCHA, JANAINA ESMERALDO ; FREITAS, PRISCILA RAMOS ; DE ARAÚJO, ANA CAROLINA JUSTINO ; FREITAS, THIAGO SANTIAGO ; NOGUEIRA, CARLOS EMÍDIO SAMPAIO ; DE LIMA-NETO, PEDRO ; BANDEIRA, PAULO NOGUEIRA ; TEIXEIRA, ALEXANDRE MAGNO RODRIGUES ; COUTINHO, HENRIQUE DOUGLAS MELO ; DOS SANTOS, HÉLCIO SILVA . Structural characterization, DFT calculations, ADMET studies, antibiotic potentiating activity, evaluation of efflux pump inhibition and molecular docking of chalcone (E)-1-(2-hydroxy-3,4,6-trimethoxyphenyl)-3-(4-methoxyphenyl)prop-2-en-1-one. JOURNAL OF MOLECULAR STRUCTURE **JCR**, v. 1227, p. 129692, 2021.  
**Citações:** WEB OF SCIENCE™ 3
2. DE OLIVEIRA, MAURO M. ; NOGUEIRA, CARLOS E.S. ; **ALMEIDA-NETO, FRANCISCO WAGNER Q.** ; SANTOS, HELCIO S. ; TEIXEIRA, ALEXANDRE M.R. ; DE LIMA-NETO, PEDRO ; MARINHO, EMMANUEL S. ; DE MORAES, MANOEL O. ; PESSOA, CLAUDIA ; BARROS-NEPOMUCENO, FRANCISCO WASHINGTON A. . Full Spectroscopic Characterization and Cytotoxicity Activity of Synthetic Dibenzalacetone Derivatives.. JOURNAL OF MOLECULAR STRUCTURE **JCR**, v. 1231, p. 129670, 2021.
- 3.



COSTA, STEFANE N. ; **ALMEIDA-NETO, FRANCISCO W.Q.** ; CAMPOS, OTHON S. ; FONSECA, THIAGO S. ; DE MATTOS, MARCOS C. ; FREIRE, VALDER N. ; HOMEM-DE-MELLO, PAULA ; MARINHO, EMMANUEL S. ; MONTEIRO, NORBERTO K.V. ; CORREIA, ADRIANA N. ; DE LIMA-NETO, PEDRO . Carbon steel corrosion inhibition in acid medium by imidazole-based molecules: Experimental and molecular modelling approaches. JOURNAL OF MOLECULAR LIQUIDS **JCR**, v. 326, p. 115330, 2021.

Citações: WEB OF SCIENCE™ 2

4. **Q. ALMEIDA-NETO, FRANCISCO WAGNER**; CASTRO MATOS, MARIA GEYSILLENE ; MARINHO, EMANUELLE MACHADO ; MARINHO, MÁRCIA MACHADO ; RÓSEO PAULA PESSOA BEZERRA DE MENEZES, RAMON ; SAMPAIO, TIAGO LIMA ; BANDEIRA, PAULO NOGUEIRA ; CELEDONIO FERNANDES, CARLA FREIRE ; MAGNO RODRIGUES TEIXEIRA, ALEXANDRE ; MARINHO, EMMANUEL SILVA ; DE LIMA-NETO, PEDRO ; SILVA DOS SANTOS, HÉLCIO . In silico study of the potential interactions of 4-acetamidochalcones with protein targets in SARS-CoV-2. BIOCHEMICAL AND BIOPHYSICAL RESEARCH COMMUNICATIONS **JCR**, v. 537, p. 71-77, 2021.

5. MARINHO, MÁRCIA M. ; **ALMEIDA-NETO, FRANCISCO WAGNER Q.** ; MARINHO, EMANUELLE M. ; DA SILVA, LEONARDO P. ; MENEZES, RAMON R.P.P.B. ; DOS SANTOS, RICARDO P. ; MARINHO, EMMANUEL S. ; DE LIMA-NETO, PEDRO ; MARTINS, ALICE M.C. . Quantum computational investigations and molecular docking studies on amentoflavone. HELIYON, v. 7, p. e06079, 2021.

Citações: WEB OF SCIENCE™ 1

6. PASCOAL, KARLA L.L. ; SIQUEIRA, SÔNIA M.C. ; DE AMORIM, ANTÔNIA F.V. ; RICARDO, NÁGILA M.P. SILVA ; DE MENEZES, JANE E.S.A. ; DA SILVA, LUANA C. ; DE ARAÚJO, TAMARA G. ; **ALMEIDA-NETO, FRANCISCO W.Q.** ; MARINHO, EMMANUEL S. ; DE MORAIS, SELENE M. ; SARAIVA, GILBERTO D. ; DE LIMA-NETO, PEDRO ; DOS SANTOS, HÉLCIO S. ; TEIXEIRA, ALEXANDRE M.R. . Physical-chemical characterization, controlled release, and toxicological potential of galactomannan-bixin microparticles. JOURNAL OF MOLECULAR STRUCTURE **JCR**, v. 1239, p. 130499, 2021.

7. VASQUES, ROBERTA BASTOS ; LEVY, MARJORY MOREIRA ; RODRIGUES, MATHEUS SOUZA ; **QUEIROZ ALMEIDA NETO, FRANCISCO WAGNER** ; SILVA, LEONARDO PAES ; VAZ, GUSTAVO LEITÃO ; MAGALHÃES, ÁLVARO AUGUSTO OLIVEIRA ; LIMA-NETO, PEDRO ; ARAÚJO, WALNEY SILVA . A theoretical and experimental study of phosphate ester inhibitors for AISI 1018 in carbon dioxide-saturated 3.5-wt% NaCl solution. MATERIALS AND CORROSION (ONLINE) **JCR**, v. x, p. maco.202112365, 2021.

Citações: WEB OF SCIENCE™ 1

8. XAVIER, JAYZE DA CUNHA ; **DE ALMEIDA-NETO, FRANCISCO W.Q.** ; ROCHA, JANÁINA E. ; FREITAS, THIAGO S. ; FREITAS, PRISCILA R. ; DE ARAÚJO, ANA C.J. ; DA SILVA, PRISCILA T. ; NOGUEIRA, CARLOS E.S. ; BANDEIRA, PAULO N. ; MARINHO, MÁRCIA M. ; MARINHO, EMMANUEL S. ; KUMAR, NITIN ; BARRETO, ANTÔNIO C.H. ; COUTINHO, HENRIQUE D.M. ; JULIÃO, MURILO S.S. ; DOS SANTOS, HÉLCIO S. ; TEIXEIRA, ALEXANDRE M.R. . Spectroscopic analysis by NMR, FT-Raman, ATR-FTIR, and UV-Vis, evaluation of antimicrobial activity, and in silico studies of chalcones derived from 2-hydroxyacetophenone. JOURNAL OF MOLECULAR STRUCTURE **JCR**, v. 1241, p. 130647, 2021.

9. FONSECA, ALUÍSIO M. ; SILVA, LEONARDO PAES DA ; **ALMEIDA-NETO, FRANCISCO WAGNER DE QUEIROZ** ; COLARES, REGILANY PAULO ; MACEDO DE OLIVEIRA, MAURO ; LUTHIERRE GAMA CAVALCANTE, ANTÔNIO ; LEMOS, TELMA L. G. ; BRAZ-FILHO, RAIMUNDO ; DE LIMA-NETO, PEDRO ; MARINHO, EMMANUEL SILVA . Synthesis of a new quinone dimer biocatalysed by the coconut water. BIOTRANSFORMATION **JCR**, v. x, p. 1-10, 2021.

10. GARCIA, TATIANA RODRIGUES ; FREIRE, PAULO DE TARSO CAVALCANTE ; BANDEIRA, PAULO NOGUEIRA ; DE SOUSA, AMANDA PEREIRA ; JULIÃO, MURILO SÉRGIO DA SILVA ; RODRIGUES, TIGRESSA HELENA SOARES ; MARINHO, MÁRCIA MACHADO ; MARINHO, EMMANUEL SILVA ; **ALMEIDA-NETO, FRANCISCO WAGNER QUEIROZ** ; FERREIRA, MARIA KUEIRISLENE AMÂNCIO ; DA SILVA, ANTONIO WLISSES ; DE MENEZES, JANE EIRE SILVA ALENCAR ; DE PAIVA, ALDENEIDE SOARES ; DA HORA, JOÃO PEDRO ; BARRETO, ANTÔNIO CÉSAR HONORATO ; DOS SANTOS, HÉLCIO SILVA ; TEIXEIRA, ALEXANDRE MAGNO RODRIGUES . Synthesis, structural and spectroscopic characterization, in silico study, and antinociceptive effect in adult zebrafish of 2-(4-isobutylphenyl)-N'-phenylpropanohydrazide. JOURNAL OF MOLECULAR STRUCTURE **JCR**, v. 1243, p. 130860, 2021.

11. LEAL, ANTÔNIO L.A.B. ; PINHEIRO, DANIEL P. ; BARROS-NEPOMUCENO, FRANCISCO W.A. ; DA SILVA, PRISCILA T. ; PESSOA, CLAUDIA ; **DE ALMEIDA-NETO, FRANCISCO W.Q.** ; MARINHO, EMMANUEL S. ; BARRETO, ANTÔNIO C.H. ; JULIÃO, MURILO S.S. ; DE PAIVA, ALDENEIDE S. ; BANDEIRA, PAULO N. ; DE LIMA-NETO, PEDRO ; DOS SANTOS, HÉLCIO S. ; TEIXEIRA, ALEXANDRE M.R. . Structural and spectroscopic analysis and evaluation of cytotoxic activity of 2-hydroxychalcones against human cancer cell lines. JOURNAL OF MOLECULAR STRUCTURE **JCR**, v. x, p. 131135, 2021.

12. DE ARAÚJO, JOSÉ ISMAEL F. ; AIRES, NATÁLIA L. ; **ALMEIDA-NETO, FRANCISCO W. Q.** ; MARINHO, MÁRCIA M. ; MARINHO, EMANUELLE M. ; PAULA MAGALHÃES, EMANUEL ; DE MENEZES, RAMON R. P. P. B. ; SAMPAIO, TIAGO L. ; MARIA COSTA MARTINS, ALICE ; TEIXEIRA, EDSON H. ; RAFAELA FREITAS DOTTO, ANA ; AMARAL, WANDERLEI DO ; TEIXEIRA, ALEXANDRE MAGNO R. ; DE LIMA-NETO, PEDRO ; MARINHO, EMMANUEL S. ; DOS SANTOS, HÉLCIO S. . Antiproliferative activity on Trypanosoma cruzi (Y strain) of the triterpene 3 $\beta$ ,6 $\beta$ ,16 $\beta$ -trihidroxi-20 (29)-ene isolated from Combretum leprosum. Journal of Biomolecular Structure and Dynamics **JCR**, v. x, p. 1-14, 2021.

13. DA SILVA, P.T. ; DA CUNHA XAVIER, J. ; FREITAS, T.S. ; OLIVEIRA, M.M. ; COUTINHO, H.D.M. ; LEAL, A.L.A.B. ; BARRETO, H.M. ; BANDEIRA, P.N. ; NOGUEIRA, C.E.S. ; SENA, D.M. ; **ALMEIDA-NETO, F.W.Q.** ; MARINHO, E.S. ; SANTOS, H.S. ; TEIXEIRA, A.M.R. . Synthesis, spectroscopic characterization and antibacterial evaluation by chalcones derived of acetophenone isolated from Croton anisodontus Müll.Arg.. JOURNAL OF MOLECULAR STRUCTURE **JCR**, v. 1226, p. 129403, 2021.

Citações: WEB OF SCIENCE™ 8

14. **ALMEIDA-NETO, FRANCISCO WAGNER Q.**; DA SILVA, LEONARDO P. ; FERREIRA, MARIA KUEIRISLENE A. ; MENDES, FRANCISCO ROGÊNIO S. ; DE CASTRO, KEVIN K.A. ; BANDEIRA, PAULO N. ; DE MENEZES, JANE EIRE S.A. ; DOS SANTOS, HÉLCIO S. ; MONTEIRO, NORBERTO K.V. ; MARINHO, EMMANUEL S. ; DE LIMA-NETO, PEDRO . Characterization of the structural, spectroscopic, nonlinear optical, electronic properties and antioxidant activity of the N-{4-[(E)-3-

(Fluorophenyl)-1-(phenyl)-prop-2-en-1-one]}-acetamide. JOURNAL OF MOLECULAR STRUCTURE **JCR**, v. 1220, p. 128765, 2020.

**Citações:** WEB OF SCIENCE™ 4

15. XAVIER, JAYZE DA CUNHA ; **ALMEIDA-NETO, FRANCISCO WAGNER QUEIROZ** ; DA SILVA, PRISCILA TEIXEIRA ; MARINHO, EMMANUEL SILVA ; FERREIRA, MARIA KUEIRISLENE AMÂNCIO ; MAGALHÃES, FRANCISCO ERNANI ALVES ; NOGUEIRA, CARLOS EMÍDIO SAMPAIO ; BANDEIRA, PAULO NOGUEIRA ; DE MENEZES, JANE EIRE SILVA ALENCAR ; TEIXEIRA, ALEXANDRE MAGNO RODRIGUES ; SANTOS, HÉLCIO SILVA DOS . Structural characterization, electronic properties, and anxiolytic-like effect in adult zebrafish (Danio rerio) of cinnamaldehyde chalcone. JOURNAL OF MOLECULAR STRUCTURE **JCR**, v. 1222, p. 128954, 2020.

**Citações:** WEB OF SCIENCE™ 4

16. MAGALHÃES, HERBERT S. ; DA SILVA, ALISON B. ; NASCIMENTO, NILBERTO R.F. ; DE SOUSA, LUIS GUSTAVO F. ; DA FONSECA, MARIA JÚLIA S. ; LOIOLA, MARIA IRACEMA B. ; MONTEIRO, NORBERTO K.V. ; **ALMEIDA NETO, FRANCISCO WAGNER Q.** ; CANUTO, KIRLEY M. ; PESSOA, OTILIA DEUSDÊNIA L. . Effect of indole alkaloids from roots of Rauvolfia ligustrina in the noradrenergic neurotransmission. FITOTERAPIA **JCR**, v. 143, p. 104545, 2020.

**Citações:** WEB OF SCIENCE™ 1

17. **ALMEIDA-NETO, F. W. Q.** ; SANTOS-CASTRO, G. ; DA SILVA, M. B. ; DE SOUSA, J. S. ; CAETANO, E. W. S. ; LIMA-NETO, P. ; FREIRE, V. N. . Structural, electronic, and optical properties of inhomogeneous Ca 1-x Mg x O alloys. JOURNAL OF APPLIED PHYSICS **JCR**, v. 125, p. 155102, 2019.

**Citações:** WEB OF SCIENCE™ 3

18. SOUSA, TICYANO P. ; CASTRO, CAIO B. ; SOUSA, MAYARA N.V. ; SILVA, THIAGO T. ; **ALMEIDA-NETO, FRANCISCO W.Q.** ; QUEIROS, MARCOS V.A. ; RODRIGUES, BÁRBARA S.F. ; OLIVEIRA, MARIA C.F. ; PAULO, TÉRCIO F. ; CAVADA, BENILDO S. ; NASCIMENTO, KYRIA S. ; TEMPERINI, MARCIA L.A. ; DIÓGENES, IZAURA C.N. . SAM of Gliotoxin on Gold: A Natural Product Platform for Sugar Recognition based on the Immobilization of Canavalia brasiliensis lectin (ConBr). ELECTROCHIMICA ACTA **JCR**, v. 241, p. 116-123, 2017.

**Citações:** WEB OF SCIENCE™ 5

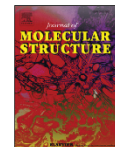
#### Demais tipos de produção técnica

1. **ALMEIDA-NETO, FRANCISCO W.Q.**. Mini Curso de Matemática aplicada à Química. 2013. (Curso de curta duração ministrado/Outra).

## Eventos

#### Participação em eventos, congressos, exposições e feiras

- VII Semana da Química da Universidade Federal do Ceará. 2016. (Outra).
- Workshop do Grupo de Eletroquímica e Corrosão (GELCORR). 2016. (Outra).
- Encontros Universitários UFC - XXXIV Encontro de Iniciação Científica.FUNCIONALIZAÇÃO DE SUPERFÍCIE DE VIDRO COM ORGANOSSILANOS. 2015. (Encontro).
- V Semana da Química da Universidade Federal do Ceará / II ENCEQUI. 2014. (Outra).
- Encontros Universitários UFC - XXII Encontro de Iniciação à Docência.A REAÇÃO OSCILANTE DE BRIGGS-RAUSCHER COMO ILUSTRAÇÃO DO CONCEITO DE CINÉTICA QUÍMICA. 2013. (Encontro).



## Characterization of the structural, spectroscopic, nonlinear optical, electronic properties and antioxidant activity of the N-{4'-[(E)-3-(Fluorophenyl)-1-(phenyl)-prop-2-en-1-one]}-acetamide

Francisco Wagner Q. Almeida-Neto<sup>a,\*</sup>, Leonardo P. da Silva<sup>a</sup>,  
 Maria Kueirislene A. Ferreira<sup>b</sup>, Francisco Rogênio S. Mendes<sup>c</sup>, Kevin K.A. de Castro<sup>d</sup>,  
 Paulo N. Bandeira<sup>c,d</sup>, Jane Eire S.A. de Menezes<sup>b</sup>, Hécio S. dos Santos<sup>d</sup>,  
 Norberto K.V. Monteiro<sup>a</sup>, Emmanuel S. Marinho<sup>e</sup>, Pedro de Lima-Neto<sup>a</sup>

<sup>a</sup> Departamento de Química Analítica e Físico-Química, Universidade Federal do Ceará, Campus do Pici, bloco 940, 60440-900, Fortaleza, CE, Brazil

<sup>b</sup> Universidade Estadual do Ceará, Centro de Ciência e Tecnologia (CCT), Itaperi Campus, Laboratório de Química de Produtos Naturais - LQPN-S, Fortaleza, CE, Brazil

<sup>c</sup> Departamento de Química Biológica, Universidade Regional do Cariri, Crato, CE, Brazil

<sup>d</sup> Centro de Ciências Exatas e Tecnologia, Universidade Estadual do Vale do Acaraú, Sobral, CE, Brazil

<sup>e</sup> Faculdade de Filosofia Dom Aureliano Matos, Universidade Estadual do Ceará, Ceará, Brazil

### ARTICLE INFO

#### Article history:

Received 12 May 2020

Received in revised form

13 June 2020

Accepted 24 June 2020

Available online 27 June 2020

#### Keywords:

Bond dissociation energy

Claisen-schmidt aldol condensation

Fukui function

Nonlinear optical

Natural bond orbital

### ABSTRACT

The molecule N-[4'-[(E)-3-(Fluorophenyl)-1-(phenyl)-prop-2-en-1-one]} chalcone (PAAPFBA) was recently synthesized due to the growing interest in the chemistry of the chalcone. The quantum chemical calculations were carried out to make a complete theoretical characterization (structural, spectroscopy, nonlinear optical, and electronic properties) employing three Density Functional Theory (DFT) methods like B3LYP, mPW1PW91, and M06-2X at 6-311++G(d,p) basis set. After all these characterizations, the antioxidant activity was studied using the reaction with the compound DPPH in methanol solution and the mechanism was investigated theoretically. All the three DFT methods used can describe with great accuracy the PAAPFBA chalcone: the results of infrared spectroscopy and the <sup>1</sup>H and <sup>13</sup>C isotropic shielding demonstrate to be in excellent agreement with the experimental data. The nonlinear optical (NLO) properties show that the title chalcone can be used with great potential in NLO devices and this result is in good agreement with the Natural Bond Orbital (NBO) analysis, which shows how the electronic density is delocalized within the molecule. Finally, the experimental data of the antioxidant activity showed a moderate rate of reaction with the DPPH molecule (50.92%) and this fact was proved by the theoretical mechanisms with the Hydrogen Atom Transfer (HAT) mechanism more favorable.

© 2020 Elsevier B.V. All rights reserved.

### 1. Introduction

Chalcones are natural products considered as the most important subgroup of the flavonoid family. They are chemically characterized by the presence of an open chain with two phenyl rings bonded by  $\alpha,\beta$ -unsaturated carbonyl group (1,3-diphenyl-2-propen-1-ones). For the chalcones, there are two possible

isomers, the E (trans) and Z (cis), being that E isomer occurs naturally and it is thermodynamically more stable [1]. The greatest interest in this class of compound lies in the fact that chalcones have many hydrogen atoms that can be replaced, thus generating the possibility of synthesis routes for several compounds with different possible applications. The chalcone can be used as anti-leishmanial, antibacterial, antimicrobial, immunosuppressive, antidepressant, anti-inflammatory, anti-obesity, hypnotic, and anticancer [1–11].

Despite these several applications, the chalcones exhibits antioxidant properties. Some examples about the great applicability of chalcone derivatives as antioxidants are given next. Arif et al. [12] studied the antioxidant properties of the 3-(1H-indol-3-yl)-1-p-

\* Corresponding author. Departamento de Química Analítica e Físico-Química, Universidade Federal do Ceará, Campus do Pici, Bloco 938/939, 60020-181, Fortaleza, CE, Brazil.

E-mail address: [wagnerqueirozneto@gmail.com](mailto:wagnerqueirozneto@gmail.com) (F.W.Q. Almeida-Neto).



ELSEVIER

Contents lists available at ScienceDirect

Biochemical and Biophysical Research Communications

journal homepage: [www.elsevier.com/locate/ybbrc](http://www.elsevier.com/locate/ybbrc)

## *In silico* study of the potential interactions of 4'-acetamidechalcones with protein targets in SARS-CoV-2



Francisco Wagner Q. Almeida-Neto<sup>a</sup>, Maria Geysillene Castro Matos<sup>b</sup>,  
Emanuelle Machado Marinho<sup>a</sup>, Márcia Machado Marinho<sup>c</sup>,  
Ramon Róseo Paula Pessoa Bezerra de Menezes<sup>d</sup>, Tiago Lima Sampaio<sup>d</sup>,  
Paulo Nogueira Bandeira<sup>e</sup>, Carla Freire Celedonio Fernandes<sup>f</sup>,  
Alexandre Magno Rodrigues Teixeira<sup>b</sup>, Emmanuel Silva Marinho<sup>h</sup>, Pedro de Lima-Neto<sup>a</sup>,  
Hélcio Silva dos Santos<sup>b, e, i, \*</sup>

<sup>a</sup> Universidade Federal do Ceará, Departamento de Química Analítica e Físico-Química, Campus do Pici, Fortaleza, CE, Brazil

<sup>b</sup> Universidade Regional do Cariri, Departamento de Química Biológica, Crato, CE, Brazil

<sup>c</sup> Faculdade de Educação, Ciência e Letras de Iguatu, Universidade Estadual do Ceará, Iguatu, CE, Brazil

<sup>d</sup> Departamento de Análises Clínicas e Toxicológicas, Universidade Federal do Ceará, Fortaleza, CE, Brazil

<sup>e</sup> Universidade Estadual do Vale do Acaraú, Centro de Ciências Exatas e Tecnologia, Sobral, CE, Brazil

<sup>f</sup> Fundação Oswaldo Cruz, Laboratório Multiusuário de Pesquisa e Desenvolvimento - Plataforma de Anticorpos e Nanocorpos, Eusébio, CE, Brazil

<sup>h</sup> Universidade Estadual do Ceará, Faculdade de Filosofia Dom Aureliano Matos, Limoeiro do Norte, CE, Brazil

<sup>i</sup> Universidade Estadual do Ceará, Centro de Ciências e Tecnologia, Programa de Pós-Graduação Ciências Naturais, Fortaleza, CE, Brazil

### ARTICLE INFO

#### Article history:

Received 16 December 2020

Accepted 18 December 2020

#### Keywords:

Chalcone  
Molecular docking  
SPIKE  
ACE2

### ABSTRACT

The sanitary emergency generated by the pandemic COVID-19, instigates the search for scientific strategies to mitigate the damage caused by the disease to different sectors of society. The disease caused by the coronavirus, SARS-CoV-2, reached 216 countries/territories, where about 20 million people were reported with the infection. Of these, more than 740,000 died. In view of the situation, strategies involving the development of new antiviral molecules are extremely important. The present work evaluated, through molecular docking assays, the interactions of 4'-acetamidechalcones with enzymatic and structural targets of SARS-CoV-2 and with the host's ACE2, which is recognized by the virus, facilitating its entry into cells. Therefore, it was observed that, regarding the interactions of chalcones with Main protease (Mpro), the chalcone N-(4'[(2E)-3-(4-fluorophenyl)-1-(phenyl)prop-2-en-1-one]) acetamide (PAAFP) has the potential for coupling in the same region as the natural inhibitor FJC through strong hydrogen bonding. The formation of two strong hydrogen bonds between N-(4'[(2E)-3-(phenyl)-1-(phenyl)-prop-2-en-1-one]) acetamide (PAAB) and the NSP16-NSP10 heterodimer methyltransferase was also noted. N-(4'[(2E)-3-(4-methoxyphenyl)-1-(phenyl)prop-2-en-1-one]) acetamide (PAAPM) and N-(4'[(2E)-3-(4-ethoxyphenyl)-1-(phenyl)prop-2-en-1-one]) acetamide (PAAPE) chalcones showed at least one strong intensity interaction of the SPIKE protein. N-(4'[(2E)-3-(4-dimetilaminofenyl)-1-(phenyl)-prop-2-en-1-one]) acetamide (PAAPA) chalcone had a better affinity with ACE2, with strong hydrogen interactions. Together, our results suggest that 4'-acetamidechalcones inhibit the interaction of the virus with host cells through binding to ACE2 or SPIKE protein, probably generating a steric impediment. In addition, chalcones have an affinity for important enzymes in post-translational processes, interfering with viral replication.

© 2020 Elsevier Inc. All rights reserved.

### 1. Introduction

The health problem caused by the COVID-19 pandemic can be measured by the numbers of cases and deaths confirmed by the disease globally. In Brazil, community transmission is observed,

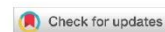
\* Corresponding author. Postgraduate Program in Biological Chemistry, Department of Biological Chemistry, Regional University of Cariri, Campus Pimenta II, CEP: 63.100-000, Crato, CE, Brazil.

E-mail address: [helcio\\_santos@uvanet.br](mailto:helcio_santos@uvanet.br) (H. Silva dos Santos).

<https://doi.org/10.1016/j.bbrc.2020.12.074>

0006-291X/© 2020 Elsevier Inc. All rights reserved.





Received: 16 February 2021 | Revised: 24 February 2021 | Accepted: 27 February 2021

DOI: 10.1002/maco.202112365

## ARTICLE

## Materials and Corrosion

# A theoretical and experimental study of phosphate ester inhibitors for AISI 1018 in carbon dioxide-saturated 3.5 wt% NaCl solution

Roberta Bastos Vasques<sup>1</sup> | Marjory Moreira Levy<sup>1</sup> |  
Matheus Souza Rodrigues<sup>1</sup> | Francisco Wagner de Queiroz Almeida Neto<sup>2</sup> |  
Leonardo Paes da Silva<sup>2</sup> | Gustavo Leitão Vaz<sup>3</sup> |  
Álvaro Augusto Oliveira Magalhães<sup>3</sup> | Pedro de Lima-Neto<sup>2</sup> |  
Walney Silva Araújo<sup>1</sup>

<sup>1</sup>Departamento de Engenharia Metalúrgica, Universidade Federal do Ceará, Fortaleza, Ceará, Brazil

<sup>2</sup>Departamento de Química Analítica e Físico-Química, Universidade Federal do Ceará, Fortaleza, Ceará, Brazil

<sup>3</sup>Centro de Pesquisa da Petrobras CENPES, Rio de Janeiro—RJ, Brazil

**Correspondence**

Roberta B. Vasques, Departamento de Engenharia Metalúrgica, Universidade Federal do Ceará, Campus do Pici, Fortaleza, CE 60440-900, Brazil.  
Email: robertabvasques@yahoo.com.br

**Funding information**

Petrobras, Grant/Award Number: 2017/00402-2

**Abstract**

Phosphate ester was investigated as a corrosion inhibitor for AISI 1018 carbon steel in carbon dioxide-saturated chloride solutions at different temperatures and pressures. The corrosion tests were realized by electrochemical techniques, weight loss measurements, bubble tests, and a high-pressure/high-temperature autoclave system. The corrosion tests demonstrated that the investigated molecule is an excellent corrosion inhibitor. The inhibiting effect is even bigger at high pressure and temperature than at atmospheric pressure and room temperature. The thermodynamic parameters were calculated and determined to obey the Langmuir isotherm. Polarization studies revealed that the evaluated inhibitor is a mixed type.

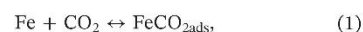
**KEYWORDS**

carbon dioxide, corrosion inhibitors, phosphate ester, temperature, pressure

## 1 | INTRODUCTION

Corrosion caused by CO<sub>2</sub> in the aqueous phase is a common problem in carbon steel pipelines used in oil and gas transportation. The formation of corrosion products is usually an essential process in the CO<sub>2</sub> corrosion mechanism, and their presence can significantly change the corrosion rate.<sup>[1,2]</sup> For the cathodic process, some papers have proposed two mechanisms: the buffering effect,<sup>[5–7]</sup> which relates the impact of the pH on the dissociation of carbonic acid and hydrogen evolution, from a combination of H<sup>+</sup>, H<sub>2</sub>CO<sub>3</sub><sup>-</sup>, HCO<sub>3</sub><sup>-</sup>, and H<sub>2</sub>O.<sup>[3,4,8–10]</sup> However, steel dissolution accounts for the anodic process.

In 1996, Nescic et al.<sup>[11]</sup> proposed different anodic mechanisms for steel dissolution in CO<sub>2</sub> solutions at a pH range from 2.5 to 6. The author proposed six reactions at pH < 4, 4 < pH < 5, and pH > 5 (Equations (1)–(6)). Then, for carbon steel, CO<sub>2</sub> corrosion rates are strongly influenced by many factors, such as flow velocity, temperature, pH, gas–liquid rates, oil–water ratio, CO<sub>2</sub> partial pressure, and chemical composition of the produced water<sup>[12–14]</sup>:





ELSEVIER

Contents lists available at ScienceDirect

Journal of Molecular Liquids

journal homepage: [www.elsevier.com/locate/molliq](http://www.elsevier.com/locate/molliq)

## Carbon steel corrosion inhibition in acid medium by imidazole-based molecules: Experimental and molecular modelling approaches



Stefane N. Costa<sup>a</sup>, Francisco W.Q. Almeida-Neto<sup>g</sup>, Othon S. Campos<sup>b</sup>, Thiago S. Fonseca<sup>c</sup>, Marcos C. de Mattos<sup>c</sup>, Valder N. Freire<sup>d</sup>, Paula Homem-de-Mello<sup>e</sup>, Emmanuel S. Marinho<sup>f</sup>, Norberto K.V. Monteiro<sup>g</sup>, Adriana N. Correia<sup>g</sup>, Pedro de Lima-Neto<sup>g,\*</sup>

<sup>a</sup> Programa de Pós-Graduação em Engenharia e Ciência de Materiais, Universidade Federal do Ceará, Campus do Pici, 60440-554 Fortaleza, CE, Brazil

<sup>b</sup> Departamento de Química e Física, Universidade Federal do Espírito Santo, Campus Guararema, 29500-000 Alegre, ES, Brazil

<sup>c</sup> Departamento de Química Orgânica e Inorgânica, Universidade Federal do Ceará, Campus do Pici, Caixa Postal 6044, 60455-970 Fortaleza, CE, Brazil

<sup>d</sup> Departamento de Física, Universidade Federal do Ceará, Campus do Pici, 60440-900 Fortaleza, CE, Brazil

<sup>e</sup> Centro de Ciências Naturais e Humanas, Universidade Federal do ABC, 09210-580 Santo André, SP, Brazil

<sup>f</sup> Faculdade de Filosofia Dom Aureliano Matos, Universidade Estadual do Ceará, 62930-000 Limoeiro do Norte, CE, Brazil

<sup>g</sup> Departamento de Química Analítica e Físico-Química, Universidade Federal do Ceará, Campus do Pici, 60440-900 Fortaleza, CE, Brazil

### ARTICLE INFO

#### Article history:

Received 3 November 2020

Received in revised form 25 December 2020

Accepted 6 January 2021

Available online 8 January 2021

#### Keywords:

Corrosion inhibitors

Imidazole derivatives

Monte Carlo

Density functional theory

Carbon steel

Acidic medium

### ABSTRACT

This paper deals with application of imidazole (IMI) and four imidazole derivative molecules: 4-(imidazole-1-yl)-phenol (PHEN), [4-(1*H*-imidazole-1-yl)-phenyl]methanol (METH), 2-(1*H*-imidazol-1-yl)-1-phenylethan-1-one (ETHAN) and 4-(1*H*-imidazole-1-yl)benzaldehyde (BENZ), towards corrosion inhibition of 1020 carbon steel in acidic medium. From IMI to ETHAN, the corrosion inhibition efficiency more than doubled in gravimetric experiments and increased 85% and 68% in the potentiodynamic polarization and electrochemical impedance assays, respectively. Both gravimetric and electrochemical tests gave the following decreasing order for the corrosion inhibition efficiency: BENZ > ETHAN > METH > PHEN > IMI. Quantum chemical calculations based on density functional theory (DFT) method showed that global hardness of the inhibitor molecules and inhibition efficiency were inversely proportional, which means that a softer molecule (or lower charge/radius ratio considering HSAB theory) leads to higher anticorrosion efficiency. Monte Carlo method (MC) was used to calculate the adsorption energies in a simulated water environment, and Compass force field was selected towards obtaining the solvation energy between inhibitor and metallic surface. The calculated solvation energy showed an inverse correlation between solvation energy and corrosion inhibition, having BENZ molecule lower solvation energy and lower global hardness which explains better anticorrosion efficiency among other IMI-based molecules, which shows the importance of molecule polarity over the corrosion inhibition of carbon steel.

© 2021 Elsevier B.V. All rights reserved.

### 1. Introduction

In modern life, all topics related to metals and alloys corrosion protection are particularly important, from a simple damaged door key to an airplane turbine [1]. Thus, the corrosion studies play a significant role in our time, and the costs related to the corrosion increase every year. The NACE Impact Report, duly published in 2016 [2], reported that the corrosion's global costs reached up to US\$ 2.5 trillion, almost 3.4% of the worldwide GDP in 2013. It is well known that the steel technology plays an important role in the general industry, and that the carbon steel is widely used in the world with many applications, such as engineering (bridges, pipelines, gears etc.), tools (blades, punches, springs etc.) and so on. Spite being one of the most versatile alloys,

carbon steel has low corrosion resistance and the search of corrosion inhibitors for this material is worthy to research [3].

The usage of organic or inorganic chemicals as corrosion inhibitors is one of the strategies adopted in industrial practice to minimize the corrosion's harmful effects. However, the most effective corrosion inhibitors used in the industries, such as the chromate ions and hydrazine, are classified as harmful to the environment and human health [3–6]. Therefore, the current challenge is to seek chemicals that are effective as corrosion inhibitors and friendly to the environment and human health.

For painted metals, the modern strategy is based in the incorporation of nanoparticles into the polymer coating to act as nanocontainers for the corrosion inhibitors. For instance, Ye et al. [7] demonstrated that an epoxy coating containing graphene modified with oligomeric silsesquioxane as a nanocontainer, and benzotriazole (BTA) as the corrosion inhibitor, presents excellent self-healing capacity due to the

\* Corresponding author.

E-mail address: [pln@ufc.br](mailto:pln@ufc.br) (P. de Lima-Neto).



## Effect of indole alkaloids from roots of *Rauvolfia ligustrina* in the noradrenergic neurotransmission



Herbert S. Magalhães<sup>a</sup>, Alison B. da Silva<sup>a</sup>, Nilberto R.F. Nascimento<sup>b</sup>, Luis Gustavo F. de Sousa<sup>b</sup>, Maria Júlia S. da Fonseca<sup>b</sup>, Maria Iracema B. Loiola<sup>c</sup>, Norberto K.V. Monteiro<sup>d</sup>, Francisco Wagner Q. Almeida Neto<sup>d</sup>, Kirley M. Canuto<sup>e</sup>, Otilia Deusdênia L. Pessoa<sup>a,\*</sup>

<sup>a</sup> Departamento de Química Orgânica e Inorgânica, Universidade Federal do Ceará, 60971-270 Fortaleza, CE, Brazil

<sup>b</sup> Instituto Superior de Ciências Biomédicas, Universidade Estadual do Ceará, 60714-903 Fortaleza, CE, Brazil

<sup>c</sup> Herbário Prisco Bezerra (EAC), Universidade Federal do Ceará, 60440-900 Fortaleza, CE, Brazil

<sup>d</sup> Departamento de Química Analítica e Físico-Química, Universidade Federal do Ceará, 60020-181 Fortaleza, CE, Brazil

<sup>e</sup> Embrapa Agroindústria Tropical, 60511-110 Fortaleza, CE, Brazil

### ARTICLE INFO

#### Keywords:

*Rauvolfia ligustrina*  
Indole alkaloids  
Neuroinhibitory effect  
GIAO <sup>13</sup>C NMR

### ABSTRACT

The new glucosyl sarpagan alkaloid designated as 21(*R*<sup>+</sup>)-(*O*-β-glucosyl)-hydroxy-sarpagan-17-oic acid, along with eleven known alkaloids were isolated from a soluble alkaloidal fraction from the ethanol extract of *Rauvolfia ligustrina*. Their structures were elucidated by interpretation of spectroscopic data (1D and 2D NMR), HRESIMS experiment, GIAO <sup>13</sup>C NMR calculations, and comparison with literature data. All the isolated alkaloids were screened by their neuroinhibitory effects using the electrically stimulated mice vas deferens bioassay. Compounds **1**, **2** and **9** presented a potent inhibitory effect in the neurotransmission while **3** and **11** showed an acute neuroexcitatory effect. Compound **10** exhibited a very effective post-synaptic inhibitory activity.

### 1. Introduction

The pantropical genus *Rauvolfia* (Apocynaceae family) comprises 74 accepted species widely distributed throughout America, Africa and Asia continents [1]. Several *Rauvolfia* species have been used in traditional medicine for different purposes such as treatment of snakebite, malaria, gastrointestinal and central nervous system disorders [2–6]. Crude extracts and constituents from *Rauvolfia* species have shown pharmacological activities, such as anxiolytic [7], antihypertensive [8], anticancer [9] and antimicrobial [10].

The genus *Rauvolfia* is known as a prolific source of structurally diversified indole alkaloids, which are subdivided in different groups as sarpagan, yohimbine, heteroyohimbine, indolenine, oxindole, and anhydronium [11]. The most investigated species is *Rauvolfia serpentina*, worldwide known by its medicinal properties and as the reserpine producer, the first alkaloid indicated to the treatment of hypertension and schizophrenia in the 50's decade [2,12]. As part of our ongoing research for bioactive alkaloids [13–16] we have investigated the root extract of *R. ligustrina*, an annual shrub found in the northeast region of Brazil. Herein, a new glucosyl sarpagan alkaloid (**1**), together with eleven known indole alkaloids are described (see Fig.1). Additionally,

their effects on the noradrenergic neurotransmission were also evaluated on the electrically stimulated mice vas deferens (biological tissue with a rich diversity of pharmacological presynaptic and postsynaptic receptors bioassay).

### 2. Experimental

#### 2.1. General experimental procedures

Optical rotation was determined using a Jasco P-2000 digital polarimeter. 1D and 2D NMR spectra were obtained on a DRX-500 (Bruker) and DPX-300 (Bruker) operating at 500 and 300 MHz frequency for <sup>1</sup>H, respectively, and 125 and 75 MHz frequency for <sup>13</sup>C, respectively. High-resolution electrospray ionization mass spectra (HRESIMS) were acquired on Acquity UPLC-QTOF-ESI-MS (Waters). Chromatographic procedures were carried out using silica gel (40–63 μm, Merck), SPE cartridge C-18 (Phenomenex), Sephadex LH-20 (Pharmacia) and thin-layer chromatography (TLC) with pre-coated silica gel 60 F<sub>254</sub> (Merck) using Dragendorff reagent to detect spots. HPLC (Shimadzu) analyses were performed with a system equipped with SPD-M20 diode array detector and semi-preparative C-18 column

\* Corresponding author.

E-mail address: [opessoa@ufc.br](mailto:opessoa@ufc.br) (O.D.L. Pessoa).

<https://doi.org/10.1016/j.fitote.2020.104545>

Received 18 December 2019; Received in revised form 4 March 2020; Accepted 5 March 2020

Available online 07 March 2020

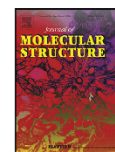
0367-326X/ © 2020 Elsevier B.V. All rights reserved.



ELSEVIER

Contents lists available at ScienceDirect

Journal of Molecular Structure

journal homepage: [www.elsevier.com/locate/molstr](http://www.elsevier.com/locate/molstr)

## Full Spectroscopic Characterization and Cytotoxicity Activity of Synthetic Dibenzalacetone Derivatives.

Mauro M. de Oliveira<sup>a,\*</sup>, Carlos E.S. Nogueira<sup>a,e</sup>, Francisco Wagner Q. Almeida-Neto<sup>f</sup>, Helcio S. Santos<sup>a,b</sup>, Alexandre M.R. Teixeira<sup>a,e</sup>, Pedro de Lima-Neto<sup>f</sup>, Emmanuel S. Marinho<sup>g</sup>, Manoel O. de Moraes<sup>c</sup>, Claudia Pessoa<sup>c</sup>, Francisco Washington A. Barros-Nepomuceno<sup>d</sup>

<sup>a</sup> Department of Biological Chemistry, Regional University of Cariri, Crato, CE, Brazil

<sup>b</sup> Science and Technology Centre - Course of Chemistry, State University Vale do Acaraú, Sobral, CE, Brazil

<sup>c</sup> Center for Research and Drug Development, Federal University of Ceará, Fortaleza, CE, Brazil

<sup>d</sup> Institute of Health Sciences, University of International Integration of the Afro-Brazilian Lusophony, Acaraú, CE, Brazil

<sup>e</sup> Department of physics, Regional University of Cariri, Crato, CE, Brazil

<sup>f</sup> Department of Analytical Chemistry and Physical Chemistry, Federal University of Ceará, Fortaleza, CE, Brazil.

<sup>g</sup> State University of Ceará, Faculty of Philosophy Dom Aureliano Matos, Limoeiro do Norte, CE, Brazil.

### ARTICLE INFO

#### Article history:

Received 26 September 2020

Revised 5 November 2020

Accepted 24 November 2020

Available online 27 November 2020

#### Keywords:

Dibenzalacetone derivatives

Cytotoxicity

DFT

Spectroscopy, Cancer cells

### ABSTRACT

Dibenzalacetone derivatives are organic compounds formed by two  $\alpha, \alpha'$  active sites that provide a large relocation of  $\pi$ -electrons. They have great polarizability that make them excellent chromophore and draw attention for their biological properties, mainly for their activity against nasopharyngeal, oral, colon, prostate and cervical cancer. Two dibenzalacetone derivatives, (1E,4E)-1,5-bis(4-ethoxyphenyl)penta-1,4-dien-3-one and (1E,4E)-1,5-bis(4-chlorophenyl)penta-1,4-dien-3-one, were synthesized. Spectroscopic characterizations as well as vibrational assignments were predicted using density Functional Theory (DFT) calculations with B3LYP exchange-correlation functional. Cytotoxicity assays of the synthesized compounds were performed against HCT-116, SNB and PC3 cells, showing promising results against cancer cells HCT-116.

© 2020 Elsevier B.V. All rights reserved.

### 1. Introduction

A double condensation reaction of a ketone that has two  $\alpha, \alpha'$ -active sites with two equivalents of aromatic aldehyde yields a molecule with an extensive delocalization of  $\pi$ -electrons, which favors an easier polarizability, that is achieved by the presence of strong electron donor (D) and strong acceptor (A) groups with a  $\pi$ -electron bridge joining D and A. These compounds are closely related to the class of organic chromophores known as "bis-chalcones" which have several multifunctional characteristics (pharmacological and biological activities) [1]. In literature, dibenzalacetone derivatives as the ones reported here, are sometimes referred to as bis-chalcones [2–4] or simply chalcone derivatives [5].

Chalcones are a class of naturally occurring or readily synthesized compounds that have a 1,3-diaryl-2-propen-1-one basic framework. They are an open-chain precursor of flavonoids and

may exist as *trans* and *cis* isomers, although the *trans* isomer is thermodynamically more stable. Natural chalcones are commonly found in fruits, vegetables, petals, bark, leaves and roots of various trees or plants [6–9]. The chalcone class and its derivatives have attracted a lot of interest, as they have a wide range of bioactivities, e.g.: anti-inflammatory [10], antimicrobial [11], anti-oxidant [12], anticancer [13], antifungal [14], antimalarial [15], anti-protozoal [16], etc. This broad spectrum of biological activity is probably related to its small structure and its characteristics as Michael acceptors, which make them tolerant to different biological molecules and allow them to bind quickly or reactively to them [9].

Several bis-chalcones have shown remarkable anticancer activity against nasopharyngeal, oral, colon, prostate and cervical cancer [13,17]. In a recent study, nine bis-chalcones were tested in vitro for cytotoxic activity against cancer cell lines of lung (A549), prostate (DU-145), nasopharyngeal carcinoma (KB) and vincristine-resistant KB subline (KB-VIN). Best results were obtained in non-substituted phenyl B rings or in *para*-methoxyphenyl B-rings [18]. Other bis-chalcones with methoxy groups inserted at *para* position of phenyl rings have displayed encouraging results by inhibit-

\* Corresponding author: Department of Biological Chemistry, Regional University of Cariri, Campus Pimenta II, CEP: 63.100-000, Crato, CE, Brazil.

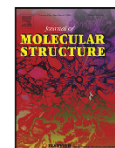
E-mail address: [mauropandi@gmail.com](mailto:mauropandi@gmail.com) (M.M. de Oliveira).





Contents lists available at ScienceDirect

Journal of Molecular Structure

journal homepage: [www.elsevier.com/locate/molstr](http://www.elsevier.com/locate/molstr)

## Physical-chemical characterization, controlled release, and toxicological potential of galactomannan-bixin microparticles



Karla L.L. Pascoal<sup>a</sup>, Sônia M.C. Siqueira<sup>a</sup>, Antônia F.V. de Amorim<sup>a</sup>,  
Nágila M.P. Silva Ricardo<sup>b</sup>, Jane E.S.A. de Menezes<sup>a</sup>, Luana C. da Silva<sup>a</sup>, Tamara G. de  
Araújo<sup>c</sup>, Francisco W.Q. Almeida-Neto<sup>d</sup>, Emmanuel S. Marinho<sup>e</sup>, Selene M. de Moraes<sup>a</sup>,  
Gilberto D. Saraiva<sup>f</sup>, Pedro de Lima-Neto<sup>d</sup>, Hécio S. dos Santos<sup>g</sup>, Alexandre M.R. Teixeira<sup>h,\*</sup>

<sup>a</sup> Department of Chemistry, State University of Ceará, Fortaleza-CE, Brazil

<sup>b</sup> Department of Organic and Inorganic Chemistry, Federal University of Ceará, Fortaleza-CE, Brazil

<sup>c</sup> Department of Pharmacy, Federal University of Ceará, Fortaleza-CE, Brazil

<sup>d</sup> Department of Analytical Chemistry and Physical Chemistry, Federal University of Ceará, Fortaleza, Ceará, Brazil

<sup>e</sup> Theoretical and Electrochemical Chemistry Group, Ceará State University, FAFIDAM Campus, Limoeiro do Norte, Ceará, Brazil

<sup>f</sup> Department of Physics, State University of Ceará, Quixadá-CE, Brazil

<sup>g</sup> Course of Chemistry, State University of the Acaraú, Sobral-CE, Brazil

<sup>h</sup> Department of Physics, Regional University of Cariri, Juazeiro do Norte-CE, Brazil

### ARTICLE INFO

#### Article history:

Received 5 November 2020

Revised 3 April 2021

Accepted 13 April 2021

Available online 22 April 2021

#### Keywords:

Encapsulation

Bixin

Galactomannan

SEM

FT-IR

Thermoanalysis

### ABSTRACT

In this study, a spray drying technique was used to encapsulate bixin in the galactomannan polymer to give greater stability to this carotenoid. The microparticles were characterized using physical-chemical techniques, quantum chemical calculations, and evaluated the particle sizes, encapsulation efficiency, stability, controlled release, and toxicological potential. The bixin was successfully encapsulated, with an average size of  $5.55 \pm 0.50 \mu\text{m}$ , and infrared spectroscopy showed no chemical reaction between bixin and galactomannan during the encapsulation process. The values for the encapsulation efficiency were higher than 90 %, indicating that galactomannan was a good encapsulating agent. A stability test revealed that microencapsulation provides significant protection for bixin. It was observed that the microparticles were capable of releasing the pigment homogeneously and gradually. The absence of toxicity of these materials allows for their use within the food industry, since there is a need for new products that combine low toxicity, efficiency, and low cost.

© 2021 Elsevier B.V. All rights reserved.

### 1. Introduction

The strong restrictions imposed by the market on the use of synthetic pigments and the toxicity of certain colorants have motivated their increasing substitution by natural pigments, and this is becoming increasingly common. Natural pigments have been shown to be as effective as those derived from chemical synthesis, with the additional benefits of being safer and providing health benefits, organoleptic features, multiple benefits (such as antioxidant and even preservative activity), and functional properties [1,2]. Annatto (*Bixa orellana* L.) is a crop of great agro-industrial interest due to the high content of red-orange pigment found in

its seeds [3,4]. In the food industry, the bixin is used as a pigment in dairy products and soft drinks and liquors [5].

Bixin is the main carotenoid found in annatto seeds and accounts for about 80 % of the carotenoids found in this material. It has an isoprene chain of 24 carbon atoms, with a carboxylic acid and a methyl ester at the ends, giving a molecular formula of  $\text{C}_{25}\text{H}_{30}\text{O}_4$  [6,7]. The bixin has been found to exhibit the highest measured potential for carotenoid oxidation to date, which is consistent with its practical protective use in cosmetics, drugs, and food [8]. The incorporation of this carotenoid into foods is mainly for coloring purposes and to confer certain functional characteristics since bixin has the ability to sequester free radicals and deactivate singlet oxygen, acting as an antimicrobial, anti-inflammatory, antioxidant, hypoglycemic, and non-toxic additive [7,9,10]. Due to its high number of conjugated pairs, bixin is susceptible to isomerization and degradation by external agents (heat, light, and oxygen), resulting in a loss of color [11,12]. Microencapsulation offers

\* Corresponding author. Department of Physics, Regional University of Cariri, Campus Crajubar, Av. Leão Sampaio, 170, Bairro Triângulo, CEP: 63040-000, Juazeiro do Norte, CE, Brazil

E-mail address: [alexandre.teixeira@urca.br](mailto:alexandre.teixeira@urca.br) (A.M.R. Teixeira).



Contents lists available at ScienceDirect

**Heliyon**

journal homepage: [www.cell.com/heliyon](http://www.cell.com/heliyon)



Research article

## Quantum computational investigations and molecular docking studies on amentoflavone



Márcia M. Marinho<sup>a, \*</sup>, Francisco Wagner Q. Almeida-Neto<sup>b</sup>, Emanuelle M. Marinho<sup>b</sup>, Leonardo P. da Silva<sup>b</sup>, Ramon R.P.B. Menezes<sup>a</sup>, Ricardo P. dos Santos<sup>c</sup>, Emmanuel S. Marinho<sup>d</sup>, Pedro de Lima-Neto<sup>b</sup>, Alice M.C. Martins<sup>a</sup>

<sup>a</sup> Departamento de Análises Clínicas e Toxicológicas, Centro de Ciências da Saúde, Universidade Federal do Ceará, Campus Porangabussu, 60430-370, Fortaleza, Ceará, Brazil

<sup>b</sup> Departamento de Química Analítica e Físico-Química, Centro de Ciências, Universidade Federal do Ceará, Campus do Pici, Bloco 940, 60440-900, Fortaleza, Ceará, Brazil

<sup>c</sup> Engenharia de Computação / Biotecnologia, Universidade Federal do Ceará, Campus de Sobral, 62010-560, Sobral Ceará, Brazil

<sup>d</sup> Faculdade de Filosofia Dom Aureliano Matos, Universidade Estadual do Ceará, 62930-000, Limoeiro do Norte, Ceará, Brazil

### ARTICLE INFO

**Keywords:**  
Antichagasic agent  
Biflavonoid  
DFT  
Fukui analysis  
NLO

### ABSTRACT

Chagas disease is a neglected tropical disease caused by the protozoan parasite *Trypanosoma cruzi*, with approximately 6–7 million people infected worldwide, becoming a public health problem in tropical countries, thus generating an increasing demand for the development of more effective drugs, due to the low efficiency of the existing drugs. Aiming at the development of a new antichagasic pharmacological tool, the density functional theory was used to calculate the reactivity descriptors of amentoflavone, a biflavonoid with proven anti-trypanosomal activity in vitro, as well as to perform a study of interactions with the enzyme cruzain, an enzyme key in the evolutionary process of *T. cruzi*. Structural properties (in solvents with different values of dielectric constant), the infrared spectrum, the frontier orbitals, Fukui analysis, thermodynamic properties were the parameters calculated from DFT method with the monomeric structure of the apigenin used for comparison. Furthermore, molecular docking studies were performed to assess the potential use of this biflavonoid as a pharmacological antichagasic tool. The frontier orbitals (HOMO-LUMO) study to find the band gap of compound has been extended to calculate electron affinity, ionization energy, electronegativity electrophilicity index, chemical potential, global chemical hardness and global chemical softness to study the chemical behaviour of compound. The optimized structure was subjected to molecular Docking to characterize the interaction between amentoflavone and cruzain enzyme, a classic pharmacological target for substances with anti-gas activity, where significant interactions were observed with amino acid residues from each one's catalytic sites enzyme. These results suggest that amentoflavone has the potential to interfere with the enzymatic activity of cruzain, thus being an indicative of being a promising antichagasic agent.

### 1. Introduction

Chagas disease is a tropical disease caused by the protozoan parasite *Trypanosoma cruzi*, classified as neglected by the World Health Organization. The Chagas disease is transmitted to humans by the triatomine insect, popularly known, in Brazil, as the barber [1]. Currently, there are approximately 6–7 million infected people in the world and it is estimated that 70 million people will be able to contract this disease. This is an endemic disease in Latin America, Africa and Asia, but also found in

non-endemic developed countries such as Canada, Spain, Japan and Australia [2,3]. Currently, benznidazole and nifurtimox are the only drugs used for the pharmacological treatment of Chagas disease, developed almost fifty years ago, have limited effectiveness in the chronic phase of the disease. However, these drugs led to the occurrence of several side effects, such as polyneuritis, bone marrow depression, lymphoma and dermatitis [4]. Therefore, it is necessary to look for new bioactive substances, as well as therapeutic strategies that promote

\* Corresponding author.  
E-mail address: [marinho.marcia@gmail.com](mailto:marinho.marcia@gmail.com) (M.M. Marinho).

<https://doi.org/10.1016/j.heliyon.2021.e06079>

Received 27 October 2020; Received in revised form 1 December 2020; Accepted 20 January 2021

2405-8440/© 2021 Published by Elsevier Ltd. This is an open access article under the CC BY-NC-ND license (<http://creativecommons.org/licenses/by-nc-nd/4.0/>).



Contents lists available at ScienceDirect

Electrochimica Acta

journal homepage: [www.elsevier.com/locate/electacta](http://www.elsevier.com/locate/electacta)

## SAM of Gliotoxin on Gold: A Natural Product Platform for Sugar Recognition based on the Immobilization of *Canavalia brasiliensis* lectin (ConBr)



Dieric S. Abreu<sup>a</sup>, Ticyano P. Sousa<sup>a</sup>, Caio B. Castro<sup>a</sup>, Mayara N.V. Sousa<sup>a</sup>, Thiago T. Silva<sup>a</sup>, Francisco W.Q. Almeida-Neto<sup>a</sup>, Marcos V.A. Queiros<sup>a</sup>, Bárbara S.F. Rodrigues<sup>a</sup>, Maria C.F. Oliveira<sup>a</sup>, Tércio F. Paulo<sup>a</sup>, Benildo S. Cavada<sup>b</sup>, Kyria S. Nascimento<sup>b</sup>, Marcia L.A. Temperini<sup>c</sup>, Izaura C.N. Diógenes<sup>a,\*</sup>

<sup>a</sup> Universidade Federal do Ceará, Departamento de Química Orgânica e Inorgânica, Laboratório de Bioinorgânica, Fortaleza, Ceará, Brazil

<sup>b</sup> Universidade Federal do Ceará, Departamento de Bioquímica e Biologia Molecular - BioMol-Lab, Fortaleza, Ceará, Brazil

<sup>c</sup> Universidade de São Paulo, Instituto de Química, Departamento de Química Fundamental, Laboratório de Espectroscopia Molecular, São Paulo, São Paulo, Brazil

### ARTICLE INFO

#### Article history:

Received 29 January 2017

Received in revised form 18 April 2017

Accepted 19 April 2017

Available online 23 April 2017

#### Keywords:

Self-assembled monolayer

Diketopiperazine

ConBr lectin

Sugar recognition

### ABSTRACT

We report the successful fabrication of a novel gold surface coated with a thiol-lectin multilayer that showed specific interaction towards D-mannose sugars. Firstly, the gold surface was spontaneously modified with gliotoxin (gtx), a sulfur containing diketopiperazine isolated from marine-derived fungus, and fully characterized by electrochemical, EIS, SPR and SERS techniques. The results indicated the sulfur bridge of gtx is broken upon adsorption and the molecules are flat lying on gold with surface coverage of  $2.3 \times 10^{-10} \text{ mol cm}^{-2}$  and reductive desorption potential of  $-0.87 \text{ V vs Ag/AgCl}$ , i.e. strongly chemisorbed on gold. The real-time monitoring of the immobilization of Concanavalin Br (ConBr) lectin ( $6.9 \times 10^{-12} \text{ mol cm}^{-2}$ ) on the gold surface modified with gliotoxin (Au/gtx) was performed by SPR which was also used to prove the recognition capability of ConBr towards D-mannose remains active on Au/gtx. Comparative studies using 11-mercaptoundecanoic acid and cysteine on gold show the interaction between the thiol layer with ConBr involves a network of hydrogen bonds and that the SAM formed with gliotoxin is the most robust monolayer. Impedimetric measurements in solution containing  $[\text{Fe}(\text{CN})_6]^{3-/4-}$  redox probe and D-mannose sugar at different concentrations indicate hydrogen bonds are the major intermolecular contributions connecting the sugar molecules to the sugar recognition sites of ConBr where  $\text{Ca}^{2+}$  and  $\text{Mn}^{2+}$  ions are inserted.

© 2017 Elsevier Ltd. All rights reserved.

### 1. Introduction

Self-assembled monolayers (SAMs) on solid substrates is one of the most common methods to produce surfaces with desired properties [1–4]. In particular, SAMs of sulfur containing compounds on gold have been examined in a huge variety of interests ranging from the physical chemistry aspect of the adsorption process itself to applications in bioelectronics and bioelectrochemistry [4–11]. In the context of bioelectrochemistry, immobilization of biomolecules without the loss of the biological activity is a prerequisite for successful preparation of any biosensor.

Unfortunately, the direct adsorption of proteins on metallic surfaces usually results in denaturation and, consequently, in the loss of the biological activity [12–15]. Thiolate SAMs have been used, therefore, as a platform to immobilize proteins aiming to inhibit denaturation and preserve the biological activity [5,16–22]. The immobilization of such molecules on SAMs is highly relevant and should be considered as a key step in constructing high-performance biosensors. Lectins have been used as bioreceptor in several biosensing devices due to their capacity to recognize and specifically bind carbohydrates with high selectivity [23–26]. Carbohydrates present on cell surfaces play an important role in a wide range of biological and pathological processes like the interaction between cells and their environment, inflammations and cancer metastasis. In addition, carbohydrates are commonly used as biomarkers of pathological changes occurring during

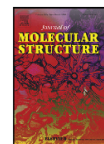
\* Corresponding author.

E-mail address: [izaura@dqoi.ufc.br](mailto:izaura@dqoi.ufc.br) (I.C.N. Diógenes).



Contents lists available at ScienceDirect

Journal of Molecular Structure

journal homepage: [www.elsevier.com/locate/molstr](http://www.elsevier.com/locate/molstr)

## Spectroscopic analysis by NMR, FT-Raman, ATR-FTIR, and UV-Vis, evaluation of antimicrobial activity, and *in silico* studies of chalcones derived from 2-hydroxyacetophenone



Jayze da Cunha Xavier<sup>a</sup>, Francisco W.Q. de Almeida-Neto<sup>b</sup>, Janaína E. Rocha<sup>a</sup>, Thiago S. Freitas<sup>a</sup>, Priscila R. Freitas<sup>a</sup>, Ana C.J. de Araújo<sup>a</sup>, Priscila T. da Silva<sup>a</sup>, Carlos E.S. Nogueira<sup>a,c</sup>, Paulo N. Bandeira<sup>d</sup>, Márcia M. Marinho<sup>e</sup>, Emmanuel S. Marinho<sup>f</sup>, Nitin Kumar<sup>g</sup>, Antônio C.H. Barreto<sup>h</sup>, Henrique D.M. Coutinho<sup>a</sup>, Murilo S.S. Julião<sup>b</sup>, Hélcio S. dos Santos<sup>a,d</sup>, Alexandre M.R. Teixeira<sup>a,c,\*</sup>

<sup>a</sup> Department of Biological Chemistry, Regional University of Cariri, CE, Brazil

<sup>b</sup> Department of Analytical Chemistry and Physical Chemistry, Federal University of Ceará, Fortaleza, CE, Brazil

<sup>c</sup> Department of Physics, Regional University of Cariri, Juazeiro do Norte, CE, Brazil

<sup>d</sup> Center for Exact Sciences and Technology, Chemistry Course, Vale do Acaraú University, Sobral, CE, Brazil

<sup>e</sup> State University of Ceará, Faculty of Education, Science and Letters of Iguatu, Iguatu, CE, Brazil

<sup>f</sup> State University of Ceará, Faculty of Philosophy Dom Aureliano Matos, Limoeiro do Norte, CE, Brazil

<sup>g</sup> KR Mangalan University, Sohna Road, Gurugram, India

<sup>h</sup> Department of Physics, Federal University of Ceará, Fortaleza, CE, Brazil

### ARTICLE INFO

**Article history:**  
Received 13 March 2021  
Revised 25 April 2021  
Accepted 5 May 2021  
Available online 19 May 2021

**Keywords:**  
Chalcones  
Spectroscopy  
ADMET  
Antimicrobial activity  
Efflux pump

### ABSTRACT

Six 2'-hydroxychalcones were synthesized and characterized by NMR, FT-Raman, ATR-FTIR, and UV-Vis. These chalcones alone and in combination with the ciprofloxacin, penicillin, and erythromycin antibiotics were tested against multiresistant strains of *Staphylococcus aureus*. It was also verified by *in vitro* and *in silico* studies the capacity of these chalcones to inhibit the NorA efflux pump. The MICs values of ciprofloxacin were reduced in the presence of all tested chalcones. For norfloxacin antibiotic, the chalcones A1, A4, A5 and A6 promoted the reduced in the MIC values. The A2 chalcone was the only one to reduce the MIC values when associated with penicillin. Any chalcones were not able to reduce MIC values when associated with erythromycin. These results indicate that the synergistic effects demonstrated for the synthesized chalcones were influenced by the introduction of a furanic ring (A1), a chlorine atom and a methoxy group at the C4 position (A2 and A4), a second double bond (A5), and a fluorine atom at the C2 position (A6). The ADMET analysis predicts that the chalcones A2, A3, A5 and A6 have easier cell permeation. The nucleophilic region makes the A5 chalcone capable of covalently bonding with plasma proteins, and the presence of oxygenated aromatic substitutions makes the chalcones A1 and A4 more water-soluble and consequently easier to excrete. On the other hand, the substitution of the methoxy group of the A4 chalcone makes it more susceptible to O-demethylation reactions by the CYP3A4 isoenzyme. The molecular docking revealed that all six chalcones could hinder the binding of norfloxacin to the NorA efflux pump.

© 2021 Elsevier B.V. All rights reserved.

### 1. Introduction

The prevalence of bacteria resistant to antibiotics has increased dramatically in recent years. The infections caused by multidrug-

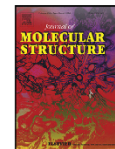
resistant bacteria result at approximately 700,000 deaths per year, and it estimates they will rise to ten million lives annually by 2050 [1]. Due to the emergence and spread of multidrug-resistant strains, the treatment of *staphylococcal* infections with traditionally used antibiotics, such as penicillin and cephalosporin, has become ineffective [2]. Despite the effectiveness of vancomycin against multidrug-resistant strains of *S. aureus*, this antibiotic has some limitations, such as toxicity and poor absorption [3]. Fluoroquinolones such as norfloxacin and ciprofloxacin have been used

\* Corresponding author at: Dr. Alexandre Magno Rodrigues Teixeira, Postgraduate Program in Biological Chemistry, Department of Biological Chemistry, Regional University of Cariri, Campus Pimenta II, CEP: 63.100-000, Crato, CE, Brazil.  
E-mail address: [alexandre.teixeira@urca.br](mailto:alexandre.teixeira@urca.br) (A.M.R. Teixeira).



Contents lists available at ScienceDirect

Journal of Molecular Structure

journal homepage: [www.elsevier.com/locate/molstr](http://www.elsevier.com/locate/molstr)

## Structural and spectroscopic analysis and evaluation of cytotoxic activity of 2-hydroxychalcones against human cancer cell lines



Antonio L.A.B. Leal<sup>a</sup>, Daniel P. Pinheiro<sup>b</sup>, Francisco W.A. Barros-Nepomuceno<sup>b,c</sup>, Priscila T. da Silva<sup>a</sup>, Claudia Pessoa<sup>b</sup>, Francisco W.Q. Almeida-Neto<sup>d</sup>, Emmanuel S. Marinho<sup>e</sup>, Antônio C.H. Barreto<sup>f</sup>, Murilo S.S. Julião<sup>g</sup>, Aldeneide S. de Paiva<sup>g</sup>, Paulo N. Bandeira<sup>g</sup>, Pedro de Lima-Neto<sup>d</sup>, Hécio S. dos Santos<sup>a,g</sup>, Alexandre M.R. Teixeira<sup>a,\*</sup>

<sup>a</sup> Department of Biological Chemistry, Regional University of Cariri, Campus Pimenta II, CEP: 63.100-000 Crato, Ceará, Brazil

<sup>b</sup> Center for Research and Drug Development, Federal University of Ceará, Fortaleza, Ceará, Brazil

<sup>c</sup> Institute of Health Sciences, University of International Integration of the Afro-Brazilian Lusophony, Redenção, Ceará, Brazil

<sup>d</sup> Department of Analytical Chemistry and Physical Chemistry, Federal University of Ceará, Fortaleza, Ceará, Brazil

<sup>e</sup> Group of Theoretical Chemistry and Electrochemistry, State University of Ceará, Campus FAFIDAM, Limoeiro do Norte, Ceará, Brazil

<sup>f</sup> Department of Physics, Federal University of Ceará, Fortaleza, CE, Brazil

<sup>g</sup> Center for Exact Sciences and Technology - Chemistry Course, State University of Vale do Acaraú, Sobral, CE, Brazil

### ARTICLE INFO

#### Article history:

Received 15 February 2021

Revised 14 July 2021

Accepted 15 July 2021

Available online 19 July 2021

#### Keywords:

Chalcones

NMR

ATR-FTIR

FT-Raman

UV-vis

Cytotoxic activity

### ABSTRACT

Chalcones and their derivatives exhibit a broad spectrum of pharmacological activities, including antiproliferative activities. Accordingly, they are deemed robust anticancer candidates for cytotoxicity assays. Herein, we synthesized and characterized four chalcones using nuclear magnetic resonance (<sup>1</sup>H NMR and <sup>13</sup>C NMR), Fourier transform Raman (FT-Raman), attenuated total reflection Fourier transform infrared (ATR-FTIR), and ultraviolet-visible (UV-vis) spectroscopy. Theoretical calculations of quantum chemistry were performed to obtain data regarding normal vibration modes, frontier molecular orbitals, molecular electrostatic potential maps, theoretical UV-vis spectra, and quantum chemical parameters expected for these chalcones. In addition, we evaluated the cytotoxic potential of these compounds. For synthesized compounds, quantum chemical calculations demonstrated excellent correlation with experimental data. The electronic properties revealed that chalcones 1 and 4 possess a higher electrophilic character, while chalcones 2 and 3 possess a higher nucleophilic character. Chalcone 3 demonstrated the highest value of HOMO energy, indicating the greatest propensity to donate electronic density among the four compounds. According to the HOMO-LUMO energy gap and global hardness, the reactivity of chalcones should follow the order 1 < 2 < 4 < 3. Regarding the cytotoxic potential, chalcones 1 and 4 exhibited superior activity against HL-60 acute promyelocytic leukemia cells (IC<sub>50</sub> = 14.09 ± 1.001 and 28.02 ± 1.47 μM, respectively) and HCT-116 colon cancer cells (IC<sub>50</sub> = 22.64 ± 0.64 and 42.74 ± 4.63 μM, respectively).

© 2021 Elsevier B.V. All rights reserved.

### 1. Introduction

Cancer is a leading cause of death worldwide. In 2020, the Global Cancer Observatory (GLOBOCAN) estimated the incidence of 19.3 million new cases of cancer and 10 million deaths [1]. It is projected that by 2030, between 10 and 11 million cancers will be diagnosed each year in low- and middle-income countries [2]. In Brazil, cancer remains the second leading cause of death due to illness. Reportedly, 337,535 new cases and 122,600 deaths are

recorded annually [3,4]. It is estimated that non-melanoma skin cancer (114,000 new cases) accounts for the most commonly detected cancer in the Brazilian population, followed by prostate tumors (52,000), female breast (49,000), colon and rectal (28,000), lung (28,000), stomach (21,000), and cervical (18,000) cancers [3].

Currently, several anticancer drugs are available for cancer therapy, including cyclophosphamide, camptothecin, mitoxantrone, podophyllotoxin, vincristine, vinblastine, taxol, and thiopeta [5–7]. However, in many cases, therapeutic success is eluded owing to failures in therapeutic regimens, high relapse rates, reduced patient survival, and adverse effects, resulting in an ongoing search for novel therapeutic agents [8]. Numerous natural products with

\* Corresponding author.

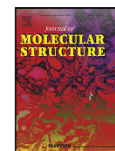
E-mail address: [alexandre.teixeira@urca.br](mailto:alexandre.teixeira@urca.br) (A.M.R. Teixeira).





Contents lists available at ScienceDirect

Journal of Molecular Structure

journal homepage: [www.elsevier.com/locate/molstr](http://www.elsevier.com/locate/molstr)

## Structural characterization, DFT calculations, ADMET studies, antibiotic potentiating activity, evaluation of efflux pump inhibition and molecular docking of chalcone (*E*)-1-(2-hydroxy-3,4,6-trimethoxyphenyl)-3-(4-methoxyphenyl)prop-2-en-1-one



Jayze da Cunha Xavier<sup>a</sup>, Francisco Wagner de Queiroz Almeida-Neto<sup>b</sup>, Priscila Teixeira da Silva<sup>a</sup>, Amanda Pereira de Sousa<sup>f</sup>, Emmanuel Silva Marinho<sup>c</sup>, Márcia Machado Marinho<sup>g</sup>, Janaina Esmeraldo Rocha<sup>a</sup>, Priscila Ramos Freitas<sup>a</sup>, Ana Carolina Justino de Araújo<sup>a</sup>, Thiago Santiago Freitas<sup>a</sup>, Carlos Emídio Sampaio Nogueira<sup>a,e</sup>, Pedro de Lima-Neto<sup>b</sup>, Paulo Nogueira Bandeira<sup>f</sup>, Alexandre Magno Rodrigues Teixeira<sup>a</sup>, Henrique Douglas Melo Coutinho<sup>a</sup>, Hércio Silva dos Santos<sup>a,d,f,\*</sup>

<sup>a</sup> Department of Biological Chemistry, Regional University of Cariri, Crato, CE, Brazil

<sup>b</sup> Group of Theoretical Chemistry, Department of Analytical Chemistry and Physical Chemistry, Federal University of Ceará, Fortaleza, CE, Brazil

<sup>c</sup> Group of Theoretical Chemistry and Electrochemistry, State University of Ceará, Campus FAFIDAM, Limoeiro do Norte, CE, Brazil

<sup>d</sup> Science and Technology Center, Postgraduate Program in Natural Sciences, State University of Ceará, Fortaleza, CE, Brazil

<sup>e</sup> Department of Physics, Regional University of Cariri, Juazeiro do Norte, CE, Brazil

<sup>f</sup> Center for Exact Sciences and Technology - Chemistry Course, Vale do Acaraú University, Sobral, CE, Brazil

<sup>g</sup> Iguatu Faculty of Education, Science and Letters (Fectl), State University of Ceará, Iguatu, Ceará, Brazil

### ARTICLE INFO

#### Article history:

Received 2 August 2020

Revised 12 November 2020

Accepted 26 November 2020

Available online 29 November 2020

#### Keywords:

Chalcone

ATR-FTIR

UV-vis

Fukui

Efflux pump

### ABSTRACT

Chalcones are open-chain flavonoids characterized by two aromatic rings joined by a three-carbon  $\alpha,\beta$ -unsaturated carbonyl system. Over the last several years, chalcones have instigated the interest of chemical and pharmacological researchers due to their simple chemical structure and varied biological activities. Here, we performed the electronic properties, of the chalcone, (*E*)-1-(2-hydroxy-3,4,6-trimethoxyphenyl)-3-(4-methoxyphenyl) prop-2-en-1-one synthesized by Claisen-Schmidt condensation reaction. The density functional theory method was used with the B3LYP/6-311++G(d,p) level of theory to compute the structural, electronic, and reactivity properties of the chalcone. In addition, microbiological tests were performed to investigate the modulator potential and efflux pump inhibition on *Staphylococcus aureus* multi-resistant strains. The spectroscopic data analyses allowed drawing the molecular structure of the chalcone synthesized with subsequent confirmation using the quantum chemical calculations. The addition of chalcone to the growth medium caused a synergic effect by reduction of the minimum inhibitory concentration (MIC) values for ciprofloxacin strain. Docking results showed that the chalcone docks in almost the same way as the antibiotic against a MepA model. Druglikeness criteria based on the rules of Lipinski and Veber evaluated that the chalcone has the ideal physicochemical and pharmacokinetic properties to be a good candidate for drug orally. The results confirm the structure of the synthesized chalcone and revealing that the compound can be used as a possible inhibitor of the MepA efflux pump.

© 2020 Elsevier B.V. All rights reserved.

### 1. Introduction

The search for new drugs is increasing due to the rapid growth of bacterial resistance that has become a medical concern today [1-3]. The bacterial resistance comes from factors such as selectiv-

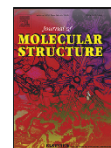
\* Corresponding author at: Postgraduate Program in Biological Chemistry, Department of Biological Chemistry, Regional University of Cariri, Campus Pimenta II, CEP: 63.100-000, Crato, CE, Brazil.

E-mail address: [helcio\\_santos@uvanet.br](mailto:helcio_santos@uvanet.br) (H.S. dos Santos).



Contents lists available at ScienceDirect

Journal of Molecular Structure

journal homepage: [www.elsevier.com/locate/molstr](http://www.elsevier.com/locate/molstr)

## Structural characterization, electronic properties, and anxiolytic-like effect in adult zebrafish (*Danio rerio*) of cinnamaldehyde chalcone

Jayze da Cunha Xavier<sup>a</sup>, Francisco Wagner Queiroz Almeida-Neto<sup>b</sup>, Priscila Teixeira da Silva<sup>a</sup>, Emmanuel Silva Marinho<sup>c</sup>, Maria Kueirislene Amâncio Ferreira<sup>d</sup>, Francisco Ernani Alves Magalhães<sup>d,g</sup>, Carlos Emídio Sampaio Nogueira<sup>a,e</sup>, Paulo Nogueira Bandeira<sup>f</sup>, Jane Eire Silva Alencar de Menezes<sup>d</sup>, Alexandre Magno Rodrigues Teixeira<sup>a,e</sup>, Hécio Silva dos Santos<sup>a,d,f,\*</sup>

<sup>a</sup> Department of Biological Chemistry, Regional University of Cariri, Crato, CE, Brazil

<sup>b</sup> Group of Theoretical Chemistry, Department of Analytical Chemistry and Physical Chemistry, Federal University of Ceará, Fortaleza, CE, Brazil

<sup>c</sup> Group of Theoretical Chemistry and Electrochemistry, State University of Ceará, Campus FAFIDAM, Limoeiro do Norte, CE, Brazil

<sup>d</sup> Science and Technology Center, Postgraduate Program in Natural Sciences, State University of Ceará, Fortaleza, CE, Brazil

<sup>e</sup> Department of Physics, Regional University of Cariri, Juazeiro do Norte-CE, Brazil

<sup>f</sup> Center for Exact Sciences and Technology - Chemistry Course, Vale do Acaraú University, Sobral, CE, Brazil

<sup>g</sup> State University of Ceará, Department of Chemistry, Laboratory of Natural Products Bioprospecting and Biotechnology, CECITEC Campus, Tauá, CE, Brazil

### ARTICLE INFO

#### Article history:

Received 1 June 2020

Revised 15 July 2020

Accepted 21 July 2020

Available online 22 July 2020

#### Keywords:

RMN

IR

Fukui functions

Anxiolytic-like effect

Zebrafish

Cinnamaldehyde chalcone

### ABSTRACT

Zebrafish is a model animal that is used for neurobehavioral studies. It is an excellent model organism for pharmacological studies and/or safety research at an early stage of drug development. In this work, the chalcone (2*E*, 4*E*)-1-(2-hydroxy-3,4,6-trimethoxyphenyl)-5-phenylpenta-2,4-dien-1-one, was synthesized by the Claisen-Schmidt condensation from two natural products: 2-hydroxy-3,4,6-trimethoxyacetophenone and cinnamaldehyde. The molecular structure of this compound was confirmed by spectroscopic methods such as NMR, Infrared, UV-vis, and quantum chemical calculations. In addition, the anxiolytic-like effect of the cinnamaldehyde chalcone in adult zebrafish (*Danio rerio*) was evaluated. The results showed that chalcone caused an approximately 80% reduction in zebrafish locomotor activity and induced maximum permanence of zebrafish in the clear zone (61.16%) at a dose of 0.5 mg kg<sup>-1</sup>. The data suggest that the cinnamaldehyde chalcone has anxiolytic activity.

© 2020 Elsevier B.V. All rights reserved.

### 1. Introduction

Zebrafish (*Danio rerio*) (Fig. 1) are used in behavioral neuroscience, including research involving the brain and psychopharmacology [1]. This fish is a suitable model to study the central nervous system because its genotype has 70% homology with mammalian neurotransmitter receptors [2]. Because of the side effects associated with allopathic drugs, there is a growing interest in the development of alternative therapies to treat psychiatric disorders [3]. Natural products were selected over the years with the needed efficiency and selectivity to reach cellular targets, and would be a molecular inspiration for medicinal chemists or the source of drugs with high complex chemical structures. Previous studies demon-

strated the anxiolytic action of several phytochemical groups such as polyphenols and chalcones [4–6].

The genus *Croton*, which belongs to the Euphorbiaceae family, is the second largest genus of a large and diverse group of plants rich in tropical species. Around 712 species of *Croton* are recognized [7,8], and they generally have important pharmacological properties, which were already reported in literature [9]. The substance 2-hydroxy-3,4,6-trimethoxyacetophenone (Fig. 1b) was isolated from *Croton anisodontus* (Fig. 1a) [10]. This structure can basically be used to synthesize new chalcones from reactions between acetophenones and aromatic aldehydes.

Chalcones have at least two aromatic rings linked together by a three-carbon unsaturated  $\alpha,\beta$ -bond (Fig. 2). Natural chalcones are precursors of flavonoids and isoflavonoids [11]. They can also be obtained by organic synthesis. This compound class attracted much interest because of the wide spectrum of pharmacological activities that they represent, including antimicrobial [12], antioxidant [13],

\* Corresponding author: Science and Technology Center - Chemistry Course, State University of Vale do Acaraú, Sobral, Ceará, Brazil. Address: 850 University Avenue, Sobral, CE 62040370, Brazil.

E-mail address: [helcio.silva@uece.br](mailto:helcio.silva@uece.br) (H.S.d. Santos).

<https://doi.org/10.1016/j.molstruc.2020.128954>

0022-2860/© 2020 Elsevier B.V. All rights reserved.

# Structural, electronic, and optical properties of inhomogeneous $\text{Ca}_{1-x}\text{Mg}_x\text{O}$ alloys

Cite as: J. Appl. Phys. 125, 155102 (2019); doi: 10.1063/1.5053102

Submitted: 21 August 2018 · Accepted: 26 March 2019 ·

Published Online: 16 April 2019



F. W. Q. Almeida-Neto,<sup>1</sup> G. Santos-Castro,<sup>2</sup> M. B. da Silva,<sup>2</sup> J. S. de Sousa,<sup>2,a)</sup> E. W. S. Caetano,<sup>3</sup> P. Lima-Neto,<sup>1</sup> and V. N. Freire<sup>2</sup>

## AFFILIATIONS

<sup>1</sup>Departamento de Química Analítica e Físico-Química, Universidade Federal do Ceará, 60440-900 Fortaleza-CE, Brazil

<sup>2</sup>Departamento de Física, Universidade Federal do Ceará, 60440-900 Fortaleza-CE, Brazil

<sup>3</sup>Instituto Federal de Educação, Ciência e Tecnologia do Ceará, 60040-531 Fortaleza-CE, Brazil

<sup>a)</sup>Electronic mail: jeanlex@fisica.ufc.br

## ABSTRACT

The structural, electronic, and optical properties of homogeneous and inhomogeneous  $\text{Ca}_{1-x}\text{Mg}_x\text{O}$  alloys are studied with the density functional theory (DFT) under the assumption of polymorphism. Large supercells ( $2 \times 2 \times 2$  and above) with different lattice symmetries and varying Mg molar fraction  $x$  were constructed, representing distinct solid phases that may coexist in micro/nanodomains of inhomogeneous alloys. We demonstrate that these polymorphs exhibit rich phenomenology like similar formation enthalpies for a given concentration  $x$ , but different electronic and optical properties. For example,  $\text{Ca}_{0.5}\text{Mg}_{0.5}\text{O}$  may have crystallites with four possible lattice symmetries using a  $2 \times 2 \times 2$  supercell for its description, with bandgaps varying between 3.26 eV (direct) and 4.46 eV (indirect). The DFT-simulated X-ray diffraction shows that polymorphism causes broadening and shift of the diffraction peaks. We also performed a detailed calculation of the bandgaps, optical absorption, and dielectric constants as a function of  $x$  for each polymorph, and they exhibit a structured bandgap behavior with maxima and minima in the  $0.0 < x < 1.0$  range, which is in marked contrast to Vegard's law rule of mixtures. We also report a direct-to-indirect bandgap transition occurring between  $0.072 \leq x \leq 0.1094$  for the  $FM3M$  symmetry.

Published under license by AIP Publishing. <https://doi.org/10.1063/1.5053102>

## I. INTRODUCTION

In bulk  $\text{A}_{1-x}\text{B}_x\text{C}$  alloys, the spatial distribution of the atomic species can be either homogeneous or inhomogeneous. The homogeneous case  $h\text{A}_{1-x}\text{B}_x\text{C}$  is obtained when the whole structure is well described by a single unit cell (UC) that can be determined by X-ray diffraction. In contrast, inhomogeneous alloys  $i\text{A}_{1-x}\text{B}_x\text{C}$  may exhibit distinct crystallographic domains or completely random distribution of the atomic species. In this case, the X-ray diffraction exhibits broader and shifted peaks as compared to the homogeneous alloy. Depending on the thermodynamical conditions during crystal growth and the formation enthalpies of each type of crystal, a given symmetry can prevail or coexist with other symmetries forming a polycrystalline structure. The empirical Vegard's law for a solid solution of two constituents,<sup>1</sup> which proposes a linear dependence on  $x$  for the lattice parameters and energy bandgaps, is regularly used to describe the physical properties of homogeneous alloys. However, the associated polymorphism in inhomogeneous alloys rules out the application of Vegard's law. Therefore, new

methods to study alloys considering the possibility of polymorphism are necessary.

Theoretical solid state usually applies constraints such as translational symmetry, Bloch's theorem, and small UCs in order to reduce the complexity of the calculations. However, the formation of  $\text{A}_{1-x}\text{B}_x\text{C}$  alloys from the ordered solids AC and BC is inevitably associated with a loss of long-range order. Alloyed materials break translational symmetry, complicating the definition of a band structure. From a given concentration  $x$ , one can construct a perfectly random or a perfectly ordered alloy  $\text{A}_{1-x}\text{B}_x\text{C}$ , or any intermediate state. Thus, the most appropriate method to deal with alloyed materials is the supercell (SC) approach. The larger the supercell, the larger the number of accessible  $x$  concentrations. It is also possible to investigate different crystal structures for a given value of  $x$ .<sup>2,3</sup> The disadvantage of the SC method is the increasing complexity of the calculations and the Brillouin zone folding due to the use of large SCs in real space, which results in Brillouin zones (BZs) smaller than the BZ of the smallest UC in real space, projecting





## Synthesis of a new quinine dimer biocatalysed by the coconut water

Aluísio M. Fonseca<sup>a,b</sup>, Leonardo Paes da Silva<sup>c</sup>, Francisco Wagner de Queiroz Almeida-Neto<sup>c</sup>, Regilany Paulo Colares<sup>b</sup>, Mauro Macedo de Oliveira<sup>a,d</sup>, Antônio Luthierre Gama Cavalcante<sup>c</sup>, Telma L. G. Lemos<sup>e</sup>, Raimundo Braz-Filho<sup>f</sup>, Pedro de Lima-Neto<sup>c</sup> and Emmanuel Silva Marinho<sup>c,g</sup>

<sup>a</sup>Mestrado Acadêmico em Sociobiodiversidades e Tecnologias Sustentáveis – MASTS, Instituto de Engenharias e Desenvolvimento Sustentável, Universidade da Integração Internacional da Lusofonia Afro-Brasileira, Acarape, Brazil; <sup>b</sup>Instituto de Ciências Exatas e da Natureza, Universidade da Integração Internacional da Lusofonia Afro-Brasileira, Acarape, Brazil; <sup>c</sup>Grupo de Química Teórica, Departamento de Analítica e Físico-Química, Universidade Federal do Ceará, Fortaleza, Brazil; <sup>d</sup>Departamento de Química, Centro Universitário Paraíso – UNIFAP, Juazeiro do Norte, Brazil; <sup>e</sup>Laboratório de Biotálise e Produtos Naturais, Departamento de Química Orgânica e Inorgânica, Universidade Federal do Ceará, Fortaleza, Brazil; <sup>f</sup>Centro de Ciências e Tecnologias, Universidade Estadual do Norte Fluminense Darcy Ribeiro, Campos Dos Goytacazes, Brazil; <sup>g</sup>Faculdade de Filosofia Dom Aureliano Matos - FAFIDAM, Universidade Estadual do Ceará, Centro, Brazil

### ABSTRACT

The obtaining of bis-quinine, a novel alkaloid dimer, has been successfully achieved starting from quinine and the raw coconut juice (*Cocos nucifera*) as biocatalyst dimerization-like reaction, in mild conditions, with a mass yield of 64.7% in 72 h. The structural elucidation was made based on the spectral data, mainly by a high-field NMR and a mass spectrometry. In a second step, theoretical calculations were performed, an optimised energy structure of the new compound was obtained, the energy gap of the boundary orbitals (HOMO and LUMO) as well as the chemical reactivity descriptors were estimated.

### GRAPHICAL ABSTRACT

### ARTICLE HISTORY

Received 23 August 2020  
 Revised 7 May 2021  
 Accepted 23 May 2021

### KEYWORDS

Quinine; biotransformations;  
 crude enzyme;  
 coconut water

## 1. Introduction


In the recent decades, the current model of economic, scientific and technological development, combined with unrestrained consumerism, has generated a significant increase in the consumption of goods and raw materials, as well as an unbridled growth in industrial production and the usage of synthetic chemicals (Chi et al. 2019). This actions have generated an unseen picture of environmental degradation leading to an environmental crisis. Therefore, It is necessary to develop processes and actions that would minimise the harmful entropic effects in the natural and human environments (Faber et al. 2019; Schwarz 2017).

With the purpose to maintain and improve the quality of life around the planet and considering the need for continuous sustainable economic, social and environmental developments, a new chemical conduct would become imperative for the improvement of the techniques and methodologies with the rising generation of toxic residues and effluents. This particular trend, known as Green Chemistry, can be defined as "the creation, development and application of

chemicals, as well as the processes to reduce or eliminate the use in the generation of substances that are harmful to human health and the environment" (Iravani 2011; Lazar 2008; Lewandowski 2014). Hence, this previously mentioned way, provides enzymes that will increasingly replace many conventional catalysts, since they are a sustainable path, because they are ecologically more viable. The usage of enzymes (isolated from vegetables or microorganisms) as catalysts to promote specific changes in a given substrate, is known as biocatalysis, which is considered an interdisciplinary area by correlating studies in organic chemistry and biology, therefore, contributing to the development of new synthetic strategies with the use of easily accessible raw materials (Sheldon and Woodley 2018).

Previous studies have reported the presence of enzymes in all parts of fruits that have been used as biocatalysts in several organic reactions (Chittamuru et al. 2016). Research continues to find sources of enzymes in the Brazilian plants for a later use in biocatalysis, such as the juice of *Cocos nucifera* L. Among

**CONTACT** Aluísio M. Fonseca [aluisiomf@unilab.edu.br](mailto:aluisiomf@unilab.edu.br) Institute of Exact and Nature Sciences – ICEN, University for the International Integration of the Afro-Brazilian Lusophony, Acarape, CE, CEP 62785-000, Brazil

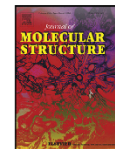
 Supplemental data for this article can be accessed [here](#).

© 2021 Informa UK Limited, trading as Taylor & Francis Group



Contents lists available at ScienceDirect

Journal of Molecular Structure

journal homepage: [www.elsevier.com/locate/molstr](http://www.elsevier.com/locate/molstr)

## Synthesis, spectroscopic characterization and antibacterial evaluation by chalcones derived of acetophenone isolated from *Croton anisodontus* Müll.Arg.



P.T. da Silva<sup>a</sup>, J. da Cunha Xavier<sup>a</sup>, T.S. Freitas<sup>a</sup>, M.M. Oliveira<sup>a</sup>, H.D.M. Coutinho<sup>a</sup>, A.L.A.B. Leal<sup>d</sup>, H.M. Barreto<sup>d</sup>, P.N. Bandeira<sup>b</sup>, C.E.S. Nogueira<sup>a,c</sup>, D.M. Sena Jr.<sup>a</sup>, F.W.Q. Almeida-Neto<sup>e</sup>, E.S. Marinho<sup>f</sup>, H.S. Santos<sup>a,b</sup>, A.M.R. Teixeira<sup>a,c,\*</sup>

<sup>a</sup> Department of Biological Chemistry, Regional University of Cariri, CE, Brazil

<sup>b</sup> Center for Exact Sciences and Technology - Chemistry Course, State University Vale do Acaraú, Sobral, CE, Brazil

<sup>c</sup> Department of Physics, Regional University of Cariri, Juazeiro do Norte-CE, Brazil

<sup>d</sup> Laboratory of Research in Microbiology, Federal University of Piauí, Teresina, Piauí, Brazil

<sup>e</sup> Department of Analytical Chemistry and Physical Chemistry, Group of Theoretical Chemistry (GQT), Federal University of Ceará, Fortaleza-CE, Brazil

<sup>f</sup> Department of Chemistry, Group of Theoretical Chemistry and Electrochemistry (GGTE), State University of Ceará, Limoeiro do Norte, Ceará, Brazil

### ARTICLE INFO

#### Article history:

Received 10 April 2020

Revised 14 September 2020

Accepted 4 October 2020

Available online 7 October 2020

#### Keywords:

NMR

Molecular spectroscopy

DFT

Molecular docking

Antibacterial activity

Chalcones

### ABSTRACT

Chalcones and their derivatives have been widely studied at research institutions and industries, in order to verify their biological properties against various diseases. In this work, it was carried out the synthesis of chalcones (*E*)-3-(furan-2-yl)-1-(2-hydroxy-3,4,6-trimethoxyphenyl) prop-2-en-1-one (HYTFURFURAL) and (*E*)-1-(2-hydroxy-3,4-dimethoxyphenyl)-3-(thiophen-2-yl) prop-2-en-1-one (HYTTIOPHENE) by Claisen-Schmidt aldolic condensation reaction. The molecular structures of these new heteroaryl chalcones have been elucidated and characterized by <sup>1</sup>H and <sup>13</sup>C Nuclear Magnetic Resonance, Fourier transform Raman (FT-Raman), Attenuated Total Reflectance Fourier Transform Infrared (ATR-FTIR), and Ultraviolet-Visible (UV-Vis) spectroscopy. Calculations using the Functional Density Theory (DFT) were performed to predict the vibrational wavenumbers and to obtain the HOMO (highest occupied molecular orbital) and LUMO (lowest unoccupied molecular orbital) molecular orbitals, and starting from them, the quantum descriptors: vertical ionization energy (I), vertical electron affinity (A), chemical potential ( $\mu$ ), electronegativity ( $\chi$ ), global hardness ( $\eta$ ), and electrophilicity index ( $\omega$ ). Antimicrobial and modulatory antibiotic activities of these chalcones were also investigated. The mechanism of the NorA and MepA efflux pump inhibition was also studied by means of molecular docking. The HYTFURFURAL and HYTTIOPHENE chalcones did not present intrinsic activity against the tested bacterial strains; however, they were able to potentiate the activity of norfloxacin against the SA1199B (NorA) strain, as well as the activity of ciprofloxacin against the K2068 (MepA) strain. These results indicate that the HYTFURFURAL and HYTTIOPHENE chalcones are promising compounds as adjuvants to the norfloxacin and ciprofloxacin antibiotics in the treatment of infections caused by *S. aureus*.

© 2020 Elsevier B.V. All rights reserved.

### 1. Introduction

The societal burden of bacterial infections has increased in recent years, and from the moment we began to use antibiotics clinically, pathogenic bacteria began to resist them. These bacteria have spread across the globe and have now become a problem for healthcare systems, causing not only financial damage, but se-

rious harm to the health of patients with multidrug-resistant infections, with an orderly death rate corresponding to 6% of the total of these infections. Furthermore, the financial losses reach absurd heights. In the European Union, treatment costs caused by multidrug-resistant bacterial diseases reached up to 1.6 billion Euros, and days of prolonged hospitalization due to the same problem cost can reach up to 2.5 million Euros [1]. In this sense, strategies involving the development of new antimicrobial molecules is paramount.

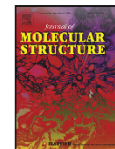
Nature provides us with a broad spectrum of bioactive molecules that can serve as a structural blueprint for rational

\* Corresponding author. Department of Biological Chemistry, Regional University of Cariri, Campus Pimenta II, CEP: 63.100-000, Crato, CE, Brazil.  
E-mail address: [alexandre.teixeira@urca.br](mailto:alexandre.teixeira@urca.br) (A.M.R. Teixeira).



Contents lists available at ScienceDirect

Journal of Molecular Structure

journal homepage: [www.elsevier.com/locate/molstr](http://www.elsevier.com/locate/molstr)

## Synthesis, structural and spectroscopic characterization, *in silico* study, and antinociceptive effect in adult zebrafish of 2-(4-isobutylphenyl)-N'-phenylpropanohydrazide



Tatiana Rodrigues Garcia<sup>a,b</sup>, Paulo de Tarso Cavalcante Freire<sup>a,c</sup>, Paulo Nogueira Bandeira<sup>d</sup>, Amanda Pereira de Sousa<sup>d</sup>, Murilo Sérgio da Silva Julião<sup>d</sup>, Tigressa Helena Soares Rodrigues<sup>d</sup>, Márcia Machado Marinho<sup>e</sup>, Emmanuel Silva Marinho<sup>e</sup>, Francisco Wagner Queiroz Almeida-Neto<sup>f</sup>, Maria Kueirislene Amâncio Ferreira<sup>g</sup>, Antonio Wlisses da Silva<sup>h</sup>, Jane Eire Silva Alencar de Menezes<sup>g</sup>, Aldeneide Soares de Paiva<sup>d</sup>, João Pedro da Hora<sup>d</sup>, Antônio César Honorato Barreto<sup>c</sup>, Hécio Silva dos Santos<sup>a,d,g,h</sup>, Alexandre Magno Rodrigues Teixeira<sup>a,h,\*</sup>

<sup>a</sup> Departamento de Química Biológica, Universidade Regional do Cariri, Crato, CE, Brasil

<sup>b</sup> Indústria Química Farmacêutica Coarense, Juazeiro do Norte, CE, Brasil

<sup>c</sup> Departamento de Física, Universidade Federal do Ceará, Fortaleza, CE, Brasil

<sup>d</sup> Centro de Ciências e Tecnologia, Curso de Química, Universidade Vale do Acaraú, Sobral, CE, Brasil

<sup>e</sup> Grupo de Química Teórica e Eletroquímica, Universidade Estadual do Ceará, Limoeiro do Norte, CE, Brasil

<sup>f</sup> Departamento de Química Analítica e Físico-Química, Universidade Federal do Ceará, Fortaleza, Ceará, Brasil

<sup>g</sup> Programa de Pós-Graduação em Ciências Naturais, Laboratório de Química de Produtos Naturais, Universidade Estadual do Ceará, Fortaleza, CE, Brasil

<sup>h</sup> Programa de Doutorado em Biotecnologia da Rede Nordeste de Biotecnologia (RENORBIO), Universidade Estadual do Ceará, Fortaleza, CE, Brasil

### ARTICLE INFO

#### Article history:

Received 3 March 2021

Revised 31 May 2021

Accepted 1 June 2021

Available online 10 June 2021

#### Keywords:

Ibuprofen derivative

Vibrational spectroscopy

UV-Vis

Molecular docking

ADMET

### ABSTRACT

In this work, an ibuprofen derivative 2-(4-isobutylphenyl)-N'-phenylpropanohydrazide (ACPHZN) was synthesized and characterized by NMR, ATR-FTIR, FT-Raman, and UV-Vis spectroscopy, while their structural and spectroscopic properties were investigated using DFT calculations. *In vivo* study using animal model in an adult Zebrafish (*Danio rerio*), and molecular docking was performed. In addition, molecular descriptors of the properties of absorption, distribution, metabolism and excretion, and toxicity (ADMET) were obtained. The data calculated for ibuprofen derivative are in accordance with the experimental values. From the assays in adult zebrafish, it was found that the ibuprofen derivative was non-toxic and exhibited analgesic properties through the TRPA1, TRPV1 and TRPM8 channels. Molecular docking revealed six interactions of ACPHZN with residues of the capsaicin binding site, and a more favorable affinity energy (-9.0 kcal / mol). ADMET studies suggest that ACPHZN has a pharmacological principle as an oral drug based on a longer half-life in the human body.

© 2021 Elsevier B.V. All rights reserved.

### 1. INTRODUCTION

Ibuprofen (C<sub>13</sub>H<sub>18</sub>O<sub>2</sub>) with the chemical name 2-(4-isobutylphenyl)propanoic acid is a non-steroidal anti-inflammatory drug (NSAID) that has analgesic, antipyretic, and anti-inflammatory activity [1,2]. It is mainly known for its use in arthritis pain [3,4].

Its prolonged use results in gastrointestinal ulceration, bleeding, and nephrotoxicity [5]. This compound has been used to produce hybrid molecules through a two-carbon ethyl bridge [6]. The preparation of new hybrid molecules stem from a lead compound can improve its pharmacokinetic parameters resulting in the discovery of safe drugs, or at least with fewer side effects.

Traditional NSAIDs, such as ibuprofen, contain a free carboxylic acid group, which is appointed as responsible for gastrointestinal damage for long-term use [7]. A strategy to eliminate this effect is to obtain ibuprofen derivatives without the carboxylic acid group [7,8]. Lolli *et al.* showed that ibuprofen derivatives reduced gastric

\* Corresponding author at: Postgraduate Program in Biological Chemistry, Department of Biological Chemistry, Regional University of Cariri, Campus Pimenta II, CEP: 63.100-000, Crato, CE, Brazil.

E-mail address: [alexandre.teixeira@urca.br](mailto:alexandre.teixeira@urca.br) (A.M.R. Teixeira).



## Antiproliferative activity on *Trypanosoma cruzi* (Y strain) of the triterpene 3 $\beta$ ,6 $\beta$ ,16 $\beta$ -trihidroxilup-20 (29)-ene isolated from *Combretum leprosum*

José Ismael F. de Araújo<sup>a</sup>, Natália L. Aires<sup>d</sup>, Francisco W. Q. Almeida-Neto<sup>b</sup> , Márcia M. Marinho<sup>c</sup>, Emanuelle M. Marinho<sup>d</sup>, Emanuel Paula Magalhães<sup>d</sup>, Ramon R. P. B. de Menezes<sup>d</sup>, Tiago L. Sampaio<sup>d</sup>, Alice Maria Costa Martins<sup>d</sup>, Edson H. Teixeira<sup>i</sup>, Ana Rafaela Freitas Dotto<sup>h</sup>, Wanderlei do Amaral<sup>j</sup>, Alexandre Magno R. Teixeira<sup>a,f</sup>, Pedro de Lima-Neto<sup>b</sup> , Emmanuel S. Marinho<sup>g</sup>  and Hécio S. dos Santos<sup>a,e,f</sup>

<sup>a</sup>Programa de Pós-Graduação em Biotecnologia - PPG-B-Renorbio, Universidade Estadual do Ceará, Fortaleza, CE, Brazil; <sup>b</sup>Departamento de Química Analítica e Físico-Química, Universidade Federal do Ceará, Fortaleza, Brazil; <sup>c</sup>Faculdade de Educação, Ciência e Letras de Iguatu, Universidade Estadual do Ceará, Iguatu, Brazil; <sup>d</sup>Laboratório de Bioprospecção Farmacêutica e Bioquímica Clínica (LBFBC), Departamento de Análises Clínicas e Toxicológicas, Universidade Federal do Ceará, Fortaleza, Brazil; <sup>e</sup>Centro de Ciências Exatas e Tecnologia, Universidade Estadual do Vale do Acaraú, Sobral, Brazil; <sup>f</sup>Departamento de Química Biológica, Universidade Regional do Cariri, Crato, Brazil; <sup>g</sup>Faculdade de Filosofia Dom Aureliano Matos, Universidade Estadual do Ceará, Limoeiro do Norte, Brazil; <sup>h</sup>Programa de Pós-Graduação em Desenvolvimento Territorial Sustentável, Universidade Federal do Paraná, Matinhos, PR, Brazil; <sup>i</sup>Laboratório Integrado de Biomoléculas (LIBS), Departamento de Patologia e Medicina Legal, Universidade Federal do Ceará, Fortaleza, Brazil; <sup>j</sup>Departamento de Engenharia Química, Universidade Federal do Paraná, Curitiba, Paraná, Brasil

Communicated by Ramaswamy H. Sarma

### ABSTRACT

Chagas disease infects approximately seven million people worldwide. Benznidazole is effective only in the acute phase of the disease, with an average cure rate of 80% between acute and recent cases. Therefore, there is an urgent need to find new bioactive substances that can be effective against parasites without causing so many complications to the host. In this study, the triterpene 3 $\beta$ -6 $\beta$ -16 $\beta$ -trihydroxilup-20 (29)-ene (CLF-1) was isolated from *Combretum leprosum*, and its molecular structure was determined by NMR and infrared spectroscopy. The CLF-1 was also evaluated *in vitro* and *in silico* as potential trypanocidal agent against epimastigote and trypomastigote forms of *Trypanosoma cruzi* (Y strain). The CLF-1 demonstrated good results highlighted by lower IC<sub>50</sub> (76.0 ± 8.72  $\mu$ M, 75.1 ± 11.0  $\mu$ M, and 70.3 ± 45.4  $\mu$ M) for epimastigotes at 24, 48 and 72 h, and LC<sub>50</sub> (71.6 ± 11.6  $\mu$ M) for trypomastigotes forms. The molecular docking study shows that the CLF-1 was able to interact with important TcGAPDH residues, suggesting that this natural compound may preferentially exert its effect by compromising the glycolytic pathway in *T. cruzi*. The ADMET study together with the MTT results indicated that the CLF-1 is well-absorbed in the intestine and has low toxicity. Thus, this work adds new evidence that CLF-1 can potentially be used as a candidate for the development of new options for the treatment of Chagas disease.

### ARTICLE HISTORY

Received 29 June 2021  
Accepted 15 August 2021

### KEYWORDS

*Combretum*; triterpene;  
chagas disease;  
benznidazole


### 1. Introduction

Chagas disease is a tropical disease caused by the *Trypanosoma cruzi* parasite, classified as neglected by the World Health Organization (WHO). Currently, there are approximately seven million people infected in the world, and it is estimated that 70 million people will be able to contract this disease (Chatelain & Jean-Robert, 2011). Benznidazole is the only drug used in Brazil for the treatment of Chagas disease. It is effective only in the acute phase of the disease, with an average cure rate of 80% between acute and recent cases. Benznidazole has significant side effects such as skin reactions, fever, atopic dermatitis, erythematous, light-sensitive rashes, purple, weight loss, and gastrointestinal disorders in the first weeks of treatment (Coura & Borges-Pereira, 2012). Thus, there is a need to

search for new bioactive substances that promote greater control of parasites without causing so many complications to the host. During the past few years, isolated triterpenes from different plant species have been reported in the literature because they have a variety of biological activities (Akihisa et al., 1996; Dzubak et al., 2006; Topçu, 2006).

Among the bioactive triterpenes isolated from plants, it can be highlighted the pentacyclic triterpene of the lupine class 3 $\beta$ , 6 $\beta$ , 16 $\beta$ -trihydroxilup-20(29)-eno (C<sub>30</sub>H<sub>50</sub>O<sub>3</sub>, hereafter named CLF-1) isolated from *Combretum leprosum* (Figure 1), a shrub plant, found in the Northeast region of Brazil, popularly known as “mufumbo”, “mofumbo” or “cipoaba” (de Sousa Lira et al., 2002) which has received attention due to its great pharmacological importance, evidenced by its anti-oxidant, anti-inflammatory, antiviral, antiparasitic,

**CONTACT** Hécio S. dos Santos  [helciiodossantos@gmail.com](mailto:helciiodossantos@gmail.com)  Postgraduate Program in Biological Chemistry, Department of Biological Chemistry, Regional University of Cariri, Campus Pimenta II, CEP: 63.100-000, Crato, CE, Brazil

 Supplemental data for this article can be accessed online at <https://doi.org/10.1080/07391102.2021.1970025>

© 2021 Informa UK Limited, trading as Taylor & Francis Group

According to Elsevier's permission and Author's rights to reproduce copyright work, the author can use in part or full the published articles when included in a thesis if there aren't commercial purposes. The following information was taken from Elsevier's website accessed on September 18, 2021.

ELSEVIER

About Elsevier Products & Solutions Services Shop & Discover Search Q

Permission guidelines ScienceDirect content ClinicalKey content Tutorial videos Help and support

Do I need to request permission to re-use work from another STM publisher? +

Do I need to request permission to text mine Elsevier content? +

Can I include/use my article in my thesis/dissertation? -

Yes. Authors can include their articles in full or in part in a thesis or dissertation for non-commercial purposes.

Which uses of a work does Elsevier view as a form of 'prior publication'? +

How do I obtain permission to use Elsevier Journal material such as figures, tables, or text excerpts, if the request falls within the STM permissions guidelines? +

How do I obtain permission to use Elsevier Journal material such as figures, tables, or text excerpts, if the amount of material I wish to use does not fall within the free limits set out in the STM permissions guidelines? +

How do I obtain permission to use Elsevier Book material such as figures, tables, or text excerpts? +

Source: <https://www.elsevier.com/about/policies/copyright/permissions>



## Author rights

The below table explains the rights that authors have when they publish with Elsevier, for authors who choose to publish either open access or subscription. These apply to the corresponding author and all co-authors.

Author rights in Elsevier's proprietary journals	Published open access	Published subscription
Retain patent and trademark rights	✓	✓
Retain the rights to use their research data freely without any restriction	✓	✓
Receive proper attribution and credit for their published work	✓	✓
Re-use their own material in new works without permission or payment (with full acknowledgement of the original article): 1. Extend an article to book length 2. Include an article in a subsequent compilation of their own work 3. Re-use portions, excerpts, and their own figures or tables in other works.	✓	✓
Use and share their works for scholarly purposes (with full acknowledgement of the original article): 1. In their own classroom teaching. Electronic and physical distribution of copies is permitted 2. If an author is speaking at a conference, they can present the article and distribute copies to the attendees 3. Distribute the article, including by email, to their students and to research colleagues who they know for their personal use 4. Share and publicize the article via Share Links, which offers 50 days' free access for anyone, without signup or registration 5. Include in a thesis or dissertation (provided this is not published commercially) 6. Share copies of their article privately as part of an invitation-only work group on commercial sites with which the publisher has a hosting agreement	✓	✓
Publicly share the preprint on any website or repository at any time.	✓	✓
Publicly share the accepted manuscript on non-commercial sites	✓	✓ using a CC BY-NC-ND license and usually only after an embargo period (see Sharing Policy for more information)
Publicly share the final published article	✓ in line with the author's choice of end user license	×
Retain copyright	✓	×

Source: <https://www.elsevier.com/about/policies/copyright>